

**Investigation of LPA₁ Receptor Antagonism/ATX Inhibition by a Scaffold
Hopping Approach and SAR Analysis**

Diana Castagna

Thesis

February 2016

**Investigation of LPA₁ Receptor Antagonism/ATX Inhibition by a Scaffold
Hopping Approach and SAR Analysis**

Thesis submitted to the University of Strathclyde in fulfilment of the requirements for
the degree of Doctor of Philosophy

By

Diana Castagna

February 2016

Declaration of Copyright

This thesis is a result of the author's original research. It has been composed by the author and has not been previously submitted for examination which has led to the award of a degree.

The copyright of this thesis belongs to the author under the terms of the United Kingdom Copyright Acts as qualified by University of Strathclyde Regulation 3.50. Due acknowledgement must always be made of the use of any material contained in, or derived from, this thesis.

Signed:

Date: February 2016

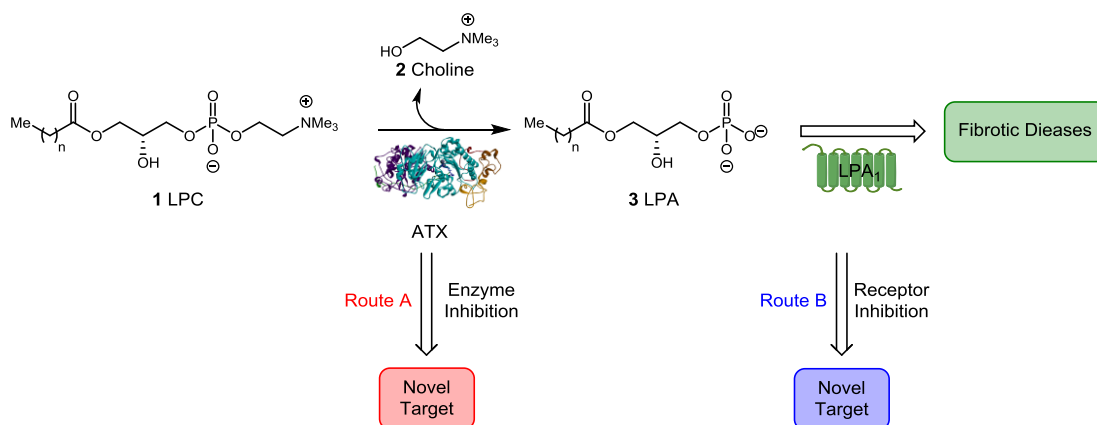
Publication List

1. "Identification of a Novel Class of ATX Inhibitors Through Cross-Screening": Diana Castagna, Emma L. Duffy, Louise C. Young, John M. Pritchard, Simon J. F. Macdonald, Craig Jamieson and Allan J. B. Watson, *Med. Chem. Commun.*, **2015**, 6, 1149-1155.
2. "The Development of Autotaxin Inhibitors: An Overview of the Patent and Primary Literature": Diana Castagna, David Budd, Simon J. F. Macdonald, Craig Jamieson and Allan J. B. Watson, *J. Med. Chem.* DOI:10.102/acs.jmedchem.5b01599
3. "Structure-Activity Relationships of Autotaxin Inhibitors": Diana Castagna, Lisa M. Miller, Emma L. Duffy, Frances M. Potjewyd, Louise, C. Young, John M. Pritchard, Simon J. F. Macdonald, Craig Jamieson and Allan J. B. Watson, *Manuscript in Preparation*.
4. "A Scaffold Hopping Approach to Novel Autotaxin Inhibitors": Emma L. Duffy, Frances M. Potjewyd, Diana Castagna, Lisa M. Miller, Louise C. Young, John M. Pritchard, Simon J. F. Macdonald, Craig Jamieson and Allan J. B. Watson, *Manuscript in Preparation*.
5. "A Quantitative Assessment of the Effect of Reaction Variables on Racemization During Peptide Coupling of α -Amino Acids": Diana Castagna, Amy Ott, Craig Jamieson and Allan J. B. Watson, *Manuscript in Preparation*.

Abstract

The Autotaxin-Lysophosphatidic acid (ATX-LPA) signalling pathway has been implicated in a variety of human disease states including angiogenesis, autoimmune diseases, cancer, fibrotic disease, inflammation, neurodegeneration, and neuropathic pain, amongst others.

Two methods have been pursued in attempts to develop novel targets for this disease state which include: Route A – the development of novel LPA₁ receptor antagonist, and Route B – the inhibition of the enzyme ATX required for the production of LPA (Scheme 1). Both of these routes will be pursued within this study with a view to developing novel targets for the inhibition of the LPA-ATX signalling pathway.



Scheme 1: Proposed routes for the development of novel LPA-ATX inhibitors.

A small compound library was constructed to target Route A, where of the compounds analysed none exhibited LPA₁ receptor antagonism. Pleasingly, cross screening against ATX inhibition revealed several hit compounds, indicating the ability of cross-talk between these two signalling pathways.

In regards to the second route, an extensive compound library was built based on the development of SAR surrounding a known potent ATX inhibitor by Amira Pharmaceuticals. The designed compounds were screened using a dual assay procedure (LPC and (bis-*p*-nitrophenyl)phosphate assay) which indicated a range of active compounds, as well as indicating the complexity associated with the binding mode of this particular motif.

Acknowledgements

First and foremost I would like to thank my supervisor Dr Allan Watson for giving me the opportunity to work within his group and for his continued support and motivation throughout my project.

I would also like to thank my second supervisor Dr Craig Jamieson for his help and advice throughout my PhD. I am grateful to my industrial supervisor Dr Simon Macdonald for his continuing support by providing industrial insight and guidance throughout. I would also like to thank the other members of team fibrosis, Emma Duffy, Lisa Miller, and Frances Potjewyd who have helped contribute to this project and have been a constant source of help and support.

Also, I would like to give a special thank you to my fellow members of the Watson group and the Jamieson group for all of their help and support and making the lab such an enjoyable place to work. It has been a pleasure to have worked with you all.

Lastly, I would like to thank my friends and family for their love and support. This wouldn't have been possible without you.

Abbreviations

3D	3-Dimensional
AA	Acyl Aniline Series
AcOH	Acetic acid
AECs	Alveolar epithelial cells
AI	Acyl Indole Series
ADME	Absorption, Distribution, Metabolism and Excretion
Asn	Asparagine
Asp	Aspartic Acid
aq.	Aqueous
Arl	Aryl Indole Series
ATX	Autotaxin
Bis- <i>p</i> NPP	bis-(<i>p</i> -Nitrophenyl)phosphate
B-gla	β -galactosidase
Br	Bromine
br	Broad
cat.	Catalyst
CaCl ₂	Calcium chloride
CbzCl	Benzyl chloroformate
CDCl ₃	Chloroform-d
CF ₃	Trifluoromethyl
CHCl ₃	Chloroform
CHO-K1	Chinese Hamster Ovary derived cell line

c-Hex	Cyclohexane
CN	Cyano
CO ₂	Carbon dioxide
Conc.	Concentration
Cpd. No.	Compound number
CPF4	Coumarin phosphodiester fluorescein 4
c-Pent	Cyclopentane
c-Pr	Cyclopropyl
Cs ₂ CO ₃	Caesium carbonate
CuI	Copper Iodide
CuO	Copper oxide
Cys	Cystein
d	Doublet
DBU	1,8-Diazabicycloundec-7-ene
DCE	Dichloroethane
DCM	Dichloromethane
dd	Double doublet
DIPEA	N,N-Diisopropylethylamine
DMEM	Dulbecco's Modified Eagle's Medium
DMF	Dimethylformamide
DMSO	Dimethyl sulfoxide
DNA	Deoxyribonucleic Acid
ECM	Extracellular matrix

ENPP2	Ecto-nucleotide pyrophosphates/phosphodiesterase
Et	Ethyl
et. al.	et alia
EtOAc	Ethyl acetate
EtOH	Ethanol
Equiv.	Equivalents
FBS	Fetal Bovine Serum
FS3	Fluorogenic substrate 3
FTIR	Fourier transform infrared spectroscopy
g	Grams
GDP	Guanosine-diphosphatase
Glu	Glutamic acid
GTP	Guanosine-triphosphatase
GPCR	G-coupled protein receptor
GSK	GlaxoSmithKline
h	Hours
H	Hydantoin Series
HCl	Hydrogen chloride
HPLC	High-pressure liquid chromatography
HRMS	High-resolution mass spectrometry
HRP	Horseradish peroxidase
Hs 27	Human foreskin, fibroblast cells
H ₂ SO ₄	Sulfuric acid

HVA	Homovanilic acid
Hz	Hertz
IC ₅₀	Half maximal inhibitory concentration
ILD	Interstitial lung disease
IPF	Idiopathic pulmonary fibrosis
<i>i</i> -Pr	Isopropanol
K ₂ CO ₃	Potassium carbonate
Ki	Kinetic inhibitor
KOAc	Potassium acetate
K ₃ PO ₄	Potassium phosphate
L1	Linker 1
L2	Linker 2
LC-MS/MS	Liquid chromatography-tandem mass spectrometry
Leu	Leucine
LiOH	Lithium hydroxide
LPA	Lysophosphatidic acid
LPC	Lysophosphatidylcholine
LysoPLD	Lysophospholipase D
M	Molar
m	Multiplet
MDAP	Mass directed auto purification system
MeCN	Acetonitrile
MeOH	Methanol

MeOD	Methanol-d
mg	Milligrams
mL	Millilitres
mM	millimolar
mmol	Millimole
Mo(CO) ₆	Molybdenum hexacarbonyl
m/z	Mass-to-charge ratio
N ₂	Nitrogen
Me	Methyl
MeOH	Methanol
2-MeTHF	2-Methyltetrahydrofuran
MHz	Megahertz
min	Minutes
MW	Molecular weight
NaH	Sodium hydride
NaHB(OAc) ₃	Sodium triacetoxyborohydride
NaHCO ₃	Sodium hydrogen carbonate
NaOH	Sodium hydroxide
Na ₂ SO ₄	Sodium sulfate
NCRI	National Cancer Institute
ng	Nanograms
NH ₃ Cl	Ammonium chloride
nm	Nanometers

nM	Nanomolar
NMR	Nuclear magnetic resonance
NNP	Nucleotide pyrophosphatase/phosphodiesterase
NUC	Nuclease-like domain
OMe	Methoxy
p	Pentet
PAI-1	Plasminogen activator inhibitor-1
P_{app}	Apparent permeability
PC3	Prostate cancer 3
PCy ₃	Tricyclohexylphosphine
PDB	Protein Data Bank
Pd(dppf)Cl ₂	[1,1'-Bis(diphenylphosphino)ferrocene]dichloropalladium(II)
PDE	Phosphodiesterase domain
PDGF	Platelet derived growth factor
p-ERK	Phosphorylated ERK
Ph	Phenyl
Phe	Phenylglycine
1,10-phen	1,10-phenanthroline
PIP2	Phosphatidylinositol-biphosphate
pK _a	Negative log of the acid dissociation constant
PKC	Protein Kinase C
PK/PD	Pharmacokinetic/pharmacodynamic
PLC	Phospholipase C

PLD	Phospholipase D
<i>p</i> NP-TMP	Thymidine 5'-mono-phosphate <i>p</i> -nitrophenyl
Pos.	Position
ppm	Parts per million
Pr	Propyl
PSA	Polar Surface Area
Py	Pyridine
q	Quartet
quin.	Quintet
RPMI	Roswell Park Memorial Institute
s	Singlet
S1P	Sphingosine 1-phosphate
SAR	Structure Activity Relationship
sat.	Saturated
SDS	Sodium dodecyl sulfate
SEM	Standard error of the mean
SMB1	Somatomedin B1
SMB2	Somatomedin B2
S _N Ar	Nucleophilic aromatic substitution
SOCl ₂	Thionyl chloride
Sol.	Solubility
SPC	Sphingosylphosphorylcholine
t	Triplet

^t BuOH	tert-Butyl alcohol
TCA	Trichloroacetic acid
TGF-β	Transforming growth factor β
TLC	Thin layer chromatography
THF	Tetrahydrofuran
THP	Tetrahydropyran
Thr	Threonine
TNF-α	Tumor necrosis factor α
uPAR	Urokinase-type plasminogen activator
UV	Ultraviolet
UV-Vis	Ultraviolet-visible spectroscopy
μg	Micrograms
μM	Micromolar
Val	Valine
yr	Year
w/v	percentage weight per volume
w/w	percentage weight per weight
XaNPP	Xanthomonas axonopodis

Table of Contents

1	Introduction.....	1
1.1	Cancer.....	1
1.1.1	Disease Progression	2
1.2	Respiratory Disorders	2
1.2.1	Idiopathic Pulmonary Fibrosis: Disease Background	2
1.2.2	Pathogenesis of IPF	3
1.2.3	Proposed Mechanism of IPF.....	4
1.3	Structure and Function of the Autotaxin Enzyme	8
1.4	Assays for the Identification of ATX Inhibition.	15
1.4.1	Natural Substrate ATX Assays	15
1.4.2	Unnatural Substrate ATX Assays	17
1.5	Inhibitors.....	19
1.5.1	LPA ₁ and LPA ₃ Antagonists.....	19
2	Project Overview	26
3	Chapter 1: Development of Novel LPA ₁ Receptor Antagonist	27
3.1	Proposed Work and Aims	27
3.2	Results and Discussion	30
3.2.1	Structural Development of Acyl Aniline, Acyl Indole and Hydantoin Series	30
3.2.2	Physicochemical Data	33
3.2.3	Acyl Aniline Series.....	35
3.2.4	Acyl Indole Series.....	40
3.3	Pharmacology.....	44
3.3.1	LPA ₁ receptor Agonism/Antagonism.....	44
3.3.2	ATX Inhibition	48
3.4	Conclusions.....	56
3.5	Future Work.....	58

3.6	Experimental	60
3.6.1	General	60
3.6.2	General Procedures	61
3.6.3	Characterisation Data.....	64
3.7	Biology	84
3.7.1	PathHunter® CHO-K1 EDG2 β -Arrestin Compound Screen Study	84
3.7.2	Methods for [³ H]-Thymidine Incorporation Assay	85
3.7.3	Cytotoxicity	86
4	Chapter 2: Investigation of the Origin of Activity in the Amira Non-Lipid Like ATX Inhibitor.....	87
4.1	Proposed Work and Aims	87
4.2	Results and Discussion	89
4.2.1	Amira Patent SAR Data.	89
4.2.2	Molecular Docking Studies	93
4.2.3	Development of Deletion Analogues.....	96
4.2.4	Section A: Substitution on the Benzenoid Ring.....	102
4.2.5	Section B: Core Modifications.....	106
4.2.6	Section C: Derivatisation of the Acid Warhead	108
4.2.7	Section D: Indole Substitution.....	113
4.3	Pharmacology.....	115
4.3.1	Section A: Substitution on the Benzenoid Ring.....	117
4.3.2	Section B: Core Changes	120
4.3.3	Section C: Derivatisation of the Acid Warhead	122
4.3.4	Section D: Indole Nitrogen Substitution	123
4.3.5	Assay Kinetics	126
4.4	Conclusions.....	130
4.5	Future Work.....	133
4.5.1	Biological Evaluation	133

4.5.2	Supplementary SAR	133
4.6	Experimental	136
4.6.1	General	136
4.6.2	General Experimental Procedures.....	137
4.6.3	Compound Characterisation Data.....	141
4.7	Biology	183
4.7.1	Autotaxin Inhibition Assay.....	183
4.7.2	Choline Release Assay.....	184
5	References	185

List of Figures, Schemes, and Tables

Figure 1: Six most common cancer cases worldwide in 2014, data obtained from the National Cancer Institute (NCRI). ⁴	1
Figure 2: 5-year survival rate of a range of cancers compared to IPF. Statistics obtained from the US National Cancer Institute. ¹²	3
Figure 3: Proposed pathway for the progression of IPF. a) Normal Cell structure. b) External stimuli causing damage to the epithelial cells. c) Release of growth factors and leakage of coagulant proteins into the airspace. d) Migration of fibroblasts to the site.....	5
Figure 4: Simplified representation of the four main components of the ATX enzyme; N is the nuclease-like domain; C is the catalytic domain containing the hydrophobic pocket; and SMB1 and SMB2 are the two somatomedin B domains. LPC is introduced into the catalytic site where it is subsequently hydrolysed to LPA and transported to the GPCR, resulting in their activation.....	7
Figure 5: Signalling pathways activated by LPA ₁₋₆	8
Figure 6: a) Schematic representative diagram of ATX domains (PDB 2XR9). (b) 3D structure of ATX representing the four main domains, SMB1 in orange, SMB2 in brown, catalytic domain in cyan, nuclease like domain in purple, L1 in red, and L2 in green.	10
Figure 7: a) Representation of ATX with the catalytic site highlighted (PDB 2XRN). b) Enlarged image of the catalytic site illustrating the Zn ²⁺ ions, and the essential residues: Thr209 (red) and the catalytic triad made up of His359 (orange), Asp358 (blue), and Asn230 (green).	11
Figure 8: (a) Representation of the ATX active site, hydrophobic pocket, and tunnel with LPA (PDB 3NKN). (b) A representation of the T-shaped structure.	12
Figure 9: Structure of LPA (14:0) (4) complexed within the active site of ATX (PDB 3NKN). a) Ribbon representation of ATX, coloured as follows: SMB1 domain in orange, SMB2 domain in brown, catalytic domain in cyan, nuclease-like domain in purple, L1 in red, L2 in green, Zn ²⁺ in grey, and 4 in pink. b) Structure of 4 . c) and d)	

Enlargement of the catalytic site indicating the interactions between the phosphate group with the Thr209 residue and one of the Zn²⁺ ions.....13

Figure 10: Co-crystal of **5** within the catalytic domain of ATX (PDB 2XRG). a) Ribbon representation of ATX, coloured as follows: SMB1 domain in orange, SMB2 domain in brown, catalytic domain in cyan, nuclease-like domain in purple, L1 in red, L2 in green, Zn²⁺ in grey, and **5** in pink. b) Structure of **5**. c) and d) Enlargement of the catalytic site indicating the interactions between the boronic acid and both the Thr209 residue and one of the Zn²⁺ ions.....14

Figure 11: Potential antagonists of LPA₁ and LPA₃.....20

Figure 12: Illustrative examples of patented ATX inhibitors.....21

Figure 13: Compound **19** docked within ATX using MOE docking software using PDB 3NKR. a) Ribbon representation of ATX, coloured as follows: SMB1 domain in orange, SMB2 domain in brown, the catalytic domain in cyan, nuclease-like domain in purple, L1 in red, L2 in green, Zn²⁺ in grey, and **19** in pink. b) Illustrating close proximity of the acidic head group (benzoxazolidinone) to one of the Zn²⁺ ions and the Thr209 residue. c) Alternative view of **19** within the active site of the enzyme...22

Figure 14: Compound **4** (in green) and **20** (in pink) co-crystallised within ATX (PDB 4ZG7). a) Ribbon representation of ATX, coloured as follows: SMB1 domain in orange, SMB2 domain in brown, the catalytic domain in cyan, nuclease-like domain in purple, L1 in red, L2 in green, and Zn²⁺ in grey. b) Structure of **20**. c) Enlarged image of the active site illustrating the space occupied by **4** (in green) and **20** (in pink). d) Simplified representation of the active site.23

Figure 15: ATX-related publications since 1992. Data collected from SciFinder and Espacenet.¹24

Figure 16: Illustrative examples of the four generally chemotype within the patent literature: **18** Amira-like; **19** Pfizer-like; **21** lipid-like; and **5** other.24

Figure 17: Schematic representation of the three proposed disconnections from the backbone compounds **16**, followed by the overlaid diagrams of each of the exemplars where **16** in shown in grey.28

Figure 18: Proposed compounds to be synthesised within the three main series (i) the acyl aniline (AA), (ii) the acyl indole (AI), and (iii) the hydantoin (H).	31
Figure 19: AA overlay alignments where AM095 (16) in grey, and AA (22) in blue.	32
Figure 20: AI overlay diagram where AM095 (16) in grey, and AI (23) in green.	33
Figure 21: H overlay diagram where AM095 (16) in grey and H (24) is in red.	33
Figure 22: AA compounds targeted for synthesis.....	35
Figure 23: Catalyst 45	38
Figure 24: Proposed compounds for synthesis within the substituted AA series. ...	38
Figure 25: Overlay of Arl compound 75 (green) with AM095 16 (grey).....	43
Figure 26: Synthesised compounds taken forward for biological evaluation.....	43
Figure 27: Activation of GPCR leads to β -arrestin recruitment and formation of a functional enzyme which is then capable of hydrolysing the substrate and generating a chemiluminescent signal.	44
Figure 28: Overlaid diagram of compounds 22 in blue, 25 in purple, 26 in red, and 27 in green, illustrating all four compounds contain the same conformation.....	50
Figure 29: ^3H -thymidine incorporation into LPA (2 μM), AM095 (16) (graph a), compound 22 (graph b), compound 28 (graph c), or compound 35 (graph d) (10 μM), stimulated PC3 cell line, cells were quiesced for 24 hours and treated for 18 h with compounds (16 , 22 , 28 , or 35). n=9, data represented as Mean \pm S.E.M.	55
Figure 30: Additional SAR surrounding the hydantoin series.....	59
Figure 31: Typical structure of ATX inhibitors within the literature with the key motifs highlighted.	87
Figure 32: Potent literature ATX inhibitors 18 and 19 with the main structural motifs highlighted.	88
Figure 33: Representative compounds from Amira illustrating the three assay categories.....	89
Figure 34: Four main sections studied by Amira Pharmaceuticals.	90

Figure 35: SAR around section A - substitution on the aromatic ring.....	90
Figure 36: SAR around section B - derivatisation of the acid.....	91
Figure 37: SAR around section C - substitution on the indole nitrogen.....	92
Figure 38: SAR around Section D at the C ₂ position of the indole.	92
Figure 39: SAR deduced from Amira Pharmaceutical patents.....	93
Figure 40: Compound 18 modelled within the active site of ATX (PDB 2XRG), where the blue surface represents the space occupied by the ligand. ⁹⁷	94
Figure 41: Docking of 18 illustrating the interactions of the pyridyl acid with one of the Zn ²⁺ ions in the active site (PDB 2XRG). ⁹⁷	94
Figure 42: Compound 18 docked within the active site (PDB 2XRG) indicating the main binding interactions: a) 6-chloro indole projecting into a cleft and picking up interactions with Glu308 and Val227 residues; b) methyl of the indole picking up interactions with Glu308 and Val227 residues; b) methyl of the indole picking up interactions with Phe210, Thr209, and Leu213 residues; c) the pyrazole functionality projecting into a cleft; d) enlarged image of the cleft where the methyl pyrazole resides indicating the space available. ⁹⁷	95
Figure 43: Four main sections of 18 targeted for SAR analysis: Section A – substitution on the benzenoid ring; Section B – core changes; Section C – derivatisation of the acid warhead; and, Section D – indole nitrogen substitution, with the proposed compounds outlined within each section.	97
Figure 44: Molecular overlay of compound 137 in red and compound 18 by Amira in green.	98
Figure 45: Catalytic site and hydrophobic pocket of ATX: Complex of LPA 14:0 (4) (yellow) in Mouse ATX (PDB ID 3NKN) with the docked position of bis- <i>p</i> NPP (blue) overlaid. ⁹⁸	102
Figure 46: Compound 137	121
Figure 47: Single shot data at 30 μM for a selection of the compounds tested.....	127

Figure 48: Ki curve data illustrating a tailing off at 40% hydrolysis indicated by the red line.....	128
Figure 49: Ribbon representation of ATX coloured as follows: SMB1 domain in orange, SMB2 domain in brown, catalytic domain in cyan, nuclease-like domain in purple, L1 in red, L2 in green, and Zn ²⁺ in grey. a) Structure of 228 complexed within ATX (PDB 4ZG7). b) Structure of 20 complexed within ATX (PDB 4ZG7)...	129
Figure 50: Structure of 20 in yellow and LPA 14:0 (4) in pink complexed within ATX, illustrating the remote binding of 20 from the active site.....	129
Figure 51: Four main sections probed in the SAR study.	130
Figure 52: Summary of the associated SAR developed from the bis- <i>p</i> NNP data for the developed compound library.	131
Figure 53: Proposed addition SAR surrounding the functionality of the indole ring.	134
Figure 54: Alternative functionality on the benzenoid ring.....	134
Figure 55: Additional SAR proposed for the acid region.....	135
Scheme 1: Proposed routes for the development of novel LPA-ATX inhibitors.....	iv
Scheme 2: ATX mediated hydrolysis of LPC (1) to LPA (3) with the release of choline (2).....	6
Scheme 3: Hydrolysis of SPC (6) to S1P (7) catalysed by ATX.....	15
Scheme 4: Regions of 20 highlighted to indicated the lipophilic tail (in red), the core spacer (in blue), and the acidergic head group (in green).	25
Scheme 5: Proposed route for the development of novel ATX-LPA inhibitors from 16	26
Scheme 6: Proposed route for the development of novel ATX inhibitors from 18	26
Scheme 7: Retrosynthetic analysis for the synthesis of 22 from the AA series.....	36

Scheme 8: Synthetic route for the construction of the acyl aniline series compounds (22, 25, 26, and 27). *Synthesised using commercially available phenyl boronic acid.	37
Scheme 9: Synthetic route of 28, 29, and 30 for the functionalised AA series.	39
Scheme 10: Adapted synthetic route for the formation of compound 23.....	40
Scheme 11: Synthetic route for the synthesis of compound 23.	41
Scheme 12: Revised synthetic route for the synthesis of 23.....	41
Scheme 13: Revised route for the synthesis of the AI series.....	42
Scheme 14: Bis-pNPP assay mechanism, where i) inactive compounds have no effect on the ATX enzyme allowing hydrolysis of the substrate which can be monitored by UV and ii) active compounds will inhibit the ATX enzyme inhibiting the hydrolysis process.	49
Scheme 15: Three target series developed using from AM095 (16), i) the AA series, ii) the Arl series, and iii) the H series.....	56
Scheme 16: Alternative SAR surrounding compound 28.....	58
Scheme 17: Alternative route to the development of the acyl indole compounds. ..	59
Scheme 18: Specific compounds proposed for synthesis within Section A.....	103
Scheme 19: Retrosynthetic analysis for the synthesis of compounds 18 and 127-129.	103
Scheme 20: Synthesis of Section A compounds.....	104
Scheme 21: Synthesis of compounds within Section A with alternative substitution on the benzenoid ring.	106
Scheme 22: Compounds proposed for synthesis within Section B.	107
Scheme 23: Retrosynthetic analysis for the synthesis of compound 137.....	107
Scheme 24: Synthetic route for the preparation of compound 132 within Section B.	108

Scheme 25: Specific compounds proposed for synthesis within Section C.	109
Scheme 26: Retrosynthetic analysis for the synthesis of the benzoic acid series compounds within Section C.....	110
Scheme 27: Synthetic route for compounds 104 , and 146 within Section C.....	111
Scheme 28: Retrosynthetic analysis for the synthesis of compounds 147 and 148 within Section C.....	112
Scheme 29: Synthetic route for the construction of compounds 147 and 148 within Section C.....	113
Scheme 30: Specific compounds proposed for synthesis within Section D.	113
Scheme 31: Synthesis towards compounds proposed in Section D.	115
Scheme 32: Amplex® Red assay procedure where the choline released from LPC hydrolysis is quantified using a two-step enzymatic colouring reaction.	116
Table 1: Splice variant of ATX.....	9
Table 2: Natural substrate ATX assays.	16
Table 3: Unnatural substrate ATX assays.	18
Table 4: Calculated physicochemical data for AA and AI series. ^a	34
Table 5: Control compounds.	45
Table 6: Aryl indole compounds.	45
Table 7: Hydantoin compounds.....	46
Table 8: Acyl aniline compounds.....	47
Table 9: Biological and Physicochemical Data for Acyl Aniline Series.....	50
Table 10: Biological and physicochemical data for substituted acyl aniline series. .	51
Table 11: Biological and physicochemical data for substituted aryl indole series....	52
Table 12: Biological and physicochemical data for hydantoin series.....	53
Table 13: Calculated physicochemical values for 137 Section B. ^a	98

Table 14: Calculated physicochemical values for exemplars from section C. ^a	100
Table 15: Calculated physicochemical values for exemplars from section D. ^a	101
Table 16: Chlorine regiochemical analysis biological data	117
Table 17: Alternative substitution on the benzenoid ring biological data	119
Table 18: Section B - core changes biological data	120
Table 19: Section C - Derivatisation of the acid warhead biological evaluation.....	122
Table 20: Section D - Indole nitrogen substitution on pyridyl system biological data.	124
Table 21: Section D - Indole nitrogen substitution on benzoic acid system biological data.	126

1 Introduction

The top five causes for premature death in the UK can be attributed to cancer, heart disease, stroke, respiratory disease, and liver disease.¹ It has been proposed by the Department of Health that the number of deaths associated with these diseases could be dramatically reduced by earlier diagnosis, which could be achieved by obtaining a more in-depth knowledge of the disease states and their associated symptoms.¹ Of the five most common causes of premature death, cancer is perhaps the most studied, followed closely by respiratory diseases due to their high mortality rates and the requirement for more efficacious and better tolerated therapies.

1.1 Cancer

Cancer is one of the leading causes of mortality with around 160,000 deaths each year in the UK alone,² and an estimated 8.2 million deaths worldwide, with an expected increase in incidence of 70% in the next two decades.³ With more than 200 variants of cancer, where breast, prostate, lung, and bowel are the most prevalent (Figure 1),³ the investigation into new therapeutic targets for the treatment of cancer has become of pivotal importance. As a result, a substantial amount of funding has been invested into the development of novel treatments to inhibit or slow the progression of the disease. This can be seen by the dramatic increase in funding associated with cancer research, which has increased from £257 million in 2002 to a current spending of over £500 million.⁴

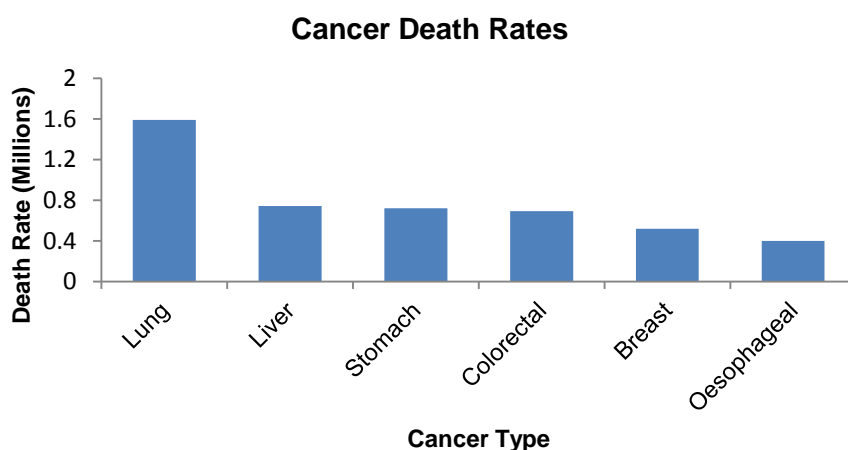


Figure 1: Six most common cancer cases worldwide in 2014, data obtained from the National Cancer Institute (NCRI).³

1.1.1 Disease Progression

The general disease progression associated with cancers stems from the mutation of cells, which will in turn increase their likelihood of proliferation, survival, invasion, and metastasis in an abnormal way.⁵ The increased proliferation of abnormal cells will then lead to the formation of outgrowths of cells, also known as tumours. There are a number of different carcinogens which have been implicated in the development of cancerous tissue which include cigarette smoking, radiation, chemicals, and viruses; however, it should be noted that cancer development is a complex process with many factors to be considered.⁵

1.2 Respiratory Disorders

In addition to cancer, another disease state which has developed increased interest is respiratory disorders. These are a class of disorders which affect the organs and tissue that make gas exchange possible. There is a wide range of common disorders which can be classified by this term. One such class of diseases is known as interstitial lung diseases (ILDs). This refers to inflammation of the interstitium (tissue surrounding and separating the alveoli) of the lungs. The causes associated with ILD are thought to involve over-stimulation of the normal wound healing process when damage occurs. However, when there is no outside stimulus, ILDs can still occur and this is classed as idiopathic interstitial lung disease, where idiopathic signifies that the cause is unknown. There are seven distinct disorders associated with ILD which are; (i) idiopathic pulmonary fibrosis (IPF) (47-64% of ILDs), (ii) nonspecific interstitial pneumonia (14-36%), (iii) cryptogenic organising pneumonia (4-12%), (iv) respiratory bronchial interstitial pneumonia, (v) desquamative interstitial pneumonia (10-17%), (vi) acute interstitial pneumonia (<2%), and (vii) lymphoid intestinal pneumonia (<2%).⁶ ILDs are becoming an increasing problem: 2006 ILDs cost the NHS over £6.6 billion and accounted for 1 in 5 deaths in the UK.⁷

1.2.1 Idiopathic Pulmonary Fibrosis: Disease Background

IPF is a chronic, progressive and potentially fatal lung disease.^{8,9} IPF affects around 13-20 per 100,000 people,⁹ and is becoming increasingly common, with an additional 5,000 cases reported each year in the UK alone. IPF exhibits a higher mortality rate than most cancers, as illustrated in Figure 2, where only lung and

pancreatic cancer have a lower five year survival rate.¹⁰ Once diagnosed, sufferers on average have a survival of around 3-5 years.⁸ IPF seems to have no specific demographic, however, it has been found to be prevalent in the older generation (median age range of 55-75 years) with a slight predominance in males.^{6,9} Some research has suggested there may be environmental factors which could attribute to the onset of IPF. These include cigarette smoking, drug/environmental factors, occupational exposure (from metal and wood dusts), viral infections (such as Epstein-Barr virus, hepatitis C, and gastroesophageal reflux disease),⁶ and genetic transmission.⁹

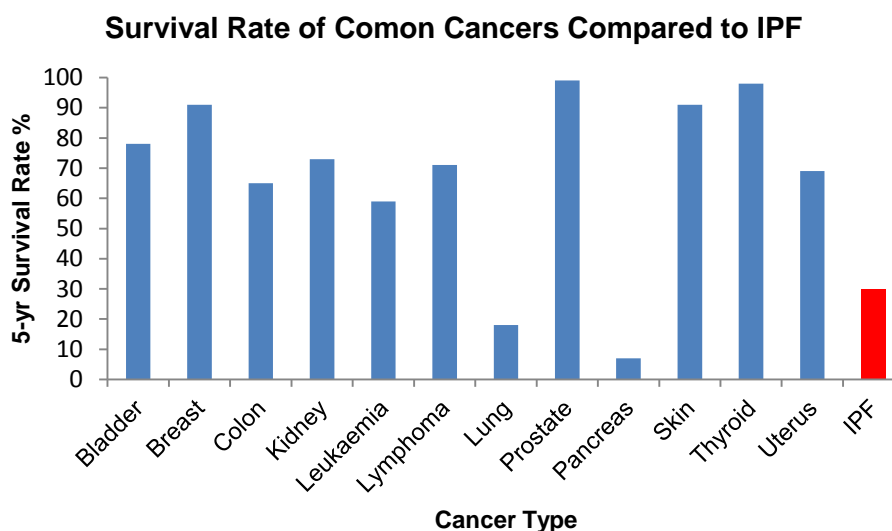


Figure 2: 5-year survival rate of a range of cancers compared to IPF. Statistics obtained from the US National Cancer Institute.¹¹

1.2.2 Pathogenesis of IPF

The causes behind IPF are not yet fully understood, however, it is believed to be connected to the abnormal behaviour of the alveolar epithelial cells (AECs) following lung injury. This promotes migration, proliferation, and activation of mesenchymal cells which can differentiate into connective tissue and fibroblasts, the latter of which are responsible for the production of extracellular matrix (ECM) molecules and collagen.^{9,12} The overstimulation of AECs results in the accumulation of ECM molecules, and it is the excessive production of these fibroblasts which cause irreversible damage and destruction of the lung through hardening and scarring of the lung tissue between the alveoli, honeycombing on the surface of the lung tissue,

loss of function of the capillary unit, impaired gas exchange, and finally, can lead to respiratory failure causing death.^{9,13}

1.2.3 Proposed Mechanism of IPF

The extent of the role that AECs have within IPF remains unknown, however, it has been proven that those suffering from IPF have a reduced number of Type I AECs and hyperplastic and elongated Type II epithelial cells, as evidenced through lung biopsies.⁹ The process by which IPF proceeds is not fully understood; however, a proposed scenario is illustrated in Figure 3.⁹

IPF is believed to develop after the normal epithelial and endothelial cells, (Figure 3a) become damaged (Figure 3b), and this can be caused by a range of stimuli including; viral infections, cigarette smoking, environmental factors such as working with wood and metal dust, and age.^{9,14} Once the basement membrane and endothelial cells are damaged this will result in the release of growth factors and leakage of proteins such as coagulant proteins into the airspace (Figure 3c). This process then becomes over-activated as more growth factors will be produced to try and aid the wound healing process (*i.e.*, regeneration of the basement membrane) and as a consequence this will result in the accumulation of fibroblasts within the airspace, (Figure 3d). The accumulation of these fibroblasts will then result in hardening and scarring of the tissue, impaired gas exchange, and the tell-tale honeycombing of the tissue, (Figure 3e).¹⁴

Recent investigations into the pathogenesis of both cancer and IPF have led to the discovery of several similarities between these disease states. These fall into five categories: i) genetic alterations, ii) epigenetic alterations, iii) uncontrolled proliferation, iv) tissue invasion, and v) signal transduction pathways.¹¹ In addition to these traits, it has been established that elevated levels of the extracellular enzyme autotaxin (ATX), the bioactive phospholipid lysophosphatidic acid (LPA), and, in particular, the LPA₁ receptor have been found in both patients suffering from IPF¹⁵ and a large number of cancers including breast cancer,^{16,17} renal cell carcinoma,¹⁸ thyroid carcinoma,¹⁹ and ovarian cancer,²⁰ amongst others.

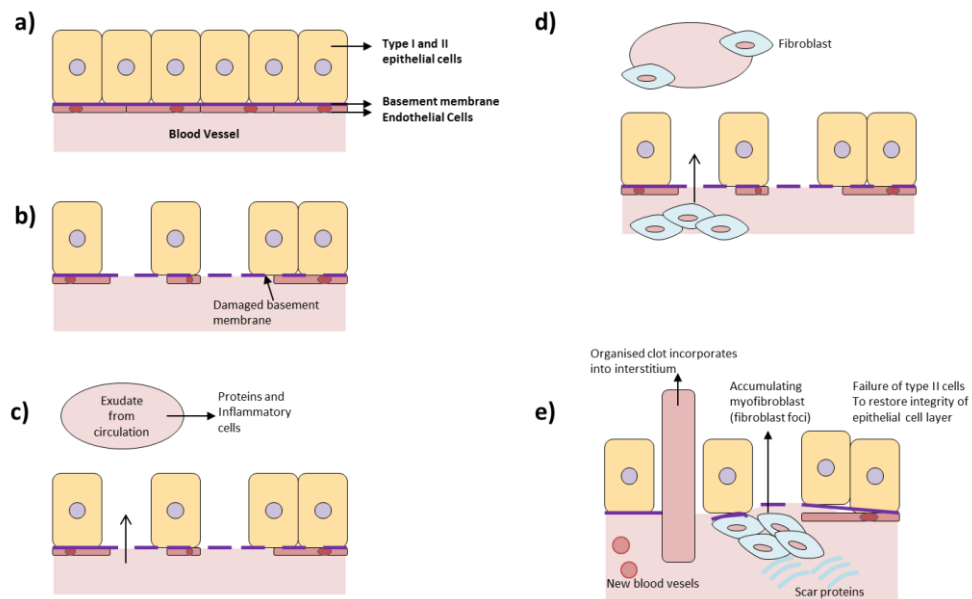


Figure 3: Proposed pathway for the progression of IPF. a) Normal Cell structure. b) External stimuli causing damage to the epithelial cells. c) Release of growth factors and leakage of coagulant proteins into the airspace. d) Migration of fibroblasts to the site

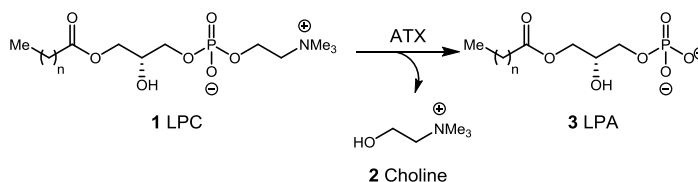
In the context of lung fibrosis, locally produced LPA has been suggested to drive several different pathological processes leading to excessive production of ECM molecules, permanent scarring of the lung, irreversible loss of tissue structure, and a reduction in lung function. Increased expression of ATX has been reported in the lungs of bleomycin-treated mice and patients with IPF²¹ in which the pattern of expression suggests that epithelial cells and macrophages (type of white blood cells which remove foreign substances) exhibit the highest intensity of ATX expression.²¹ In line with the reports of increased expression of ATX in the fibrotic lung, increased levels of LPA isoforms, notably the 22:4 species, have been reported in exhaled breath condensate of IPF patients compared to healthy volunteers.¹⁵ The mechanisms underlying the LPA pathway in the lung are complex but have been linked to accumulation of fibroblasts in the lung through increased migration and proliferation,²² increased vascular leakage,²² and apoptosis of lung epithelial cells.²² The finding that mice genetically deficient in macrophage-specific ATX expression are refractory to bleomycin-induced lung fibrosis²¹ also suggests an important role for this cell type in driving LPA-mediated pro-fibrotic responses in this organ. Some dispute exists regarding the identity of the LPA receptors responsible for driving the pro-fibrotic actions of LPA in the lung with data supporting a role for the LPA₁

receptor,²² LPA₂ receptor,²³ and LPA₃ receptor²⁴ based on a combination of pharmacological and genetic approaches. The use of ATX inhibitors might circumvent the issue of molecular redundancy with regards to which combination of receptor isoform targeting would be most effective with regards to achieving anti-fibrotic efficacy.

1.2.3.1 Autotaxin

ATX is an extracellular enzyme, which is part of the ecto-nucleotide pyrophosphatase/phosphodiesterase family (ENPP2), of which there are seven members.^{25,26} ATX was first isolated in 1992 from A2058 melanoma cells and categorised as an autocrine mobility factor, and was subsequently found to be responsible for cell proliferation, survival, invasion, migration, and neovascularization.^{20,27}

Following the initial discovery, further analysis by Tokumura *et al.*²⁸ and Umezugoto *et al.*²⁹ established that ATX was in fact the glycoprotein lysophospholipase D (lysoPLD),^{28,29} which is responsible for the hydrolysis of lysophosphatidylcholine (LPC) **1** to the bioactive phospholipid lysophosphatidic acid (LPA) **3** with the release of choline **2** (Scheme 2).³⁰



Scheme 2: ATX mediated hydrolysis of LPC (**1**) to LPA (**3**) with the release of choline (**2**).

1.2.3.2 Hydrolysis Process

As mentioned above, the biologically active phospholipid LPA can be synthesised by the hydrolysis of LPC by ATX. The enzyme itself is structurally designed for this process by the presence of a hydrophobic pocket which accommodates the acyl chain of the LPC molecule and allows for substrate discrimination. Once the LPC molecule is introduced to the active site it will subsequently be hydrolysed to the active LPA substrate, it is then believed that the channel present between the catalytic site and the somatomedin 1 (SMB1) domain binds the LPA and transports

the newly synthesised LPA molecule to the G-protein coupled receptors (GPCRs)³¹ (Figure 4).

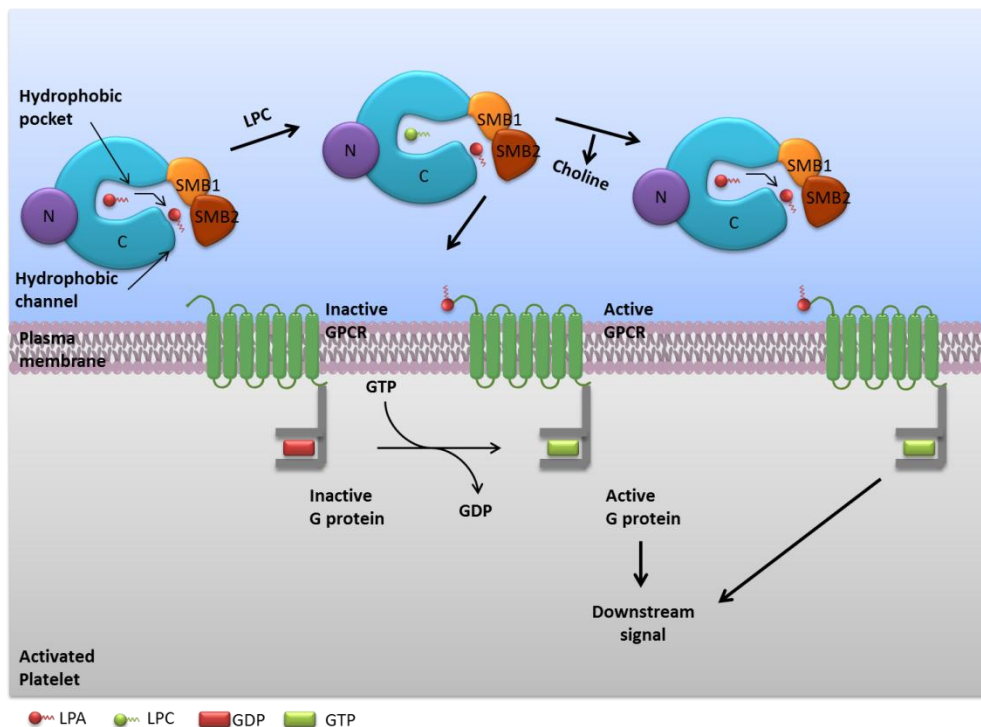


Figure 4: Simplified representation of the four main components of the ATX enzyme; N is the nuclease-like domain; C is the catalytic domain containing the hydrophobic pocket; and SMB1 and SMB2 are the two somatomedin B domains. LPC is introduced into the catalytic site where it is subsequently hydrolysed to LPA and transported to the GPCR, resulting in their activation.

Once generated, LPA can promote a range of physiological events which include cell proliferation, survival, and motility, amongst others, by acting through a set of six GPCRs known as LPA₁₋₆.^{20,32,33} The LPA receptor family can be further divided into two categories: (i) the EDG sub-family consisting of LPA₁₋₃ and (ii) LPA₄₋₆, which contain less than 40% homology to LPA₁₋₃.^{34,35} Each receptor couples to specific G_α proteins (G_s, G_i, G_q, and G_{12/13}), as illustrated in Figure 5, which will in turn initiate a range of cellular signalling cascades.²⁰ Some of the main pathways include: the activation of phospholipase C (PLC) leading to the hydrolysis of phosphatidylinositol-bisphosphate (PIP₂), which will, in turn, initiate calcium mobilisation and protein kinase C (PKC) activation; activation of the Ras, MERK, ERK pathway leading to cell proliferation; activation of the P13K-AKT survival

pathway responsible for the suppression of apoptosis; and, lastly, activation of the Rho pathway which leads to cytoskeletal remodelling, shape change, and cell migration.³⁶

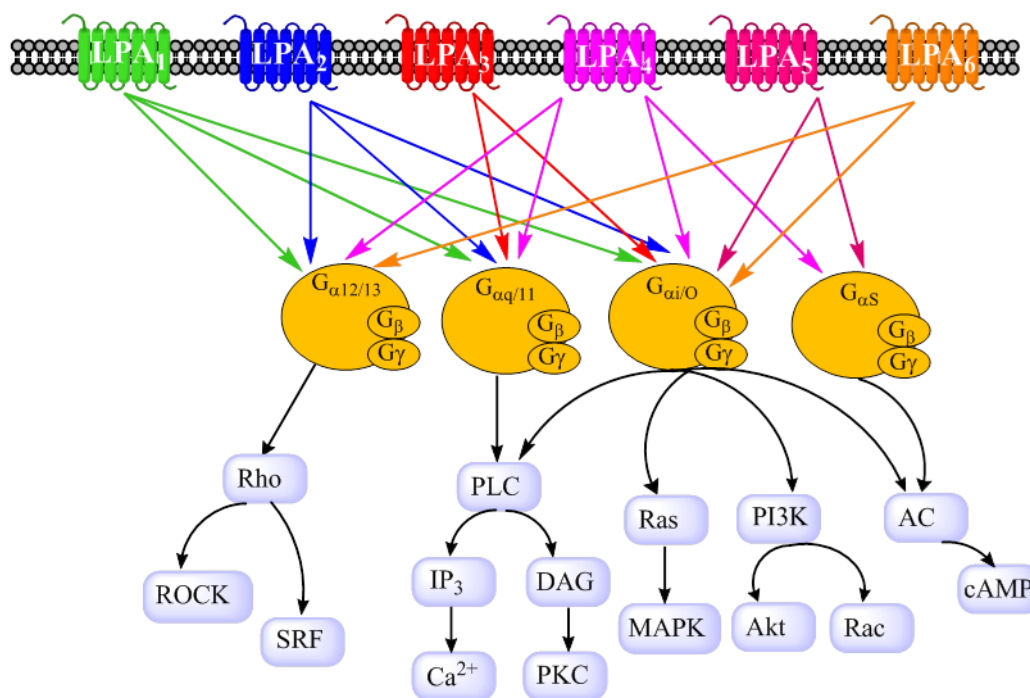


Figure 5: Signalling pathways activated by LPA₁₋₆.

1.3 Structure and Function of the Autotaxin Enzyme

Based on its perceived therapeutic potential, a substantial amount of effort has been invested into understanding both the structure and function of this enzyme. Currently, it has been established that there are five known variants of ATX referred to as ATX α (ATX m), ATX β (ATX t), ATX γ (PD-1 α), ATX δ , and ATX ϵ , all of which are catalytically active.^{20,25,37}

In 2008, the cloning and tissue distribution of the three main isoforms (α , β , and γ) using both human and mouse tissue was undertaken in order to characterise and develop an understanding of their functions, a summary of which is presented in Table 1.³⁸

Table 1: Splice variant of ATX.

Splice Variant	Isoform	Location	Comment
ATX α (ATXm)	Minor	Low quantities present in the central and peripheral nervous system. ³⁸	Original isoform isolated from melanoma cells.
ATX β (ATXt)	Major	Predominately in the brain and peripheral tissue. ³⁸ Small quantities present in central nervous system. ³⁸	Originally cloned from teratocarcinoma cells and found to be identical to lysoPLD. ²⁰
ATX γ (PD-1 α)	Minor	Central nervous system. ³⁸	Similar structure to ATX β and their biochemical functions are indistinguishable. ²⁰

Following the characterisation of the different isoforms of ATX, its crystal structure was resolved in 2011 by Nishimasu and Hausmann, of rat and mouse ATX respectively, and were found to share 93% similarity to the human ATX enzyme.^{39–41} The enzyme was found to consist of three main domains; the *N*-terminal, of which there are two SMB-like domains, known as SMB1 and SMB2; a catalytic phosphodiesterase domain (PDE), situated in the centre; and, the *C*-terminal nuclease-like domain (NUC). In addition to these there are two linker portions referred to as the L1 linker, which connects the SMB2 domain to the catalytic domain, and the L2 linker (or the lasso loop) connecting the catalytic domain to the nuclease-like domain, as illustrated in Figure 6.^{40,42}

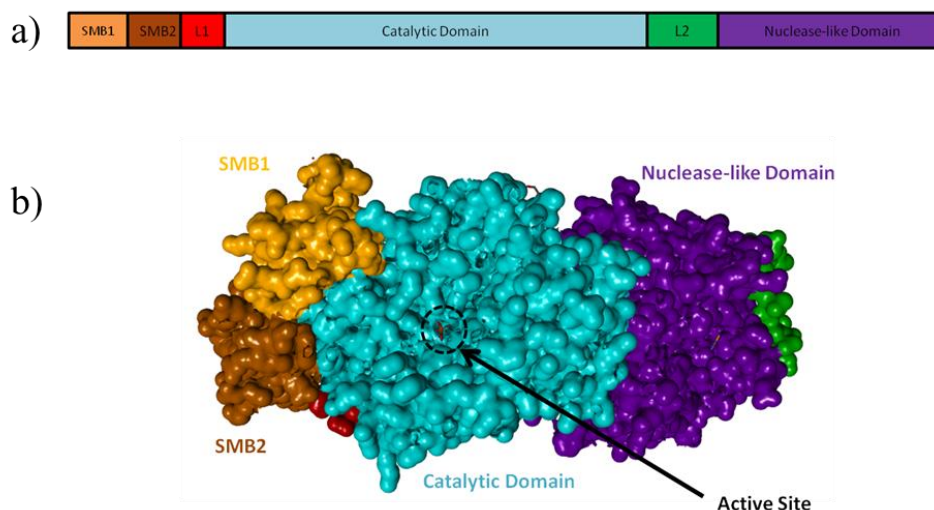


Figure 6: a) Schematic representative diagram of ATX domains (PDB 2XR9). (b) 3D structure of ATX representing the four main domains, SMB1 in orange, SMB2 in brown, catalytic domain in cyan, nuclease like domain in purple, L1 in red, and L2 in green.

The modular domain arrangement of ATX is such that the two SMB domains and the nuclease-like domain encapsulate the catalytic domain, with the two linkers (L1 and L2) reinforcing the structure and maintaining its active conformation.^{20,40} Further structural characteristics which underpin the association between the PDE and the NUC domains include the presence of an interdomain disulfide bond between Cys413-Cys801, the Asn524-linked glycan, as well as the presence of a number of hydrophobic and hydrophilic interactions.⁴⁰ In addition to these there are a number of well-ordered water molecules situated between the catalytic and nuclease-like domain, which results in an extensive hydrogen-bonding network, ensuring a further degree of thermodynamic stability.⁴⁰

The two SMB domains form a cysteine knot fold,⁴⁰ which consists of four pairs of crossed disulfide bonds. These domains are structurally similar to the SMB domains present in the integrin ligand vitronectin, which is an extracellular matrix protein that interacts with plasminogen activator inhibitor-1 (PAI-1) and urokinase-type plasminogen activator (uPAR).⁴⁰ It has also been shown that these domains are important for binding of newly generated LPA to ATX, and are also speculated to be involved in the subsequent release of LPA.³⁹

The catalytic domain itself can be broken down into two main parts known as the core and the insertion sub-domains. The core adopts an alkaline phosphatase fold

and coordinates to the two essential Zn^{2+} ions *via* conserved aspartic acid and histidine residues, Figure 7.^{20,40} In 2003, Gijbsers reported that the presence of the threonine (Thr209) residue, located within the phosphodiesterase domain, along with two Zn^{2+} ions were responsible for the hydrolytic activity of the enzyme (Figure 7).^{40,42,43} These structural features are conserved among the ENPP family, which is further exemplified by the similarity in the catalytic domain to that of *Xanthomonas axonopodis* (XaNPP), a bacterial NPP enzyme.

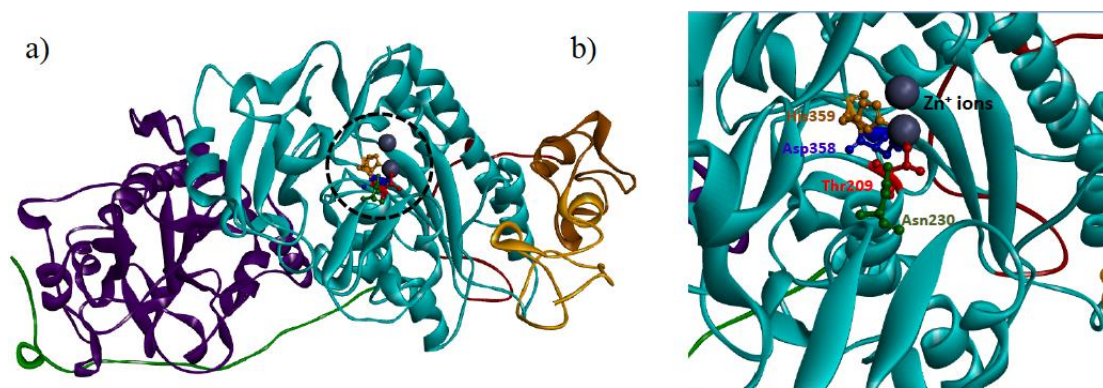


Figure 7: a) Representation of ATX with the catalytic site highlighted (PDB 2XRN). b) Enlarged image of the catalytic site illustrating the Zn^{2+} ions, and the essential residues: Thr209 (red) and the catalytic triad made up of His359 (orange), Asp358 (blue), and Asn230 (green).

Lastly, the C-terminal nuclease-like domain contains a mixed α/β fold and binds to Ca^{2+} , Na^{+} , and K^{+} . These ions are coordinated by residues present in this domain, and are bound close to the interface of the catalytic and the nuclease-like domains, implying an important role in the interaction of the two domains.⁴⁰

An interesting structural feature of the enzyme is the presence of a hydrophobic channel connecting the large binding pocket (containing an estimated volume of 800 \AA^3 and around 15 \AA deep),³¹ situated within the catalytic domain of the enzyme (Figure 8a), through a T-shaped junction⁴⁴ (as illustrated in Figure 8b). This can accommodate monoacyl phospholipids such as LPA and LPC. The function of this hydrophobic tunnel remains under discussion as it could play two potential roles: the first to release newly generated LPA to the cellular microenvironment allowing activation of the cognate GPCRs. Conversely, the tunnel entrance may promote

LPC uptake or act as an entrance and exit tunnel,⁴⁴ additional experimental analysis is required in order to validate either of these hypotheses.

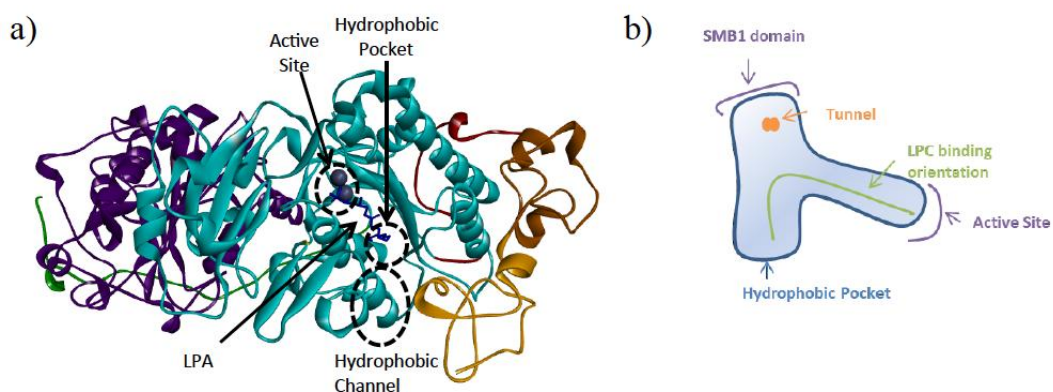


Figure 8: (a) Representation of the ATX active site, hydrophobic pocket, and tunnel with LPA (PDB 3NKN). (b) A representation of the T-shaped structure.

Nishimasu and co-workers conducted further structural analysis of the hydrophobic pocket and have disclosed crystal structures of mouse ATX complexed with LPA molecules of varying chain length (14:0, 16:0, 18:1, 18:3, and 22:6 where the first number is representative of the chain length and the second the degree of saturation).⁴⁵ The data generated indicated that the phosphate group, glycerol portion, and the acyl-chain of the various forms of LPA are all recognised in a similar way by the enzyme where one of the oxygen atoms from the phosphate group binds to one of the Zn^{2+} ions while another forms hydrogen bonds to the side chain of Asn230 and the OH and NH of the Thr209. This is exemplified in Figure 9, which shows LPA 14:0 (**4**) bound within the active site of ATX.

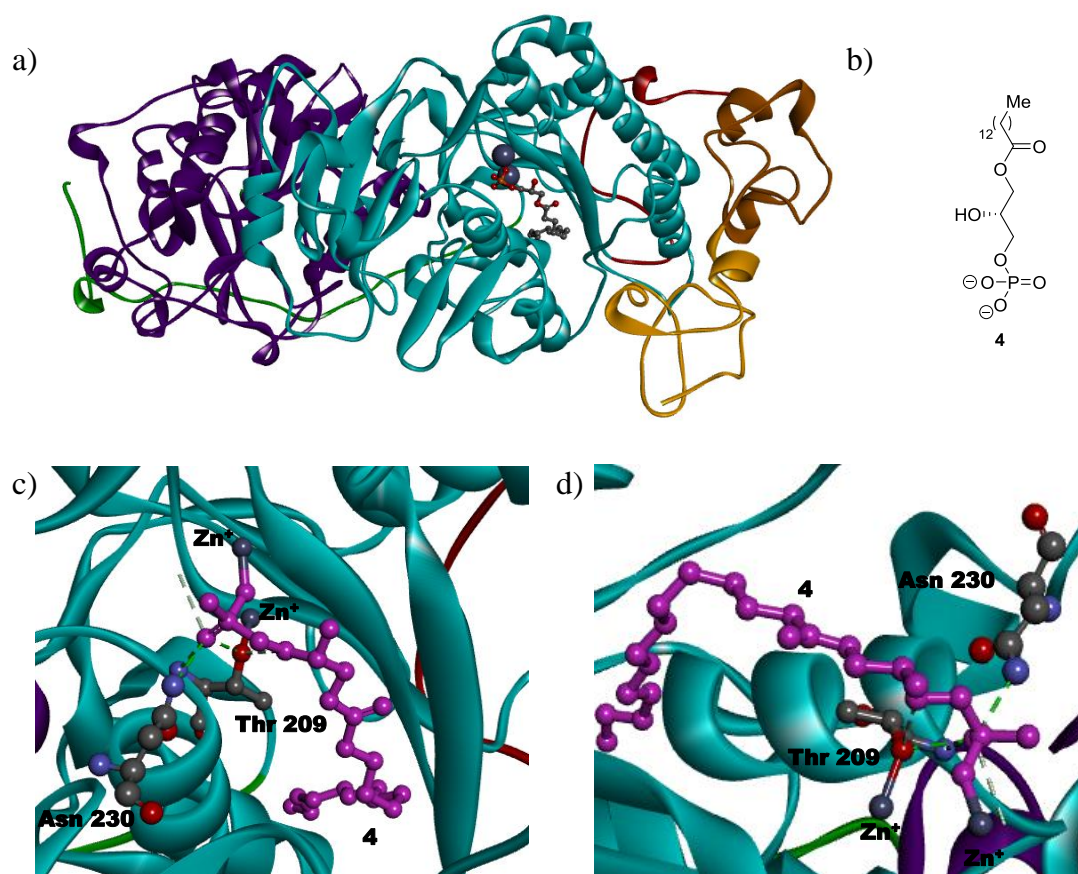


Figure 9: Structure of LPA (14:0) (**4**) complexed within the active site of ATX (PDB 3NKN). a) Ribbon representation of ATX, coloured as follows: SMB1 domain in orange, SMB2 domain in brown, catalytic domain in cyan, nuclease-like domain in purple, L1 in red, L2 in green, Zn²⁺ in grey, and **4** in pink. b) Structure of **4**. c) and d) Enlargement of the catalytic site indicating the interactions between the phosphate group with the Thr209 residue and one of the Zn²⁺ ions.

A notable feature of the binding pocket, which differs from other phospholipases, is that no protein plasticity is observed regardless of whether the enzyme is in either a bound state (*i.e.*, with orthosteric ligand) or an unbound state.⁴⁴

In addition to the LPA co-crystal structure data with murine ATX, Hausman and co-workers disclosed the crystal structure of the apo form of rat ATX, as well as a co-crystal structure of a potent inhibitor HA155 (**5**, Figure 10b).⁴⁶ Based on this analysis, it was possible to correlate inhibition with the observed binding mode.^{39,46}

From this crystal structure data it was possible to establish key interactions between the enzyme and the boronic acid-derived inhibitor **5** (Figure 10). The data generated

illustrated that the boronic acid forms a reversible covalent bond with the nucleophilic hydroxyl group of the Thr209 residue, while one of the hydroxyl groups can be effectively stabilised between the two Zn^{2+} ions present in the pocket. The hydrophobic ring of the inhibitor forms a network of van der Waals interactions. The fluorobenzene moiety points directly into the hydrophobic pocket and is orientated perpendicular to the protein surface. Therefore, this data implies that the presence of an acidic warhead to coordinate to one of the Zn^{2+} ions, the presence of a moiety which can interact with the Thr209 residue, and a lipophilic tail which can be accommodated within the hydrophobic pocket are all beneficial properties for potential inhibitors. Many of these features are conserved in inhibitors which bind at the catalytic site (*vide infra*).

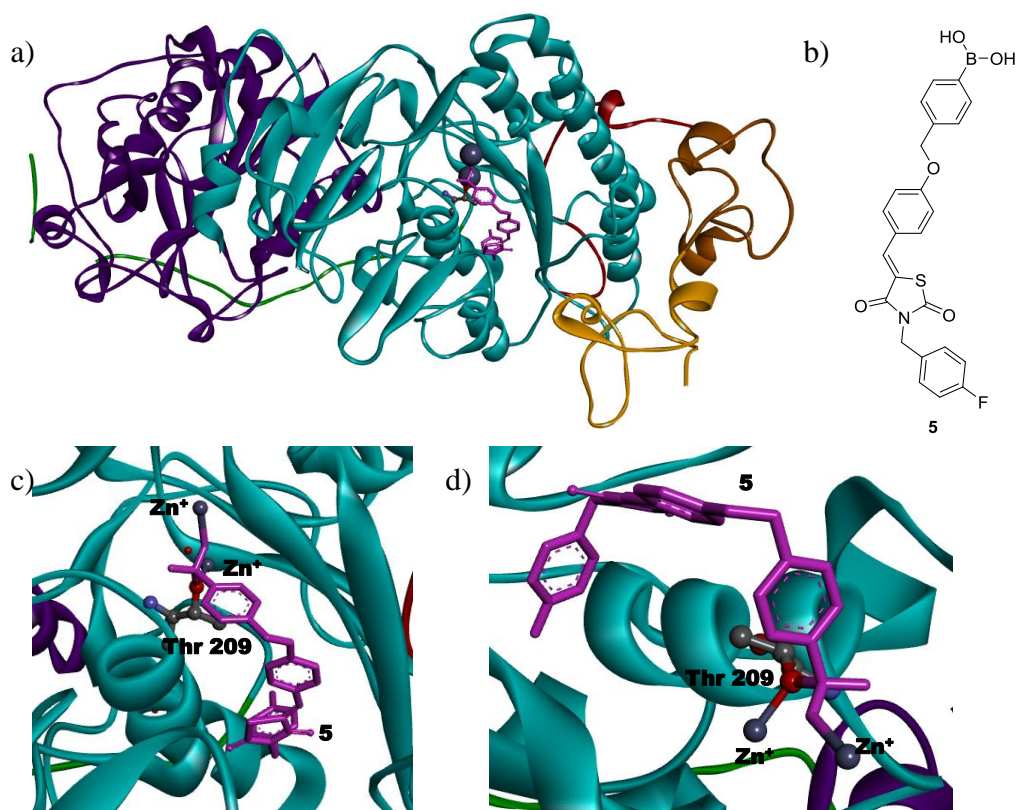


Figure 10: Co-crystal of **5** within the catalytic domain of ATX (PDB 2XRG). a) Ribbon representation of ATX, coloured as follows: SMB1 domain in orange, SMB2 domain in brown, catalytic domain in cyan, nuclease-like domain in purple, L1 in red, L2 in green, Zn^{2+} in grey, and **5** in pink. b) Structure of **5**. c) and d) Enlargement of the catalytic site indicating the interactions between the boronic acid and both the Thr209 residue and one of the Zn^{2+} ions.

As stated previously, it is well established that ATX is responsible for the hydrolysis of phospholipids such as LPC,³⁰ yet this is not its only function as it is also known to hydrolyse other phospholipid species. For example, sphingosylphosphorylcholine (SPC) **6** is converted into sphingosine 1-phosphate (S1P) **7** by ATX (Scheme 3).⁴⁷ S1P is a bioactive lipid displaying similar signalling properties to LPA (as well a range of other signalling consequences via other receptor families);^{25,48,49} however, it should be noted that this is not the main route for S1P synthesis – the primary source is believed to originate predominately from phosphorylation of sphingosine by sphingosine kinases.^{25,50}



Scheme 3: Hydrolysis of SPC (**6**) to S1P (**7**) catalysed by ATX.

1.4 Assays for the Identification of ATX Inhibition.

The availability of a robust and reliable assay to assess ATX inhibition is of great importance in the development of new inhibitors for this target. Currently, there are a range of different *in vitro* assays which have been developed to determine ATX inhibition. These can be divided into two main categories: those using the natural enzyme substrate (LPC) and those using unnatural substrates, such as bis-(*p*-nitrophenyl) phosphate (bis-*p*NPP). Both of these are discussed below.

1.4.1 Natural Substrate ATX Assays

As ATX hydrolyses LPC to LPA and choline, the monitoring of either species can be used to measure ATX activity. There are a number of methods that can be used to achieve this, including using radiolabelled substrates, liquid chromatography-tandem mass spectrometry (LC-MS), and a choline release method, as illustrated in Table 2.

Table 2: Natural substrate ATX assays.

Assay	Substrate	Analyte	Comments
Radiolabelling ^{29,44}	¹⁴ C-LPC	¹⁴ C-LPA	<p><i>Source of Enzyme:</i> Recombinant ATX.</p> <p><i>Analysis:</i> Autoradiography.⁴⁸</p> <p><i>Comments:</i> Most direct method.</p> <p>Robust and sensitive assay.</p> <p>Less suitable for high-throughput screening.²⁵</p>
LC-MS/MS ³⁷	LPC	LPA	<p><i>Source of Enzyme:</i> Recombinant ATX.</p> <p><i>Analysis:</i> LC-MS detection of LPA.</p> <p><i>Comments:</i> Very sensitive.</p> <p>Can be used to detect naturally occurring LPA in biological fluids.²⁵</p> <p>High-throughput screening possible.</p>
Amplex Red Choline release	LPC	Choline	<p><i>Source of Enzyme:</i> Recombinant ATX.</p> <p><i>Analysis:</i> Absorbance at 405 nm of colouring reagent.</p> <p><i>Comments:</i> Routinely used.</p> <p>High-throughput screening possible.</p> <p>Assay interference possible.</p>

Of the assays described in Table 2, the choline release assay is the most popular; however, caution must be taken when using this protocol as there is the potential for small molecules to react with the colouring agent or hydrogen peroxide (generated in the reaction), or inhibit the associated enzymes (horseradish peroxidase (HRP) or choline oxidase) leading to false positives.⁵² This can be circumvented by incubation of the test compound with choline followed by addition of the colouring agent. This has been shown to be an effective way of assessing whether interference has been/will be an issue.²⁵

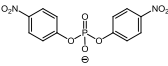
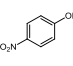
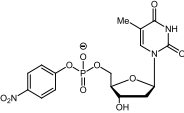
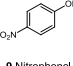
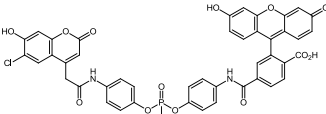
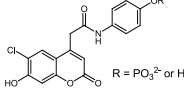
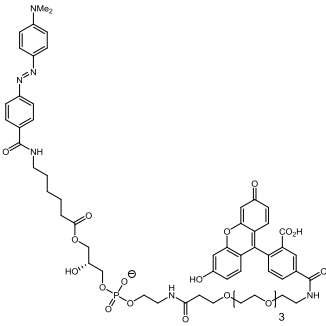
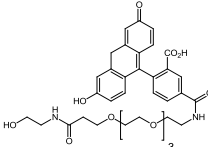
1.4.2 Unnatural Substrate ATX Assays

An alternative means to test for ATX inhibition is through the use of unnatural substrates, which include bis-*p*NPP **8**,^{48,53} thymidine 5'-mono-phosphate *p*-nitrophenyl ester (*p*NP-TMP) **10**,²⁸ CPF4 **11**,^{48,54} and FS-3 **13**,⁵⁵ with *p*NP-TMP and bis-*p*NPP being the simplest methods to measure lysoPLD activity (Table 3).

One of the main disadvantages of using synthetic unnatural substrates in place of the natural substrate is the potential lack of specificity for ATX over other phosphatases. These substrates can be readily hydrolysed by other members of the ENPP family, as well as by other less specific phosphodiesterase enzymes. Therefore, it is recommended that these assays should only be used with purified enzyme to ensure accuracy and correct interpretation of the data generated.⁵⁶

Of the assays described, using either natural and unnatural substrates, the two most commonly used methods to measure ATX activity are the lysoPLD assay using the natural substrate LPC and the unnatural substrate bis-*p*NPP. There has been, however, some debate regarding the reliability of these assays. For example, problems have been encountered when using the endogenous substrate LPC due to the presence of choline or the colouring reagents present in the assay, which as discussed above, can react with test compounds generating false positives.⁵⁷ An additional problem has been found when using unnatural substrates, such as *p*NP-TMP, as these interact differently in terms of enzyme binding compared to the natural LPC substrate.

Table 3: Unnatural substrate ATX assays.

Substrate	Analyte	Comments
 <p data-bbox="472 607 528 618">8 bis-pNPP</p>	 <p data-bbox="767 595 823 607">9 Nitrophenol</p>	<p data-bbox="927 398 1318 427"><i>Analysis:</i> Absorbance at 405 nm.</p> <p data-bbox="927 472 1375 591"><i>Comments:</i> Routinely used. Facile, high throughput capability, and commercially available.</p> <p data-bbox="927 636 1375 757">Caution when using: compound binding remote from the catalytic site will give false negative.⁴¹</p>
 <p data-bbox="480 976 536 987">10 pNP-TMP</p>	 <p data-bbox="767 943 823 954">9 Nitrophenol</p>	<p data-bbox="927 824 1318 853"><i>Analysis:</i> Absorbance at 405 nm.</p> <p data-bbox="927 898 1375 1025"><i>Comments:</i> Caution when using: compound binding remote from the catalytic site will give false negative.⁵⁸</p>
 <p data-bbox="480 1245 536 1256">11 CPF4</p>	 <p data-bbox="775 1279 791 1290">12</p> <p data-bbox="815 1245 887 1256">R = PO₃²⁻ or H</p>	<p data-bbox="927 1093 1375 1211"><i>Analysis:</i> Fluorescence assay (excitation at 355 nm, emission at 460 and 520 nm).</p> <p data-bbox="927 1256 1375 1384"><i>Comments:</i> Use with serum free conditioned culture medium isolated from cells expressing the enzyme.</p>
 <p data-bbox="472 1783 488 1794">13</p>	 <p data-bbox="799 1671 815 1682">14</p>	<p data-bbox="927 1458 1375 1536"><i>Analysis:</i> Fluorescence (excitation at 485 nm and emission at 528 nm).</p> <p data-bbox="927 1581 1375 1794"><i>Comments:</i> Caution when using: compounds may exhibit autofluorescence (false positive) or fluorescence quenching (false positive).^{41,57}</p>

This hypothesis has been validated in molecular modelling studies by Fells *et al*,⁵² and Hoeglund *et al*,⁵⁹ which indicated that compounds binding in the hydrophobic pocket of the enzyme may not be correctly identified as inhibitors due to a competitive binding mode in a space distinct from the hydrophobic tunnel of the enzyme. This, however, is not the case for the FS-3 assay, as the long lipophilic portion of the structure is accommodated within the hydrophobic pocket, and as such may prove to be a more accurate method for identifying inhibitors which bind at a proximal site.^{52,58} Having stated this, while the FS-3 substrate binds in the hydrophobic pocket, it is remote from the hydrophobic channel and, as such, any compounds which bind in this position will be unable to hydrolyse the FS-3 substrate and may lead to a false negative.⁴¹

In essence, from the data generated regarding the different ATX assays it seems it may be prudent to evaluate test compounds using a range of assays in order to confirm any activity as ATX inhibitors instead of relying on one assay in isolation.

1.5 Inhibitors

A substantial amount of research has been conducted into the development of novel pharmaceutical targets for the treatment of both IPF and cancer. There are two main routes which have been employed for the development of novel inhibitors to target these diseases which are: i) targeting the LPA receptor; and ii) inhibition of the enzyme ATX.

1.5.1 LPA₁ and LPA₃ Antagonists

The first of these categories involves the development of LPA receptor antagonists. As indicated previously, there are six LPA receptors (LPA₁₋₆) which are responsible for different biological processes, therefore selective inhibition of these receptors could lead to the development of novel therapeutic molecules. Of these six it has been established that the LPA₁ receptor has been linked to IPF, as *in vivo* studies conducted on mice illustrated that subjects which lacked this particular receptor were significantly protected from fibrosis.⁶⁰

The identification of this link between IPF and LPA resulted in the development of several LPA receptor antagonists being reported in the literature, with the main compounds being developed by Kirin Brewery,⁶¹ Amira Pharmaceuticals,⁶² and

Hoffmann La-Roche³³ (Figure 11). The first of these antagonists was developed by Kirin Brewery (Ki1645) **15**. This was developed after screening 150,000 low molecular weight fragments for LPA antagonism, and was found to be effective against both the LPA₁ and LPA₃ receptors with K_i values of 0.25 and 0.36 μM respectively.⁶¹ Following on from this, Amira pharmaceuticals developed AM095 **16**, a potent and selective LPA₁ antagonist possessing a similar chemotype to **15**.⁶³ Lastly, Hoffman La-Roche developed compound **17**, building on the previously published work by Amira Pharmaceuticals and Kirin Brewery, and conducted a bioisosteric approach. From this it was found that the pyrazole and triazole containing compounds exhibited LPA₁ and dual LPA_{1/3} antagonist behaviour, which in turn led to the development of the LPA₁ selective antagonist **17**.³³

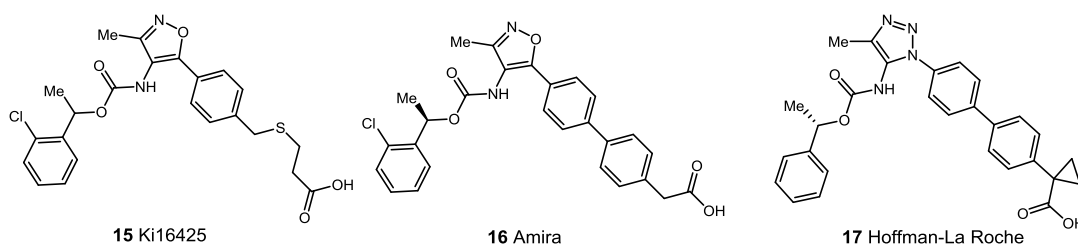


Figure 11: Potential antagonists of LPA₁ and LPA₃.

One aspect to note of these three structures is their similarity; each contains a heterocyclic core functionalised with a benzyl carbamate on one side, and an acid moiety on the other. This, as well as the structural activity relationship (SAR) described by Hoffman-La Roche, indicate that both the heterocyclic core and the acidic moiety are important for biological activity. However, the absence of a crystal structure of the receptor means that detailed elaboration of the binding cannot be determined.

Although these compounds may prove to be active against LPA using *in vitro* assays, targeting the inhibition of LPA *in vivo* is complex due to the large concentrations of LPA already present within the body. In addition to this, as stated previously, due to the uncertainties regarding which LPA receptors are responsible for driving the action of LPA it is believed that the development of ATX inhibitors could avoid this issue. In view of this, a large volume of data has been generated within the literature regarding the development of novel ATX inhibitors, perhaps two

of the most interesting compounds reported are **18** by Amira Pharmaceuticals and PF-8380 by Pfizer (**19**), Figure 12.

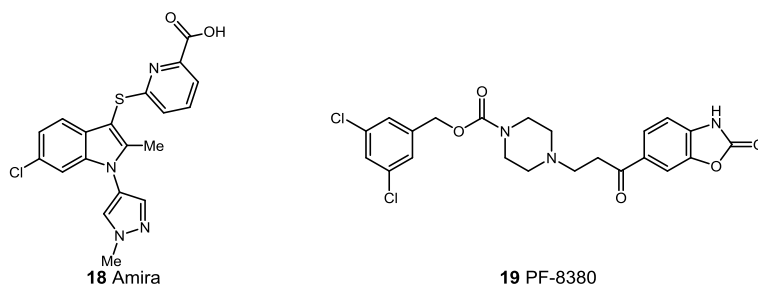


Figure 12: Illustrative examples of patented ATX inhibitors.

PF-8380 (**19**), is one of most extensively studied ATX inhibitors (followed by HA155 **5**) as well as being used as a tool compound for elucidating the role of LPA in inflammations.⁶⁴ **19** was originally patented by Merck KGA in 2010,⁶⁵ however, no biological data was disclosed. Following this, it was reported by Pfizer researchers and found to have an IC_{50} of 2.8 nM (human enzyme FS-3 assay).⁶⁴ In terms of binding to the ATX active site, it is believed that the benzoxazolone makes an essential interaction with one of the Zn^{2+} ions and the long lipophilic portion resides in a channel adjacent to the catalytic site (Figure 13).

A range of pharmacokinetic and pharmacodynamic studies have also been conducted.⁶⁴ The pharmacokinetic profile of **19** was generated using both intravenous doses of 1 mg/kg and oral doses of 1 to 11 mg/kg over a 24 h period, and was found to have a mean clearance of 31 mL/min/kg and an effective $t_{1/2}$ of 1.2 h. In addition to this, **19** exhibits good oral bioavailability with values ranging from 43-83% depending on the oral dose (ranging from 1 mg/kg to 100 mg/kg).⁶⁴ A pharmacokinetic/pharmacodynamic (PK/PD) relationship was also determined by measuring plasma LPA, where it was found that LPA levels were rapidly reduced following oral dosing implying that LPA present at basal levels in the plasma is rapidly degraded.⁶⁴

Compound **19** was also subjected to an *in vivo* study using the rat air pouch model of inflammation to determine the concentration of LPA both in the plasma and at the site of inflammation. Oral dosing showed the concentration of **19** in the plasma ranged from 0.08 μ M at 3 mg/kg to 2.68 μ M at 100 mg/kg at 4 h, and it was determined that ATX was inhibited up to 95% in both plasma and air pouch at a

dose of 100 mg/kg.⁶⁶ To date, no further work has been reported with **19** and no data is available regarding its progression into clinical trials.

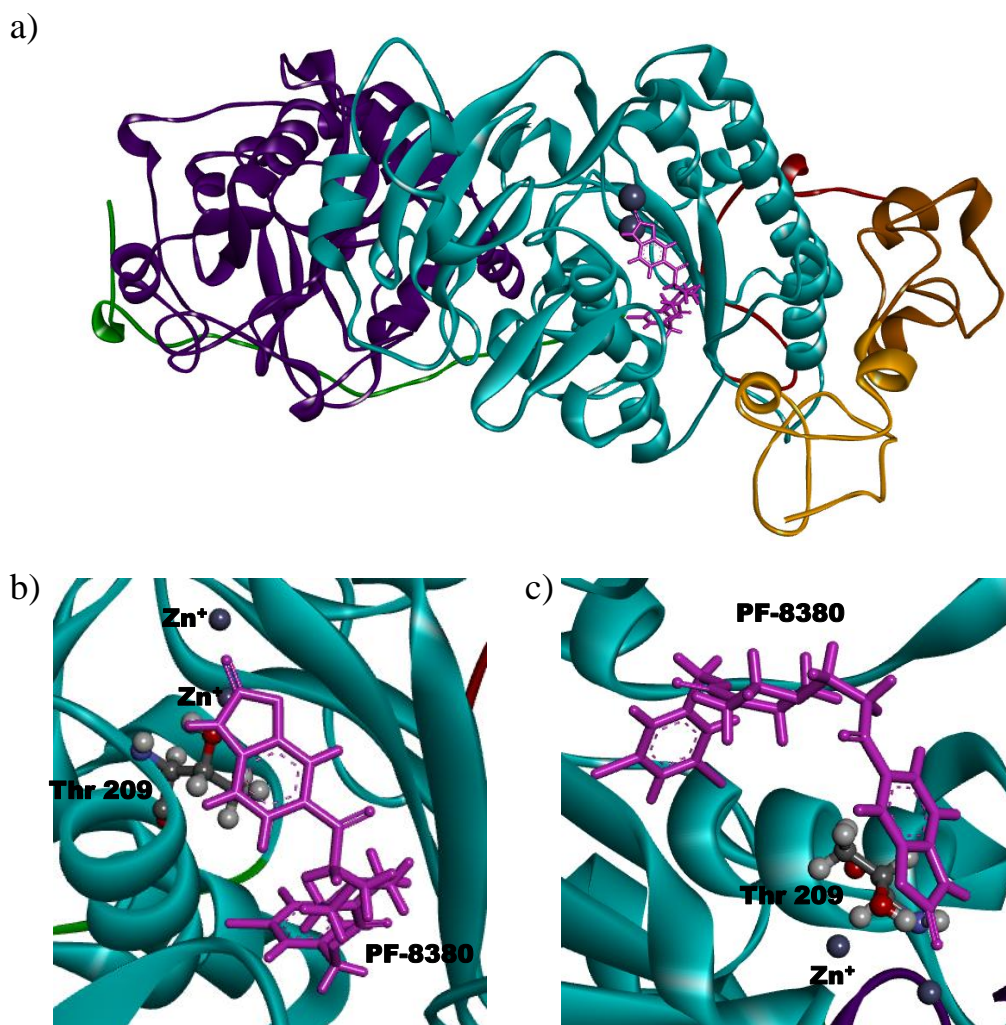


Figure 13: Compound **19** docked within ATX using MOE docking software using PDB 3NKR. a) Ribbon representation of ATX, coloured as follows: SMB1 domain in orange, SMB2 domain in brown, the catalytic domain in cyan, nuclease-like domain in purple, L1 in red, L2 in green, Zn^{2+} in grey, and **19** in pink. b) Illustrating close proximity of the acidic head group (benzoxazolidinone) to one of the Zn^{2+} ions and the Thr209 residue. c) Alternative view of **19** within the active site of the enzyme.

In contrast to PF-8380 (**19**), an alternative and novel non-lipid chemotype was discovered by Amira Pharmaceuticals which involves the removal of the lipophilic tail portion to produce smaller structures such as **18** which was found to have a K_i of $<0.3 \mu M$ (native choline release assay). Up until the beginning of this year, little attention has been focused on this chemotype, and as a result it is only starting to

become clear how this structure may bind within the active site of the enzyme. Recent studies by Stein *et al.*⁴¹ have indicated that the indole chemotype can adopt a range of different binding modes. One example is indicated in Figure 14, where compound **20** was the most similar chemotype to **18**. In this case, it can be seen that **20** does not reside within the active site of the enzyme; instead it occupies a position within the hydrophobic tunnel, this can be further illustrated in Figure 14b and c which shows both LPA (**4**) and **20** co-crystallised within the enzyme.

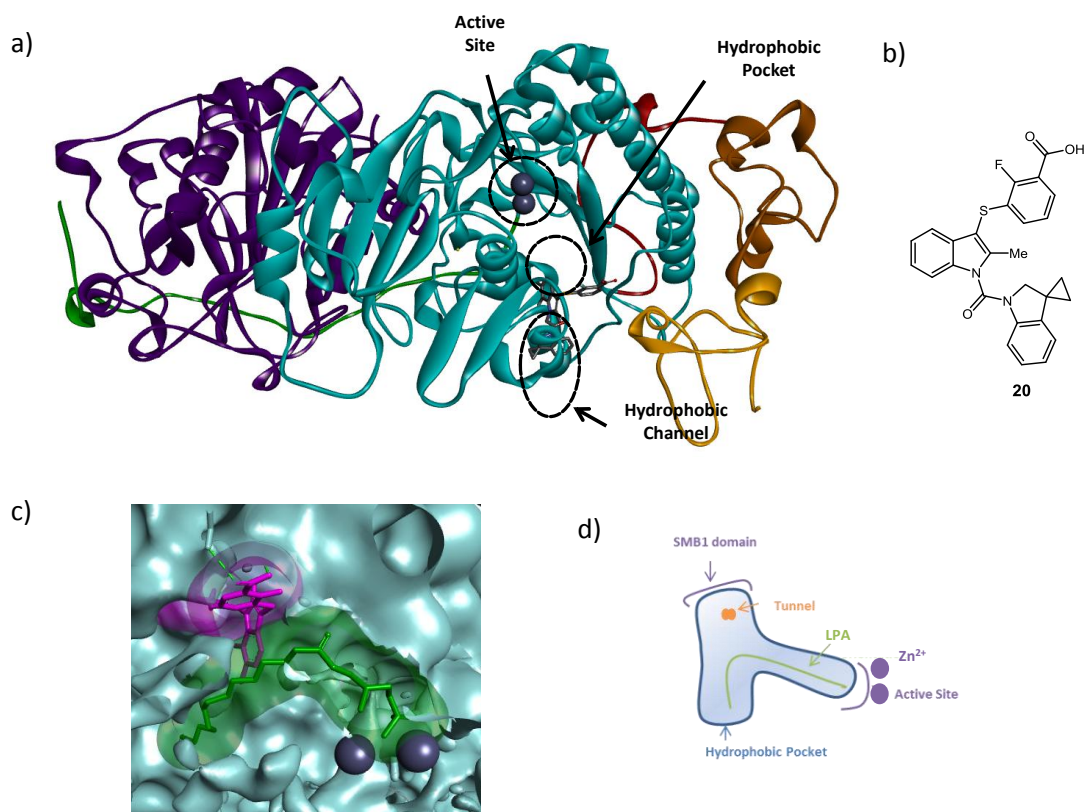


Figure 14: Compound **4** (in green) and **20** (in pink) co-crystallised within ATX (PDB 4ZG7). a) Ribbon representation of ATX, coloured as follows: SMB1 domain in orange, SMB2 domain in brown, the catalytic domain in cyan, nuclease-like domain in purple, L1 in red, L2 in green, and Zn²⁺ in grey. b) Structure of **20**. c) Enlarged image of the active site illustrating the space occupied by **4** (in green) and **20** (in pink). d) Simplified representation of the active site.

A substantial amount of research has been conducted into the design and synthesis of novel compounds with increased potency towards ATX inhibition, where over the last decade an increasing number of publications have been released as exemplified in Figure 15.

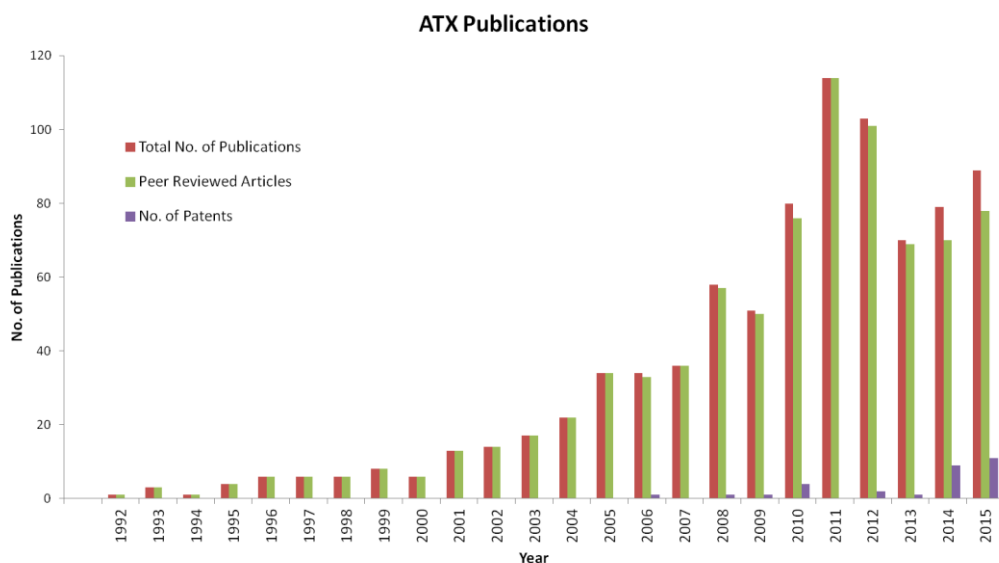


Figure 15: ATX-related publications since 1992. Data collected from SciFinder and Espacenet.⁶⁷

An increasing number of patents have been published in the past decade which focuses on the development of novel ATX inhibitors, these can be generally divided into four main categories; lipid-like, Pfizer-like, Amira-like, and other, where an exemplar of each is illustrated in Figure 16.

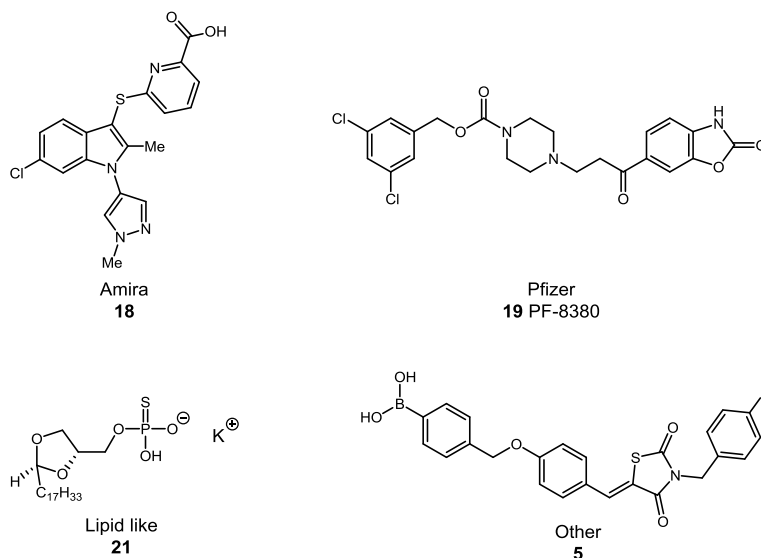
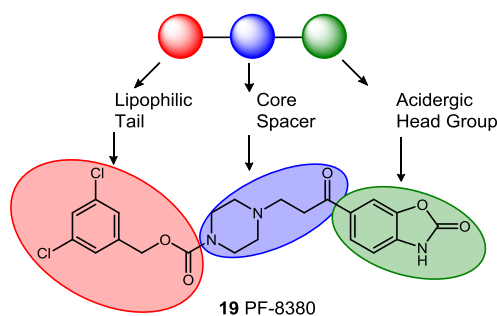


Figure 16: Illustrative examples of the four generally chemotype within the patent literature: **18** Amira-like; **19** Pfizer-like; **21** lipid-like; and **5** other.

Some of the first ATX inhibitors were lipid-like structures that mimicked the natural LPC and LPA phospholipids, where compound **21** was one of the first ATX inhibitors developed. An alternative non-lipid chemotype was then developed by Amira^{68,69} and PharmAkea.⁷⁰⁻⁷² This chemotype lacked the long lipophilic portion producing much smaller and more compact structures. Perhaps the most studied category is that associated with the Pfizer-like structure where extensive patent literature is available from Merck KGA,⁶⁵ and Novartis.^{73,74} This chemotype exhibits the general chemotype of lipophilic tail, core spacer, and acidic head group, as exemplified by PF-8380 (**19**) which contains a benzoxazolone as the acidergic head group, a functionalised piperazine as the spacer, and the dichlorocarbamate moiety as the lipophilic portion (Figure 17). Lastly, in terms of other chemotypes these encapsulate a range of compounds which do not conform to any of the three previously described categories.



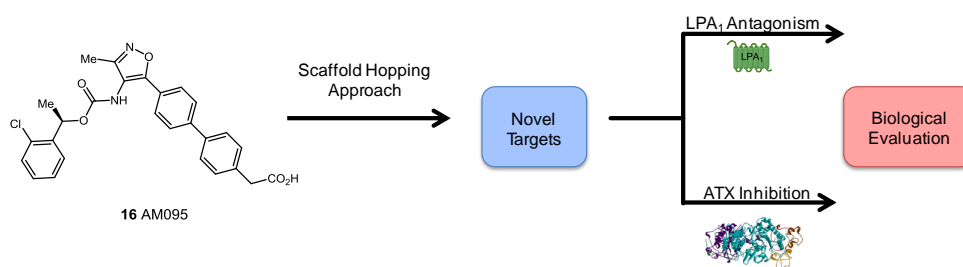
Scheme 4: Regions of **20** highlighted to indicated the lipophilic tail (in red), the core spacer (in blue), and the acidergic head group (in green).

In general, the vast majority of the compounds described within these patents adhere to the Pfizer-like chemotype as shown from the co-crystallographic data of HA155 (**5**) within the ATX enzyme, which involves the presence of a long lipophilic tail, which will be accommodated in the hydrophobic pocket, a core spacer, and an acidic head group, green section, to bind to the Zn^{2+} .

Due to the difference of **18** compared to the standard chemotype, as illustrated by PF-8380 and a large number of the patent data, in addition to the lack of any consistent SAR studies surrounding this motif it was thought to be an interesting topic of study.

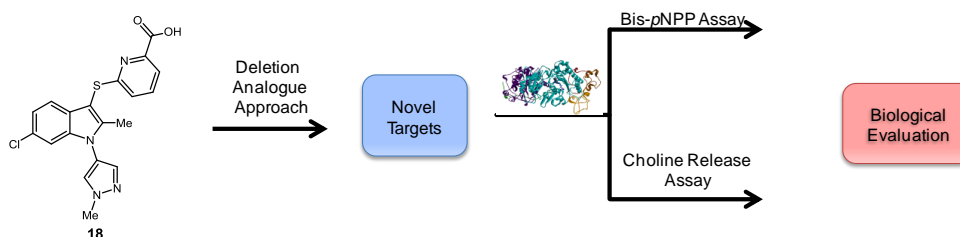
2 Project Overview

The main goal of this research project was to focus on the development of novel inhibitor compounds to target the LPA-ATX signalling pathway. This would be achieved using two main strategies. The first involved the development of compounds to selectively target the LPA₁ receptor, which would be achieved by conducting a scaffold hopping approach from **16**, a known LPA₁ receptor antagonist developed by Amira Pharmaceuticals, as a skeletal backbone and conducting a range of structural modifications to discover novel structures. The developed compound library would then be analysed for both LPA₁ receptors antagonism and ATX inhibition in a view to probe the potential cross-talk of the LPA-ATX signalling pathway (Scheme 5).



Scheme 5: Proposed route for the development of novel ATX-LPA inhibitors from **16**.

The second approach involved targeting the production of LPA by inhibiting the ATX enzyme itself. This was achieved by conducting a detailed SAR study on the known inhibitor **18**, again developed by Amira Pharmaceuticals, which was chosen due to its unique chemotype. The synthesised compound library would then be analysed for ATX inhibition using a dual assay procedure involving analysis with the native LPC assay and the unnatural bis-*p*NPP assay. Doing this would allow for biological evolution of the compounds as well as give information regarding possible binding modes (Scheme 6).



Scheme 6: Proposed route for the development of novel ATX inhibitors from **18**.

Chapter 1

Development of Novel LPA₁ Receptor Antagonists

3 Chapter 1: Development of Novel LPA₁ Receptor Antagonist

3.1 Proposed Work and Aims

The aim of this project was to design and construct new ligands to target the LPA₁ receptor in an effort to identify an effective lead compound that may be developed towards a treatment for IPF in the long term. At the outset of this project, there were two key compounds that had progressed to clinical trials. These were AM095 (**16**) from Amira Pharmaceuticals and Ki16425 (**15**) from Kirin Brewery. Due to the increased selectivity of **16** towards the LPA₁ receptor, this compound was used as the backbone for a scaffold hopping approach (i.e., conducting structural modification on a known active compound in order to discover novel compounds)⁷⁵ towards the development of a novel chemotype for the inhibition of the LPA-ATX pathway.

As LPA binds to both the LPA₁ receptor and ATX, it suggests there may be a level of cross-talk between the types of chemical entity which interact with both targets. As such, it was decided that a dual screening process would be pursued in order to test for both LPA₁ receptor antagonism and ATX inhibition.

To this end, three unique series were designed by performing simple disconnections from AM095 **16** to give the Acyl Aniline series (AA), the Acyl Indole series (AI), and the Hydantoin series (Figure 17) with the latter being pursued by a fellow member of the group.⁷⁶

The main structural alteration proposed was the removal of the isoxazole ring. This was done in an effort to reduce the molecular weight of the target compounds, as well as probing the importance of this polar heterocycle for biological activity.

In each of the three series the main disconnection involved the removal of the isoxazole ring, followed by reconnection in three different ways. The first involves the formation of a new C-N bond between the nitrogen of the side chain and C_a on the aromatic ring (**22**) to give rise to the AA series. The second involved the formation of a new C-N bond in the form of an indole ring (**23**) to give the AI series, and lastly formation of two new bonds, the first being a C-N bond between C_a and the nitrogen, and a second connection between the nitrogen and the oxygen on the side chain (**24**), to give rise to the hydantoin series. In addition to the representative

examples depicted, the regiochemistry of the biaryl and the acetic acid moiety would be probed.

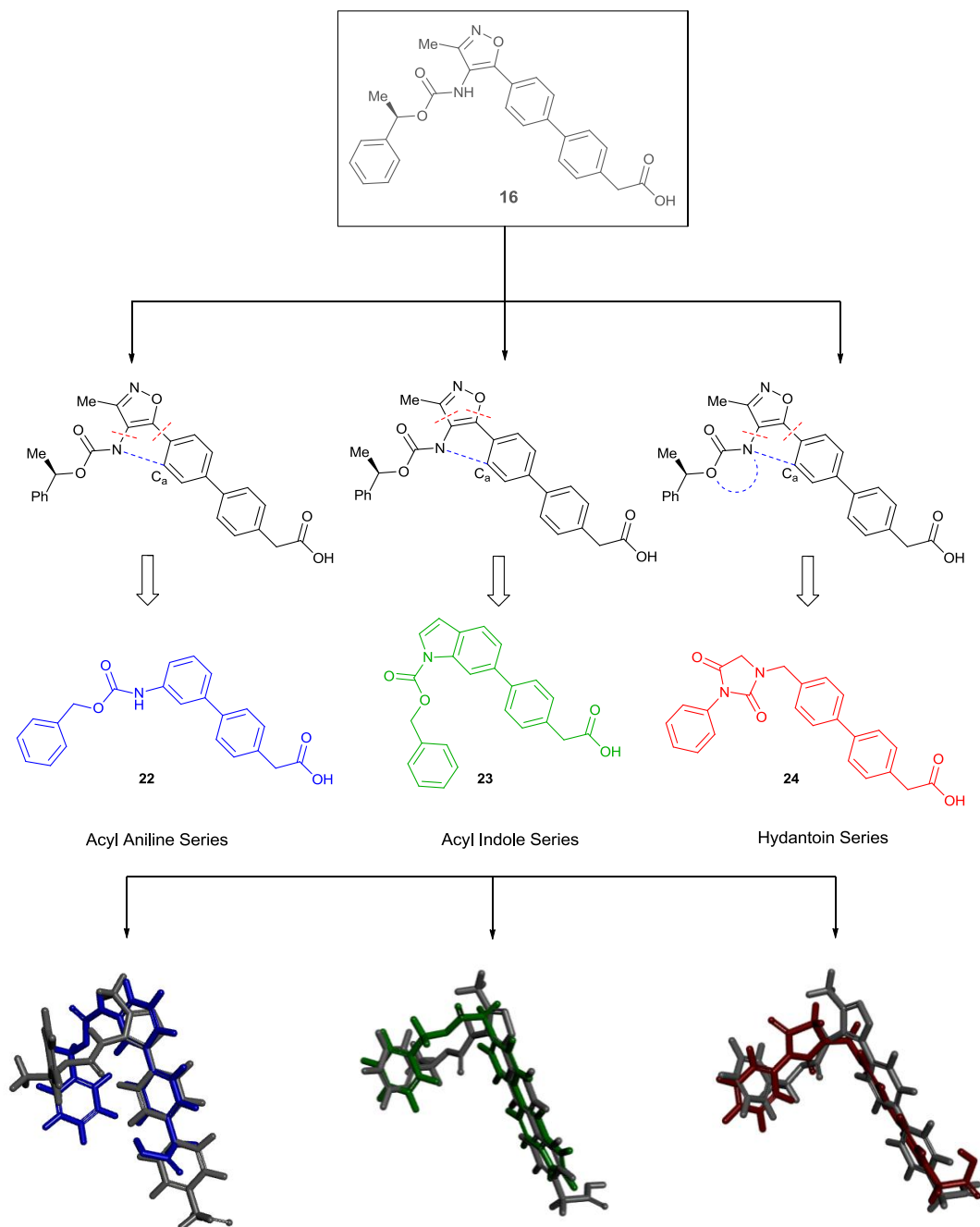


Figure 17: Schematic representation of the three proposed disconnections from the backbone compounds **16**, where the red dotted lines represent bonds to be broken, and blue dotted lines represent bonds to be formed. Followed by the overlaid diagrams of each of the exemplars where **16** is shown in grey.

In order to assess the similarity of the proposed compounds to **16**, a series of overlays were produced using exemplars from each of the three series. These were developed using Gaussian to generate the energy minimised structures, which were then overlaid manually with **16** using Discovery Visualizer. From the data generated it was evident that the proposed structures contained a reasonable degree of overlap with **16** and hence were synthesised in order to validate their biological properties against both LPA₁ receptor antagonism and ATX inhibition.

To summarise, the main aims outlined in this section include: i) conducting a series of deletion analogues utilising **16** as the backbone, resulting in the development of three main series; the acyl aniline, the acyl indole, and the hydantoin series; ii) synthesis of a range of compounds within each series to probe both the regiochemical importance of the acetic acid moiety as well as probing functional group tolerance, and iii) to analyse the compound library produced for both LPA₁ receptor antagonism and ATX inhibition.

3.2 Results and Discussion

3.2.1 Structural Development of Acyl Aniline, Acyl Indole and Hydantoin Series

The three series which were the focus of this study were the acyl aniline (AA), the acyl indole (AI), and the hydantoin series (H), Figure 18, which were designed based on the skeletal backbone of AM095 (**16**) (a known LPA₁ selective antagonist).

The principal structural alteration involved the deletion of the isoxazole functionality from the skeletal backbone of AM095 (**16**) in an attempt to lower the molecular weight and improve developability from a medicinal chemistry point of view compared to the parent compound. At the beginning of this project no structural data surrounding the LPA₁ receptor had been established and so the importance of the isoxazole functionality was unknown. Therefore, in order to gain insight into the biology, the SAR landscape would be probed by preparing a range of regioisomers for the three series. Based on modelling studies (*vide infra*), the most promising connectivity of the biaryl species for the AA series would be *meta*-aniline and *para*-acetic acid, as this gave a promising overlay with the backbone of AM095 (**16**). This also built upon previous SAR studies conducted by Hoffman La-Roche,³³ which indicated the presence of the acetic acid functionality at the 4-position of the biphenyl system was crucial for LPA₁ binding, as well as conferring high selectivity against LPA₃ (>850 fold). As a result, this key pharmacophoric moiety would be retained within the proposed compounds, and its regiochemistry would be probed in order to validate this hypothesis. For the AI series, a similar reasoning suggested that the acetic acid moiety should remain in the *para*-position of the phenyl unit, and the position of the biaryl ring would be preferable in either the 5- or the 6-position of the indole.

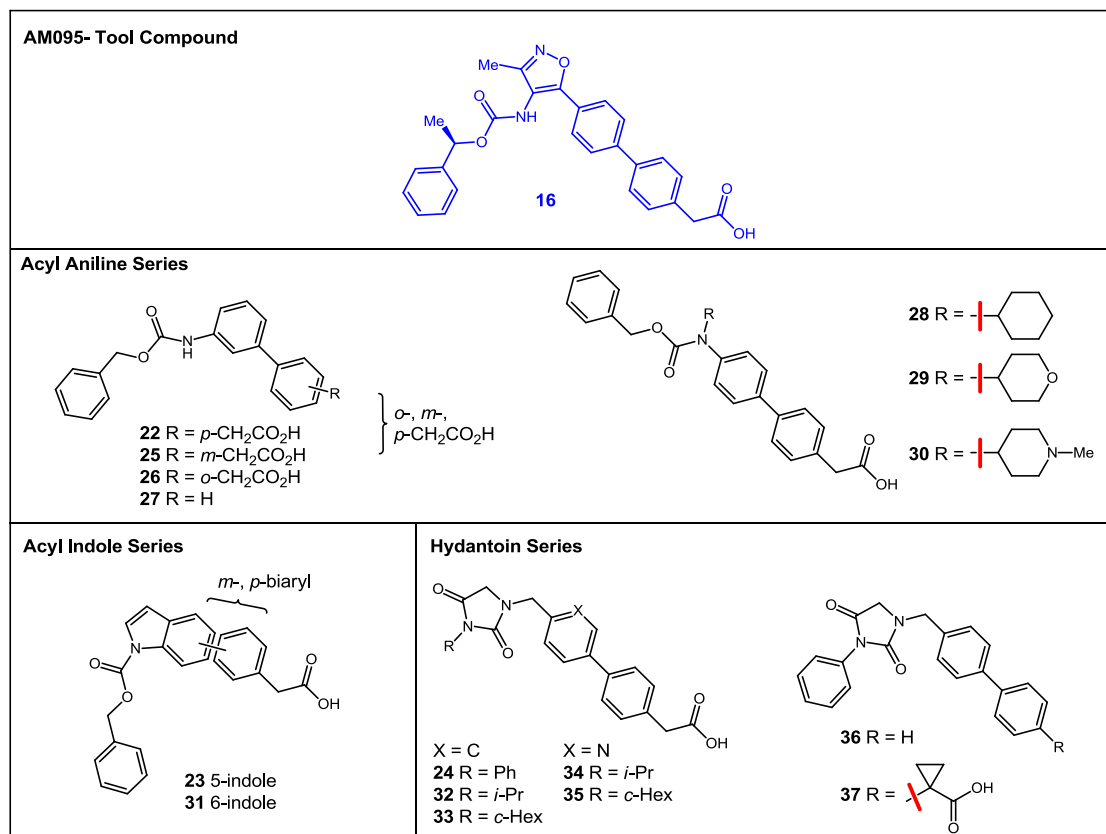


Figure 18: Proposed compounds to be synthesised within the three main series (i) the acyl aniline (AA), (ii) the acyl indole (AI), and (iii) the hydantoin (H).

Lastly, the H series was divided into two sub groups: i) the benzyl series and ii) the pyridyl series. Within both of these series the functionality on the hydantoin would be probed with the introduction of isopropyl (*i*-Pr), cyclohexyl (*c*-Hex), or phenyl (Ph) groups (with the latter only in the benzyl series) in order to ascertain if these isosteres would retain biological activity, but allow for more attractive developability profiles due to the decrease in cLogP and the number of aromatic rings. In terms of the benzyl series, the importance of the acetic acid moiety would be probed as well as the introduction of a cyclopropyl (*c*-Pr) substitution alpha to the carboxylic acid (similar to the work conducted by Hoffman-La Roche, who found that this motif was equipotent in terms of LPA₁ activity to the acetic acid moiety within their SAR study)³³ in order to determine the effect these alterations would have on the biological activity.

Due to the absence of a crystal structure of LPA binding to the receptor site, at the beginning of this study it was difficult to determine how the target structures would

interact. Therefore, in order to attempt to understand if the proposed ligands may prove to be potential ligands for LPA₁, a series of overlays were calculated with AM095 (**16**) to determine if good overlap could be achieved which may relate to similar binding modes and affinity. For the overlay models, one key compound from each series was selected. The data was generated by firstly minimising the energy of the Amira compound AM095 (**16**) and the key compound from each series; this was achieved using MM2 calculation. The key compound from each series was then superimposed onto that of AM095 (**16**) in order to compare the geometry of the structures. It was believed that if the structures had a similar geometry then this may allow for similar binding interactions to AM095 (**16**). The results of these overlays are illustrated in Figure 19-21.

From Figure 19, it was evident that when the key pharmacophoric moieties were aligned for compound **22** (blue structure) and AM095 (grey structure) (**16**), good overlap was displayed with the biaryl ring systems of both structures. The removal of the isoxazole ring from AM095 (**16**) did not appear to have a large impact on the geometry of the ligand, suggesting it may interact in a similar manner. A slight variation is apparent in the conformation of the carbamate side chain, however due to the flexibility in this region it was believed not to be a major concern at this stage.

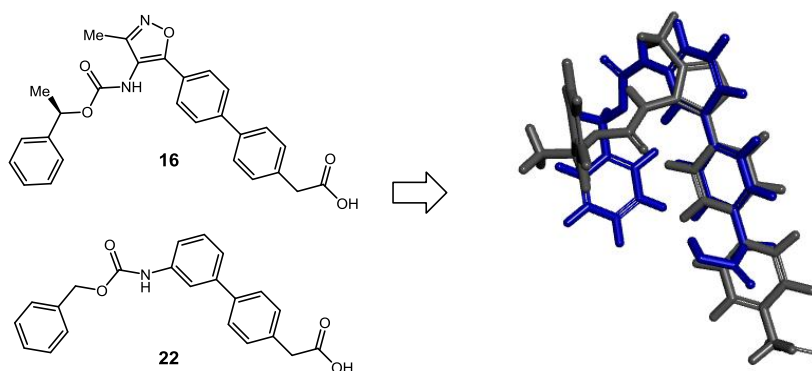


Figure 19: AA overlay alignments where AM095 (**16**) in grey, and AA (**22**) in blue.

A similar overlay was developed for the key ligand from the AI series, compound **23** Figure 20, where there was good alignment between the biaryl system of the target molecule with that of AM095 (**16**). The replacement of the isoxazole with the indole motif allowed for a slight variation in length, however, this was believed not to be a major issue.

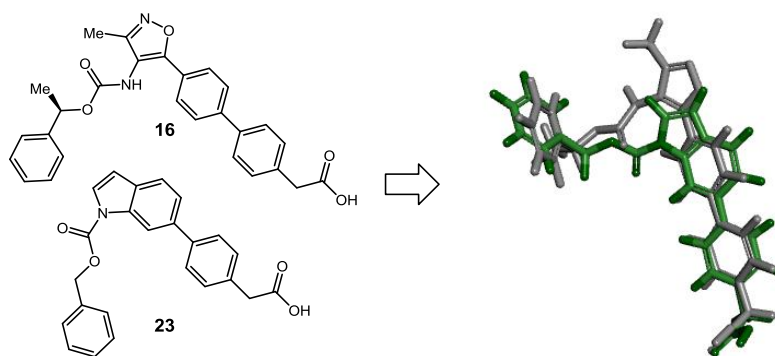


Figure 20: AI overlay diagram where AM095 (**16**) in grey, and AI (**23**) in green.

In terms of the hydantoin series, compound **24** again provided good structural similarity with AM095 (**16**), Figure 21. Where the substituted hydantoin section overlaid well with the carbamate portion of AM095 (**16**) and the biaryl section also contained good correlation to backbone.

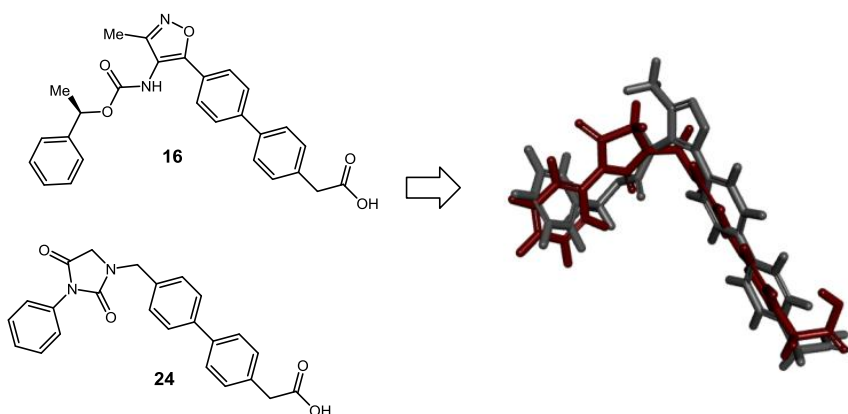
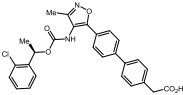
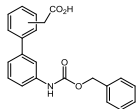
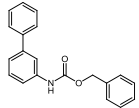
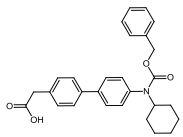
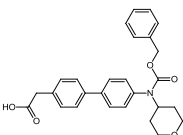
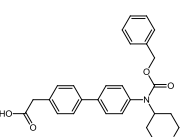
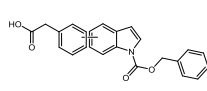


Figure 21: H overlay diagram where AM095 (**16**) in grey and H (**24**) is in red.

3.2.2 Physicochemical Data

In order to obtain as much information as possible on the proposed ligands, physicochemical calculations were conducted to determine if the proposed AA and AI compounds exhibited molecular properties aligned with modern medicinal chemistry concepts, while also allowing for a direct comparison between the proposed ligands and **16**. The calculations were made using JChem software,⁷⁷ and the resulting data is depicted in Table 4.

Table 4: Calculated physicochemical data for AA and AI series.^a

Entry	Cpd. No. ^b	Structure	MW ^c	CLogP	LogD	PSA ^d
1	16		456	5.3	2.7	104
2	22, 25, 26		361	4.8	2.0	78
3	27		303	5.2	5.2	38
4	28		443	6.5	3.7	70
5	29		446	4.6	1.9	79
6	30		459	2.0	2.0	74
7	81, 82		385	5.0	2.3	71

^aColour coded according to correlation with Lipinski⁷⁸ (MW < 500 and log P < 5) and Veber⁷⁹ (PSA < 140 Å): red = outwith guidelines; amber = borderline correlation; green = desirable. Data were obtained using JChem for Excel software.⁷⁷ ^bCompound number, ^cMolecular weight, ^dPolar surface area.

The calculated physicochemical data illustrated that as a whole the two series contained overall improved properties compared with **16**, with the exception of compound **28** (entry 4) which contained somewhat higher than desirable cLogP value which could be problematic further in the developability process; however, this would be considered further following biological evaluation (see Section 4.1). In terms of the remaining data set it was found that pleasingly the proposed ligands all contained values aligned with common medicinal chemistry guidelines with molecular weights (MW) <500 and cLogP <5 (which were in accordance with the guidelines developed by Lipinski)⁷⁸ and a polar surface area (PSA) was typically <100 Å², which correlates with Veber's guidelines of having a PSA ≤140 Å.⁷⁹

3.2.3 Acyl Aniline Series

3.2.3.1 Retrosynthetic Analysis

The first series targeted for synthesis was the AA series (Figure 22). In order to probe the SAR, the connectivity of the acetic acid would be altered and functionalisation on the nitrogen would be investigated. Removal of the acetic acid group (**27**) was targeted in order to determine what effect the removal of, what was believed to be, the key pharmacophoric moiety would have on the binding ability of the ligand. The introduction of substitution on the aniline nitrogen (**28-30**) was designed to probe the SAR around the location of the isoxazole in AM095 (**16**). More polar groups could then be introduced in this region to mimic the isoxazole should interesting results be obtained.

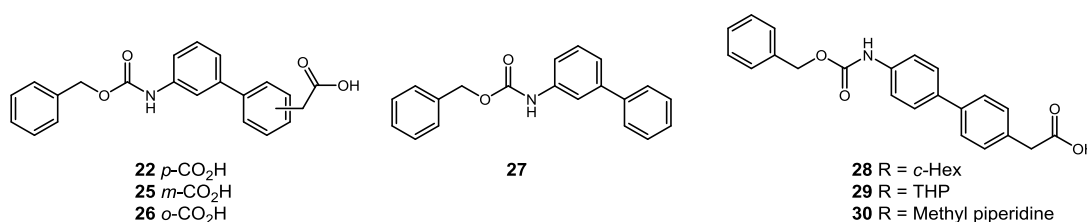
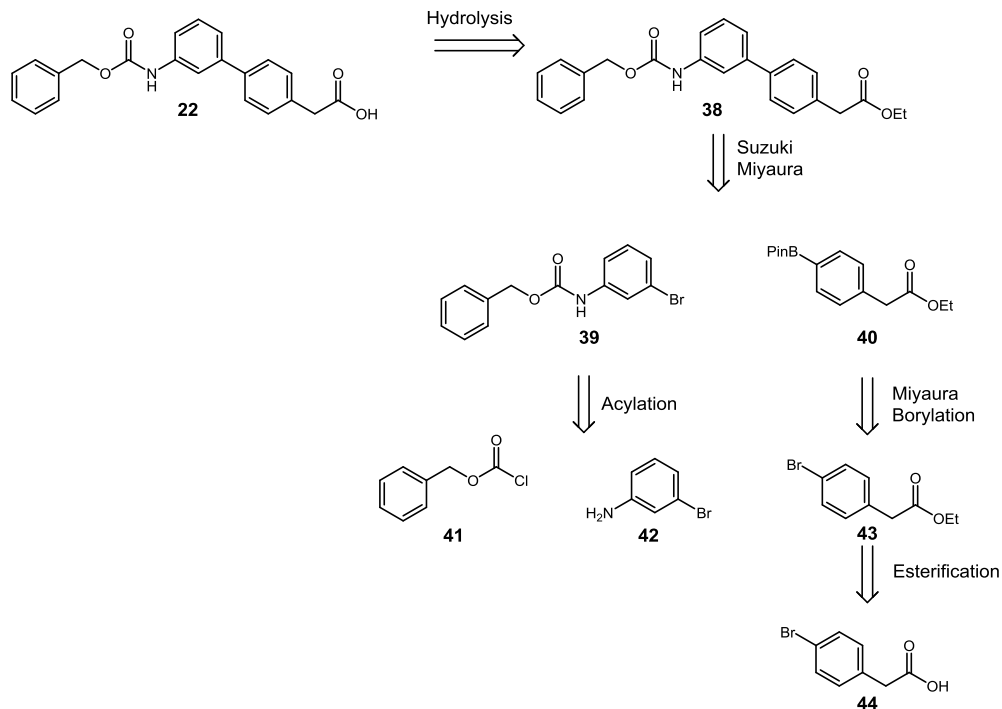


Figure 22: AA compounds targeted for synthesis.

A general synthetic strategy was developed for the AA compounds. Using *para*-isomer **22** as an example, the retrosynthetic analysis is shown in Scheme 7. It was determined that through the use of four key reactions: Acylation, Miyaura borylation, Suzuki-Miyaura cross-coupling, and hydrolysis the desired compounds could be effectively prepared. A similar method could then be employed for the construction

of the other ligands (compounds **25** and **26**). In the case of compound **28-30** where functionalisation was required on the aniline nitrogen, it was envisaged that this would be introduced by reductive amination prior to acylation with benzyl chloroformate (CbzCl).

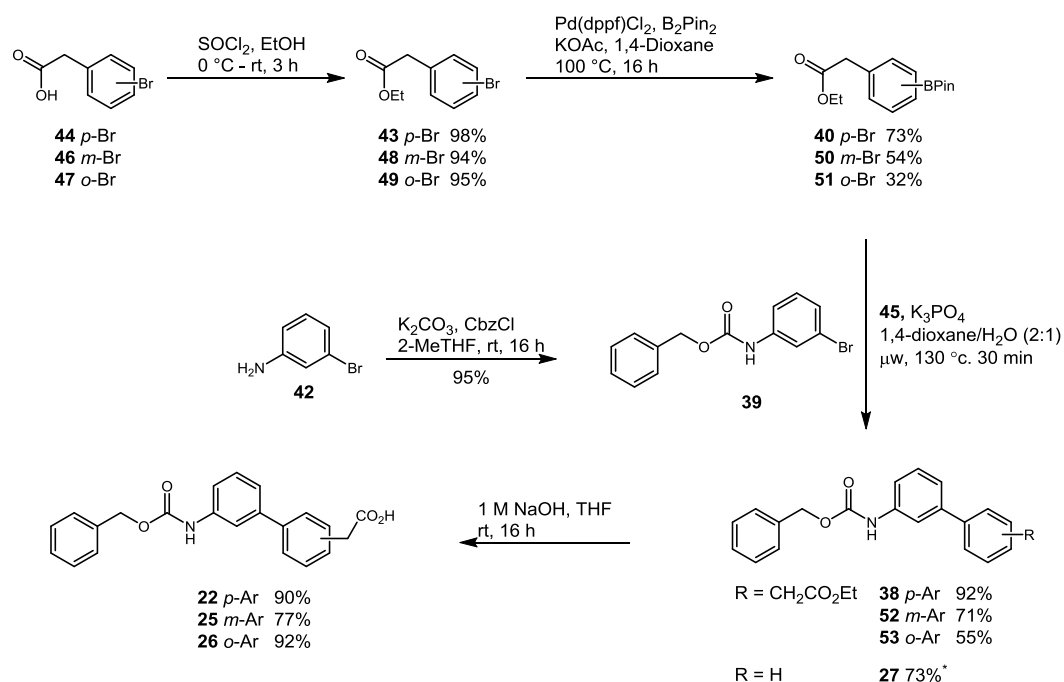


Scheme 7: Retrosynthetic analysis for the synthesis of **22** from the AA series.

3.2.3.2 Synthetic Route

The key step in the synthetic route involved the Suzuki-Miyaura cross-coupling reaction between pinacol esters (**40**, **50**, and **51**) and the acylated 3-bromoaniline (**39**). The first of the coupling partners, the pinacol boronic esters, were prepared by esterification of 4-, 3- and 2-bromophenylacetic acid (**44**, **46**, and **47**) using thionyl chloride and EtOH to give ethyl(bromophenyl)acetates **43**, **48**, and **49** in quantitative yields. The synthesised esters **43**, **48**, and **49** were then converted into the corresponding pinacol boronic esters using standard Miyaura borylation conditions³³ (Scheme 8). A significant decrease in yield was found on going from *para*- (**40**) to *ortho*-substituted pinacol ester (**51**), which may be attributed to the increased steric hindrance due to the proximity of the ester unit.

The second of the coupling partners, the acylated aniline, was prepared *via* the reaction of 3-bromoaniline (**42**) with benzyl chloroformate (CbzCl) **21** in the presence of K_2CO_3 .⁸⁰



Scheme 8: Synthetic route for the construction of the acyl aniline series compounds (**22**, **25**, **26**, and **27**). *Synthesised using commercially available phenyl boronic acid.

In an effort to adopt greener protocols into the synthetic route a small solvent screen was conducted in order to find a suitable replacement to chloroform (a literature-based method) which is classed by many solvent guides as highly hazardous.^{80,81} Building on previous work conducted in our laboratories on alternative, more environmentally friendly solvents,^{82–84} 2-MeTHF was selected. Pleasingly, this allowed for the synthesis of **39** in a high yield of 95%, Scheme 8.

With the two coupling partners in hand, these could then be coupled together *via* a Suzuki-Miyaura reaction in order to generate the required biaryl motif of the target compounds. A set of conditions routinely employed in the labs of our collaborators at GlaxoSmithKline(GSK) were trialled which involved the use of 10 mol% of a dinorbornyl phosphine complex catalyst **45**, (Figure 23)⁸⁵ with K_3PO_4 as the base and a 2:1 mixture of 1,4-dioxane and water as the solvent system under microwave irradiation at 130 °C for 30 min. These conditions afforded the desired biaryl species (**27**, **43**, **52**, and **53**) in moderate to high yields. Similar to the previous Miyaura

borylation conditions there was a noticeable drop in yield when going from the *para* to the *ortho* substituted products, which again may be attributed to the increase in steric hindrance.

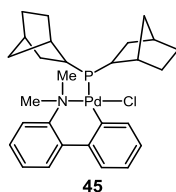


Figure 23: Catalyst **45**.

The final step in the synthetic route involved hydrolysis of the ester moiety to the corresponding acetic acid compounds (**22**, **25**, and **26**). Initial conditions attempted involved the use of LiOH (0.3 M) in a solution of MeOH/THF/H₂O (1:1:0.5), however, it was found that an undesirable transesterification occurred with the MeOH present in the reaction mixture. Therefore, the reaction was repeated omitting the MeOH, however, no hydrolysis was observed. As a result, a stronger base was employed in the form of NaOH (1 M), using THF as the solvent (Scheme 8). Pleasingly, this afforded the desired compounds cleanly and in good yields.

3.2.3.3 Reductive Amination

A similar route was envisaged for the synthesis of the *N*-substituted AA's (Figure 24) in order to probe the SAR around the region occupied by the isoxazole in AM095 (**16**), which was truncated in the ligand design. Reductive amination, prior to the acylation reaction, was anticipated to be effective for the introduction of *c*-Hex, tetrahydro-4*H*-pyran (THP), and *N*-methylpiperidine functionality onto the aniline.

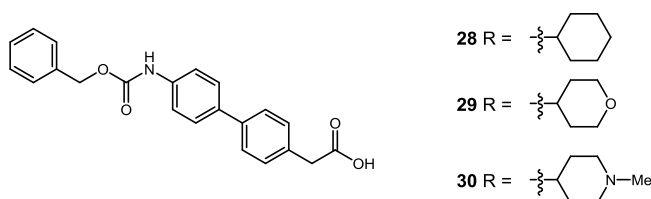
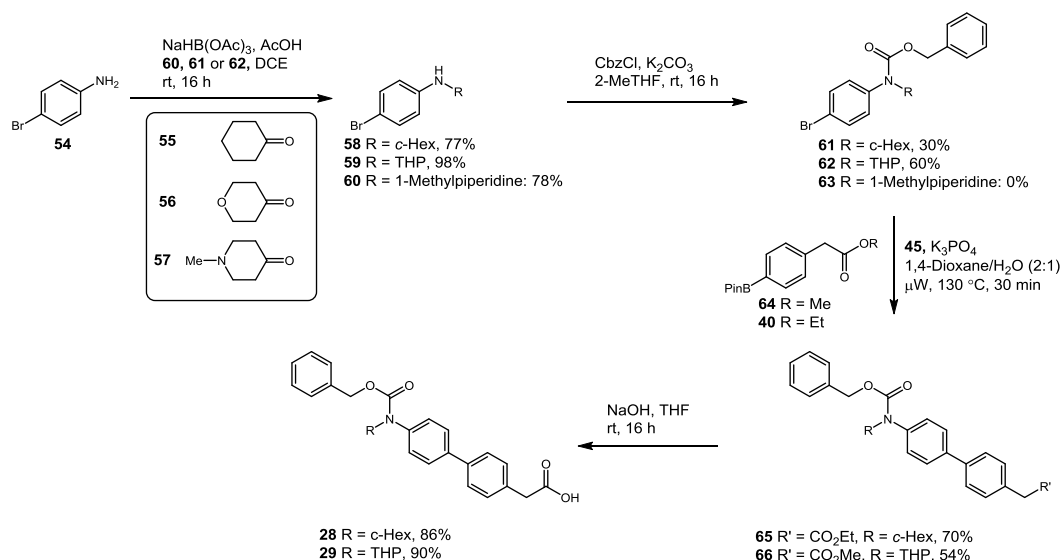


Figure 24: Proposed compounds for synthesis within the substituted AA series.

The first step of the synthetic route involved the reductive amination reaction between 4-bromoaniline (**54**) and either cyclohexanone (**55**), tetrahydro-4*H*-pyran-4-one (**56**), or 1-methylpiperidin-4-one (**57**). As 2-MeTHF had proved to be a good

replacement solvent within the acylation reaction, it was envisioned that this may also be the case for the reductive amination process. Unfortunately, due to solubility issues with the tetrahydro-4*H*-pyran-4-one and 1-methylpiperidin-4-one it was quickly discarded and replaced with the conventional DCE which gave modest to good yields of the three desired products **58-60**, Scheme 9.



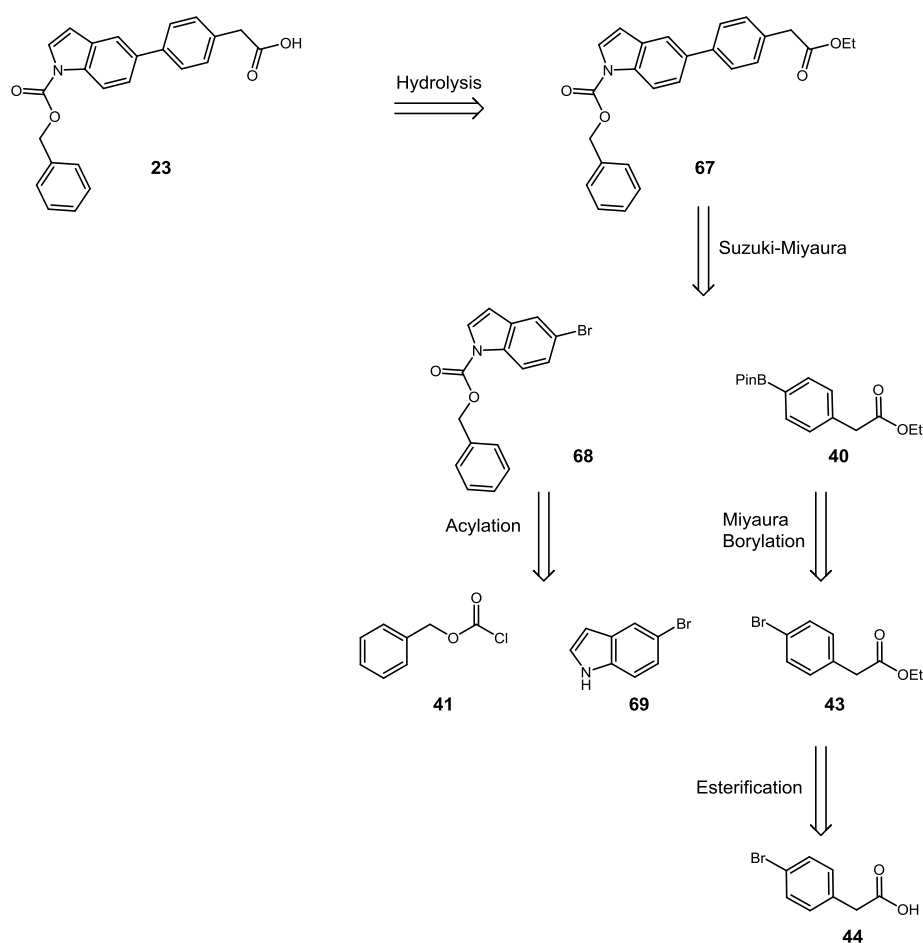
Scheme 9: Synthetic route of **28**, **29**, and **30** for the functionalised AA series.

With these compounds in hand, they were taken forward to the acylation step, using the same conditions as previously employed for the AA series, with **41**. The THP alkylation proceeded moderately well obtaining the desired product **62** in a modest yield of 60%, however, on moving to the *c*-Hex functionality (**61**) a drop in yield to 30% was observed. Additional complications were encountered with the acylation of the *N*-methylpiperidine substituted aniline, as upon purification it was found that the benzyl carbonate functionality was not stable and readily removed. Therefore, due to the difficulties associated with the synthesis of compound **63**, only the *c*-Hex (**62**) and THP (**63**) derivatives were carried forward to the Suzuki-Miyaura reaction. Again, construction of the biaryl motif was achieved using the previously optimised conditions delivering the desired products **65** and **66** in moderate yields 70% and 54%, respectively. Hydrolysis then provided the target compounds **28** and **29** in 86% and 90% yield respectively (Scheme 9).

3.2.4 Acyl Indole Series

3.2.4.1 Retrosynthetic Analysis

Following completion of the desired AA compounds, focus was transferred to the synthesis of the AI compounds. It was proposed to base the synthesis of compounds **23** and **31** on the already established route used for the acyl aniline series, as can be illustrated in the retrosynthetic analysis for compound **23** (Scheme 10). As previously stated, the route involved four main reactions, acylation (to install the carbamate functionality), Miyaura borylation, Suzuki-Miyaura cross-coupling, and lastly, hydrolysis.

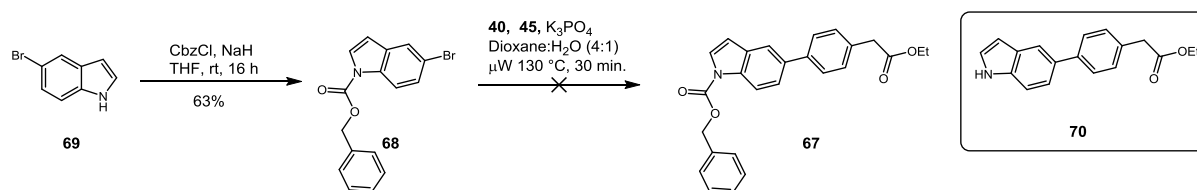


Scheme 10: Adapted synthetic route for the formation of compound **23**.

3.2.4.2 Synthetic Route

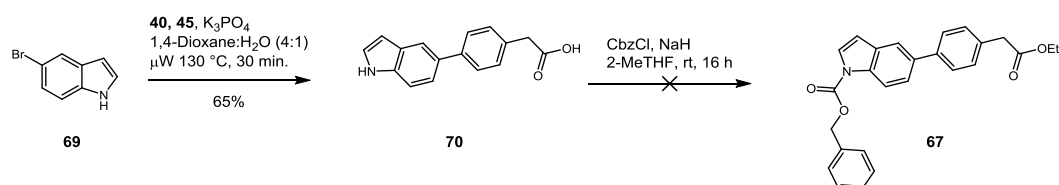
The first step of the synthetic route involved the introduction of the benzyl carbamate functionality on the nitrogen of the indole. To achieve this, the previous acylation conditions used for the AA series were trialled (K_3PO_4 in 2-MeTHF), however, these resulted in a slow reaction, and proved difficult to purify. Therefore, after a slight optimisation of the conditions, it was found that altering the base to sodium hydride and using THF as the solvent gave access to the desired product **68** in 63% yield.

With the acylated indole **68** in hand, coupling to the pinacol boronic ester **40** using the Suzuki-Miyaura conditions developed previously was trialled. Unfortunately, it became evident, from LCMS analysis, that although the Suzuki-Miyaura was successful in installing the biaryl motif, the reaction conditions resulted in the removal of the benzyl carbamate to give compound **70** (Scheme 11). This could be attributed to the carbamate group not being stable to the basic and high temperature conditions of the reaction.



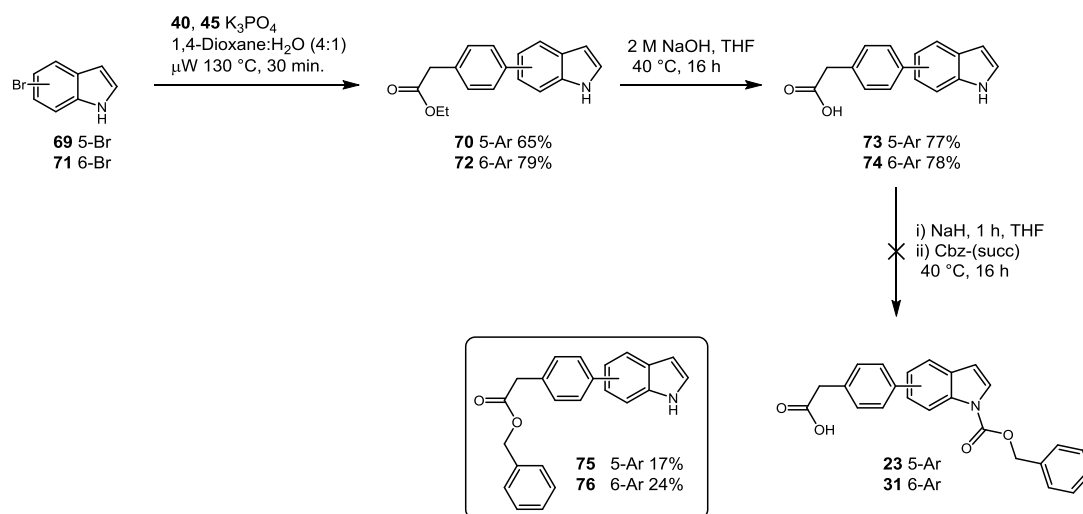
Scheme 11: Synthetic route for the synthesis of compound **23**.

In an attempt to rectify this problem the order of the reaction was altered to firstly construct the biaryl system using 5-bromoindole (**69**) and pinacol boronic acid **40** to give compound **70**, which was then subjected to the acylation conditions to introduce the carbamate functionality on the nitrogen of the indole (Scheme 12). This reaction, however, proved troublesome and only resulted in the isolation of unreacted starting material even after the introduction of additional base and $CbzCl$.



Scheme 12: Revised synthetic route for the synthesis of **23**.

In a final attempt to rectify this problem reorganisation of the steps was trialled in order to introduce the troublesome carbamate functionality at the end of the route, to avoid removal under the reactions conditions. The new route developed is illustrated in Scheme 13, beginning with the Suzuki-Miyaura cross-coupling, followed by hydrolysis of the ester, and lastly the acylation reaction to install the carbamate group, this time using *N*-(benzyloxycarbonyloxy)succinamide as the carbamate source. The first three steps proceeded well; however, the acylation step proved troublesome yet again and unfortunately did not afford the desired products **23** and **31**, affording compounds **75** and **76** instead.



Scheme 13: Revised route for the synthesis of the AI series.

Although it had not been possible to gain access to the previously proposed compounds **23** and **31**, two interesting compounds **75** and **76** had been developed. On further analysis, it was thought that these could provide valuable information in terms of structural binding, challenging the binding hypothesis previously stated as they lacked the key pharmacophoric moiety, the acetic acid.

In order to further assess the utility of these compounds as potential LPA₁ receptor antagonists a similar structural analysis was conducted, as seen previously for the three main proposed series. Compound **75** was used as an exemplar compound and its structure was compared against the known LPA₁ receptor antagonist **16**. The overlaid structures are illustrated in Figure 25 and pleasingly indicate that **75** occupied a similar structure space to the known inhibitor, and as a result it could be

hypothesised that these aryl indole (Arl) compounds (**75** and **76**) could bind in a similar manner. Therefore, they would be evaluated within the biological assay.

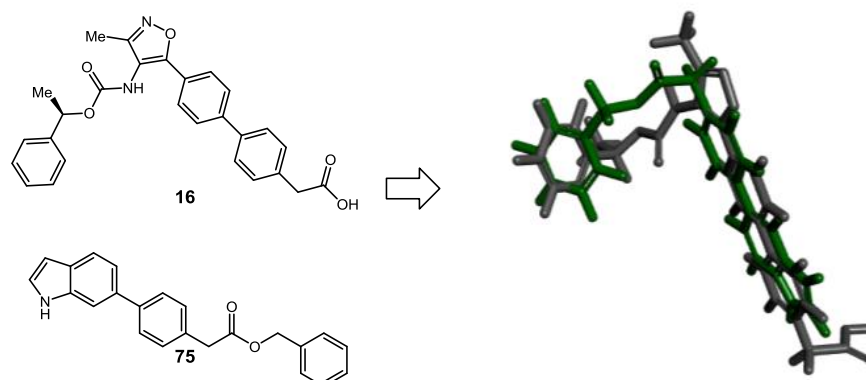


Figure 25: Overlay of Arl compound **75** (green) with AM095 **16** (grey).

The complete compound library (containing synthesised compounds from AA, Arl, and H series), Figure 26, would then be tested for both LPA₁ and ATX inhibition.

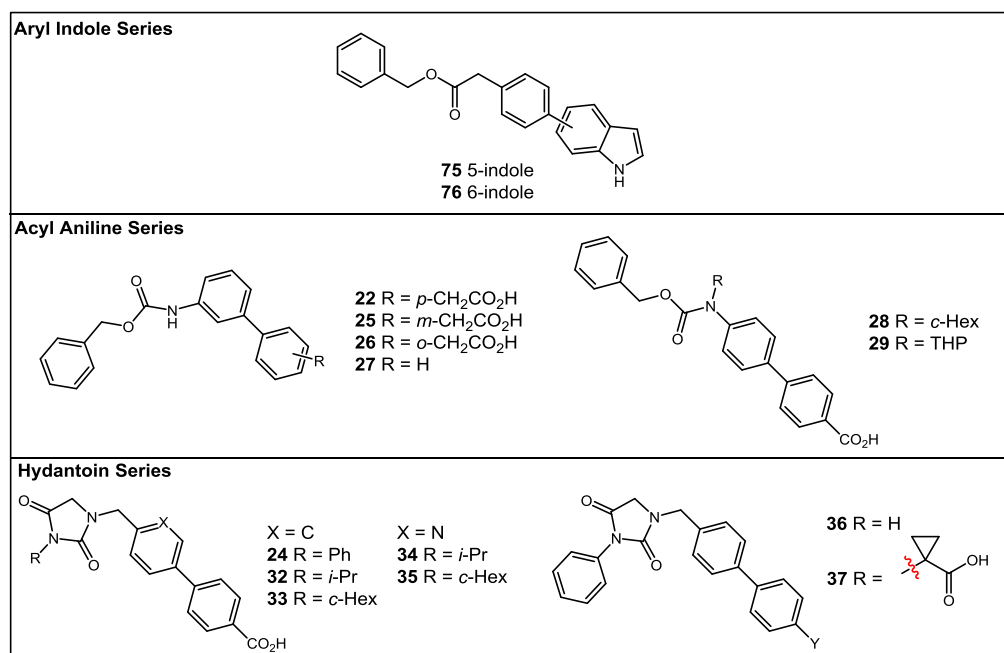


Figure 26: Synthesised compounds taken forward for biological evaluation.

3.3 Pharmacology

3.3.1 LPA₁ receptor Agonism/Antagonism

Once synthesised, the compounds were then evaluated for LPA₁ receptor agonism and antagonism using CHO-K1 EDG2 β -arrestin cell line in a single dose format (10 μ M) using 1-oleoyl-LPA (**4**), Ki16425 (**15**), and AM095 (**16**), as controls.

The assay functions by monitoring GPCR activity by detecting the interaction between β -arrestin and a fragment of β -galactosidase (β -gal) termed ProLink. The GPCR of interest is tagged with the ProLink fragment. Activation of the GPCR stimulates binding of β -arrestin to the ProLink tag which will in turn force pairing of the two enzyme fragments forming an active β -gal enzyme, which can then hydrolyse the substrate generating a chemiluminescent signal which can be measured (Figure 27).⁸⁶

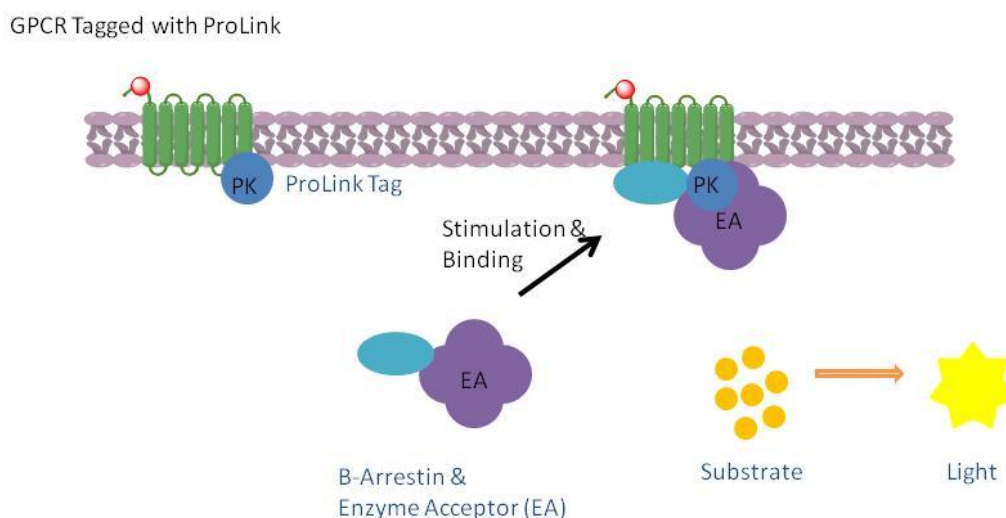
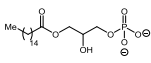
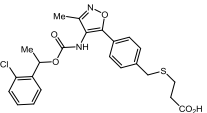
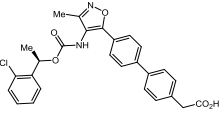


Figure 27: Activation of GPCR leads to β -arrestin recruitment and formation of a functional enzyme which is then capable of hydrolysing the substrate and generating a chemiluminescent signal.

The biological data obtained from the assay is quoted in terms of a percentage of agonism where 100% refers to complete agonism and 0% refers to complete antagonism.

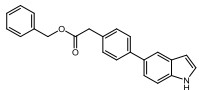
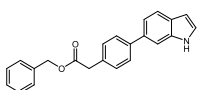
The compound library developed previously was then evaluated using this assay and the data generated is illustrated in Table 5-8 associated with the controls, Arl, AA and H series respectively.

Table 5: Control compounds.

Entry	Cpd. No.	Structure	% Activation (Agonism)	% Activation (Antagonism)
1	4		100	105
2	15		-5	16
3	16		4	11

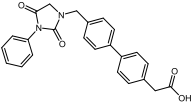
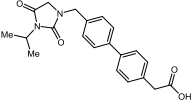
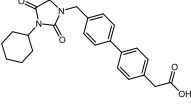
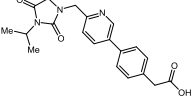
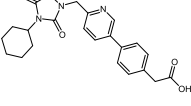
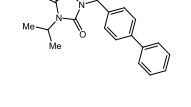
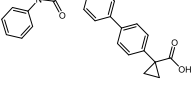
*Data generated by DiscoverX.⁸⁷

Table 6: Aryl indole compounds.

Entry	Cpd. No.	Structure	% Activation (Agonism)	% Activation (Antagonism)
1	75		-1	98
2	76		-3	88

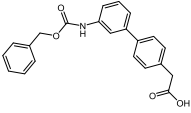
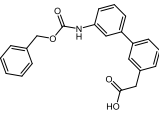
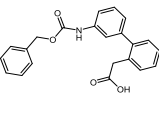
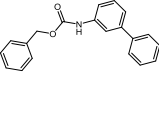
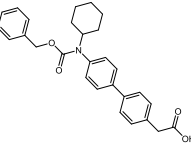
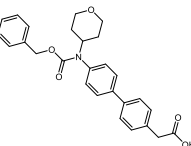
*Data generated by DiscoverX.⁸⁷

Table 7: Hydantoin compounds.

Entry	Cpd. No.	Structure	% Activation (Agonism)	% Activation (Antagonism)
1	24		-2	102
2	32		5	111
3	33		9	118
4	34		5	100
5	35		36	95
6	36		5	106
7	37		4	95

*Data generated by DiscoverX Corporation.⁸⁷

Table 8: Acyl aniline compounds.

Entry	Cpd. No.	Structure	% Activation (Agonism)	% Activation (Antagonism)
1	22		-5	88
2	25		1	102
3	26		-4	68
4	27		7	101
5	28		0	82
6	29		0	113

*Data generated by DiscoverX Corporation.⁸⁷

The control samples included; the natural substrate LPA (**4**), and two known LPA₁ receptor antagonists Ki16425 (**15**), and AM095 (**16**). Compound **4** was a negative control within the antagonist format and a positive control in the agonist format. Whereas **15** and **16** were positive controls within the antagonist format, and negative controls for the agonist format. Control compound **4** was found to contain no activity in the antagonist form, but 100% activity within the agonist form. This was

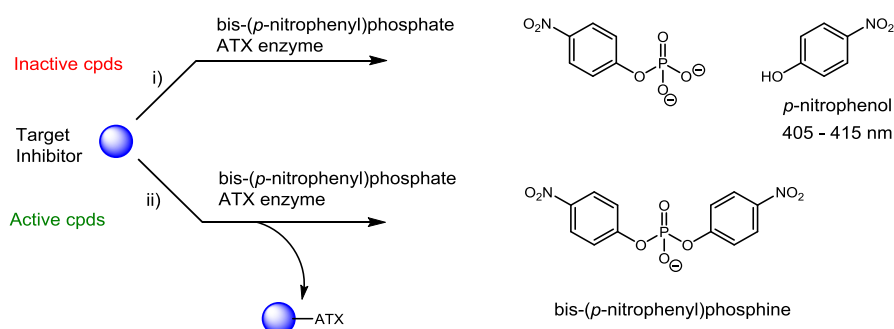
to be expected as it is the natural substrate produced from the LPC hydrolysis reaction. In addition to this, compounds **15** and **16**, the known LPA₁ receptor inhibitors, as expected, only illustrated LPA₁ antagonism and no agonism was observed. In terms of the Arl and the H series, unfortunately both illustrated no activity in either screening procedure, Table 6 and 7. In the AA series (Table 8) only compound **26** suggested it may be acting as a partial antagonist due to the slight decrease in the % activity, however, further biological evaluation would be required in order to verify this.

From this study, it became evident that the original hypothesis that the isoxazole unit present in AM095 (**16**) was just a spacer unit between the important carbamate and acetic acid functionalities was incorrect, and in fact the elimination of this moiety was not tolerated within this chemotype. Literature evidence has however illustrated that the isoxazole can be derivitised into functionalities such as triazoles and pyrazole analogues which retain LPA₁ receptor antagonism, as demonstrated by Qian *et. al.*³³

3.3.2 ATX Inhibition

In addition to analysing the compounds for LPA₁ receptor antagonism they were also put forward to evaluate their potential use as ATX inhibitors due to the degree of cross-talk between the two pathways.^{88,89} The compound library was evaluated using the commercially available, and conventionally used, bis-*p*NPP assay with the inclusion of PF-8380 (**19**), a known ATX inhibitor, as a standard for comparison.

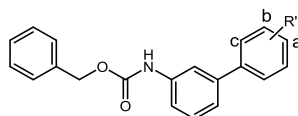
The assay proceeds using the unnatural substrate bis-(*p*-nitrophenyl)phosphate which can undergo hydrolysis by ATX, forming *p*-nitrophenol which can be subsequently detected using UV-Vis, Scheme 14. The percentage of inhibition can then be measured from the percentage hydrolysis of the substrate, as these will be inversely proportional.



Scheme 14: Bis-pNPP assay mechanism, where i) inactive compounds have no effect on the ATX enzyme allowing hydrolysis of the substrate which can be monitored by UV and ii) active compounds will inhibit the ATX enzyme inhibiting the hydrolysis process.

Compounds derived from each of the three series were then analysed using a concentration-response method (1 nM – 30 μ M) to generate inhibitor constants (K_i). In addition to the biological evaluation, the compounds were also subjected to pharmacokinetic assays so that their drug-like properties could be evaluated (Tables 9-12).

Biological evaluation of the unsubstituted AA compounds (Table 9) illustrated the importance of the acetic acid functionality as its removal (compound **27**) resulted in a complete loss of activity, supporting the hypothesised binding mode. Interestingly, it was discovered that within this series the presence of the acetic acid moiety was important for activity. However, its regiochemistry around the aromatic ring (*i.e.* *ortho*, *meta* or *para* to the ring) was not, as **22**, **25** and **26** were all equipotent with K_i values of around 4 μ M.

Table 9: Biological and Physicochemical Data for Acyl Aniline Series.

Entry	Cpd. No. ^a	Pos. R	R'	Ki (μM) ⁹⁰	LogD ^b	Sol. (ug/mL) ^c	P _{app} (nm/s) ^d
1	22	A	CH ₂ CO ₂ H	4.5	3.19	198	73
2	25	B	CH ₂ CO ₂ H	3.5	3.10	221	64
3	26	C	CH ₂ CO ₂ H	4	3.06	287	140
4	27	-	H	> 30	7.52	5	450

^aCompound Number (Cpd), ^bChromlogD at pH 7.4 (LogD), ^cChemiluminescent nitrogen detection (CLND) kinetic aqueous solubility assay (Sol.), ^dPermeability pH 7.4 assay (P_{app}).

In an attempt to rationalise this data an additional set of overlay diagrams were produced (Figure 28) which indicated the backbone of all four compounds (**22**, **25-27**) contained the same conformation, and the acetic acid moieties all pointed in the same spacial orientation which may be indicative of beneficial interactions within the catalytic pocket.

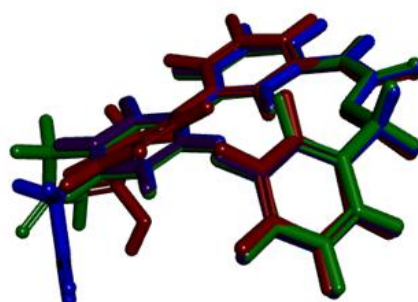
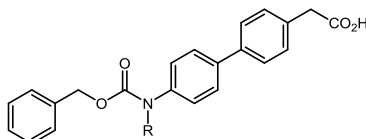


Figure 28: Overlaid diagram of compounds **22** in blue, **25** in purple, **26** in red, and **27** in green, illustrating all four compounds contain the same conformation.

In terms of drug-like properties, these compounds **22**, **25**, and **26** contained good LogD values which are in accordance with the guidelines produced by Lipinski⁷⁸ and Gleeson,⁹¹ as well as having good solubility, >100 ug/mL and moderate permeability, in accordance to general guidelines produced by GSK. On moving to **27**, the solubility decreases dramatically and the LogD increases. This can be attributed to the loss of the acetic acid moiety resulting in the compound being more lipophilic which is consistent with the increase in cell permeability. As such, from this data it is evident that **27** may not be a viable as a drug compound due to its increased lipophilicity which could lead reduction in the solubility of the drug, and hence reduce its possibility of becoming a drug candidate.

The introduction of substitution on the nitrogen of the aniline also resulted in some interesting data (Table 10), as it was found that functionalisation was tolerated as illustrated in compound **28** with the introduction of a *c*-Hex unit giving a Ki of 2 μ M. However, when this substitution was altered to THP, compound **29** resulted in complete loss of activity. A possible explanation for this data may be a result of an unfavourable polar interaction with the oxygen present in the THP moiety which is absent in *c*-Hex, thus implying other polar functionalities may not be tolerated in this position.

Table 10: Biological and physicochemical data for substituted acyl aniline series.



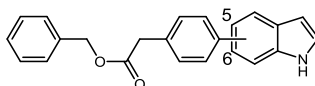
Entry	Cpd. No. ^a	R	Ki (uM) ⁹⁰	LogD ^b	Sol. (ug/mL) ^c	P _{app} (nm/s) ^d
1	28	<i>c</i> -Hex	2	4.92	189	150
2	29	THP	>30	3.13	212	23

^aCompound Number (Cpd), ^bChromlogD at pH 7.4 (LogD), ^cChemiluminescent nitrogen detection (CLND) kinetic aqueous solubility assay (Sol.), ^dPermeability pH 7.4 assay (P_{app}).

In terms of the pharmacokinetic analysis, as expected the more polar THP group results in a decrease in LogD compared to **28**, which is on the higher end of the spectrum in terms of the conventionally used guidelines.^{78,91} Solubility of the two compounds are comparable, but the permeability differs greatly as **29** is much less permeable. This may be attributed to the more polar functionality of the THP group.

For the aryl indole (Arl) compound series (Table 11) it became apparent that the substitution of the biaryl ring proved important for biological activity as moving the aryl side chain from the five to the six position resulted in Ki values of 1.1 μM to >30 μM respectively. Strikingly, this data also illustrates that the acid moiety which was previously labelled as being the key pharmacophoric moiety, and found to be important for activity in regards to the acyl aniline compounds, seemed not to be required within the aryl indole series, indicating a potential alternative hydrophobic binding mode.

Table 11: Biological and physicochemical data for substituted aryl indole series.



Entry	Cpd No. ^a	Pos.	Ki (μM) ⁹⁰	LogD ^b	Sol. ^c ($\mu\text{g/mL}$)	P _{app} ^d (nm/s)
1	75	5	1.1	7.25	70	445
2	76	6	>30	7.43	110	510

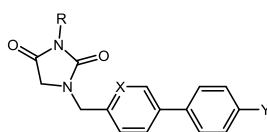
^aCompound Number (Cpd), ^bChromlogD at pH 7.4 (LogD), ^cChemiluminescent nitrogen detection (CLND) kinetic aqueous solubility assay (Sol.), ^dPermeability pH 7.4 assay (P_{app}).

From a developability perspective both compounds contain a high LogD and cell permeability, which are undesirable and so may lead to problems if taken further.

Finally, the data generated for the hydantoin series (Table 12) illustrated that in general all the compounds showed ATX inhibition properties except compound **37**. Interestingly it was found that compounds **24** and **36** gave comparable Ki values of 1.3 and 3.6 μM respectively, indicating the acetic acid functionality (present on **24**,

and absent on **37**) may again not be as important as for activity as was previously hypothesised. In addition to this, it was found that both the pyridyl and benzyl hydantoin compounds were well tolerated as well as the alternative functionality (Ph, and *c*-Hex) on the hydantoin. As mentioned, compound **37** displayed no ATX inhibition which when compared to compound **36** indicated that the *c*-Pr group adjacent to the acid group is not tolerated, possibly due to a steric clash in the active site of the enzyme.

Table 12: Biological and physicochemical data for hydantoin series.



Entry	Cpd. No. ^a	R	X	Y	Ki (μM) ⁹⁰	LogD ^b	Sol. ^c (μg/mL)	P _{app} ^d (nm/s)
1	24	Ph	C	CH ₂ CO ₂ H	3.6	2.18	174.5	3
2	32	<i>i</i> -Pr	C	CH ₂ CO ₂ H	1.2	1.10	190	3
3	33	<i>c</i> -Hex	C	CH ₂ CO ₂ H	1.8	1.12	185.5	22
4	34	<i>i</i> -Pr	N	CH ₂ CO ₂ H	4	-1.38	108	<10
5	35	<i>c</i> -Hex	N	CH ₂ CO ₂ H	3.9	-0.35	93	<30
6	36	Ph	C	H	1.3	6.24	7.5	540
7	37	Ph	C	C(<i>c</i> -propy) CO ₂ H	>30	1.50	195	16

^aCompound Number (Cpd), ^bChromlogD at pH 7.4 (LogD), ^cChemiluminescent nitrogen detection (CLND) kinetic aqueous solubility assay (Sol.), ^dPermeability pH 7.4 assay (P_{app}).

In general, the H series compounds contained a poorer pharmacokinetic profile (Table 12) where permeability was dramatically reduced compared to the values obtained for the AA (Table 10) and the Arl series (Table 11). In addition to this, the LogD values associated with the pyridyl derivatives (**34** and **35**) and compound **36** fell out with the desired ranges, however, in terms of the benzyl derivatives these were generally good. Therefore, from a developability perspective, if these compounds were to be taken further then the problems with cell permeability would need to be addressed.

In addition to the synthesised compounds discussed above, Ki16245 (**15**), and AM095 (**16**), two known LPA₁ antagonists, were also analysed for ATX inhibition at a single-shot concentration (30 µM) in order to further probe the cross-talk between the two pathways. Unfortunately, these compounds showed less than 20% ATX inhibition and thus were deemed inactive towards ATX inhibition.

In addition to screening against LPA₁ receptor antagonism and ATX inhibition, further assay work was conducted in order to evaluate the impact of these potential inhibitors on in-cell proliferation through ATX modulation. This was achieved through the use of a [³H]-thymidine incorporation assay. This proceeds by quantifying the amount of radiolabelled tritiated thymidine incorporated into the cell, in this case prostate cancer (PC3) cells. The amount of which will be proportional to the quantity of newly synthesised DNA.

Three of the most active compounds **22**, **28**, and **35** as well as **16** were analysed using [³H]-thymidine incorporation assay, and the data generated is illustrated in Figure 29. From these graphs it is evident that there was a significant increase in DNA synthesis within PC3 cells when stimulated with LPA ($p < 0.05$). Upon treatment with **22**, **28**, **35** and **16**, DNA synthesis was inhibited to a statistically significant level ($p < 0.05$) with respect to the control. Compounds **22**, **28**, and **35** illustrated ATX inhibitory potency and blocked baseline [³H]-thymidine incorporation in PC3 cells, suggesting that the inhibitory effect is due to the compounds blocking the endogenous production of LPA by ATX. Visual inspection of the cells showed no apparent cell death.

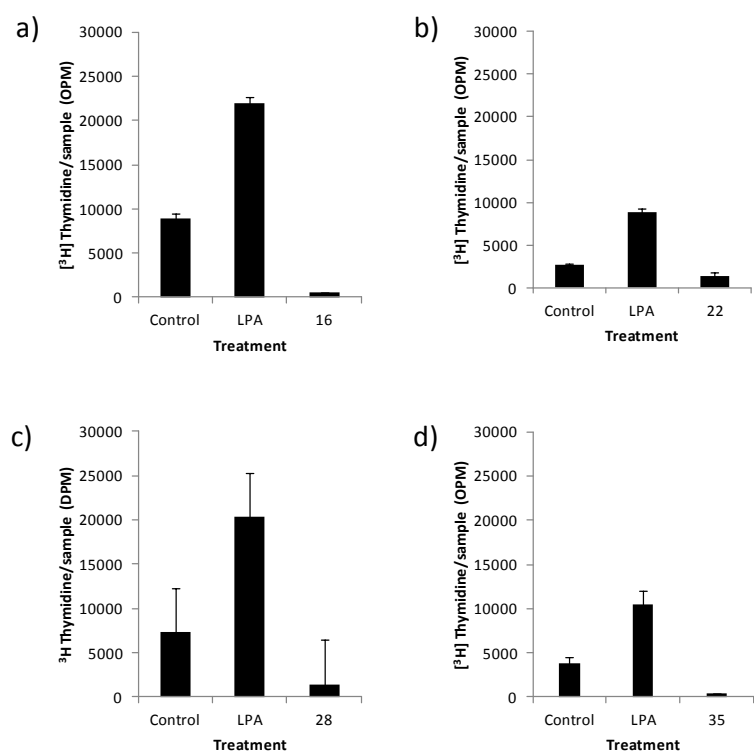
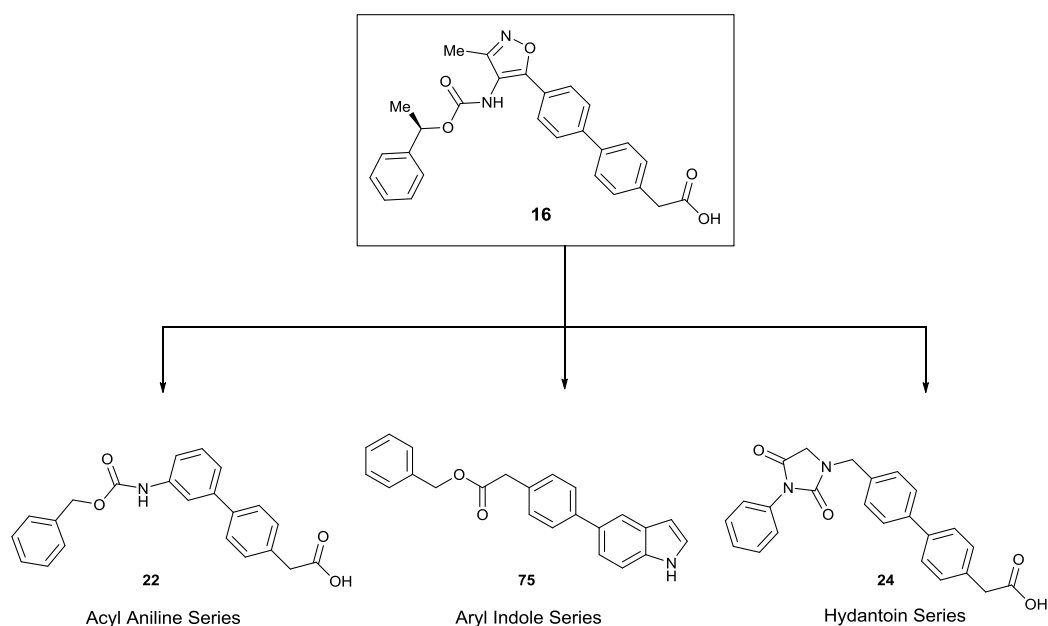


Figure 29: ^3H -thymidine incorporation into LPA (2 μM), AM095 (**16**) (graph a), compound **22** (graph b), compound **28** (graph c), or compound **35** (graph d) (10 μM), stimulated PC3 cell line, cells were quiesced for 24 hours and treated for 18 h with compounds (**16**, **22**, **28**, or **35**). n=9, data represented as Mean \pm S.E.M.

3.4 Conclusions

AM095 (**16**), a known LPA₁ antagonist, was used as the basis for a scaffold hopping approach for the design and synthesis of novel compounds to target the LPA-ATX signalling pathway. From this skeletal backbone, three novel chemotypes were developed by performing three main disconnections from the AM095 (**16**) backbone giving rise to the Acyl Aniline, the Acyl Indole, and the Hydantoin series. Unfortunately, due to synthetic problems associated with the original proposed Acyl Indole compounds these were unable to be synthesised, however, a new series in the form of the Aryl Indole were synthesised. Thus, giving rise to three novel series of compounds, Scheme 15.



Scheme 15: Three target series developed using from AM095 (**16**), i) the AA series, ii) the Arl series, and iii) the H series.

From these three main series a variety of compounds were then synthesised and evaluated in a range of biological assays which included testing for LPA₁ receptor antagonism, ATX inhibition, in-cell proliferation through ATX modulation using [³H]-thymidine assay, and cytotoxicity.

From the generated biological data it was found that unfortunately, the compounds synthesised proved to be inactive towards LPA₁ receptor antagonism. From this, it became apparent that perhaps the previous hypothesis of the isoxazole functionality

acting as a spacer between the important carbamate and acetic acid moieties may not be correct, and in fact it seemed to be essential for activity. Pleasingly, in cross-screening the compounds for ATX inhibition, using the conventionally used bis-*p*NNP assay, several of the compounds illustrated inhibitory activity towards the ATX enzyme in the μM range. Surprisingly, compounds lacking the acetic acid component, **83** and **36**, also illustrated inhibitory properties against ATX, perhaps indicating that these compounds were binding in an alternative manner than previously envisioned, *i.e.* with the acetic acid pointing towards the Zn^{2+} ions within the active site.

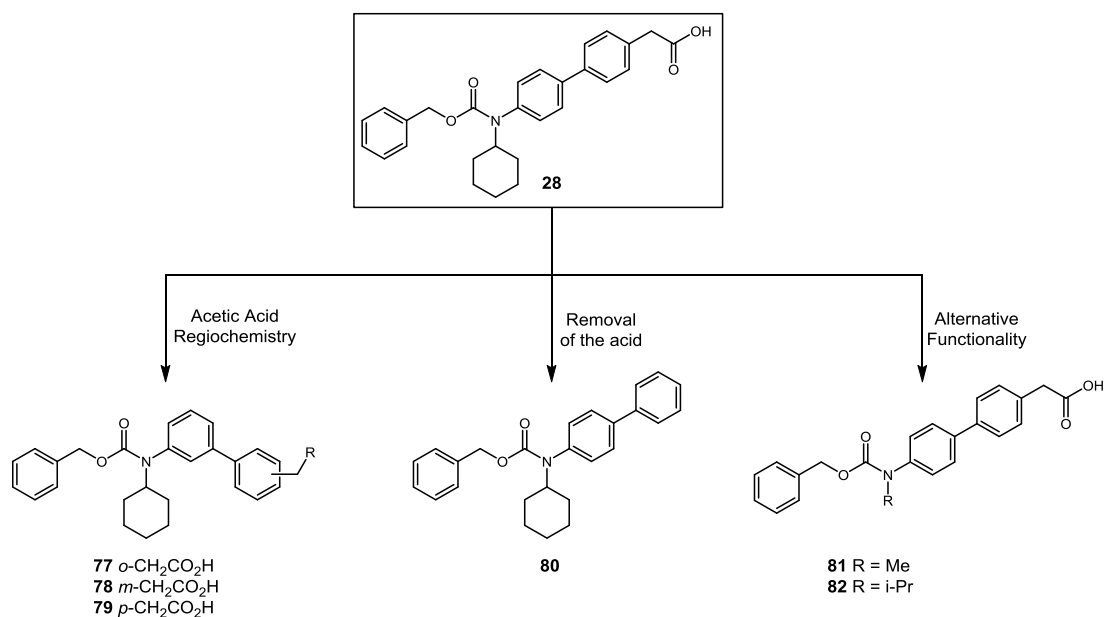
In addition to testing for LPA_1 receptor antagonism and ATX inhibition, three of the more active compounds (**22**, **28**, and **35**) were also analysed to determine what effect, if any, they would have on in-cell proliferation through ATX modulation. This was determined by using a [^3H]-thymidine incorporation assay, where it was found that of compounds tested all illustrated ATX inhibitory potency as well as effectively blocking baseline [^3H]-thymidine incorporation in PC3 cells. As a result it is possible to conclude from this data that compounds **22**, **28**, and **35** may be blocking the endogenous production of LPA by ATX.

Lastly, to ensure that any data obtained from the cell based assays was in fact a result of the inhibitory properties of the compound and not due to cytotoxicity resulting in cell death, the compound library was further validated for cytotoxicity where it was pleasingly found that none of the synthesised compounds exhibited any cytotoxic effects.

To conclude, this study indicated that there is the potential for cross-talk between both the LPA_1 receptor and the ATX signalling pathways. This can be demonstrated as the original study was based upon a known LPA_1 receptor antagonist and through a scaffold hopping approach this led to the development of novel compounds with ATX inhibition properties.

3.5 Future Work

Using the information obtained from this study, additional SAR could be conducted within each of the three series in order to gain additional information regarding the beneficial attributes which gave rise to biological activity. From the AA series, compound **28** proved to be the most active, therefore additional compounds could be synthesised building from this to include: i) changing the regiochemistry of the ring system, and ii) probing the tolerance of altered functionality of the nitrogen of the aniline, Scheme 16.



Scheme 16: Alternative SAR surrounding compound **28**.

In terms of the H series, compounds **24**, **32** and **33** proved to contain the best attributes in terms of activity and physicochemical properties. Therefore, using these compounds as a backbone, a more extensive analysis of the functional group tolerance could be conducted (Figure 30). This would allow further probing of the functional group tolerance of the hydantoin ring, with the introduction of alternative groups such as Me, CF₃, (trifluoromethyl)benzene, and chlorobenzene. These particular groups were proposed in a view to increase the cell permeability.

The additional compound library could then be analysed against both LPA₁ receptor antagonism and ATX inhibition in order to further probe the potential cross-talk between the two pathways.

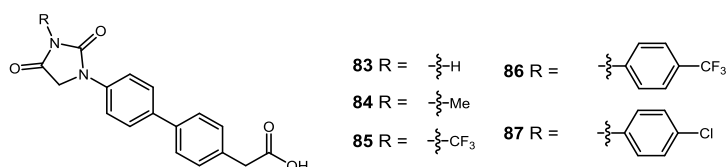
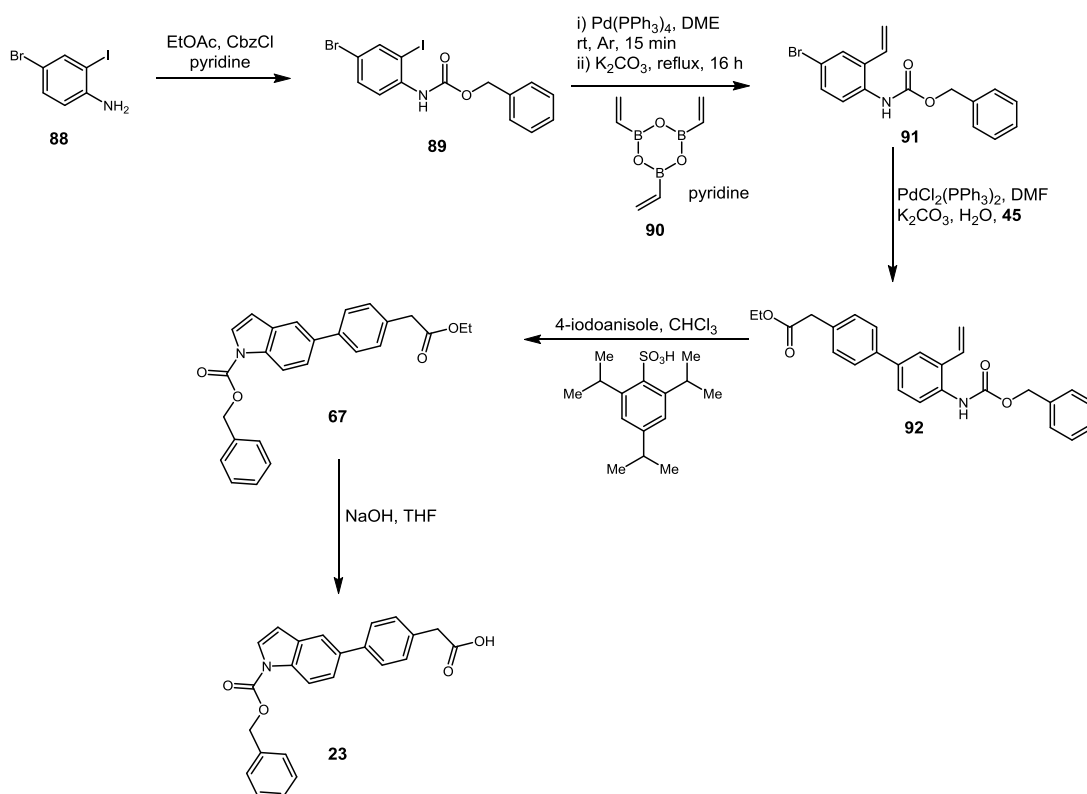


Figure 30: Additional SAR surrounding the hydantoin series.

Lastly, due to the difficulty in synthesising the original AI compounds an alternative approach could be utilised (Scheme 17) based on recent literature.⁹² This would allow for the evaluation of the previously proposed compounds for both LPA₁ receptor antagonism and ATX inhibition. The synthetic route proposed involves late stage construction of the acylated indole *via* acylation of 4-bromo-2-iodoaniline (**88**) to give **89** followed by two consecutive Suzuki cross-coupling reactions to give intermediate **92**. The desired indole is then formed through an acid catalysed hypervalent iodide promoted intramolecular cyclisation to give **67**, which after hydrolysis would give the desired compound **23**. A similar route could then be developed for the construction of **24**.



Scheme 17: Alternative route to the development of the acyl indole compounds.

3.6 Experimental

3.6.1 General

All reagents and solvents were obtained from commercial suppliers and were used without further purification unless otherwise stated. Purification was carried out according to standard laboratory methods.⁹³

3.6.1.1 Experimental Details

Reactions were carried out using conventional glassware. Room temperature was generally 18 °C. Reactions were carried out at elevated temperatures using a temperature-regulated hotplate/stirrer.

3.6.1.2 Purification of Products

Thin layer chromatography was carried out using Merck silica plates coated with fluorescent indicator UV254. These were analysed under 254 nm UV light or developed using potassium permanganate solution. Normal phase flash chromatography was carried out using ZEOprep 60 HYD 40-63 µm silica gel.

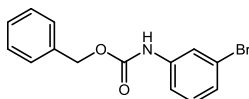
3.6.1.3 Analysis of Products

Fourier Transformed Infra-Red (FTIR) spectra were obtained on a Shimadzu IRAffinity-1 machine. ¹H and ¹³C, NMR spectra were obtained on a Bruker AV 400 at 400 MHz and 125 MHz, respectively. Chemical shifts are reported in ppm and coupling constants are reported in Hz with CDCl₃ referenced at 7.26 (¹H) and 77.1 ppm (¹³C) and methanol-d₄ referenced at 3.31 (¹H) and 49.0 ppm (¹³C). High-resolution mass spectra were obtained through analysis at the EPSRC UK National Mass Spectrometry Facility at Swansea University.

3.6.2 General Procedures

3.6.2.1 General Procedure A: Acylation Reaction

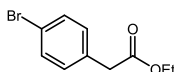
For example, for the preparation of benzyl(3-bromophenyl)carbamate, **48**



A mixture of 3-bromoaniline (6.3 mL, 58 mmol, 1 equiv.) and K_2CO_3 (8.8 g, 64 mmol, 1.1 equiv.) in 2-MeTHF (175 mL) was cooled to 0 °C before dropwise addition of CbzCl (10 mL, 70 mmol, 1.2 equiv.) over a period of 10 min. The reaction mixture was allowed to warm to room temperature and left to stir for 24 h. The reaction mixture was then quenched using ice water (50 mL) and saturated $NaHCO_3$ (2 mL) and extracted using EtOAc with 2% MeOH (2 x 100 mL). The organics were then collected, dried (hydrophobic frit), and concentrated under vacuum to a residue that was purified by silica chromatography (10-40% EtOAc in petroleum ether) to afford the desired product as a white solid (17 g, 95%).

3.6.2.2 General Procedure B: Esterification Reaction

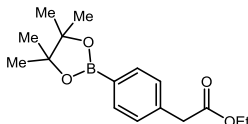
For example, for the preparation of 2-(4-Bromophenyl)acetate, **43**



To a round-bottomed flask was added 4-bromophenylacetic acid (2.7 g, 12.5 mmol, 1 equiv.) and EtOH (50 mL). The reaction mixture was then cooled to 0 °C before the drop-wise addition of $SOCl_2$ (1.2 mL, 16.5 mmol, 1.3 equiv.). The reaction mixture was then allowed to warm to room temperature and stirred for 3 h. The crude mixture was then evaporated under reduced pressure, diluted with DCM (20 mL) and extracted using sat. aq. $NaHCO_3$ (2 x 25 mL). The organic layer was then dried (hydrophobic frit) and evaporated under reduced pressure to afford the desired compound as a colourless oil (3.0 g, 98%).

3.6.2.3 General Procedure C: Miyaura Borylation Reaction

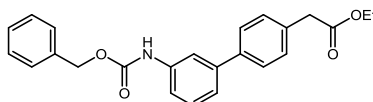
For example, for the preparation of 4-ethylphenylacetateboronic acid pinacol ester, **40**



To a round-bottomed flask was added ethyl(4-bromophenyl)-acetate **43** (2.0 g, 8.3 mmol, 1 equiv.), bis(pinacolato)diborane (2.1 g, 8.3 mmol, 1 equiv.), KOAc (2.4 g, 24.7 mmol, 3 equiv.), Pd(dppf)Cl₂ (0.2 g, 0.25 mmol, 0.03 equiv.). The flask was sealed and purged with N₂ before addition of 1,4-dioxane (44 mL). The reaction mixture was then heated to 100 °C for 24 h. The mixture was allowed to cool to room temperature and evaporated under reduced pressure. The crude mixture was then diluted with EtOAc (20 mL) and filtered through a silica plug (eluent EtOAc). The filtrate was collected and evaporated under reduced pressure and the resulting residue purified using silica chromatography (eluent 3-15% EtOAc/ petroleum ether) to afford the desired product as a white solid (1.7 g, 70 %).

3.6.2.4 General Procedure D: Suzuki-Miyaura Cross-Coupling

For example, for the preparation of ethyl 2-(3'-(((benzyloxy)carbonyl)amino)-[1,1'-biphenyl]-4-yl)acetate, **38**

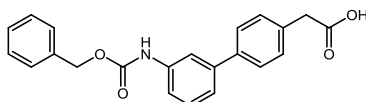


A mixture of 4-ethylphenylacetateboronic acid pinacol ester **40** (0.65 g, 2.24 mmol, 2 equiv.), 2'-(dimethylamino)-2-biphenyl-palladium(II)chloride dinorbornylphosphine complex **45** (28.30 mg, 0.05 mmol, 10 mol%), K₃PO₄ (0.63 g, 3.00 mmol, 3 equiv.), benzyl (3-bromophenyl)carbamate (0.30 g, 1.00 mmol, 1 equiv.), and 1,4-dioxane (2.40 mL) water (0.60 mL) was purged with N₂ and heated to 130 °C for 30 min under microwave irradiation. The reaction mixture was allowed to return to room temperature and evaporated to dryness under reduced pressure. The crude material was then diluted using EtOAc (10 mL) and filtered through a silica plug (eluent EtOAc), the solution was evaporated under reduced pressure and purified using

silica chromatography (eluent ethyl acetate in petroleum ether 40-60%) to afford compound the desired compound as a yellow oil (357.8 mg, 92%).

3.6.2.5 General Procedure E: Hydrolysis

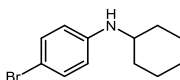
For example, for the preparation of 2-(3'-(3-phenylpropanamido)-[1,1'-biphenyl]-4-yl)acetic acid, **22**



To a round-bottomed flask was added ethyl 2-(3'-(3-phenylpropanamido)-[1,1'-biphenyl]-4-yl)acetate **38** (50 mg, 0.1 mmol), NaOH (1 M, 0.5 mL), and THF (0.5 mL). The reaction was then stirred at room temperature for 16 h. The reaction mixture was quenched using saturated NH₃Cl (2 mL), acidified with 2 M HCl, and extracted with EtOAc (2 x 10 mL). The organics were combined, dried (hydrophobic frit), and concentrated under vacuum to afford the desired product as a white solid (39 mg, 92%).

3.6.2.6 General Procedure G: Reductive Amination

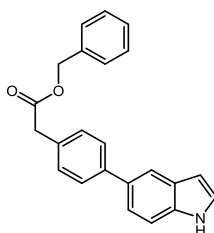
For example, for the preparation of 4-bromo-*N*-cyclohexylaniline, **58**



To a round-bottomed flask was added 4-bromoaniline (1.0 g, 5.8 mmol, 1 equiv.), cyclohexanone (0.8 mL, 7.6 mmol, 1.3 equiv.), AcOH (0.5 mL), and 2-MeTHF (25 mL). NaBH(OAc)₃ (1.8 g, 8.7 mmol, 1.5 equiv.) was then added and the mixture was stirred at room temperature for 16 h. The reaction mixture was diluted with Na₂HCO₃ (20 mL) and extracted with CHCl₃ (3 x 20 mL). The organics were collected, washed with brine (50 mL), dried (Na₂SO₄), and concentrated under vacuum to give a residue that was purified by silica chromatography (15-30% EtOAc in petroleum ether) to afford the desired product as a white solid (1.5 g, 93%).

3.6.2.7 General Procedure H: Indole Acylation

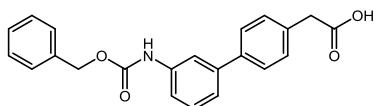
For example, for the preparation of benzyl 5-bromo-1*H*-indole-1-carboxylate, **75**



To a round-bottomed flask was added 2-(4-(1*H*-indol-6-yl)phenyl)acetic acid **74** (260 mg, 1.0 mmol, 1 equiv.) and DMF (3 mL) and cooled to 0 °C. NaH (49 mg, 2.0 mmol, 2 equiv.) was then added portion wise and the mixture was stirred for 1 hr at 0 °C. *N*-(Benzyloxycarbonyloxy)succinimide (374 mg, 1.5 mmol, 1.5 equiv.) was then added and allowed to warm to room temperature and stirred for 16 h. The reaction was quenched with ice H₂O (10 mL) and saturated NaHCO₃ (10 mL) and extracted using EtOAc (2 x 100 mL). The organics were collected, dried (hydrophobic frit) and concentrated under vacuum to a residue that was purified using silica chromatography (5-20% EtOAc in petroleum ether) to afford the desired product as a red solid (59 mg, 17%).

3.6.3 Characterisation Data

Compound 22: 2-(3'-(3-Phenylpropanamido)-[1,1'-biphenyl]-4-yl)acetic acid



2-(3'-(((benzyloxy)carbonyl)amino)-[1,1'-biphenyl]-4-yl)acetic acid
Chemical Formula: C₂₂H₁₉NO₄
Molecular Weight: 361.3970

Prepared according to General Procedure E using ethyl 2-(3'-(3-phenylpropanamido)-[1,1'-biphenyl]-4-yl)acetate **38** (50 mg, 0.1 mmol), NaOH (1 M, 0.5 mL) and THF (0.5 mL) to afford the desired product as a white solid (39 mg, 92%).

ν_{\max} (neat): 3270, 3034, 1694, 1591, 1543, 1519 cm⁻¹.

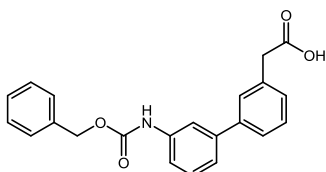
¹H NMR (400 MHz, CDCl₃): δ 7.63 (s, 1H), 7.55 (d, *J* = 8.2 Hz, 2H), 7.45 – 7.27 (m, 10H), 6.76 (s, 1H), 5.23 (s, 2H), 3.71 (s, 2H). OH not observed.

Experimental

^{13}C NMR (151 MHz, CDCl_3): δ 176.3, 141.7, 139.8, 138.2, 136.0, 132.6, 129.8, 129.5, 128.7, 128.4 (2C) 127.4, 122.4, 67.2, 40.5. Three carbons not observed/coincident.

HRMS: exact mass calculated for $[\text{M}+\text{H}^+]$ ($\text{C}_{22}\text{H}_{20}\text{NO}_4$) requires m/z 362.1392, found m/z 362.1390.

Compound 25: 2-(3'-(((benzyloxy)carbonyl)amino)-[1,1'-biphenyl]-3-yl)acetic acid



2-(3'-(((benzyloxy)carbonyl)amino)-[1,1'-biphenyl]-3-yl)acetic acid
Chemical Formula: $\text{C}_{22}\text{H}_{19}\text{NO}_4$
Molecular Weight: 361.3970

Prepared according to General Procedure E using ethyl 2-(3'-(((benzyloxy)carbonyl)amino)-[1,1'-biphenyl]-3-yl)acetate **52** (48.1 mg, 1.24 mmol), NaOH (0.5 mL), and THF (0.5 mL) to afford the desired product as an off white solid (34.5 mg, 77%).

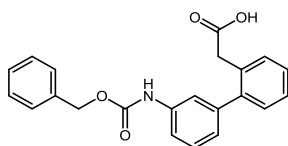
ν_{max} (neat): 1697, 1604, 1531, 1508 cm^{-1} .

^1H NMR (500 MHz, CDCl_3): δ 7.63 (s, 1H), 7.50 (s, 2H), 7.45 – 7.28 (m, 11H), 6.76 (s, 1H), 5.23 (s, 2H), 3.73 (s, 2H).

^{13}C NMR (151 MHz, CDCl_3): δ 176.7, 141.8, 141.1, 138.2, 136.0, 133.9, 129.5, 129.0, 128.7, 128.5, 128.4, 128.3 (2C), 126.2, 122.5, 67.2, 41.0. Three carbons not observed/coincident.

HRMS: exact mass calculated for $[\text{M}+\text{H}^+]$ ($\text{C}_{22}\text{H}_{20}\text{NO}_4$) requires m/z 360.1241, found m/z 360.1240.

Compound 26: 2-(3'-(((Benzyloxy)carbonyl)amino)-[1,1'-biphenyl]-2-yl)acetic acid



2-(3'-(((benzyloxy)carbonyl)amino)-[1,1'-biphenyl]-2-yl)acetic acid
 Chemical Formula: C₂₂H₁₉NO₄
 Molecular Weight: 361.3970

Prepared according to General Procedure E using ethyl 2-(3'-(((benzyloxy)carbonyl)amino)-[1,1'-biphenyl]-2-yl)acetate **53** (46.1 mg 0.18 mmol), NaOH (0.5 mL), and THF (0.5 mL) to afford the desired product as a brown solid (39.3 mg, 92 %).

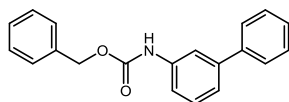
ν_{max} (neat): 1701, 1535, 1408 cm⁻¹.

¹H NMR (400 MHz, CDCl₃): δ 7.43 – 7.28 (m, 12H), 7.02 – 6.98 (m, 1H), 5.17 (s, 2H), 3.61 (s, 2H). NH and OH not observed.

¹³C NMR (101 MHz, CDCl₃): δ 177.0, 141.6, 141.3, 137.3, 135.5, 130.8, 130.0, 129.7, 128.5, 128.1, 127.9, 127.3, 126.9, 124.0, 66.7, 38.1. Three carbons not observed/coincident.

HRMS: exact mass calculated for [M+H⁺] (C₂₂H₂₀NO₄) requires *m/z* 360.1241, found *m/z* 360.1240.

Compound 27: Benzyl [1,1'-biphenyl]-3-ylcarbamate



Benzyl [1,1'-biphenyl]-3-ylcarbamate
 Chemical Formula: C₂₀H₁₇NO₂
 Molecular Weight: 303.3610

Prepared according to General Procedure D using phenylboronic acid (366 mg, 3.00 mmol, 3 equiv.), benzyl-(3-bromophenyl)acetate **39** (306.2 mg, 1.00 mmol, 1 equiv.), K₃PO₄ (637 mg, 3.00 mmol, 3 equiv.), 2'(dimethylamino)-2-biphenylpalladium(II)chloride dinorbonylphosphine complex (56 mg, 0.01 mmol, 10 mol%), 1,4-dioxane (2.4 mL, 0.24 M), and H₂O (0.6 mL, 0.06 M) to afford the desired product as a yellow oil (220 mg, 73%).

ν_{max} (neat): 1708, 1597, 1539, 1496 cm⁻¹.

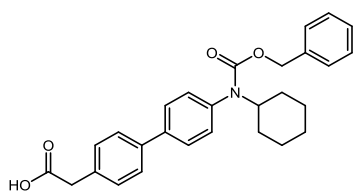
Experimental

^1H NMR (400 MHz, CDCl_3): δ 7.65 (s, 1H), 7.58 (d, $J = 7.2$ Hz, 2H), 7.47 – 7.28 (m, 11H), 6.73 (s, 1H), 5.23 (s, 2H).

^{13}C NMR (101 MHz, CDCl_3): δ 166.0, 141.8, 140.2, 137.7, 135.5, 128.9, 128.2 (2C), 127.9, 127.8, 127.0, 126.7, 121.9, 117.1, 117.0, 66.6.

HRMS: exact mass calculated for $[\text{M}+\text{H}^+]$ ($\text{C}_{20}\text{H}_{18}\text{NO}_2$) requires m/z 304.1335, found m/z 304.1332.

Compound 28: 2-(4'-(((Benzyloxy)carbonyl)(cyclohexyl)amino)-[1,1'-biphenyl]-4-yl)acetic acid



2-(4'-(((benzyloxy)carbonyl)(cyclohexyl)amino)-[1,1'-biphenyl]-4-yl)acetic acid
Chemical Formula: $\text{C}_{28}\text{H}_{29}\text{NO}_4$
Molecular Weight: 443.5430

Prepared according to General Procedure E ethyl 2-(4'-(((benzyloxy)carbonyl)(cyclohexyl)amino)-[1,1'-biphenyl]-4-yl)acetate] **65** (50 mg, 1.06 mmol), NaOH (0.5 mL), and THF (0.5 mL) to afford the desired product as a yellow oil (40 mg, 86%).

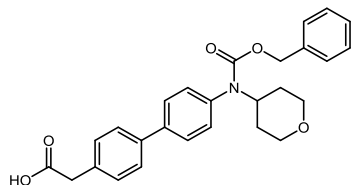
ν_{max} (neat): 2930, 1699, 1550, 1403, 1313 cm^{-1} .

^1H NMR (400 MHz, CDCl_3) δ 7.59 (m, 4H), 7.40 (d, $J = 8.1$ Hz, 2H), 7.36 – 7.26 (m, 3H), 7.20 (m, 4H), 5.15 (s, 2H), 4.22 (m, 1H), 3.73 (s, 2H), 1.94 (d, $J = 11.1$ Hz, 2H), 1.78 (d, $J = 13.1$ Hz, 2H), 1.60 (d, $J = 12.9$ Hz, 1H), 1.50 – 1.32 (m, 2H), 1.31 – 1.14 (m, 3H). OH not observed.

^{13}C NMR (101 MHz, CDCl_3): δ 176.4, 155.1, 139.3, 139.0, 137.4, 136.5, 132.1, 129.8, 129.4, 127.8, 127.1, 126.9, 126.8, 115.1, 66.4, 56.7, 40.2, 31.5, 25.4, 24.8.

HRMS: exact mass calculated for $[\text{M}+\text{H}^+]$ ($\text{C}_{28}\text{H}_{30}\text{NO}_4$) requires m/z 444.2175, found m/z 444.2168.

Compound 29: 2-(4'-(((benzyloxy)carbonyl)(tetrahydro-2H-pyran-4-yl)amino)-[1,1'-biphenyl]-4-yl)acetic acid



2-(4'-(((benzyloxy)carbonyl)(tetrahydro-2H-pyran-4-yl)amino)-[1,1'-biphenyl]-4-yl)acetic acid
 Chemical Formula: C₂₇H₂₇NO₅
 Molecular Weight: 445.5150

Prepared according to General Procedure E using methyl 2-(4'-(((benzyloxy)carbonyl)(tetrahydro-2H-pyran-4-yl)amino)-[1,1'-biphenyl]-4-yl)acetate **66** (160 mg, 0.35 mmol), NaOH (1.6 mL), THF (1.6 mL) to afford the desired product as a brown oil (140 mg, 90%).

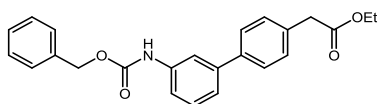
ν_{\max} (neat): 1700, 1693, 1494, 1375 cm⁻¹.

¹H NMR (400 MHz, CDCl₃) δ 7.61 – 7.53 (m, 4H), 7.38 (d, *J* = 8.2 Hz, 2H), 7.28 (d, *J* = 7.2 Hz, 2H), 7.19 (s, 1H), 7.14 (d, *J* = 8.3 Hz, 1H), 5.14 (s, 2H), 4.47 (m, 1H), 3.97 (dd, *J* = 11.3, 4.3 Hz, 2H), 3.71 (s, 2H), 3.47 (dd, *J* = 11.7, 10.7 Hz, 2H), 1.81 (dd, *J* = 12.3, 2.2 Hz, 2H), 1.59 (m, 2H). OH not observed.

¹³C NMR (101 MHz, CDCl₃): δ 176.3, 155.0, 139.8, 138.9, 136.7, 136.3, 132.3, 129.8, 129.4, 127.9, 127.3, 127.0, 126.9, 126.8, 66.9, 66.6, 53.6, 40.1, 31.3.

HRMS: exact mass calculated for [M+H⁺] (C₂₇H₂₈NO₅) requires *m/z* 446.1962, found *m/z* 446.1956.

Compound 38: Ethyl 2-(3'-(((benzyloxy)carbonyl)amino)-[1,1'-biphenyl]-4-yl)acetate



ethyl 2-(3'-(((benzyloxy)carbonyl)amino)-[1,1'-biphenyl]-4-yl)acetate
 Chemical Formula: C₂₄H₂₃NO₄
 Molecular Weight: 389.4510

Prepared according to General Procedure D using ethyl 2-(4-(4,4,5,5-tetramethyl-1,3,2-dioxaborolan-2-yl)phenyl)acetate **40** (650 mg, 2.24 mmol, 2.2 equiv.), 2'-(dimethylamino)-2-biphenyl-palladium(II)chloride dinorbornylphosphine complex (28 mg, 0.05 mmol, 10 mol%), K₃PO₄ (630 mg, 3.00 mmol, 3 equiv.), and benzyl (3-

Experimental

bromophenyl)carbamate **39** (300 mg, 1.00 mmol, 1 equiv.), 1,4-dioxane (2.4 mL) and H₂O (0.6 mL) to afford the desired product as a yellow oil (358 mg, 92%).

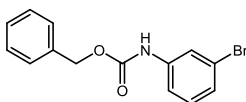
ν_{\max} (neat): 3327, 1729, 1717, 1608, 1594, 1545 cm⁻¹.

¹H NMR (400 MHz, CDCl₃): δ 7.64 (s, 1H), 7.54 (dd, J = 8.2, 2.5 Hz, 4H), 7.46 – 7.25 (m, 8H), 6.77 (s, 1H), 5.22 (s, 2H), 4.18 (q, J = 7.1 Hz, 2H), 3.65 (s, 2H), 1.27 (t, J = 7.1 Hz, 3H).

¹³C NMR (101 MHz, CDCl₃): δ 171.6, 153.3, 141.8, 139.5, 138.2, 136.0, 133.5, 133.2, 129.7, 129.4, 128.6, 128.4, 128.3, 127.3, 127.2, 122.3, 67.1, 60.9, 41.1, 14.2.

HRMS: exact mass calculated for [M+H⁺] (C₂₄H₂₄NO₄) requires m/z 390.1701, found m/z 390.1700.

Compound 39: Benzyl(3-bromophenyl)carbamate



Benzyl (3-bromophenyl)carbamate
Chemical Formula: C₁₄H₁₂BrNO₂
Molecular Weight: 306.1590

Prepared according to General Procedure A using 3-bromoaniline (6.3 mL, 58.1 mmol, 1 equiv.), K₂CO₃ (8.8 g, 63.9 mmol, 1.1 equiv.), 2-MeTHF (175 mL), and CbzCl (10 mL, 70 mmol, 1.2 equiv.) to afford the desired product as a white solid (16.9 g, 95%).

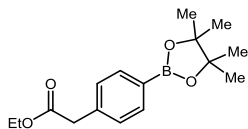
ν_{\max} (neat): 1703, 1591, 1529, 1421 cm⁻¹.

¹H NMR (400 MHz, CDCl₃): δ 7.66 (s, 1H), 7.45 – 7.11 (m, 8H), 6.71 (s, 1H), 5.20 (s, 2H).

¹³C NMR (101 MHz, CDCl₃): δ 152.6, 138.6, 135.3, 129.8, 128.2, 128.0, 127.9, 126.0, 122.3, 121.0, 116.6, 66.8.

HRMS: exact mass calculated for [M+H⁺] (C₁₄H₁₃BrNO₂) requires m/z 306.0124, 308.0104 found m/z 306.0126, 308.0103.

Compound 40: Ethyl 2-(4-(4,4,5,5-tetramethyl-1,3,2-dioxaborolane-2-yl)phenyl)acetate



Ethyl 2-(4-(4,4,5,5-tetramethyl-1,3,2-dioxaborolan-2-yl)phenyl)acetate
 Chemical Formula: C₁₆H₂₃BO₄
 Molecular Weight: 290.16

Prepared using General Procedure C using ethyl(4-bromophenyl)-acetate **43** (4.05 g, 16.7 mmol, 1 equiv.), bis-(pinacolato)diborane (4.20 g, 16.5 mmol, 1.01 equiv.), KOAc (4.82 g, 49.14 mmol, 3 equiv.), Pd(dppf)Cl₂ (0.4 g, 0.5 mmol, 0.03 equiv), and 1,4-dioxane (88 mL) to give the desired compound as an amorphous white solid (1.74 g, 73%).

ν_{\max} (neat): 1734, 1612, 1469, 1446, 1398 cm⁻¹.

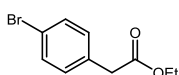
¹H NMR (400 MHz, CDCl₃): δ 7.77 (d, 2H, *J* = 8.0 Hz), 7.30 (d, 2H, *J* = 8.0 Hz), 4.14 (q, 2H, *J* = 7.1 Hz), 3.62 (s, 2H), 1.34 (s, 12H), 1.23 (t, 3H, *J* = 7.1 Hz).

¹³C NMR (101 MHz, CDCl₃): δ 170.8, 136.8, 134.5, 128.1, 83.3, 60.4, 41.2, 24.4, 13.6. One signal absent (C-B).⁹⁴

¹¹B NMR (128 MHz, CDCl₃): δ 30.48.

HRMS: exact mass calculated for [M+H⁺] (C₁₆H₂₄BO₄) requires *m/z* 290.1806, found *m/z* 290.1803.

Compound 43: Ethyl 2-(4-bromophenyl)acetate⁹⁵



Ethyl 2-(4-bromophenyl)acetate
 Chemical Formula: C₁₀H₁₁BrO₂
 Molecular Weight: 243.10

Prepared according to General Procedure B using 4-bromophenylacetic acid (2.68 g, 12.46 mmol, 1 equiv.), EtOH (50 mL), and SOCl₂ (1.2 mL, 16.54 mmol, 1.3 equiv.) to give the desired compound as a colourless oil (2.98 g, 98%).

ν_{\max} (neat): 1730, 1487, 1406, 1367 cm⁻¹.

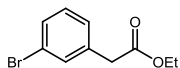
¹H NMR (400 MHz, CDCl₃): δ 7.43 (d, 2H, *J* = 8.4 Hz), 7.15 (d, 2H, *J* = 8.4 Hz), 4.14 (q, 2H, *J* = 7.1 Hz), 3.55 (s, 2H), 1.24 (t, 3H, *J* = 7.1 Hz).

¹³C NMR (101 MHz, CDCl₃): δ 170.6, 132.6, 131.1, 130.5, 120.6, 60.5, 40.3, 13.7.

Experimental

HRMS: exact mass calculated for $[M+H^+]$ ($C_{10}H_{11}^{79}BrO_2$) requires m/z 243.0015, found m/z 243.0017 and ($C_{10}H_{11}^{81}BrO_2$) requires m/z 244.9995, found m/z 244.9996

Compound 48: Ethyl 2-(3-bromophenyl)acetate



Ethyl 2-(3-bromophenyl)acetate
Chemical Formula: $C_{10}H_{11}BrO_2$
Molecular Weight: 243.10

Prepared according to General Procedure B using 3-bromophenylacetic acid (10.8 g, 50 mmol, 1 equiv.), EtOH (150 mL), and $SOCl_2$ (4.8 mL, 65 mmol, 1.3 equiv.) to give the desired compound as a colourless oil (12 g, 94%).

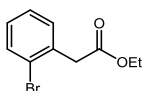
ν_{max} (neat): 1730, 1595, 1568, 1473 cm^{-1} .

1H NMR (400 MHz, $CDCl_3$): δ 7.47–7.35 (m, 2H), 7.27–7.13 (m, 2H), 4.15 (q, 2H, $J = 7.2$ Hz), 3.57 (s, 2H), 1.25 (t, 3H, $J = 7.1$ Hz).

^{13}C NMR (101 MHz, $CDCl_3$): δ 170.9, 136.3, 132.3, 130.2, 130.0, 128.0, 122.5, 61.1, 40.9, 14.2.

HRMS: exact mass calculated for $[M+H^+]$ ($C_{10}H_{11}^{79}BrO_2$) requires m/z 243.0015, found m/z 243.0017 and ($C_{10}H_{11}^{81}BrO_2$) requires m/z 244.9995, found m/z 244.9996

Compound 49: Ethyl 2-(2-bromophenyl)acetate⁹⁶



Ethyl 2-(2-bromophenyl)acetate
Chemical Formula: $C_{10}H_{11}BrO_2$
Molecular Weight: 243.10

Prepared according to General Procedure B using 2-bromophenylacetic acid (5.4 g, 25 mmol, 1 equiv.), EtOH (75 mL), and $SOCl_2$ (2.4 mL, 33 mmol, 1.3 equiv.) to give the desired compound as a colourless oil (5.8 g, 95%).

ν_{max} (neat): 1730, 1471, 1440, 1334 cm^{-1} .

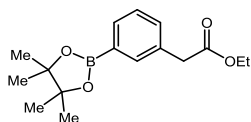
1H NMR (400 MHz, $CDCl_3$): δ 7.54 (d, 1H, $J = 8.5$ Hz), 7.28 – 7.20 (m, 2H), 7.15 – 7.06 (m, 1H), 4.16 (q, 2H, $J = 7.1$ Hz), 3.76 (s, 2H), 1.24 (t, 3H, $J = 7.1$ Hz).

^{13}C NMR (101 MHz, $CDCl_3$): δ 170.1, 133.9, 132.3, 131.0, 128.4, 127.0, 124.5, 60.6, 41.2, 13.7.

Experimental

HRMS: exact mass calculated for $[M+H^+]$ ($C_{10}H_{11}^{79}BrO_2$) requires m/z 243.0015, found m/z 243.0017 and ($C_{10}H_{11}^{81}BrO_2$) requires m/z 244.9995, found m/z 244.9993

Compound 50: Ethyl 2-(3-(4,4,5,5-tetramethyl-1,3,2-dioxaborolane-2-yl)phenyl)acetate



Ethyl 2-(3-(4,4,5,5-tetramethyl-1,3,2-dioxaborolan-2-yl)phenyl)acetate
Chemical Formula: $C_{16}H_{23}BO_4$
Molecular Weight: 290.16

Prepared according to General Procedure C using ethyl(3-bromophenyl)-acetate **48** (4.04 g, 16.61 mmol, 1 equiv.), bis-(pinacolato)diborane (4.30 g, 16.75 mmol, 1.01 equiv.), KOAc (4.84 g, 49.31 mmol, 3 equiv), Pd(dppf)Cl₂ (0.20 g, 0.24 mmol, 0.03 equiv), and 1,4-dioxane (80 mL) to give the desired compound as an amorphous white solid (2.60 g, 54%).

ν_{max} (neat): 1730, 1429, 1357, 1323 cm^{-1} .

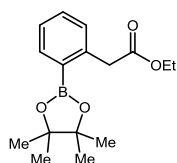
¹H NMR (400 MHz, CDCl₃): δ 7.74 (d, 2H, $J = 7.3$ Hz), 7.43–7.32 (m, 2H), 4.15 (q, 2H, $J = 7.1$ Hz), 3.63 (s, 2H), 1.35 (s, 12H), 1.25 (t, 3H, $J = 7.1$ Hz).

¹³C NMR (101 MHz, CDCl₃): δ 171.0, 135.1, 133.0, 133.0, 131.6, 127.4, 83.3, 60.2, 40.7, 24.4, 13.7. One signal absent (C-B).

¹¹B NMR (128 MHz, CDCl₃): δ 30.58.

HRMS: exact mass calculated for $[M+H^+]$ ($C_{16}H_{24}BO_4$) requires m/z 290.1806, found m/z 290.1803.

Compound 51: Ethyl 2-(2-(4,4,5,5-tetramethyl-1,3,2-dioxaborolane-2-yl)phenyl)acetate



Ethyl 2-(2-(4,4,5,5-tetramethyl-1,3,2-dioxaborolan-2-yl)phenyl)acetate
Chemical Formula: $C_{16}H_{23}BO_4$
Molecular Weight: 290.16

Prepared according to General Procedure C using ethyl(2-bromophenyl)-acetate **49** (4.02 g, 8.32 mmol, 1 equiv.), bis-(pinacolato)diborane (2.11 g, 8.31 mmol, 1.01 equiv.), KOAc (2.41 g, 24.63 mmol, 3 equiv.), Pd(dppf)Cl₂ (0.20 g, 0.25 mmol, 0.03

Experimental

equiv.), and 1,4-dioxane (40 mL) to give the desired compound as an amorphous white solid (0.80 g, 32%).

ν_{\max} (neat): 1732, 1600, 1492, 1442, 1369 cm^{-1} .

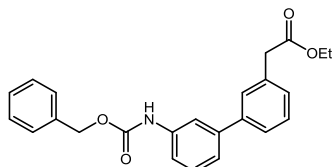
^1H NMR (400 MHz, CDCl_3): δ 7.84 (dd, 1H, $J = 7.4, 1.3$ Hz), 7.38 (td, 1H, $J = 7.5, 1.6$ Hz), 7.30 – 7.23 (m, 1H), 7.20 (d, 1H, $J = 7.6$ Hz), 4.13 (q, 2H, $J = 7.1$ Hz), 3.97 (s, 2H), 1.33 (s, 12H), 1.27 (s, 3H).

^{13}C NMR (101 MHz, CDCl_3): δ 171.9, 140.0, 135.6, 130.4, 128.7, 126.5, 83.0, 60.0, 40.6, 24.3, 13.8

^{11}B NMR (128 MHz, CDCl_3): δ 30.80.

HRMS: exact mass calculated for $[\text{M}+\text{H}^+]$ ($\text{C}_{16}\text{H}_{24}\text{BO}_4$) requires m/z 290.1806 found m/z 290.1802.

Compound 52: Ethyl 2-(3'-(((benzyloxy)carbonyl)amino)-[1,1'-biphenyl]-3-yl)acetate



Ethyl 2-(3'-(((benzyloxy)carbonyl)amino)-[1,1'-biphenyl]-3-yl)acetate
Chemical Formula: $\text{C}_{24}\text{H}_{23}\text{NO}_4$
Molecular Weight: 389.4510

Prepared according to General Procedure D using ethyl 2-(3-(4,4,5,5-tetramethyl-1,3,2-dioxaborolane-2-yl)phenyl)acetate **50** (646.2 mg, 2.2 mmol, 2.2 equiv.), benzyl-(3-bromophenyl)acetate **39** (307 mg, 1.00 mmol, 1 equiv.), K_3PO_4 (637 mg, 3.0 mmol, 3 equiv.), 2'-(dimethylamino)-2-biphenyl-palladium(II)chloride dinorbornylphosphine complex (56.7 mg, 0.01 mmol, 10 mol%), 1,4-dioxane (2.4 mL), and H_2O (0.6 mL) to afford the desired product as a yellow oil (357.8 mg, 92%).

ν_{\max} (neat): 1732, 1604, 1546, 1496, 1408 cm^{-1} .

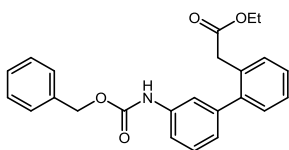
^1H NMR (400 MHz, CDCl_3): δ 7.63 (s, 1H), 7.51 – 7.26 (m 11H), 6.78 (s, 1H), 5.23 (s, 2H), 4.17 (q, $J = 7.1$ Hz, 2H), 3.67 (s, 2H), 1.27 (t, 3H). NH not observed.

Experimental

^{13}C NMR (101 MHz, CDCl_3): δ 171.0, 152.9, 141.5, 140.5, 137.7, 135.6, 134.1, 128.9, 128.5, 128.1, 127.9, 127.8, 127.7 (2C), 125.5, 122.0, 117.2, 117.1, 66.6, 60.4, 41.0, 13.7.

HRMS: exact mass calculated for $[\text{M}+\text{H}^+]$ ($\text{C}_{24}\text{H}_{24}\text{NO}_4$) requires m/z 390.1701, found m/z 390.1700.

Compound 53: Ethyl 2-(3'-(((benzyloxy)carbonyl)amino)-[1,1'-biphenyl]-2-yl)acetate



Ethyl 2-(3'-(((benzyloxy)carbonyl)amino)-[1,1'-biphenyl]-2-yl)acetate
Chemical Formula: $\text{C}_{24}\text{H}_{23}\text{NO}_4$
Molecular Weight: 389.4510

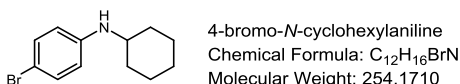
Prepared according to General Procedure D using ethyl 2-(3-(4,4,5,5-tetramethyl-1,3,2-dioxaborolane-2-yl)phenyl)acetate **51** (547.2 mg, 1.9 mmol, 1.9 equiv.), benzyl-(3-bromophenyl)acetate **39** (305.7 mg, 1.0 mmol, 1 equiv.), K_3PO_4 (686.0 mg, 3.2 mmol, 3.2 equiv.), 2'-(dimethylamino)-2-biphenyl-palladium(II)chloride dinorbornylphosphine complex (56.1 mg, 0.01 mmol, 10 mol%), 1,4-dioxane (2.4 mL), and H_2O (0.6 mL) to afford the desired product as a yellow oil (212.4 mg, 55%).

ν_{max} (neat): 1732, 1712, 1589, 1544, 1539 cm^{-1} .

^1H NMR (400 MHz, CDCl_3): δ 7.47 – 7.28 (m, 12H), 7.04 – 7.00 (m, 1H), 6.68 (s, 1H), 5.20 (s, 2H), 4.08 (q, $J = 7.1$ Hz, 2H), 3.58 (s, 2H), 1.18 (t, $J = 7.1$ Hz, 3H).

^{13}C NMR (101 MHz, CDCl_3): δ 175.6, 171.4, 141.6, 141.4, 131.5, 131.4, 129.8, 129.6, 128.4, 128.1, 127.9, 127.8, 127.2, 126.6, 124.0, 124.0, 66.6, 60.2, 38.4, 13.6.
Two carbons not observed/coincident.

HRMS: exact mass calculated for $[\text{M}+\text{H}^+]$ ($\text{C}_{24}\text{H}_{24}\text{NO}_4$) requires m/z 390.1701, found m/z 390.1700.

Compound 58: 4-bromo-*N*-cyclohexylaniline

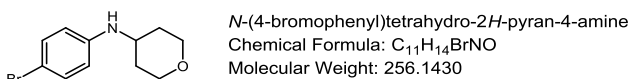
Prepared according to General Procedure D using 4-bromoaniline (1.0 g, 5.8 mmol, 1 equiv.), cyclohexanone (0.8 mL, 7.6 mmol, 1.3 equiv.), AcOH (0.5 mL), 2-MeTHF (25 mL), and NaBH(OAc)₃ (1.8 g, 8.7 mmol, 1.5 equiv.) to afford the desired product as a white solid (1.5 g, 93%).

ν_{\max} (neat): 3450, 2926, 2850, 1591, 1494, 1351 cm⁻¹.

¹H NMR (400 MHz, CDCl₃): δ 7.22 (d, J = 8.8 Hz, 2H), 6.49 (d, J = 8.7 Hz, 2H), 3.23 – 3.16 (m, 1H), 2.03 (m, 2H), 1.80 – 1.71 (m, 2H), 1.69 – 1.61 (m, 1H), 1.54 (s, 1H), 1.42 – 1.08 (m, 5H).

¹³C NMR (101 MHz, CDCl₃): δ 145.9, 131.4, 114.1, 107.6, 51.3, 32.8, 25.4, 24.4.

HRMS: exact mass calculated for [M+H⁺] (C₁₂H₁₇⁷⁹BrN) requires m/z 254.0539, found 254.0542 [M+H⁺] (C₁₂H₁₇⁸¹BrN) requires m/z 256.0518, found m/z 256.0518.

Compound 59: *N*-(4-bromophenyl)tetrahydro-2*H*-pyran-4-amine

Prepared according to General Procedure G using 4-bromoaniline (1.0 g, 5.8 mmol, 1 equiv.), tetrahydro-4*H*-pyran-one (0.7 mL, 7.6 mmol, 1.3 equiv.), AcOH (0.5 mL), and NaBH(OAc)₃ (1.8 g, 8.7 mmol, 1.5 equiv.) to afford the desired product as an off white solid (1.5 g, 98%).

ν_{\max} (neat): 3336, 2927, 2833, 1716, 1591, 1512, 1485 cm⁻¹.

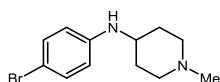
¹H NMR (400 MHz, CDCl₃): δ 7.23 (d, J = 8.9 Hz, 2H), 6.48 (d, J = 8.8 Hz, 2H), 4.03 – 3.94 (m, 2H), 3.54 – 3.39 (m, 4H), 2.00 (d, J = 11.5 Hz, 2H), 1.40-1.50 (m, 2H).

¹³C NMR (101 MHz, CDCl₃): δ 145.2, 131.5, 114.4, 108.4, 66.3, 48.7, 32.9.

Experimental

HRMS: exact mass calculated for $[M+H]^+$ ($C_{11}H_{15}^{79}BrNO$) requires m/z 256.0332, found m/z 256.0335 $[M+H]^+$ ($C_{11}H_{15}^{81}BrNO$) requires m/z 258.0311, found m/z 258.0310.

Compound 60: *N*-(4-bromophenyl)-1-methylpiperidine-4-amine



N-(4-bromophenyl)-1-methylpiperidin-4-amine
Chemical Formula: $C_{12}H_{17}BrN_2$
Molecular Weight: 269.1860

Prepared according to General Procedure G using 4-bromoaniline (1.0 g, 5.8 mmol, 1 equiv.), 1-methylpiperidin-4-one (0.9 mL, 7.6 mmol, 1.3 equiv.), AcOH (0.5 mL), and $NaBH(OAc)_3$ (1.8 g, 8.7 mmol, 1.5 equiv.) to give the desired compound as an amorphous yellow solid (1.2 g, 76%).

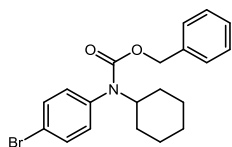
ν_{max} (neat): 3294, 2931, 1589, 1516, 1487 cm^{-1} .

1H NMR (400 MHz, $CDCl_3$): δ 7.28–7.15 (m, 2H), 6.61 – 6.53 (m, 1H), 6.50–6.43 (m, 1H), 3.38–3.29 (m, 1H), 3.10 (d, $J = 12.1$ Hz, 2H), 2.48 (s, 3H), 2.44 (d, $J = 10.5$ Hz, 2H), 2.20 – 2.06 (m, 2H), 1.82–1.61 (m, 2H). N-H signal absent.

^{13}C NMR (101 MHz, $CDCl_3$): δ 145.0, 131.6, 116.2, 114.5, 53.1, 43.9, 29.7. One carbon absent/not observed.

HRMS: exact mass calculated for $[M+H]^+$ ($C_{12}H_{17}^{79}BrN_2$) requires m/z 269.0648, found m/z 269.0647, and ($C_{12}H_{17}^{81}BrN_2$) requires m/z 271.0627, found m/z 271.0622

Compound 61: Benzyl(4-bromophenyl)(cyclohexyl)carbamate



benzyl (4-bromophenyl)(cyclohexyl)carbamate
Chemical Formula: $C_{20}H_{22}BrNO_2$
Molecular Weight: 388.3050

Prepared according to General Procedure A using 4-bromo-*N*-cyclohexylaniline **58** (504.1 mg, 1.97 mmol, 1 equiv.), K_2CO_3 (301.4 mg, 2.2 mmol, 1.1 equiv.), DCE (9 mL), H_2O (0.05 mL), and CbzCl (0.3 mL, 2.2 mmol, 1.1 equiv.) to afford the desired product as a white solid (223.5 mg, 30%).

ν_{max} (neat): 1597, 1489, 1452, 1396 cm^{-1} .

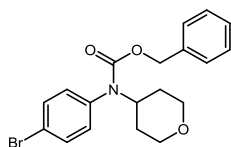
Experimental

^1H NMR (400 MHz, CDCl_3) δ 7.48 (d, $J = 8.6$ Hz, 2H), 7.29 (m, 3H), 7.18 (m, 2H), 6.96 (d, $J = 8.6$ Hz, 2H), 5.09 (s, 2H), 4.22 – 4.10 (m, 1H), 1.85 (dd, $J = 12.8, 1.6$ Hz, 2H), 1.73 (dd, $J = 12.3, 1.6$ Hz, 2H), 1.57 (m, 1H), 1.33 (app. pent, $J = 13.0$ Hz, 2H), 1.14 – 1.05 (m, 2H), 0.97 – 0.86 (m, 1H).

^{13}C NMR (101 MHz, CDCl_3): δ 154.7, 137.2, 136.3, 131.4, 131.3, 127.9, 127.3, 126.8, 120.9, 66.4, 56.4, 31.5, 25.3, 24.8.

HRMS: exact mass calculated for $[\text{M}+\text{H}^+]$ ($\text{C}_{20}\text{H}_{23}^{79}\text{BrNO}_2$) requires m/z 388.0907, found m/z 388.0904 $[\text{M}+\text{H}^+]$ ($\text{C}_{20}\text{H}_{23}^{81}\text{BrNO}_2$) requires m/z 390.0886, found m/z 390.0879.

Compound 62: Benzyl(4-bromophenyl)(tetrahydro-2H-pyran-4-yl)carbamate



Benzyl (4-bromophenyl)(tetrahydro-2H-pyran-4-yl)carbamate
Chemical Formula: $\text{C}_{19}\text{H}_{20}\text{BrNO}_3$
Molecular Weight: 390.2770

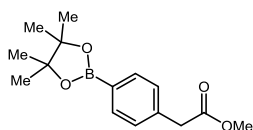
Prepared according to General Procedure G using 4-bromophenyl)(tetrahydro-2H-pyran-4-amine **59** (510 mg, 1.97 mmol, 1 equiv.), K_2CO_3 (290 mg, 2.14 mmol, 1.1 equiv.), DCE (9 mL), H_2O (0.05 mL), and CbzCl (0.3 mL, 2.15 mmol, 1.1 equiv.) to afford the desired product as an orange solid (448 mg, 60%).

ν_{max} (neat): 2970, 1732, 1502, 1473, 1413 cm^{-1} .

^1H NMR (400 MHz, CDCl_3): δ 7.50 (m, 2H), 7.38 – 7.28 (m, 3H), 7.17 (s, 2H), 6.95 (m, 2H), 5.09 (s, 2H), 4.40 (m, 1H), 3.94 (dd, $J = 11.5, 4.6$ Hz, 2H), 3.44 (t, $J = 12.7$ Hz, 2H), 1.77 – 1.73 (m, 2H), 1.51–1.42 (m, 2H).

^{13}C NMR (101 MHz, CDCl_3): δ 154.6, 136.7, 136.1, 131.6, 131.2, 127.9, 127.4, 126.9, 121.3, 66.8, 66.7, 53.6, 31.3.

HRMS: exact mass calculated for $[\text{M}+\text{H}^+]$ ($\text{C}_{19}\text{H}_{21}^{79}\text{BrNO}_3$) requires m/z 390.0699, found m/z 390.0699 $[\text{M}+\text{H}^+]$ ($\text{C}_{19}\text{H}_{21}^{81}\text{BrNO}_3$) requires m/z 392.0679, found m/z 392.0677.

Compound 64: Methyl 2-(4-(4,4,5,5-tetramethyl-1,3,2-dioxaborolan-2-yl)phenyl)acetate

methyl 2-(4-(4,4,5,5-tetramethyl-1,3,2-dioxaborolan-2-yl)phenyl)acetate
 Chemical Formula: C₁₅H₂₁BO₄
 Molecular Weight: 276.14

Prepared according to General Procedure C using methyl 2-(4-bromophenyl)acetate (3.0 g, 13.2 mmol, 1 equiv.), bis(pinacolato)diboron (3.38 g, 13.3 mmol, 1.01 equiv.), and KOAc (3.87 g, 39.5 mmol, 3 equiv.) in 1,4-dioxane (65 mL), to afford the desired product as an off-white solid (2.74 g, 75%).

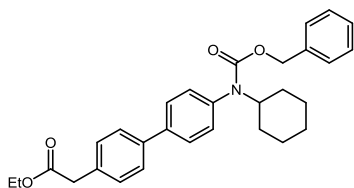
ν_{\max} (film): 2978, 1737, 1616, 1519, 1479 cm⁻¹.

¹H NMR (CDCl₃, 400 MHz): δ 7.80 (d, *J* = 7.8 Hz, 2 H), 7.32 (d, *J* = 7.8 Hz, 2 H), 3.71 (s, 3 H), 3.67 (s, 2 H), 1.37 (s, 12 H).

¹³C NMR (CDCl₃, 126 MHz): δ 171.7, 137.1, 135.1, 128.6, 83.8, 52.0, 41.4, 24.8.

¹B NMR (CDCl₃, 128 MHz): δ 31.2.

HRMS: exact mass calculated for [M+Na⁺] ((C₁₅H₂₁BO₄Na) requires *m/z* 299.1425, found *m/z* 299.1423.

Compound 65: Ethyl 2-(4'-(((benzyloxy)carbonyl)(cyclohexyl)amino)-[1,1'-biphenyl]-4-yl)acetate

Ethyl 2-(4'-(((benzyloxy)carbonyl)(cyclohexyl)amino)-[1,1'-biphenyl]-4-yl)acetate
 Chemical Formula: C₃₀H₃₃NO₄
 Molecular Weight: 471.5970

Prepared according to General Procedure D using ethyl 2-(4-(4,4,5,5-tetramethyl-1,3,2-dioxaborolan-2-yl)phenyl)acetate **40** (300 mg, 1.03 mmol, 2 equiv.), benzyl(4-bromophenyl)(cyclohexyl)carbamate **61** (200 mg, 0.51 mmol, 1 equiv.), K₃PO₄ (330 mg, 1.55 mmol, 3 equiv.), 2'-(dimethylamino)-2-biphenyl-palladium(II)chloride dinorbornylphosphine complex (28.9 mg, 0.01 mmol, 10 mol %), 1,4-dioxane (2.4 mL), and H₂O (0.6 mL) to afford the desired product as a yellow oil (170 mg, 70%).

ν_{\max} (neat): 1733, 1695, 1497, 1398, 1301 cm⁻¹.

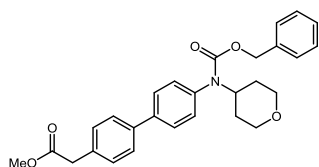
Experimental

^1H NMR (400 MHz, CDCl_3): δ 7.61 – 7.53 (m, 5H), 7.39 – 7.30 (m, 4H), 7.22 – 7.16 (m, 4H), 5.14 (s, 2H), 4.20 (q, $J = 7.1$ Hz, 2H), 3.68 (s, 2H), 1.93 (d, $J = 11.1$ Hz, 2H), 1.77 (d, $J = 13.3$ Hz, 2H), 1.45 – 1.15 (m, 10H).

^{13}C NMR (101 MHz, CDCl_3): δ 171.0, 154.9, 139.4, 138.7, 136.6, 132.9, 129.8, 129.2, 129.2, 127.8, 127.1, 126.8, 126.7, 66.3, 60.4, 56.6, 40.6, 31.5, 25.4, 24.8, 13.7.

HRMS: exact mass calculated for $[\text{M}+\text{H}^+]$ ($\text{C}_{30}\text{H}_{34}\text{NO}_4$) $[\text{M}+\text{H}^+]$ requires m/z 472.2482, found m/z 472.2474.

Compound 66: Methyl 2-(4'-(((benzyloxy)carbonyl)(tetrahydro-2H-pyran-4-yl)amino)-[1,1'-biphenyl]-4-yl)acetate



Methyl 2-(4'-(((benzyloxy)carbonyl)(tetrahydro-2H-pyran-4-yl)amino)-[1,1'-biphenyl]-4-yl)acetate
Chemical Formula: $\text{C}_{28}\text{H}_{29}\text{NO}_5$
Molecular Weight: 459.5420

Prepared according to General Procedure D using benzyl (4-bromophenyl)(tetrahydro-2H-pyran-4-yl)carbamate **62** (250 mg, 0.64 mmol, 1 equiv.), K_3PO_4 (408.2 mg, 1.92 mmol, 3 equiv.), 2'-(dimethylamino)-2-biphenylpalladium(II)chloride dinorbonylphosphine complex (18 mg, 0.03 mmol, 10 mol %), methyl 2-(4-(4,4,5,5-tetramethyl-1,3,2-dioxaborolan-2-yl)phenyl)acetate **64** (212 mg, 0.77 mmol, 1.2 equiv.), 1,4-dioxane (2.4 mL) and H_2O (0.4 mL). After 72 h, the reaction mixture was subjected to the purification outlined in General Procedure D to afford the desired product as white solid (160 mg 54 %).

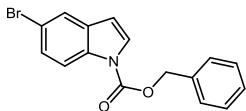
ν_{max} (neat): 1732, 1699, 1498, 1404, 1381 cm^{-1} .

^1H NMR (400 MHz, CDCl_3): δ 7.60 – 7.54 (m, 4H), 7.38 (d, $J = 8.3$ Hz, 2H), 7.33 – 7.25 (m, 3H), 7.20 (d, $J = 5.5$ Hz, 2H), 7.17 – 7.12 (m, 2H), 5.14 (s, 2H), 4.50 – 4.44 (m, 1H), 3.96 (dd, $J = 11.4, 4.4$ Hz, 2H), 3.73 (s, 3H), 3.69 (s, 2H), 3.45 – 3.44 (m, 2H), 1.81 (dd, $J = 12.3, 2.2$ Hz, 2H), 1.55-1.65 (m, 2H).

^{13}C NMR (101 MHz, CDCl_3): δ 171.4, 155.0, 139.8, 138.7, 136.8, 136.3, 132.9, 129.8, 129.3, 127.9, 127.3, 127.0, 126.8, 66.9, 66.5, 53.7, 51.6, 40.3, 31.4. One carbon not observed/coincident.

HRMS: exact mass calculated for $[M+H^+]$ ($C_{29}H_{30}NO_5$) requires m/z 460.2112, found m/z 460.2118.

Compound 68: Benzyl 5-bromo-1*H*-indole-1-carboxylate



Benzyl 5-bromo-1*H*-indole-1-carboxylate
 Chemical Formula: $C_{16}H_{12}BrNO_2$
 Molecular Weight: 330.18

Prepared according to General Procedure A using 5-bromoindole (2.01 g, 10.25 mmol, 1 equiv.), NaH (0.30 g, 12.25 mmol, 1.2 equiv.), CbzCl (1.6 mL, 11.22 mmol, 1.1 equiv.), and 2-MeTHF (50 mL) to give the desired compound as an amorphous white solid (2.14 g, 63%).

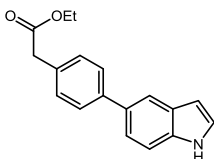
ν_{max} (neat): 1735, 1525, 1435, 1400 cm^{-1} .

1H NMR (400 MHz, $CDCl_3$): δ 8.06 (d, 1H, $J = 8.5$ Hz), 7.69 (d, 1H, $J = 1.9$ Hz), 7.63 (d, 1H, $J = 3.7$ Hz), 7.48 (dd, 2H, $J = 7.8, 1.6$ Hz), 7.45–7.34 (m, 4H), 6.53 (d, 1H, $J = 3.7$ Hz), 5.45 (s, 2H).

^{13}C NMR (101 MHz, MeOD): δ 146.1, 131.5, 130.4, 129.6, 127.8, 124.4, 124.2, 124.0, 123.0, 122.2, 119.2, 112.0, 103.0, 64.6.

HRMS: exact mass calculated for $[M+NH_4^+]$ ($C_{16}H_{16}^{79}BrN_2O_2$) requires m/z 347.0390, found m/z 347.0393, $[M+H^+]$ ($C_{16}H_{12}^{81}BrNO_2$) requires m/z 349.0396, found m/z 349.0372.

Compound 70: Ethyl 2-(4-(1*H*-indol-5-yl)phenyl)acetate



Ethyl 2-(4-(1*H*-indol-5-yl)phenyl)acetate
 Chemical Formula: $C_{18}H_{17}NO_2$
 Molecular Weight: 279.33

Prepared according to General Procedure D using 5-bromoindole (0.39 g, 2.0 mmol, 1 equiv.), ethyl 2-(4-(4,4,5,5-tetramethyl-1,3,2-dioxaborolane-2-yl)phenyl)acetate **40** (1.15 g, 3.96 mmol, 2 equiv.), K_3PO_4 (1.27 g, 6.0 mmol, 3 equiv.), 2'(dimethylamino)-2-biphenyl-palladium(II)chloride dinorbornylphosphine complex (0.11 g, 0.01 mmol, 10 mol %), 1,4-dioxane (2.4 ml), and H_2O (0.6 mL) to give the desired compound as an amorphous red solid (441.40 mg, 79%).

Experimental

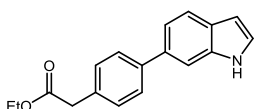
ν_{\max} (neat): 3403, 1721, 1621, 1516, 1470 cm^{-1} .

^1H NMR (400 MHz, CDCl_3): δ 8.19 (s, 1H), 7.85 (d, 1H, $J = 0.8$ Hz), 7.66–7.59 (m, 2H), 7.44 (m, 2H), 7.36 (d, 2H, $J = 8.3$ Hz), 7.24 (dd, 1H, $J = 3.1, 2.5$ Hz), 6.61 (dd, 1H, $J = 3.1, 2.1$ Hz), 4.19 (q, 2H, $J = 7.1$ Hz), 3.67 (s, 2H), 1.28 (t, 3H, $J = 7.2$ Hz).

^{13}C NMR (101 MHz, MeOD): δ 173.8, 143.0, 133.4, 133.3, 130.6, 128.2, 126.3, 121.8, 119.5, 112.4, 102.8, 102.8, 62.0, 41.7, 14.5. One carbon absent/not observed.

HRMS: exact mass calculated for $[\text{M}+\text{H}^+]$ ($\text{C}_{18}\text{H}_{18}\text{NO}_2$) requires m/z 280.1333, found m/z 280.1332.

Compound 72: Ethyl 2-(4-(1*H*-indol-6-yl)phenyl)acetate



Ethyl 2-(4-(1*H*-indol-6-yl)phenyl)acetate
Chemical Formula: $\text{C}_{18}\text{H}_{17}\text{NO}_2$
Molecular Weight: 279.3390

Prepared according to General Procedure D using 5-bromoindole (100 mg, 0.5 mmol), ethyl 2-(4-(4,4,5,5-tetramethyl-1,3,2-dioxaborolane-2-yl)phenyl)acetate **40** (260 mg, 0.91 mmol), K_3PO_4 (320 mg, 1.5 mmol), 2'-(dimethylamino)-2-biphenylpalladium(II)chloride dinorbornylphosphine complex (29 mg, 0.01 mmol, 10 mol %), 1,4-dioxane (2.4 mL), and H_2O (0.6 mL) to afford the desired product as a red solid (254 mg, 65%).

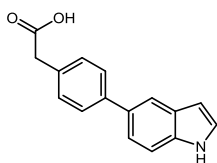
ν_{\max} (neat): 3383, 2929, 1733, 1495, 1453, 1337 cm^{-1} .

^1H NMR (400 MHz, DMSO): δ 11.15 (s, 1H), 7.64 – 7.59 (m, 4H), 7.39 – 7.36 (m, 1H), 7.35 (s, 1H), 7.33 (s, 1H), 7.29 (dd, $J = 8.2, 1.6$ Hz, 1H), 6.44 (m, 1H), 4.10 (q, $J = 7.1$ Hz, 2H), 3.69 (s, 2H), 1.20 (t, $J = 7.1$ Hz, 3H).

^{13}C NMR (101 MHz, CDCl_3): δ 172.0, 141.2, 136.5, 134.9, 132.4, 129.7, 127.6, 127.3, 125.1, 120.9, 119.60, 109.6, 102.3, 61.1, 41.1, 14.3.

HRMS: exact mass calculated for $[\text{M}+\text{H}^+]$ ($\text{C}_{18}\text{H}_{18}\text{NO}_2$) requires m/z 280.1337, found m/z 280.1335.

Compound 73: 2-(4-(1*H*-indol-5-yl)phenyl)acetic acid



2-(4-(1*H*-indol-5-yl)phenyl)acetic acid
 Chemical Formula: C₁₆H₁₃NO₂
 Molecular Weight: 251.2850

Prepared according to General Procedure E using ethyl 2-(4-(1*H*-indol-5-yl)phenyl)acetate **70** (100 mg, 0.34 mmol), NaOH (1 mL), and THF (2 mL) to give the desired product as a red solid (142 mg, 77%).

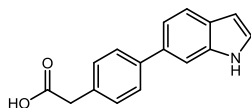
ν_{\max} (neat): 3380, 2922, 1688, 1454, 1406, 1355 cm⁻¹.

¹H NMR (400 MHz, MeOD): δ 10.46 (s, 1H), 7.60 (m, 4H), 7.34 (d, *J* = 8.3 Hz, 2H), 7.30 (d, *J* = 1.6 Hz, 1H), 7.28 (d, *J* = 1.6 Hz, 1H), 7.26 – 7.23 (m, 1H), 6.45 (s, 1H), 3.64 (s, 2H).

¹³C NMR (101 MHz, MeOD): δ 173.8, 140.7, 133.6, 132.2, 128.8, 127.0, 126.2, 124.4, 119.5, 117.8, 108.5, 100.3, 39.7. One carbon not observed/absent.

HRMS: exact mass calculated for [M+H⁺] (C₁₆H₁₄NO₂) requires *m/z* 250.0875, found *m/z* 250.0874.

Compound 74: 2-(4-(1*H*-indol-6-yl)phenyl)acetic acid



2-(4-(1*H*-indol-6-yl)phenyl)acetic acid
 Chemical Formula: C₁₆H₁₃NO₂
 Molecular Weight: 251.2850

Prepared according to General Procedure E using ethyl 2-(4-(1*H*-indol-6-yl)phenyl)acetate **72** (50 mg, 0.2 mmol), NaOH (1 mL), and THF (2 mL) to give the desired product as a red solid (34 mg, 78%).

ν_{\max} (neat): 3381, 2518, 1689, cm⁻¹.

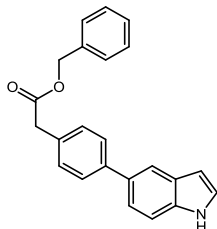
¹H NMR (400 MHz, MeOD): δ 7.64 (m, 5H), 7.39 (s, 1H), 7.37 (s, 1H), 7.33 (dd, *J* = 8.2, 1.6 Hz, 1H), 7.29 (s, 1H), 6.48 (dd, *J* = 3.1, 0.8 Hz, 1H), 3.68 (s, 2H). OH not observed.

¹³C NMR (101 MHz, MeOD): δ 173.8, 145.9, 140.7, 136.4, 133.6, 132.2, 128.8, 126.2, 124.3, 117.7, 108.5, 100.3, 39.7. One carbon absent/not observed.

Experimental

HRMS: exact mass calculated for $[M+H]^+$ ($C_{16}H_{14}NO_2$) requires m/z 252.1019, found m/z 252.1019.

Compound 75: Benzyl 2-(4-(1*H*-indol-5-yl)phenyl)acetate



Benzyl 2-(4-(1*H*-indol-5-yl)phenyl)acetate
Chemical Formula: $C_{23}H_{19}NO_2$
Molecular Weight: 341.4100

Prepared according to General Procedure H using 2-(4-(1*H*-indol-6-yl)phenyl)acetic acid **73** (150 mg, 0.60 mmol, 1 equiv.), DMF (5 mL), NaH 60% w/w (48 mg, 2.0 mmol, 3 equiv.), and *N*-(benzyloxycarbonyloxy)succinimide (223 mg, 0.90 mmol, 1.5 equiv.) to give the desired product as a red solid (148 mg, 72%).

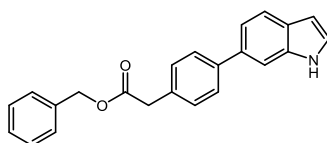
ν_{\max} (neat): 2922, 1734, 1716 cm^{-1} .

1H NMR (400 MHz, $CDCl_3$): δ 8.20 (s, 1H), 7.87 (s, 1H), 7.63 (d, $J = 8.2$ Hz, 2H), 7.47 (s, 2H), 7.41 – 7.33 (m, 6H), 7.27 (dd, $J = 2.5, 3.1$ Hz, 1H), 6.65 – 6.62 (m, 1H), 5.19 (s, 2H), 3.75 (s, 2H). NH not observed.

^{13}C NMR (101 MHz, DMSO): δ 171.1, 140.5, 136.1, 135.5, 132.1, 131.0, 129.8, 128.4, 128.2, 128.9, 127.9 (2C), 126.6, 126.0, 120.2, 118.0, 111.7, 101.5, 65.8.

HRMS: exact mass calculated for $[M+H]^+$ ($C_{23}H_{20}NO_2$) requires m/z 340.1343, found m/z 340.1334.

Compound 76: 2-(4-(1-((Benzyloxy)carbonyl)-1*H*-indol-6-yl)phenyl)acetic acid



Benzyl 2-(4-(1*H*-indol-6-yl)phenyl)acetate
Chemical Formula: $C_{23}H_{19}NO_2$
Molecular Weight: 341.4100

Prepared according to General Procedure H using 2-(4-(1*H*-indol-6-yl)phenyl)acetic acid **74** (260 mg, 1.0 mmol, 1 equiv.), NaH 60% w/w (49 mg, 2.0 mmol, 2 equiv.), *N*-(benzyloxycarbonyloxy)succinimide (374 mg, 1.5 mmol, 1.5 equiv.), and DMF (3 mL) to afford the desired product as a red solid (59 mg, 17%).

ν_{\max} (neat): 3382, 1728, 1526, 1492, 1454 cm^{-1} .

^1H NMR (400 MHz, CDCl_3): δ 8.22 (s, 1H), 7.70 (d, $J = 8.2$ Hz, 1H), 7.63 – 7.58 (m, 3H), 7.40 – 7.31 (m, 9H), 7.24 (dd, $J = 3.8, 1.7$ Hz, 1H), 6.59 – 6.56 (m, 1H), 5.17 (s, 2H), 3.73 (s, 2H).

^{13}C NMR (151 MHz, CDCl_3): δ 171.6, 141.3, 136.4, 135.9, 135.1, 132.2, 129.7, 128.6, 128.3, 128.2, 127.6, 127.3, 124.9, 120.9, 119.7, 109.5, 102.5, 66.7, 41.0.

HRMS: exact mass calculated for $[\text{M}+\text{H}^+]$ ($\text{C}_{23}\text{H}_{20}\text{NO}_4$) requires m/z 340.1343, found m/z 340.1335.

3.7 Biology

3.7.1 PathHunter® CHO-K1 EDG2 β -Arrestin Compound Screen Study

3.7.1.1 Agonist Mode Screen

17 compounds were screened against the PathHunter® CHO-K1 EDG2 cell line (DiscoverX) in agonist mode. The DiscoverX reference 1-oleoyl-LPA (LPA) specified for the EDG2 cell line was added to the screen. 5000 cells/well were plated in a 384 well assay plate, in 20 μL PathHunter® Cell Plating Reagent 18, and incubated overnight to allow cells to attach and grow. Cells were then exposed to 10 μM compound (four replicates; 1% DMSO) or buffer + 1% DMSO (80 replicates). The stocks of DiscoverX reference LPA are suspended in EtOH, rather than DMSO: therefore cells were exposed to 10 μM compound (four replicates; 5% EtOH) or buffer + 5% EtOH (4 replicates). Cells were exposed to compounds for 3 h at room temperature. Following compound incubations, PathHunter® Detection Reagent was added and the assay plates were read on an Envision luminometer.

3.7.1.2 Antagonist Mode Screen

17 compounds were profiled against the PathHunter® CHO-K1 EDG2 (DiscoverX) cell line in antagonist mode. The experiment was run concurrently with the agonist mode test. Cells were exposed to 10 μM compound (four replicates; 1% final DMSO) or buffer + 1% DMSO (80 replicates) for 1 h at 37° C, followed by exposure to 500 nM LPA (0.25% final EtOH) for 3 hours at room temperature. DiscoverX reference LPA (dissolved in EtOH) specified for the EDG2 cell line was used as the challenge agonist. E_{\max} control wells (8 replicates) were exposed to 500 nM LPA

(0.25% final EtOH) + 1% DMSO. Buffer only (negative) control wells (8 replicates) were exposed to buffer + 1% DMSO + 0.25% EtOH. The 500 nM agonist challenge dose was based on historical data from the EDG2 cell line. Following compound incubations, PathHunter® Detection Reagent was added and the assay plates were read on an Envision luminometer.

3.7.1.3 Autotaxin Inhibition Assay

Molecules were tested for their ability to inhibit autotaxin activity using the Autotaxin Inhibitor Screening Kit (Cayman Chemical) with modifications to the manufacturer's protocol. Briefly, in a 96 well plate 20 ng/mL autotaxin was incubated with 3 mM bis-*p*NPP at 30 °C for 30 min in 50 mM Tris-HCl buffer (pH 8.5) containing 10 mM CaCl₂ and 0.02% triton X. Liberated bis-*p*-nitrophenol was measured using a Wallac Victor2 1420 multilabel counter (Perkin Elmer, Beaconsfield, UK) in absorbance mode at 405 nm. The background was determined by incubating bis-*p*NPP in the absence of enzyme. Activity of the compounds was determined by subtracting the average background from all results and expressing the compound activity as a percentage of the enzyme-substrate reaction in the absence of compound. PF-8380 in the concentration range of 0.1-300 nM in half log units was included as a standard compound in every assay plate. The potential inhibitors were initially tested against autotaxin at a concentration of 30 µM (n=2); samples which showed inhibition of 60% or greater were considered to be active. Dose response curves, in the concentration range of 30 nM to 30 µM in half log units, to calculate K_i values were performed on compounds reaching the designated activity threshold (n=3). Data was expressed as mean ± SEM was plotted using Graph Pad Prism version 6.00 for Windows, GraphPad Software, La Jolla California USA, www.graphpad.com.

3.7.2 Methods for [³H]-Thymidine Incorporation Assay

3.7.2.1 Cell Culture

PC3 (human prostate cancer) cells were kept under conventional cell culture conditions at 37 °C, 5% CO₂.

3.7.2.2 Stimulating Cells

Cells were sub-cultured and grown to 70 % confluence in 24 well plates before quiescing for 24 h and then treatment with appropriate stimulus or vehicle (DMSO) for 18 h.

3.7.2.3 [³H]-Thymidine Incorporation

[³H] thymidine (9.25 kBq diluted in serum free medium) was added to each well 5 h before the expiry of the 18-20 h period. The medium was aspirated to the radioactive sink. 1 mL ice cold 10% (w/v) trichloroacetic acid (TCA) was added to each well and incubated on ice for 6 min x 3. This precipitates the protein and nuclear material remains stuck to the base of the well. The TCA was aspirated to the radioactive sink and 0.25 mL 0.1% (w/v) SDS/0.3 M NaOH was added to each well (at room temperature). This dissolves the nuclear material. The contents of each well were transferred to separate beta vials. 2 mL of scintillant was added to each vial, capped and mixed thoroughly. Each vial was counted in the scintillation counter (3 min per sample).

3.7.3 Cytotoxicity Assay.⁹⁰

Compounds were tested for any cytotoxic effects against normal fibroblasts (Hs 27 cells) and an ovarian carcinoma cell line (A2780). The cytotoxicity was evaluated by using the alamarBlue® assay. Hs 27 cells were incubated in DMEM supplemented with 10% FBS, 2 mM glutamine and 1% penicillin/streptomycin under 5% CO₂ at 37 °C in a humidified incubator. A2780 cells were cultured under the same conditions in RPMI 1640 media with 10% FBS and 1% penicillin-streptomycin. At 70-80% confluency the cells were detached from the culture flasks using Triple® Express and seeded in clear 96-well plates at a concentration of 3750 cells per well (A2780 cells) and 7500 cells per well (Hs 27 cells). The cells were allowed to adhere and equilibrate overnight before addition of compound (diluted in the relevant media). After a further 42 h incubation, 10% alamarBlue® was added to each well and incubated for 6 h. The resulting fluorescence was measured using a Wallac Victor2 1420 multilabel counter, in fluorescence mode: excitation 560, emission 590. Cells in the absence of compound were considered as 100% viable against which compound treated cells (at a concentration of 30 µM, at least n=2) were compared.

0.1% triton X was used as a negative control. Data was expressed as mean \pm SEM and plotted using Graph Pad Prism Software.

3.7.4 High Throughput Physchem Measurements⁹⁷

3.7.4.1 ChromlogD assay (LogD)

The Chromatographic Hydrophobicity Index (CHI) values were measured using reversed phase HPLC column (50 x 2 mm 3 μ M Gemini NX C18, Phenomenex, UK) with fast acetonitrile gradient at starting mobile phase of pH = 7.4. CHI values are derived directly from the gradient retention times by using a calibration line obtained for standard compounds. The CHI value approximates to the volume % organic concentration when the compound elutes. CHI is linearly transformed into ChromlogD by the formula: $\text{ChromlogD} = 0.0857\text{CHI} - 2.00$. The average error of the assay is ± 3 CHI unit or ± 0.25 ChromlogD.

3.7.4.2 Chemiluminescent nitrogen detection (CLND) kinetic aqueous solubility assay (Sol)

GSK in-house kinetic solubility assay: 5 μ l of 10 mM DMSO stock solution diluted to 100 μ l with pH 7.4 phosphate buffered saline, equilibrated for 1 h at room temperature, filtered through Millipore Multiscreen_{HTS}-PCF filter plates (MSSL BPC). The filtrate is quantified by suitably calibrated flow injection Chemi-Luminescent Nitrogen Detection. The standard error of the CLND solubility determination is ± 30 μ M, the upper limit of the solubility is 500 μ M when working from 10 mM DMSO stock solution.

3.7.4.3 Artificial Membrane Permeability assay (P_{app})

The donor cell contained 2.5 μ L of 10mM sample solution in pH 7.40 phosphate buffer. To enhance solubility, 0.5% hydroxypropyl-cyclodextrin (encapsin) has been added to the buffer. The artificial membrane is prepared from 1.8% phosphatidylcholine and 1% cholesterol in decane solution. The sample concentration in both the donor and acceptor compartment is determined by LC-MS after 3 h incubation at room temperature. The permeability ($\log P_{\text{app}}$) measuring how fast molecules pass through the black lipid membrane is expressed in nm/s. The average standard error of the assay is around ± 30 nm/s that can be higher at the low permeability range.

Chapter 2

*Investigation of the Origin of Activity in the
Amira Non-Lipid Like ATX Inhibitor*

4 Chapter 2: Investigation of the Origin of Activity in the Amira Non-Lipid Like ATX Inhibitor

4.1 Proposed Work and Aims

Following the SAR study surrounding AM095 (**16**), a potent LPA₁ antagonist, it was postulated that perhaps this process may not be the most effective method for targeting the LPA/ATX signalling pathway due to the high concentrations of LPA within the body. Therefore, it was proposed that going a step back in the signalling process may be more effective, *i.e.*, targeting the enzyme ATX which produces LPA over the receptor itself.

Two important compounds targeting ATX inhibition in the literature are a compound from Amira Pharmaceuticals (**18**), and Pfizer's PF-8380 (**19**). The latter of these compounds exemplified the typical structure associated with ATX inhibitors (lipophilic tail, core spacer, and acidic head group), highlighted in Figure 31. This chemotype has been extensively studied within recent literature by companies such as Hoffman-La Roche,⁹⁸ Novartis,⁷³ and Merck GMBH.⁶⁵ Exemplars from the patent literature are illustrated in Figure 31.

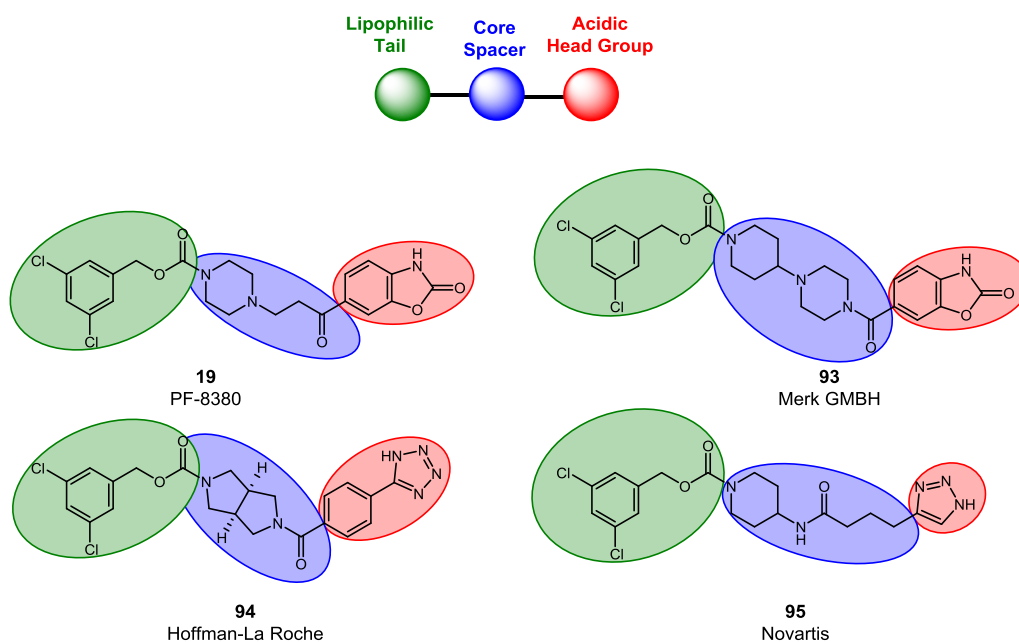


Figure 31: Typical structure of ATX inhibitors within the literature with the key motifs highlighted.

Of these, compound **18** developed by Amira is particularly interesting. This molecule is reported to exhibit similar biological activity to PF-8380 (**19**) but contains a significantly different chemotype. Specifically, it does not conform to the usual lipid-like chemotype as there is no lipophilic portion and, in general, is much more structurally compact (Figure 32). In addition, this chemotype has not been extensively studied, with structural information only becoming available in early 2015.⁴¹ At the beginning of this study only two patents,^{68,69} both from Amira Pharmaceuticals, had been published on this unique chemotype, where the data contained did not allow for in-depth analysis of the SAR. This will be discussed in more detail in Section 11.1. As a result, the origin of the biological activity of this chemotype has yet to be determined.

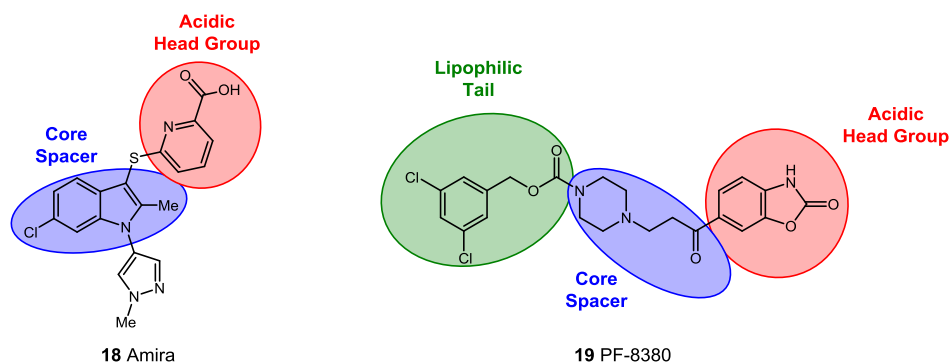


Figure 32: Potent literature ATX inhibitors **18** and **19** with the main structural motifs highlighted.

4.2 Results and Discussion

4.2.1 Amira Patent SAR Data.

In terms of existing SAR data surrounding the Amira compounds, two patents^{68,69} have been published which focus on diversification around the indole core. These patents, although extensive, do not offer a great deal in regards to the identification of important structural features needed for biological activity as all of the assay data disclosed is classified into three main categories, <0.3 μM , 0.3-1 μM , and >1 μM , for example, Figure 33.

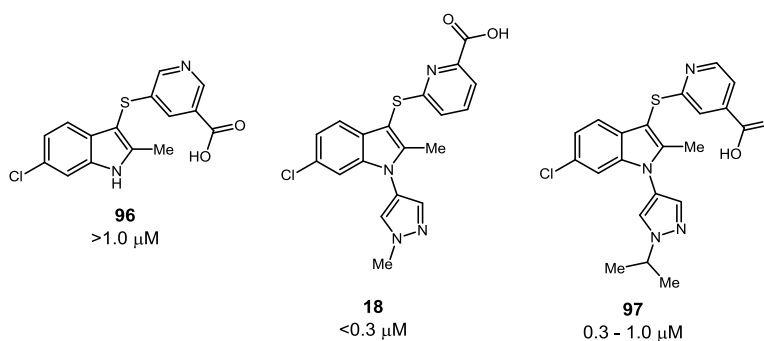


Figure 33: Representative compounds from Amira illustrating the three assay categories.

In addition to this, there is generally little correlation between compounds, *i.e.*, in the majority of cases either two or three point changes are made making it difficult to establish a confident SAR. The compound library produced by Amira was no doubt conducted in a methodical and linear manner; however, not all of this data will necessarily be disclosed in the patents.

In total a set of 175 compounds are claimed within the two Amira Pharmaceutical patents, however, as mentioned above limited SAR data can be extracted. Nevertheless, what was evident was that four main sections of the compound were analysed: Section A – substitution on the benzenoid ring; Section B – core changes; Section C – derivatisation of the acid warhead; and, Section D – indole nitrogen substitution, Figure 34.

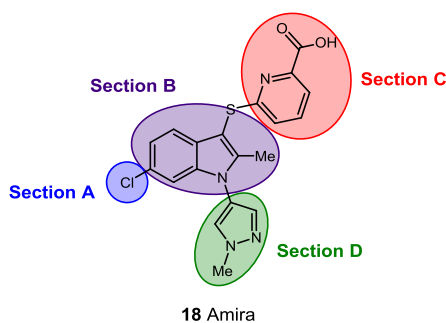


Figure 34: Four main sections studied by Amira Pharmaceuticals.

Section A

Limited variation was conducted on this section with 98% of the compounds presented containing the 6-chloro moiety. Two core structures were probed to analyse the introduction of alternative functionality on the ring, which were compounds **98-101** and **102-103** (Figure 35). From the data it became apparent that bromine (**101**) and cyano (CN) (**102**) groups were also tolerated, with values of 0.3-1 μM and $<0.3 \mu\text{M}$, respectively. However, phenyl, pyridine, and benzyl groups were less tolerated increasing the K_i values to greater than 1 μM (compounds **98-100**). This perhaps indicates the need for lipophilic character at this position. Although it has been generalised that these two functionalities are tolerated it is difficult to say with certainty as there are two point changes between compound **101** and **102** (**101** contains benzyl group on the indole nitrogen whereas **102** contains the pyrazole functionality).

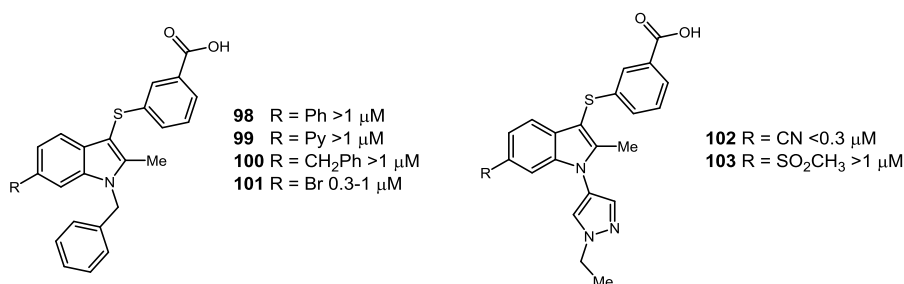


Figure 35: SAR around section A - substitution on the aromatic ring.

Section B

Analysis of the acid portion of the molecule was limited to the comparison between the phenyl and the pyridyl acid groups (Figure 36). In general, the data indicated that when methyl (Me), ethyl (Et), propyl (Pr) or *i*-Pr substituted pyrazoles were present on the nitrogen of the indole comparable activity was shown with the benzoic acid compounds **104-107** and the 5-, and 2-pyridyl acid compounds **18**, and **108-113**. Moving to the 6-pyridyl acid resulted in a drop in activity with the Me and isopropyl-*1H*-pyrazol-4-yl (**114**, and **116**), but regained activity with the ethyl-*1H*-pyrazol-4-yl (**115**) (Figure 36). This small data set suggests that with the pyrazole in place little difference in activity is associated with the benzoic or pyridyl acid. Therefore, it can be assumed that more focus was driven towards SAR around the benzoic acid core, due to the similarity and activity and the more straightforward synthesis.

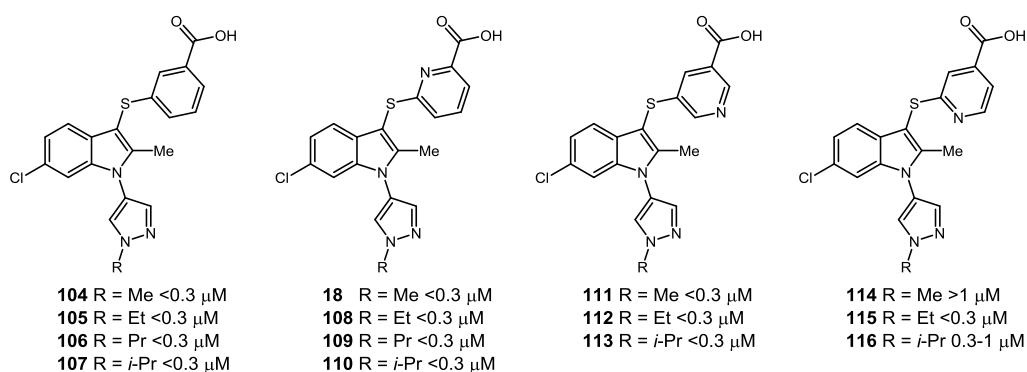


Figure 36: SAR around section B - derivatisation of the acid.

Section C

The substitution of the indole nitrogen was analysed with the most complete data set being associated with compound **104**, and **117-120** for the benzoic acid core and compounds **18**, and **121-122** pyridyl acid core, Figure 37. From this, it was found that in general for both acid groups (benzoic and pyridyl) the introduction of substituted pyrazoles (such as Me (**18**, and **104**), Et, and isopropyl-*1H*-pyrazol-4-yl) and pyridines (such as 6-ethoxy (**117**), or 5-methoxy-pyridin-3-yl) was well tolerated, giving K_i values of <0.3 μ M. Moving to unsubstituted aromatic compounds such as pyridine-2-yl (**118**) and biphenyl (**120**) on the benzoic acid core resulted in a drop in activity to 0.3-1 μ M. A further drop in activity, to >1 μ M, was shown for the pyridyl

acid core when either no substitution (**122**), or a benzyl group was present (**121**) on the nitrogen of the indole. This suggests that perhaps the increased polarity of the pyrazole is important for picking up interactions within the pocket, or perhaps the shape and size is more tolerated within the pocket than the phenyl group due to the slight drop in activity.

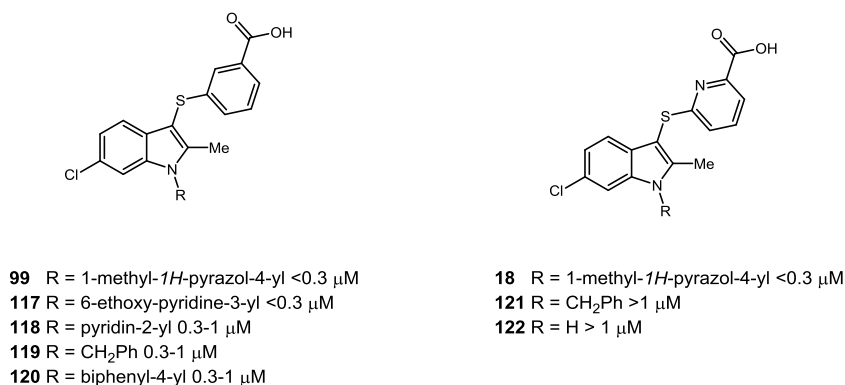


Figure 37: SAR around section C - substitution on the indole nitrogen.

Section D

In terms of core alterations, slight modifications were made on the C₂ position of the indole (Figure 38), with the benzoic acid core, where it was found that leaving this centre unsubstituted had a slight effect on the inhibition properties (compounds **124**, and **126**). Further derivatisation at this position to either an Et or CF₃ group resulted in a further drop in activity to >1 μ M (compounds **125**, and **123** respectively). However, it is difficult to compare these values as two point changes have been made, and as such the change in activity may be associated with the substitution on the indole nitrogen.

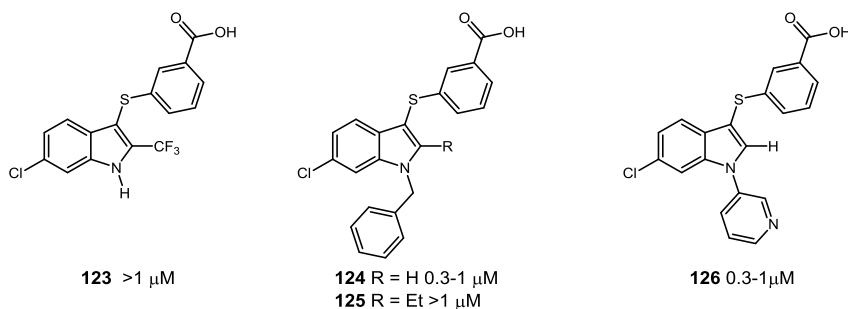


Figure 38: SAR around Section D at the C₂ position of the indole.

From this limited SAR analysis three main conclusions could be drawn which were: i) the chlorine position seemed important for activity, ii) in terms of the substitution on the indole nitrogen, pyrazole derivatives were the most heavily featured and seemed to be beneficial for biological activity, and iii) the pyridyl acid and benzoic acid were generally comparable in activity and well tolerated. A complete summary of the data illustrated within the two patents is illustrated in Figure 39, which takes into account additional features which did not fall into the generalised data given above.

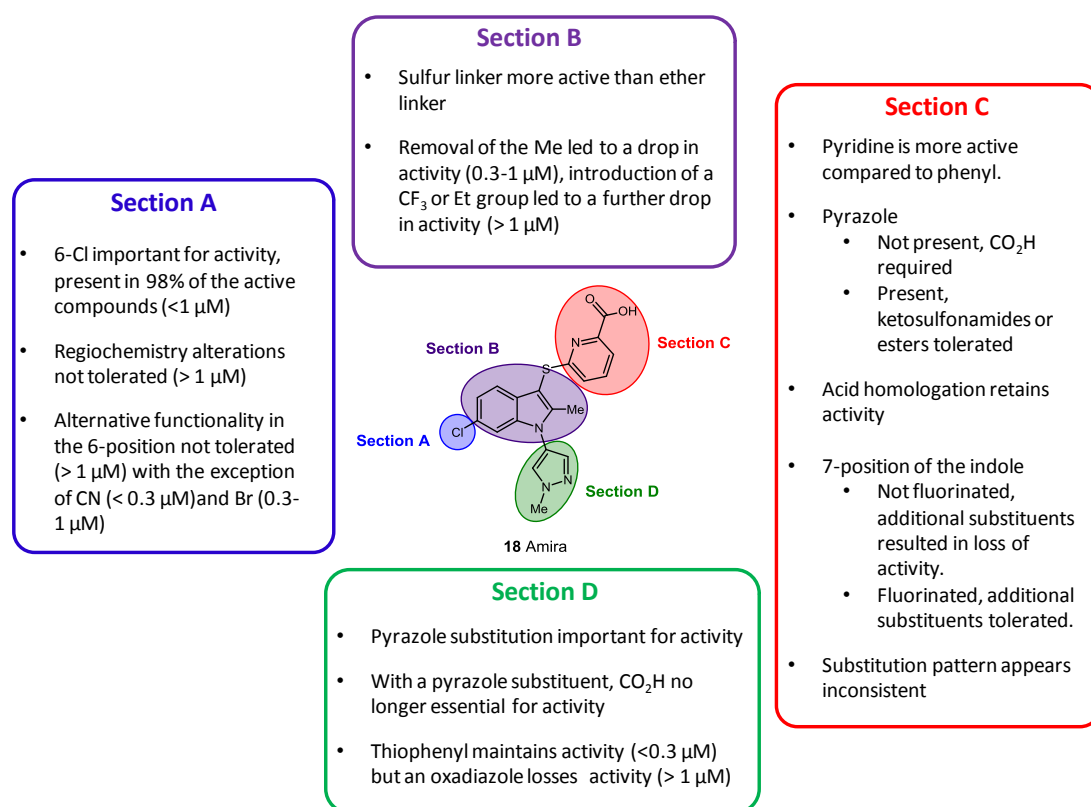


Figure 39: SAR deduced from Amira Pharmaceutical patents.

4.2.2 Molecular Docking Studies

In order to try and obtain a more in-depth understanding of how this unique chemotype may be orientated within the active site of the enzyme further structural analysis was conducted. This was achieved by undertaking a set of preliminary modelling experiments using MOE software,⁹⁹ which depicted four main binding interactions arising from: i) the chlorine residing at the 6-position of the indole ring; ii)

the pyrazole methyl; iii) the pyridyl acid; and, lastly, iv) the indole methyl (Figure 40). Interestingly, these four interactions coincided with the four sections previously highlighted for investigation from the patent data.

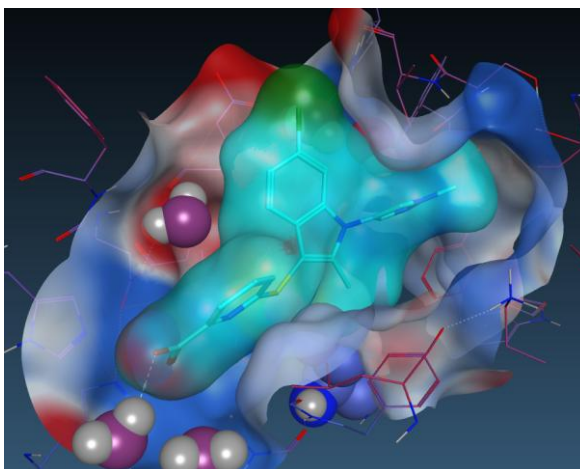


Figure 40: Compound **18** modelled within the active site of ATX (PDB 2XRG), where the blue surface represents the space occupied by the ligand.¹⁰⁰

These modelling studies suggested that **18** could potentially adopt a different binding mode to that suggested by Hausman and co-workers regarding HA155 (**5**), which binds within the active site and the hydrophobic pocket.⁴⁶ Specifically, for **18** although the pyridyl acid is believed to reside with the active site (Figure 41), the remainder of the structure may occupy a space within the hydrophobic tunnel, instead of the hydrophobic pocket, as described for the more traditional ATX chemotype binding mode.

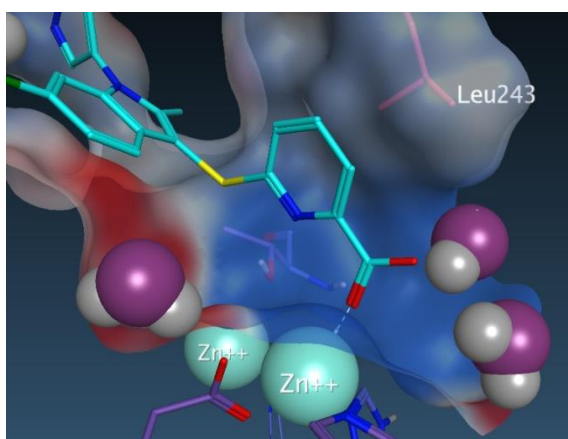


Figure 41: Docking of **18** illustrating the interactions of the pyridyl acid with one of the Zn^{2+} ions in the active site (PDB 2XRG).¹⁰⁰

In addition to the interactions associated with the acid, it became apparent in the modelling studies that the chlorine, which was highly conserved within Amira's patents, projected into a cleft within the pocket where it could pick up lipophilic interactions with the neighbouring Glu308 and Val277 residues (Figure 42a). Further lipophilic interactions were associated with both the Me on the indole ring (Figure 42b) and the Me of the pyrazole (Figure 42c and d).

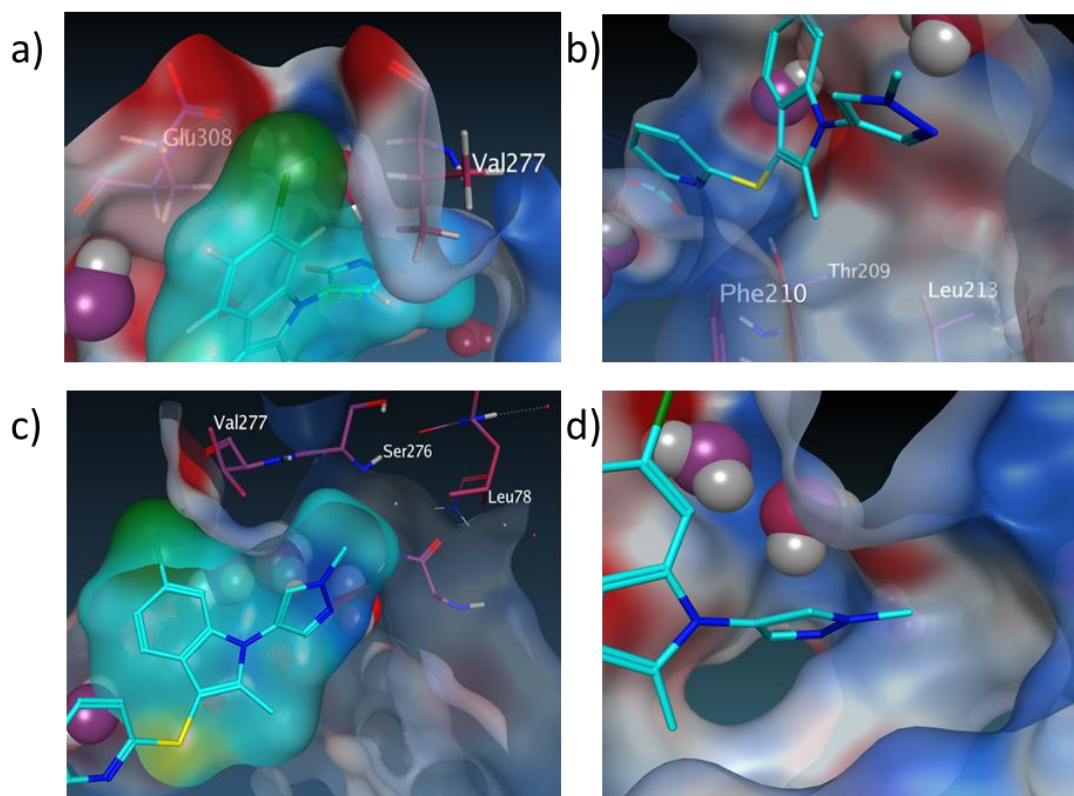


Figure 42: Compound **18** docked within the active site (PDB 2XRG) indicating the main binding interactions: a) 6-chloro indole projecting into a cleft and picking up interactions with Glu308 and Val277 residues; b) methyl of the indole picking up interactions with Glu308 and Val277 residues; b) methyl of the indole picking up interactions with Phe210, Thr209, and Leu213 residues; c) the pyrazole functionality projecting into a cleft; d) enlarged image of the cleft where the methyl pyrazole resides indicating the space available.¹⁰⁰

In terms of the C_2 substitution there is limited space within the pocket and as such only small groups such as Me or no substitution are tolerated. This can be further emphasised by the SAR data generated within the Amira patents,^{68,69} where Et and CF_3 were not tolerated. On the other hand, in the case of the substitution on the pyrazole, the cleft where this functionality is believed to reside is much larger and,

as such, this position may be more tolerant of larger functionality, with the potential to pick up additional lipophilic interactions. Again, this can be further validated using the SAR data from the Amira patents which indicated the introduction of Et, Pr, and *i*-Pr substituted pyrazole motifs was generally well tolerated and gave equipotent compounds.

4.2.3 Development of Deletion Analogues

Using both the SAR analysis from the two Amira patents and the molecular docking studies conducted, four key regions of **18** were identified for investigation which were: Section A – substitution on the benzenoid ring; Section B – core changes; Section C – derivatisation of the acid warhead; and, Section D – indole nitrogen substitution.

Therefore, due to the interesting chemotype of **18** and the lack of associated SAR, it was proposed to conduct an extensive SAR study surrounding this compound, analysing the four key sections outlined. Within each of these four sections a range of compounds would then be developed with a view to producing a detailed compound library, allowing a comprehensive analysis of the SAR and, potentially, determination of the origin of activity of compound **18** (Figure 43).

With regards to section A, two main properties would be analysed. These were the importance of the position of the chlorine and determining whether, if any, other functionality would be tolerated. To probe the latter, four main modifications were introduced, including Me, OMe, and F substituents as well as no substitution. These were chosen to determine if other halogens would be tolerated, to probe the difference in electronic and lipophilic contribution, and lastly to demonstrate if functionality was required.

In section B, the core indole ring would be analysed to ascertain if this was essential for activity. This would be achieved by the synthesis of compound **137**, which would completely remove this motif. From a structural perspective it was believed that **137** would occupy a similar space to **18**. This was validated by overlaying the energy minimised structures of **18** and **137**, using a similar method to that used for the AM095 (**16**) analogue previously. Both **18** and **137** were found to contain a good degree of overlap, with only a slight variation in the projection of the Me of the

pyrazole and the pyridyl acid, and so was believed to be a viable candidate (Figure 44).

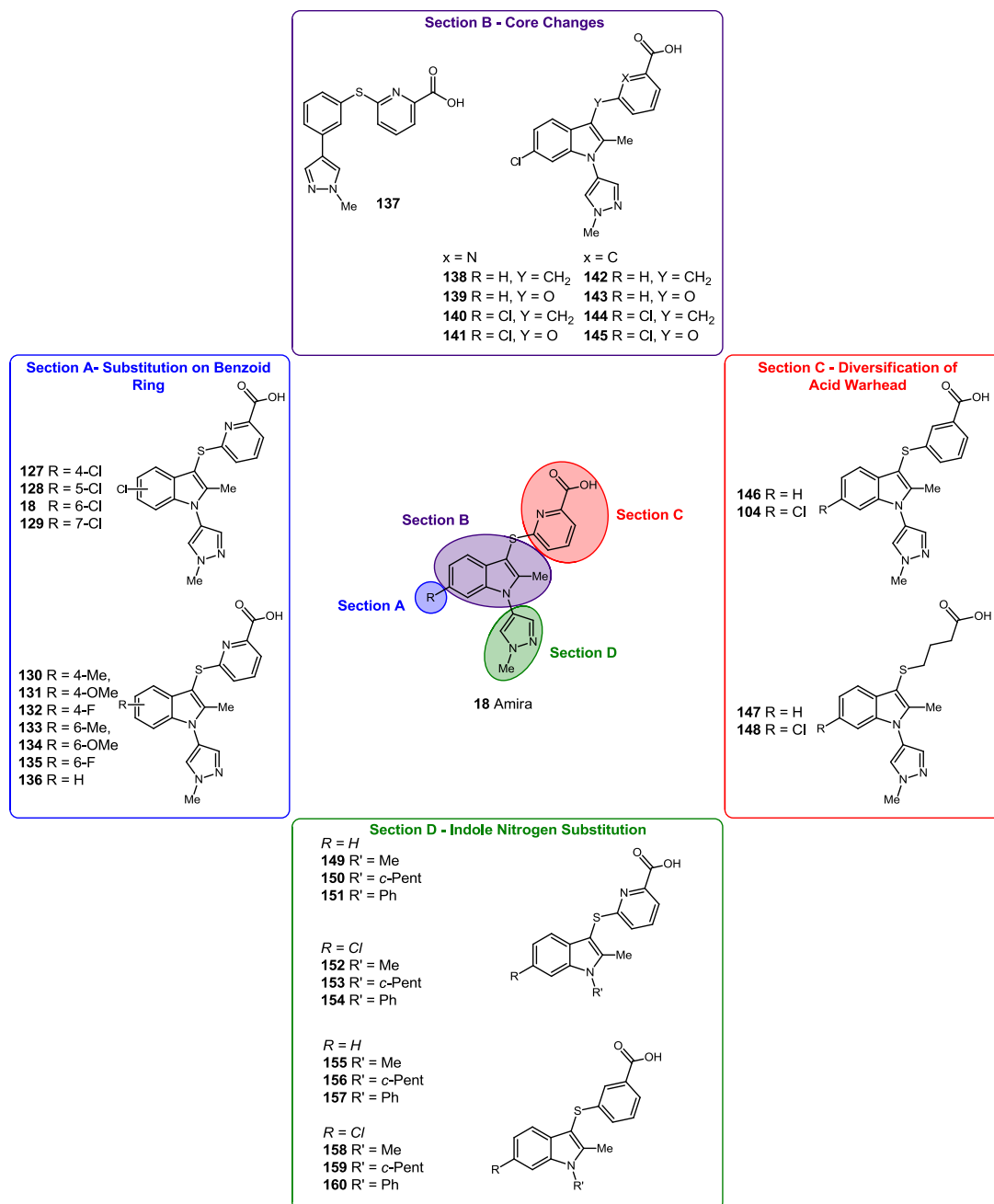


Figure 43: Four main sections of **18** targeted for SAR analysis: Section A – substitution on the benzenoid ring; Section B – core changes; Section C – derivatisation of the acid warhead; and, Section D – indole nitrogen substitution, with the proposed compounds outlined within each section.

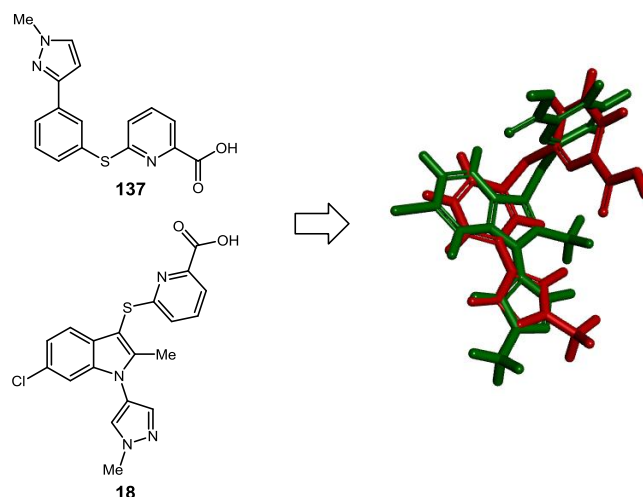
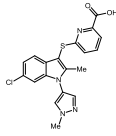
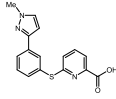


Figure 44: Molecular overlay of compound **137** in red and compound **18** by Amira in green.

In terms of the physicochemical implications of the indole removal, calculated physicochemical properties using JChem⁷⁷ illustrated a decrease in MW, as well as a decrease in the lipophilicity (cLogP) compared to the original Amira compound **18** (Table 13). Therefore, from a physicochemical perspective, **137** could be more tractable, as the cLogP is in the desirable region of <4 as stated by Gleeson.⁹¹

Table 13: Calculated physicochemical values for **137** Section B.^a

Entry	Cpd. No. ^b	Structure	MW ^c	cLogP ^d	LogD	PSA ^e
1	18		399	4.8	1.5	76
2	137		311	3.7	0.3	71

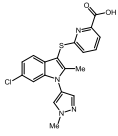
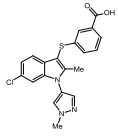
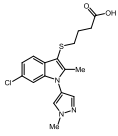
^aColour coded according to correlation with Gleeson⁹¹ (MW < 400 and log P <4) and Veber⁷⁹ (PSA < 140 Å): red = out with guidelines; amber = borderline correlation; green = desirable. Data were obtained using JChem for Excel software.⁷⁷ ^bCompound number, ^cmolecular weight, ^dcalculated LogP, ^epolar surface area

In addition to the removal of the indole, further modifications of the linker within the core would be probed by the introduction of a methylene and an ether linker. These were chosen to analyse the heteroatom tolerance, as well as probing the vector of the linker as the thioether and ether would be similar, whereas the methylene, containing increased degrees of freedom, would differ.

For section C, the acid moiety would be probed by the introduction of a pyridyl acid (as in **18**), benzoic acid, and a long chain aliphatic acid which would be approximately the same length as the aromatic acids (Table 14). This would probe whether the aromatic acid functionality is important in terms of: i) conformation, as the long chain acid would exhibit more flexibility compared to the structured aromatic ring; ii) probe the importance of lipophilicity as the LogP values increase going from long chain < benzoic < pyridyl; and, iii) analysis of altering the pK_a of the acid (pyridyl < benzoic < long chain acid). In addition to this, the long chain acid would also relate back to some of the earlier LPA₁ antagonists, for example Ki1645 (**15**), which contained a thioether aliphatic acid chain, which would also probe the potential cross-talk between the two pathways (LPA receptor antagonist and ATX inhibition signalling pathways).

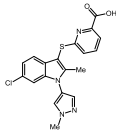
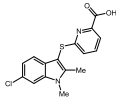
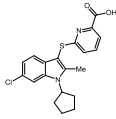
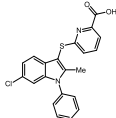
Lastly, for section D three main substituents would be introduced onto the nitrogen of the indole, Me, cyclopentane (*c*-Pent), and Ph. The Ph group was introduced to determine if any aromatic character is tolerated, or if polar functionality is required. In addition to this, Me and *c*-Pent would also be introduced in order to analyse the space available within the cleft to determine if small functionality such as the Me would be tolerated as well as the larger three-dimensional *c*-Pent group. From a physicochemical perspective (Table 15), these functionalities would probe the importance of lipophilicity, as going from Me to *c*-Pent to Ph there is a slight increase in lipophilicity, compared to the original Amira compound, making the latter two (Table 15, entry 3 and 4) outwith Gleeson⁹¹ and Lipinski's⁷⁸ guidelines which may lead to problems from a developability perspective later on.

Table 14: Calculated physicochemical values for exemplars from section C.^a

Entry	Cpd. No. ^b	Structure	MW ^c	cLogP ^d	LogD	PSA ^e	pKa
1	18		399	4.8	1.5	76	3.6
2	104		398	5.0	1.8	63	3.9
3	148		364	3.7	0.8	63	4.3

^aColour coded according to correlation with Gleeson⁹¹ (MW < 400 and log P < 4) and Veber⁷⁹ (PSA < 140 Å): red = outwith guidelines; amber = borderline correlation; green = desirable. Data were obtained using JChem for Excel software.⁷⁷ ^bCompound number, ^cmolecular weight, ^dcalculated LogP, ^epolar surface area

Table 15: Calculated physicochemical values for exemplars from section D.^a

Entry	Cpd. No. ^b	Structure	MW ^c	cLogP ^d	LogD	PSA ^e
1	18		399	4.8	1.5	76
2	152		333	4.7	1.4	58
3	153		387	6.1	2.7	58
4	154		395	6.4	3.0	58

^aColour coded according to correlation with Gleeson⁹¹ (MW < 400 and log P < 4) and Veber⁷⁹ (PSA < 140 Å): red = outwith guidelines; amber = borderline correlation; green = desirable. Data were obtained using JChem for Excel software.⁷⁷ ^bCompound number, ^cmolecular weight, ^dcalculated LogP, ^epolar surface area

As the binding site of this compound was undefined at the outset of this study, a dual assay procedure was employed where compounds would be tested using both the standard bis-*p*NNP assay as well as the native choline release assay. The rationale for the dual assay procedure stems from the potential different binding interactions of the two assays. When using the unnatural bis-*p*NPP assay, the substrate binds within the active site of the enzyme, and thus will only indicate inhibitor compounds which bind within the active site, *i.e.*, competitive inhibitors. Therefore, if compounds bind remote from this site (*i.e.*, within the hydrophobic tunnel) this may appear inactive. In order to validate if compounds described as inactive within the bis-*p*NPP assay are in fact inactive, or are instead binding remote from the active site, additional testing using the native LPC assay was proposed.

To rationalise this hypothesis, Fells *et al.*⁸ have conducted molecular docking studies using the unnatural *p*NP-TMP assay. This work indicated that when the *p*NP-TMP substrate was docked within the enzyme it resided within the catalytic site, (Figure 45) leaving the hydrophobic pocket vacant. Thus, if compounds bind remote from the active site, the *p*NP-TMP substrate will still be able to sit within the active site, resulting in a false negative.

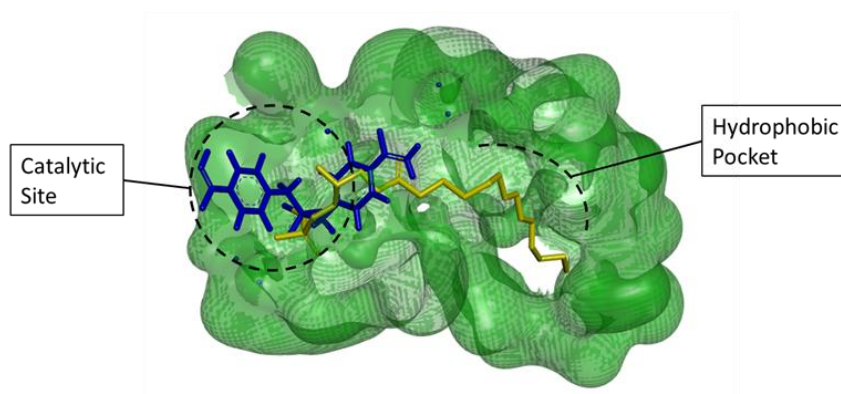
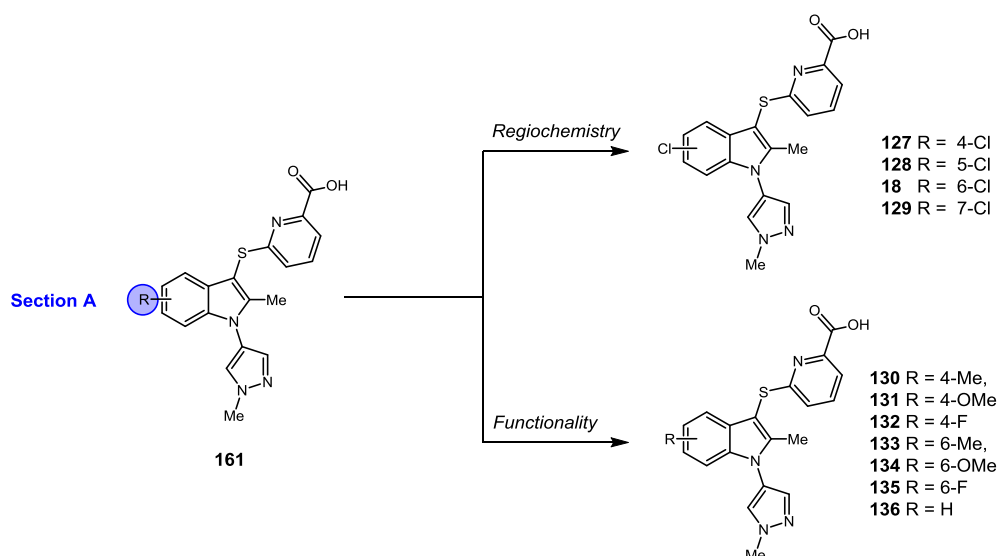


Figure 45: Catalytic site and hydrophobic pocket of ATX: Complex of LPA 14:0 (**4**) (yellow) in Mouse ATX (PDB ID 3NKN) with the docked position of bis-*p*NPP (blue) overlaid.¹⁰¹

The second assay utilised will be the native choline release assay, which is considered a more robust assay for the identification of ATX inhibitor compounds as it functions by determination of the amount of choline (**2**) released from the hydrolysis of LPC (**1**) to LPA (**3**). As a result, the binding mode of the inhibitors with the enzyme is not important as if the enzyme is inhibited in any way then this will affect the production of choline (**2**) from the hydrolysis of LPC (**1**).

4.2.4 Section A: Substitution on the Benzenoid Ring

The first of the four key regions to be analysed was Section A associated with the functionality and substitution of the benzenoid ring, which was an important SAR component from both the patent literature and the modelling studies. To achieve this, the section was further divided into two sub categories, the first involved analysis of the position of the favoured chlorine and the second involved the introduction of alternative groups, specifically Me, OMe, and F, to determine if these would be tolerated, Scheme 18.

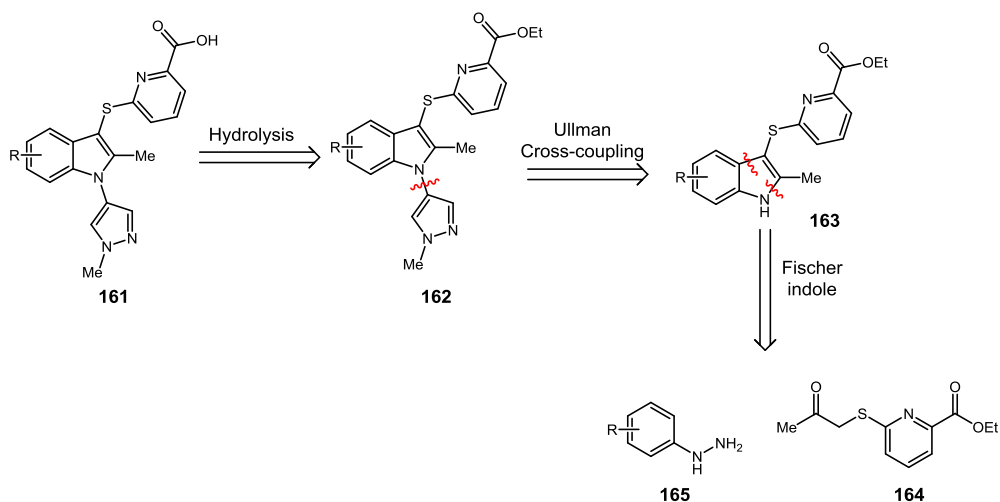


Scheme 18: Specific compounds proposed for synthesis within Section A.

4.2.4.1 Regiochemistry of the Chlorine

4.2.4.1.1 Retrosynthetic Analysis

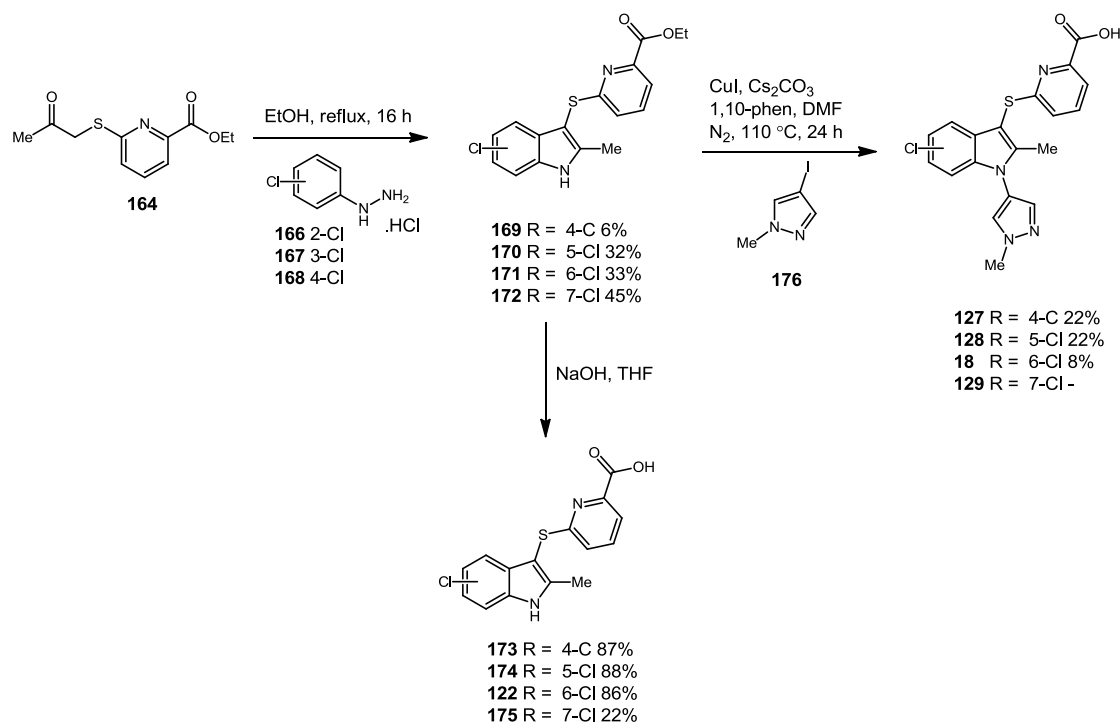
To gain access to the desired compounds **18** and **127-129** a simple retrosynthetic analysis was conducted, illustrated in Scheme 19, where it was believed that these compounds could be accessed using three main reactions: Fischer indole synthesis, Ullman cross-coupling, and hydrolysis.



Scheme 19: Retrosynthetic analysis for the synthesis of compounds **18** and **127-129**.

4.2.4.1.2 Synthetic Route

The key steps in the synthetic route involved the development of the core indole motif *via* Fischer indole synthesis, followed by an Ullman cross-coupling to introduce the methyl pyrazole on the nitrogen of the indole (Scheme 20).



Scheme 20: Synthesis of Section A compounds.

The initial step in the process involved the synthesis of the core indole scaffold containing the chlorine motif in the 4-, 5-, 6-, and 7-position of the ring. This was achieved using Fischer indole conditions with compound **164**¹⁰² and either 2-, 3-, or 4-chlorophenylhydrazine hydrochloride (**166-168**). Compounds **170-172** gave reasonable yields; however a significantly lower yield was obtained for compound **169**. This was due to the Fischer indole reaction using 3-chlorophenylhydrazine hydrochloride resulting in the formation of two regioisomers of the indole product with the chlorine in either the 6- or the 4-position of the benzenoid ring. This was beneficial from an SAR point of view as it would allow access to an additional set of compounds from the same reaction conditions. Indoles **169-172** were hydrolysed to afford the corresponding acids **122**, and **173-175**. Indoles **169-172** were also subjected to an Ullman cross-coupling reaction to install the desired methyl pyrazole

on the nitrogen of the indole (**18** and **127-129**). This was achieved using CuI, Cs₂CO₃, and 1,10-phenanthroline (1,10-phen) in DMF at 110 °C. Unfortunately, these conditions delivered low yields of the desired products. A small percentage of the hydrolysed starting material (compounds **188-194**) was also isolated, however this did not account for the remainder of the mass balance which was assumed could have been lost due to the harsh reaction conditions and the potential of complexation of the copper to the starting material. Attempts to optimise these reaction conditions proved difficult and time-consuming. Therefore, as small quantities of product were obtained, it was decided to continue with these conditions, and, if interesting biological data was obtained then a more in-depth optimisation study would be conducted to rectify this problem.

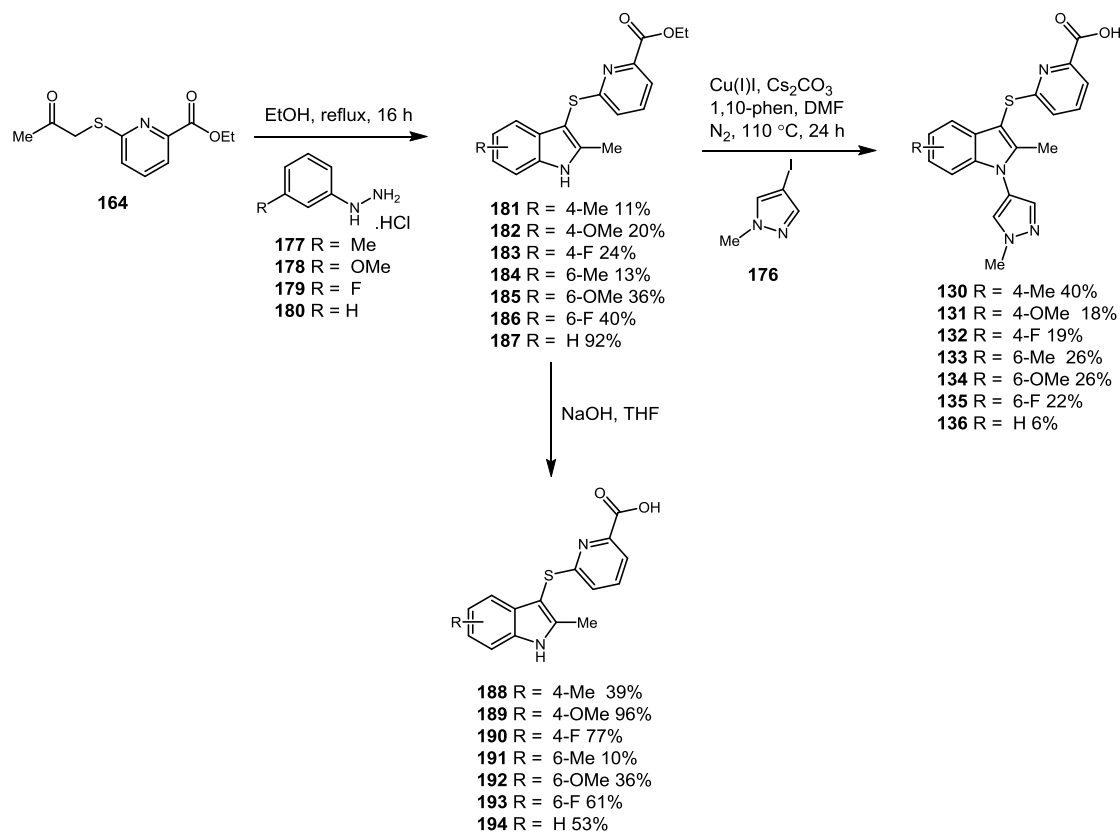
Additional problems were encountered with the synthesis of compound **129** as under the standard conditions no reaction occurred. In an attempt to push the reaction additional catalyst was added, and the reaction time was extended, however, this led to the degradation of the starting material. It was believed that the problem may be due to the unfavourable steric interaction of the chlorine and the pyrazole group. Looking back into the patented data it became apparent that Amira Pharmaceuticals⁶⁸ had claimed a similar compound, however, it had not been synthesised perhaps indicating the complexity of this structure.

4.2.4.2 Introduction of Substitution on the Indole Ring

4.2.4.2.1 Synthetic Route

The same route was used for the introduction of substitution on the indole ring. The initial step again involved the synthesis of the core indole structure which was achieved by the reaction of **164** with either *m*-tolylhydrazine hydrochloride (**177**), 3-methoxyphenylhydrazine hydrochloride (**178**), 3-fluorophenylhydrazine hydrochloride (**179**) or phenylhydrazine hydrochloride (**180**) under the Fischer indole conditions described previously. This allowed access to the desired indole backbone with substitution in either the 4-, or the 6-position due to the two regioisomers formed from the reaction (Scheme 21). In general the Fischer indole proceeded moderately well, where the slightly low yields could be attributed to the difficulty in separation of the two regioisomers which was achieved using preparative high-pressure liquid chromatography (HPLC) methods.

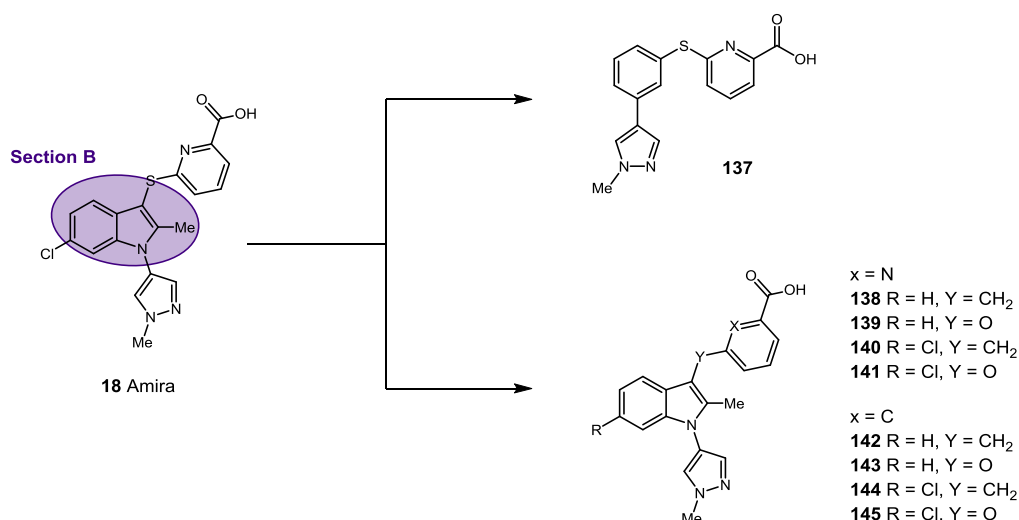
With the indole cores in hand these were then hydrolysed (Scheme 21) to gain access to the corresponding pyridyl acid compounds (compounds **188-194**), in generally good yields. Alternatively, the **181-187** were subjected to the previous Ullman cross-coupling conditions to install the desired methyl pyrazole functionality on the nitrogen of the indole (compounds **130-136**), in moderate yields of 20-40%.



Scheme 21: Synthesis of compounds within Section A with alternative substitution on the benzenoid ring.

4.2.5 Section B: Core Modifications

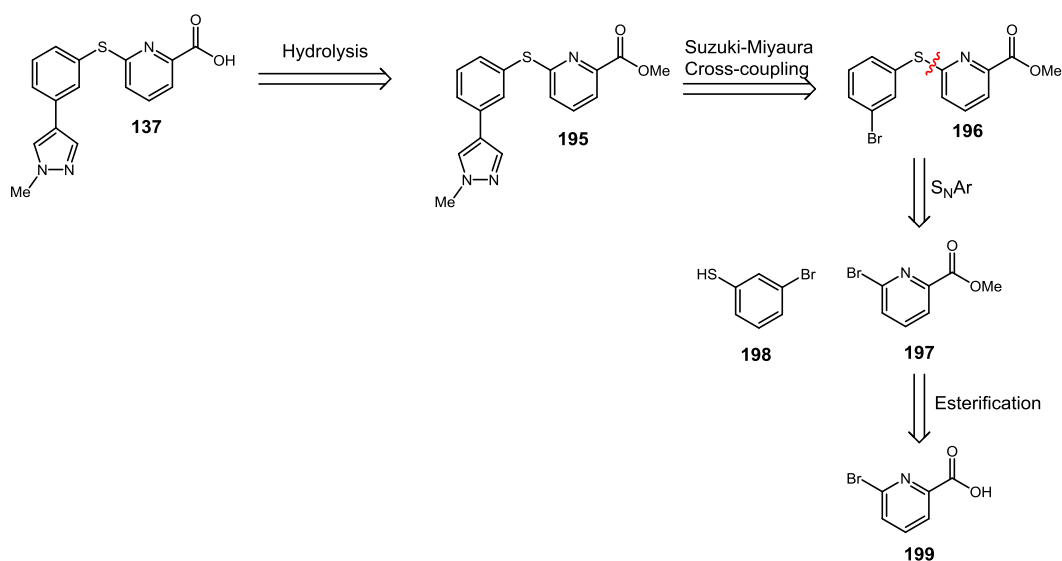
The second section of the Amira compound **18** to be analysed was the indole core. This was again broken down into two sub-groups: i) the removal of the indole core; and, ii) the introduction of different linkers, including methylene, ether, and (the original) thioether linker (Scheme 22). The latter of these core modifications was conducted by a fellow member of the group.¹⁰¹



Scheme 22: Compounds proposed for synthesis within Section B.

4.2.5.1 Retrosynthetic Analysis

The route proposed for the synthesis of **137** is illustrated in Scheme 23. This involves a four step process using esterification, S_NAr, Suzuki-Miyaura cross-coupling, and finally hydrolysis.

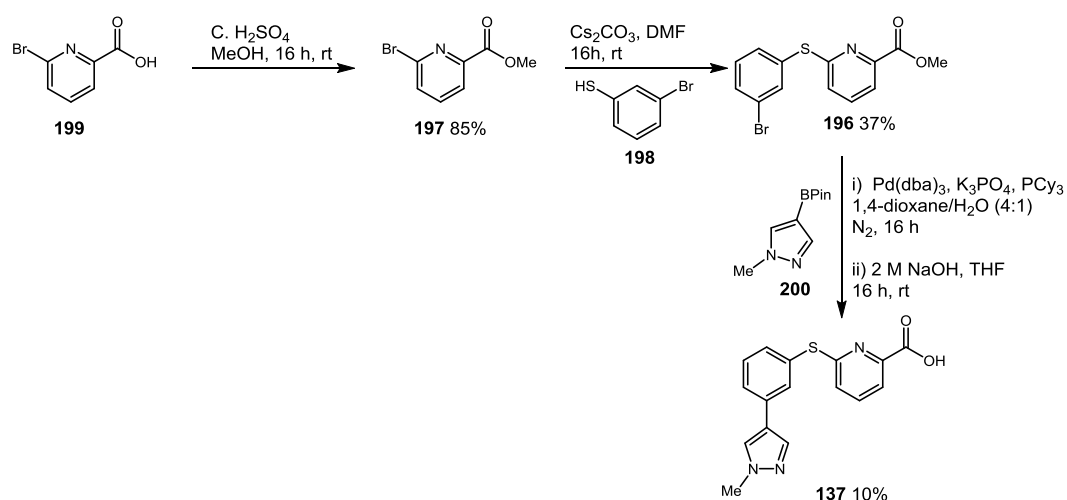


Scheme 23: Retrosynthetic analysis for the synthesis of compound **137**.

4.2.5.2 Synthetic Route

The initial step of the synthetic route involved an esterification of 6-bromo-pyridyl-2-carboxylic acid (**199**) using concentrated H₂SO₄ in MeOH to give the desired ester

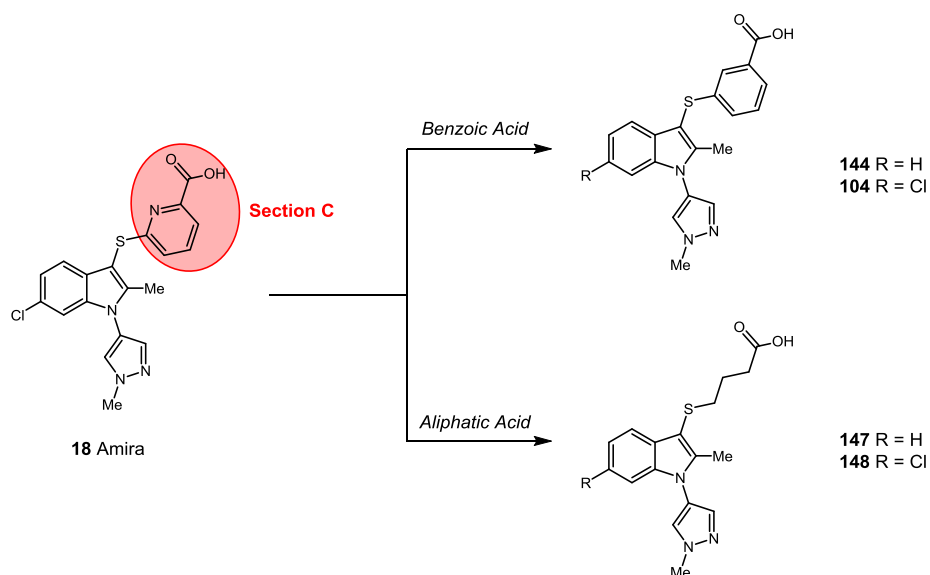
197 in an 85% yield (Scheme 24). Ester **197** was then reacted with 4-bromothiophenol (**198**) via an S_NAr reaction to obtain compound **196** in a 37% yield. With the core structure in place, the penultimate step involved the introduction of the methyl pyrazole functionality which was achieved using Suzuki-Miyaura cross-coupling conditions followed by an *in situ* hydrolysis to give the desired compound **137** in a 10% yield.



Scheme 24: Synthetic route for the preparation of compound **132** within Section B.

4.2.6 Section C: Derivatisation of the Acid Warhead

The third section studied was the acid head group. This series of compounds was split into two subgroups where the first would introduce the benzoic acid functionality in place of the pyridyl acid and the second group contained a long chain aliphatic acid to challenge the need for an aryl acid (Scheme 25).

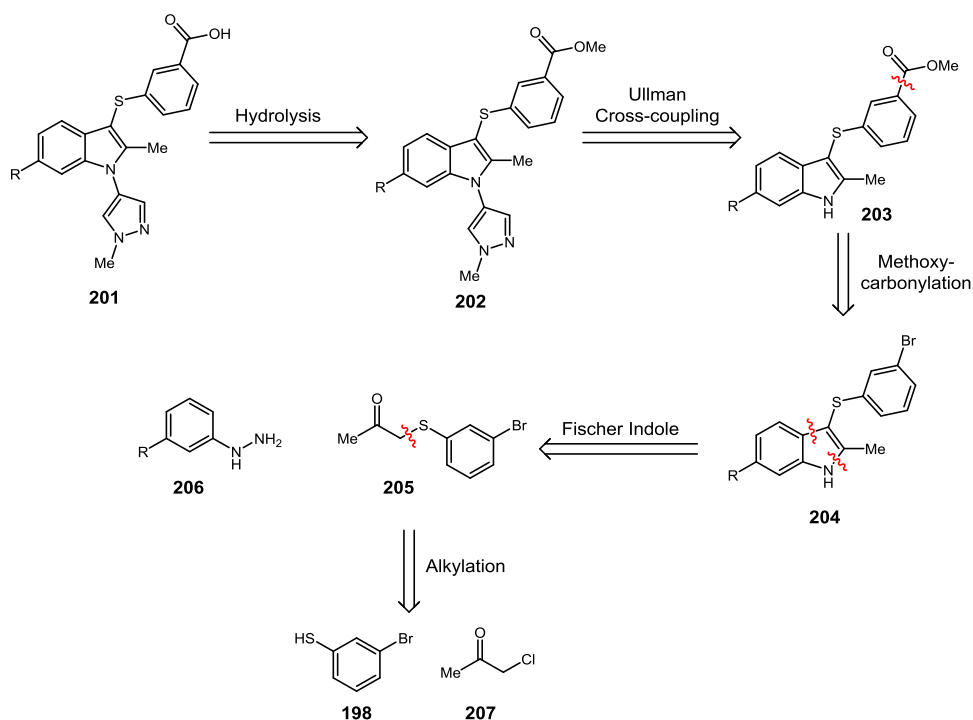


Scheme 25: Specific compounds proposed for synthesis within Section C.

4.2.6.1 Benzoic Acid SAR

4.2.6.1.1 Retrosynthetic Analysis

Retrosynthetic analysis for these benzoic acid compounds is illustrated in Scheme 26, where the main steps are aligned with those for the previously synthesised compounds in Section 11.4. However, the route varied slightly with the need to synthesise the ketone component (**205**) required for the Fischer indole reaction. The proposed route of which, therefore, would require an alkylation to afford the desired ketone which could then undergo the indole synthesis followed by a methoxycarbonylation to install the required functionality.

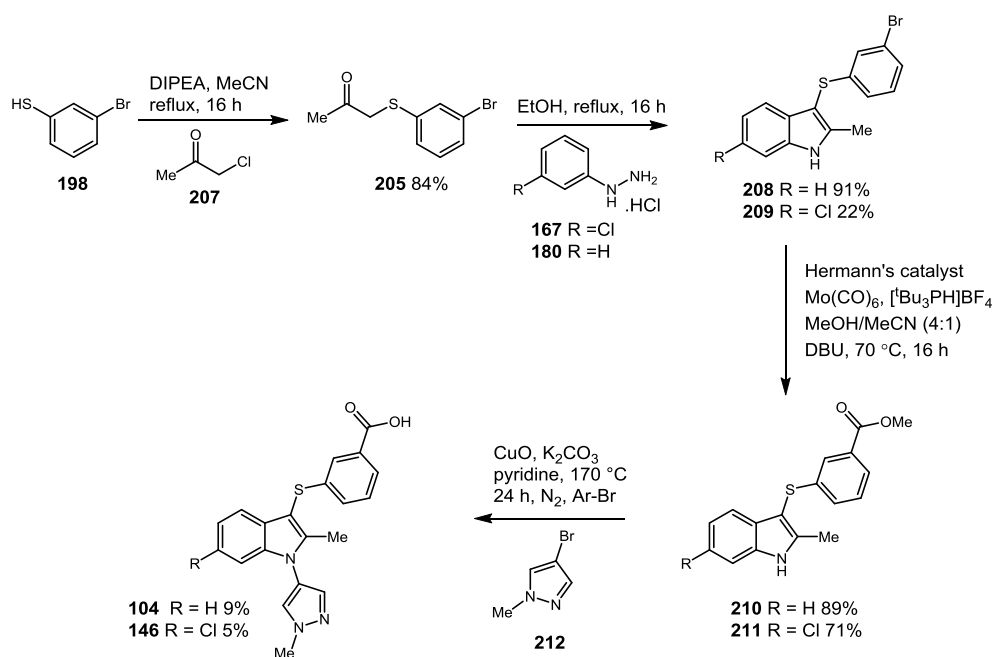


Scheme 26: Retrosynthetic analysis for the synthesis of the benzoic acid series compounds within Section C.

4.2.6.1.2 Synthetic Route

The first step of the synthetic route required the synthesis of the ketone precursor **205** for use in the Fischer indole reaction. This was synthesised using commercially available 3-bromothiophenol **198** and performing an alkylation reaction with chloroacetone **207** to give **205** in a good yield of 84% (Scheme 27). The core indole was then generated by reacting **205** with either 3-chlorophenylhydrazine hydrochloride (**167**) or phenylhydrazine hydrochloride (**180**), using similar conditions as discussed previously (Section 11.4), to obtain compounds **208** and **209** in a 91% and 22% yield, respectively. Compound **209** had a lower yield compared to the corresponding **208**, the main reason of which was due to the difficulty in separating the two regioisomers from the Fischer indole reaction (6-chloro and the 4-chloro). Indoles **208** and **209** were then converted into the corresponding carbonyl compounds **210** and **211** using methoxycarbonylation conditions routinely used within the group which use molybdenum hexacarbonyl, Hermann's catalyst, and DBU which afforded the desired compounds **210** and **211** in moderate yields of 89% and 71%, respectively. Compounds **210** and **211** were then subjected to an Ullman

cross-coupling, detailed within the Amira patent,⁶⁹ to install the desired methyl pyrazole functionality. It was found that as a result of the harsh forcing conditions of the Ullman reaction between **212** and **210** or **211** the indole ester was hydrolysed *in situ* to the corresponding acid **104** and **146**. This, however, was beneficial as the acid was ultimately required (Scheme 27). The yields obtained for **104** and **146** were low due to the difficulties associated with the Ullman cross-coupling reaction. An in-depth study into the literature precedent regarding this reaction was conducted, however, it became evident that the only information available regarding this transformation was from Amira Pharmaceuticals.

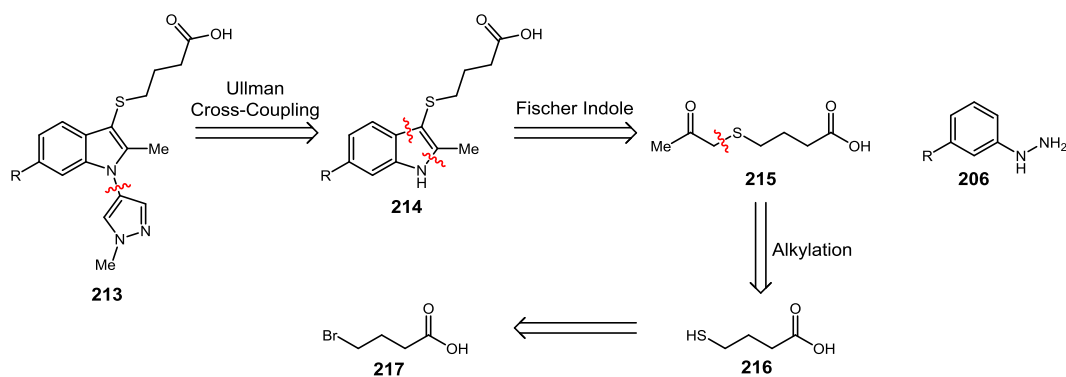


Scheme 27: Synthetic route for compounds **104**, and **146** within Section C.

4.2.6.2 Aliphatic Acid Series

4.2.6.2.1 Retrosynthetic Analysis

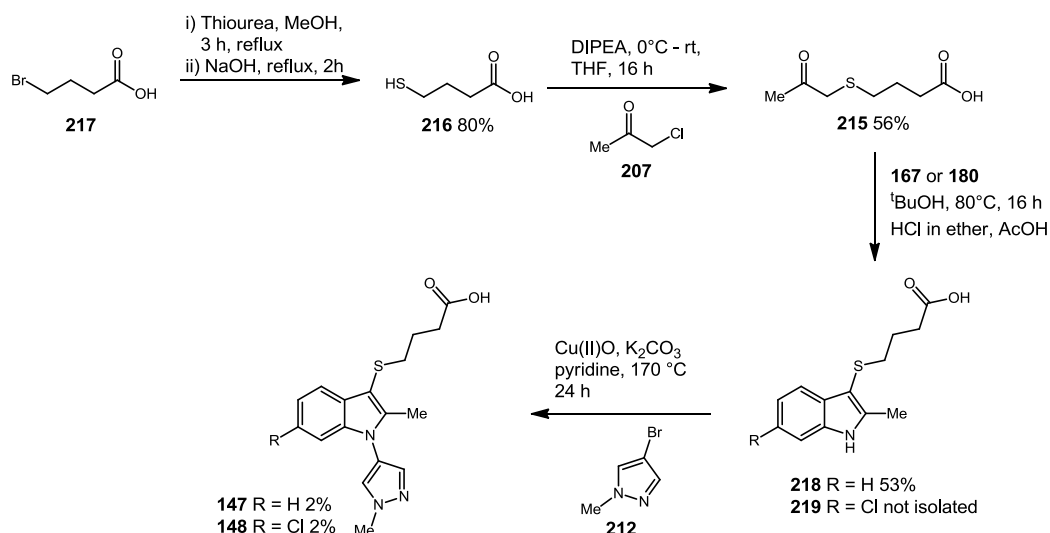
In a similar vein to the benzoic acid route, the method for the synthesis of the aliphatic acid compounds involved the Fischer indole and Ullman cross-coupling reactions. However, again the ketone required for the indole reaction would require synthesis. This was proposed to be accessed in a two-step process; the first being the conversion of bromobutyric acid **217** to the corresponding thiol **216** which could then undergo an alkylation reaction to install the required ketone functionality (Scheme 28).



Scheme 28: Retrosynthetic analysis for the synthesis of compounds **147** and **148** within Section C.

4.2.6.2.2 Synthetic Route

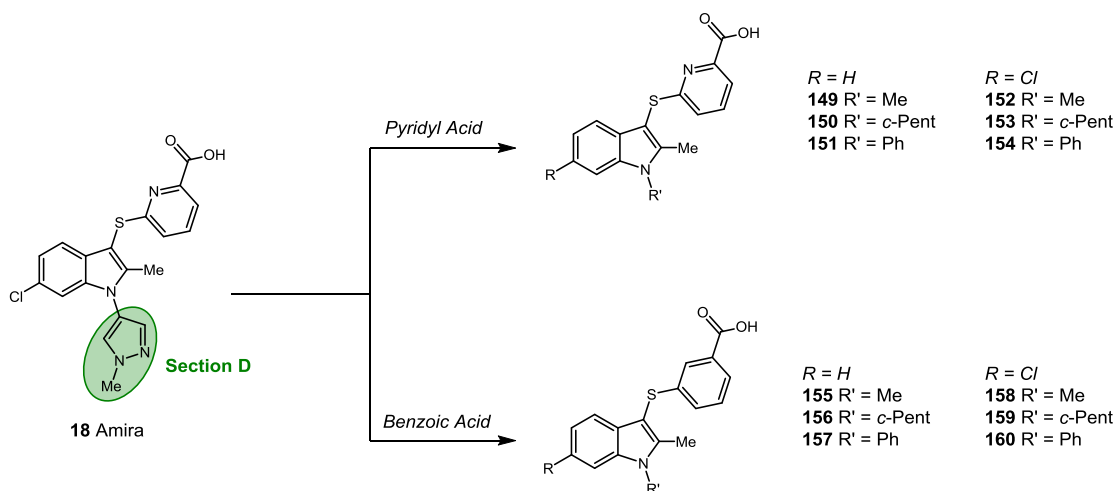
The first step of the synthetic route required the conversion of bromobutyric acid **217** to the corresponding thiol **216** which was achieved using thiourea to give the desired compound in an 80% yield (Scheme 29). Thiol **216** could then undergo an alkylation reaction with chloroacetone **207** to afford the desired ketone compound **215** in a 56% yield. With ketone **215** in hand this could be reacted with 3-chlorophenylhydrazine **167** or phenylhydrazine **180** under the Fischer indole conditions described previously to obtain the desired indoles **218** and **219**. Due to the difficulties in the separation of the 4-chloro and the 6-chloro indoles associated with **219** it was decided to telescope the mixture into the Ullman cross-coupling reaction and obtain the final product by preparative HPLC purification. Compound **218** was also subjected to the Ullman conditions to install the required methyl pyrazole giving the final compounds **147** and **148** (Scheme 29), which were again obtained in very low yields of 2%.



Scheme 29: Synthetic route for the construction of compounds **147** and **148** in Section C.

4.2.7 Section D: Indole Substitution

The last region to be studied was the diversification of the substitution on the indole nitrogen. This was again split into two sub-categories associated with probing the functionality using the pyridyl acid scaffold and the benzoic acid scaffold, as both of these were investigated initially by Amira Pharmaceuticals within their patents.^{68,69} Three main functionalities would then be introduced, two aliphatic groups (Me and *c*-Pent), and two aromatic groups (Ph and methyl pyrazole) (Scheme 30). In terms of the functionalised benzoic acid compounds these were synthesised by Lisa Miller.¹⁰¹



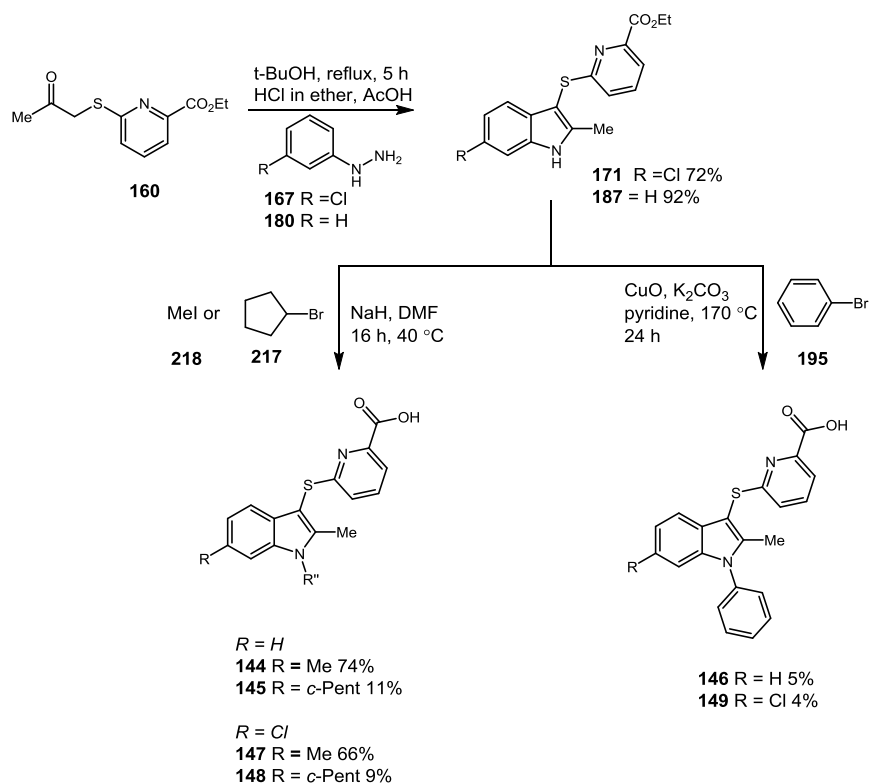
Scheme 30: Specific compounds proposed for synthesis within Section D.

4.2.7.1 Pyridyl Acid Series

4.2.7.1.1 Synthetic Route

The route to synthesise compounds **149-154** was based around the previously developed routes in section A and C. The first step involved the synthesis of the indoles **171** and **187** using the previously established Fischer indole conditions with either phenylhydrazine hydrochloride **180** or 3-chlorophenylhydrazine hydrochloride **167** and ketone **164**¹⁰² giving compound **171** and **187** in good yields of 71% and 92%, respectively (Scheme 31). Indoles **171** and **187** could then be used in the subsequent cross-coupling and alkylation reactions to install the required functionality on the indole nitrogen. The introduction of the Ph derivative was achieved using the Ullman cross-coupling method as developed previously within Sections A-C to give compounds **151** and **154**. Although, the reaction was generally very low yielding, around 10%, sufficient quantities of the desired compounds were isolated for initial biological evaluation.

Similar problems were found during attempted alkylation of the indole nitrogen of compound **171** and **187** with iodomethane (**221**) and bromocyclopentane (**222**). In order to form the desired compounds **149**, **150**, **152**, and **153** a small optimisation study indicated the need for three equivalents of sodium hydride, to push the reaction. By doing this, it was possible to gain access to the Me substituted compounds **149** and **152** in good yields of 74% and 66% respectively. Unfortunately, the *c*-Pent derivatives **150** and **153** were not as high yielding, resulting in the isolation of only 10% of the required products (Scheme 31). This nonetheless, was enough for biological evaluation.



Scheme 31: Synthesis towards compounds proposed in Section D.

The equivalent benzoic acid derivatives (**155-160**) were synthesised in a similar manner by a fellow member of the team.¹⁰¹

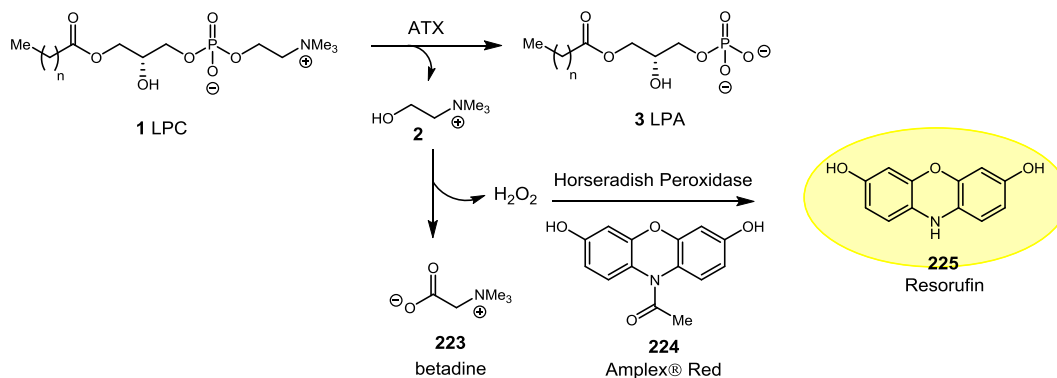
4.3 Pharmacology

The generated compound library, which focused on the four main structural sections A-D, were then evaluated for biological activity using two assay formats, the bis-*p*NPP assay, and the Amplex® Red choline release assay.

The bis-*p*NPP assay proceeds *via* the hydrolysis of the unnatural substrate bis-*p*-nitrophenyl substrate to generate *p*-nitrophenol, as described previously in Section 5.2. This has a characteristic UV signal of 450 nm allowing for quantification of the *p*-nitrophenol substrate which will in turn give an indication of the biological activity of the tested compounds as the percentage of hydrolysis is inversely proportional to the percentage of activity.

The Amplex® Red assay involves the use of the natural substrate LPC (**1**), which is hydrolysed to LPA (**3**) with the release of choline (**2**), which can be detected using a two-step enzymatic colouring reaction. This proceeds by reaction of choline (**2**) with

choline oxidase to form betadine (**223**) and hydrogen peroxide (H_2O_2), the latter of which can react with HRP and the colouring reagent Amplex® Red (**224**) to give Resorufin (**225**), which can be detected by its characteristic UV signal at 405 nm (Scheme 32).



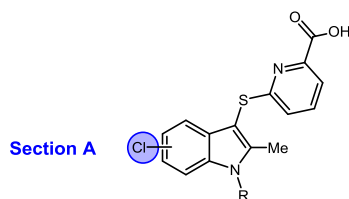
Scheme 32: Amplex® Red assay procedure where the choline released from LPC hydrolysis is quantified using a two-step enzymatic colouring reaction.

As discussed previously, the main reason for using this dual assay procedure is to assess alternative binding modes as it is unknown how these compounds bind within the pocket. Therefore, this procedure will not only give information regarding biological activity but will also allow for information to be gained regarding the location of the binding site, as the bis-*p*NPP is substrate specific for inhibitors binding within the active site whereas the LPC assay is not.

4.3.1 Section A: Substitution on the Benzenoid Ring

The screening results for Section A compounds, with altering position of the chlorine, are presented in Table 16.

Table 16: Chlorine regiochemical analysis biological data.



Entry	Cpd. No. ^a	Pos. ^b	R	Bis- <i>p</i> NPP Ki (μM) ⁹⁰	LPC IC ₅₀ (μM) ¹⁰³
1	173	4	H	>30	>30
2	127	4	1-methyl-1 <i>H</i> -pyrazole	>30	p
3	174	5	H	>30	p
4	128	5	1-methyl-1 <i>H</i> -pyrazole	>30	<1
5	122	6	H	>30	p
6	18*	6	1-methyl-1 <i>H</i> -pyrazole	0.07	<1
7	175	7	H	>30	>30

^aCompound number, ^bPosition of substituent R, p - data pending further analysis. * Original Amira compound.

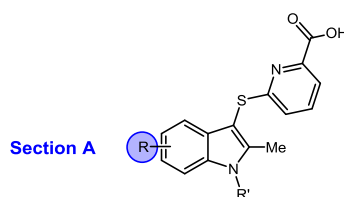
Analysis of the compound set containing different chlorine regioisomers (compounds **18**, **122**, **127**, **128**, and **173-175**) revealed that within the bis-*p*NPP assay only the original Amira compound **18** (entry 6) was able to inhibit ATX. However, analysis of the same compound set within the LPC assay indicated that the position was not as important as previously thought as compounds **128** and **18** (entry 4 and 6) displayed comparable activity of <1 μM. It is also hypothesised that compound **127** (entry 2) may also display activity within the LPC assay, however, further testing is required. This could suggest a difference in binding between the regioisomers as **128** exhibits no activity within the bis-*p*NPP but <1 μM in the LPC. This difference could be indicative of the compounds binding remote from the active site. A potential hypothesis regarding the difference in activity between the two assays could be attributed to the orientation of the molecules within the enzyme; when in the 6-

position the chlorine is believed to sit within a cleft in the pocket, as previously outlined within the molecular docking Section 11.2, thus allowing for the pyridyl acid to interact with the Zn^{2+} . For the other regioisomers it could be postulated that the chlorine still orientates so that it sits within this cleft, and as a result the orientation of the pyridyl acid will alter and no longer point towards the Zn^{2+} thus showing inactivity within the bis-*p*NPP. This hypothesis can be further validated with recent work conducted by Stein *et al*⁴¹ which indicates the differences between these two assays as the unnatural bis-*p*NPP assay is substrate specific. Thus, if compounds bind remote from the active site then the bis-*p*NPP substrate can still access the active site and subsequently become hydrolysed to *p*-nitrophenol, giving a false negative.

In addition to this, it is also evident that the methyl pyrazole is required for activity as its elimination in compound **175** (entry 7) compared to **18** (entry 6) led to a complete loss of activity within the bis-*p*NPP assay. It is also hypothesised that compounds **174** and **122** (entry 3 and 5) would also prove to be inactive within the LPC assay due to the previous data; however, additional testing is required in order to confirm the data.

The screening results for Section A compounds, with alternative functionality on the benzenoid ring, are presented in Table 17.

The presence of functionality on the benzenoid ring was found to be important for biological activity as compound **194** (entry 13) displayed no activity compared to the original Amira compound **18**. In addition, the absence of the methyl pyrazole on the nitrogen of the indole also resulted in no activity (compound **136**, entry 14) which was to be expected. Upon analysis of the compounds with alternative substitution on the benzenoid ring (Me, OMe, and F) in both the 4-, and the 6-position, significant differences were apparent between the two assays. From the bis-*p*NPP only compound **135** (entry 12), containing 6-F, displayed activity. Additional testing within the LPC assay, however, found the vast majority of the data set displayed some activity.

Table 17: Alternative substitution on the benzenoid ring biological data.

Entry	Cpd. No. ^a	Pos. ^b	R	R'	Bis-pNPP Ki (μM) ⁹⁰	LPC IC ₅₀ (μM) ¹⁰³
1	188	4	Me	H	>30	1-10
2	130	4	Me	1-methyl-1 <i>H</i> -pyrazole	>30	1-10
3	189	4	OMe	H	>30	1-10
4	131	4	OMe	1-methyl-1 <i>H</i> -pyrazole	>30	1-10
5	190	4	F	H	>30	1-10
6	132	4	F	1-methyl-1 <i>H</i> -pyrazole	>30	1-10
7	191	6	Me	H	>30	10-20
8	133	6	Me	1-methyl-1 <i>H</i> -pyrazole	>30	<1
9	192	6	OMe	H	>30	>30
10	134	6	OMe	1-methyl-1 <i>H</i> -pyrazole	>30	p
11	193	6	F	H	>30	1-10
12	135	6	F	1-methyl-1 <i>H</i> -pyrazole	3	<1
13	194	-	H	H	>30	20-30
14	136	-	H	1-methyl-1 <i>H</i> -pyrazole	>30	>30

^aCompound number, ^bPosition of substituent R, p - data pending further analysis.

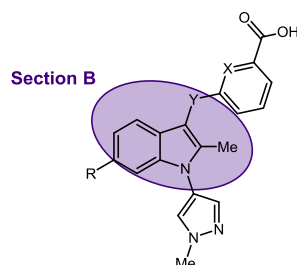
The trends established from the LPC data indicated that substitution in the four position (entry 1-6) resulted in IC₅₀ values of 1-10 μM regardless if the indole nitrogen contained substitution (compounds **130-132**, entry 2, 4, and 6) or not (compounds **188-190**, entry 1, 3, and 5). The corresponding 6-substituted regioisomers, however, indicated that substitution on the nitrogen of the indole resulted in increased activity compared to the non-substituted equivalents (compounds **191-194** entry 7, 9 and 11 compared to compounds **133-135** entry 8, 10, and 12). Interestingly, the 6-Me and 6-F compounds **133**, and **135** (entry 8, and 12) displayed comparable data within the LPC assay (IC₅₀ <1 μM) with the original

Amira compound **18** ($IC_{50} < 1 \mu M$) suggesting that alternative substitution on the benzenoid ring is tolerated. As inactivity was observed from the bis-*p*NPP assay for compound **133** it can be hypothesised that it binds remote from the active site, whereas compound **135** is presumed to bind in a similar fashion to the original Amira compound **18**, due to the activity shown in the bis-*p*NPP assay. In terms of functionality, it seems that both electron withdrawing and electron donating groups are tolerated, however, with the absence of functionality there is a loss of activity suggesting that these groups are making important interactions within the enzyme.

4.3.2 Section B: Core Changes

The screening results for Section B compounds are presented in Table 18.

Table 18: Section B - core changes biological data.



Entry	Cpd. No. ^a	R	Y	X	Bis- <i>p</i> NPP Ki (μM) ⁹⁰	LPC IC ₅₀ (μM) ¹⁰³
1	143	H	O	C	>30	>30
2	145	Cl	O	C	0.8	<1
3	142	H	CH ₂	C	>30	>30
4	144	Cl	CH ₂	C	86 nM	1-10
5	146	H	S	C	>30	>30
6	04	Cl	S	C	8.5	p
7	138	H	CH ₂	N	>30	>30
8	140	Cl	CH ₂	N	194 nM	<1
9	136	H	S	N	>30	p
10	18 *	Cl	S	N	0.07	<1

^aCompound number, p - data pending further analysis, * Original Amira compound.

Analysis of the compound set generated from the core modifications showed that in general the data obtained from both the bis-*p*NPP and the LPC assay were consistent. This allowed for two conclusions to be made which were: the chlorine moiety seemed important for activity as compound **145**, **144**, **104**, **140** and **18** (entry 2, 4, 6, 8, and 10) all displayed activity whereas **143**, **142**, **144**, **138**, and **136** (entry 1, 3, 5, 7, and 9) were inactive; altering the linker in the benzyl series illustrated that all three of the linkers were tolerated (ether, methylene, and thioether) although it is worthy to note that there was a slight drop in activity with the methylene linker when comparing the pyridyl and benzoic compounds (**140** and **144** respectively). In terms of the pyridyl derivatives both the thioether and ether linked compounds **18**, and **140** were equipotent, and also found to be more active than the corresponding benzoic acid compounds **144** and **104**.

From this, it could be hypothesised that these compounds may be binding within the active site due to activity being registered when using the bis-*p*NPP assay. From these trends it can also be hypothesised that the ether linked pyridyl compound **141** may lead to a further increase in activity compared to the thioether linked alternative. However, this was found not to be synthetically tractable.

In addition to this data, it was found that elimination of the indole ring, compound **137**, (Figure 46) resulted in a complete loss of activity. This may be due to the absence of the important 6-Cl motif, which has been shown previously to increase activity, or perhaps the truncated structure does not allow for the previous interactions within the pocket to be picked up.

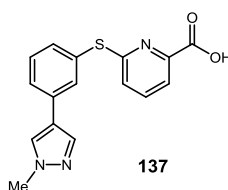
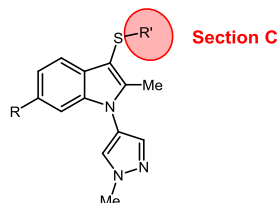


Figure 46: Compound **137**.

4.3.3 Section C: Derivatisation of the Acid Warhead

The screening results for Section C compounds are presented in Table 19.

Table 19: Section C - Derivatisation of the acid warhead biological evaluation.



Entry	Cpd. No. ^a	R	R'	Bis-pNPP Ki (μM) ⁹⁰	LPC IC ₅₀ (μM) ¹⁰³
1	146	H		>30	>30
2	104	Cl		8.5	p
3	147	H		>30	1-10
4	148	Cl		>30	1-10
5	136	H		>30	>30
6	18*	Cl		0.07	<1

^aCompound number, p - data pending further analysis. * Original Amira compound.

Analysis of the compound set containing alternative acid warheads (benzoic acid, and aliphatic acid) indicated differences between the two assays. When tested in the bis-pNPP assay with the absence of the 6-Cl (compounds **146**, and **136** entry 1 and 5) no activity was observed, which could be expected from the previous data generated indicating the importance of this moiety for activity. On moving to the corresponding 6-Cl derivatives (compounds **104**, and **148** entries 2 and 4), the benzoic acid derivative **104** exhibited activity at 8.5 μM, while the aliphatic acid compound **148** was inactive. Interestingly, however, when this data set was analysed within the LPC assay the aliphatic acid derivatives **147** and **148** (entry 3

and 4) both displayed some activity. In terms of the benzoic equivalent **104** (entry 2) additional analysis is required, but it is hypothesised that this will also display activity.

In terms of the aliphatic acid compounds **147** and **148** the absence of activity in the bis-*p*NPP assay indicates that perhaps these compounds reside remote from the active site. Comparing this data with the previous pyridyl acid derivatives **136** and **18** (entry 5 and 6) illustrates that these are not as active as the original Amira compound **18**. A reason for this may be due to the increased rotational freedom associated with the aliphatic acid.

The benzoic acid derivatives were expected to act similarly to the pyridyl acid derivatives due to the similarity in structure, and this was in fact the case as compounds **146** and **136** were both inactive and **104** and **18** were both active within the bis-*p*NPP assay, however, additional analysis is required of compound **104** within the LPC assay.

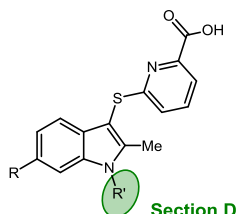
4.3.4 Section D: Indole Nitrogen Substitution

The screening results for Section D compounds are presented in Table 20.

Analysis of the compound set containing various functionality on the nitrogen of the indole again illustrated the importance of the chlorine moiety for activity as its removal led to a complete loss of activity in compounds **146**, **149-151**, and **194** (entry 1-5) compared to **18**, **122**, and **152-154** (entry 6-10). This generally tracked well with the LPC data, except in the case of compound **151** (entry 1) where, interestingly, inhibition is regained with the introduction of the Ph group on the nitrogen of the indole. This perhaps suggests again that this compound is binding remote from the active site. Moving to the corresponding 6-Cl derivatives **18**, **152-154**, and **122** (entry 6-10) it was established that substitution on the nitrogen of the indole was important as **122** (entry 10), which lacked this, exhibited no biological activity. In terms of the functionalised compounds it was found that the bis-*p*NPP assay, increased activity was associated with the aromatic moieties, compounds **154** and **18** (entry 6 and 7) compared to the aliphatic groups, compounds **152** and **153** (entry 8 and 9). A similar set of results was obtained when analysed using the native LPC assay with slight variations associated with compounds **151** and **152**, Me and Ph derivatives respectively. In terms of compound **151** it can be assumed that it

is occupying a space remote from the active site. This may be as a result of the lack of the 6-Cl group which was speculated to set the orientation of the molecule within the active site due to the cleft which the chlorine is believed to reside in, identified within the previous docking studies.

Table 20: Section D - Indole nitrogen substitution on pyridyl system biological data.



Entry	Cpd. No.	R	R'	Bis- <i>p</i> NPP Ki (μ M) ⁹⁰	LPC IC ₅₀ (μ M) ¹⁰³
1	151	H	Ph	>30	<1
2	146	H	1-methyl-1 <i>H</i> -pyrazole	>30	>30
3	149	H	Me	>30	>30
4	150	H	<i>c</i> -Pent	>30	>30
5	194	H	H	>30	20-30
6	154	Cl	Ph	0.9	<1
7	18*	Cl	1-methyl-1 <i>H</i> -pyrazole	0.07	<1
8	152	Cl	Me	>30**	<1
9	153	Cl	<i>c</i> -Pent	5	1-10
10	122	Cl	H	>30	p

^aCompound number, p - data pending further analysis, * Original Amira compound, ** Curve tailed off at 40% hydrolysis and as a result was deemed inactive.

In terms of compound **152** again the difference in activity could be associated with binding remote from the active site. An additional observation which was found with **151** within the bis-*p*NPP assay was that the percentage inhibition did not fall below 40%, this could be as a result of a non-competitive binding mode. This hypothesis will be discussed in more detail in Section 11.8.5.

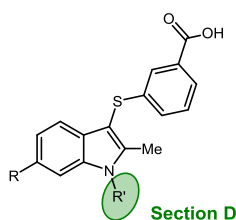
In terms of the functional group tolerance, varying results were found depending on the assay used. It can be hypothesised that in the bis-*p*NPP assay Ph, methyl pyrazole, and *c*-Pent derivatives are binding within the active site *i.e.*, with the

pyridyl acid residing in close vicinity to the Zn^{2+} ions and the functionality of the indole protruding into a cleft. In addition to this, the slight difference between the aromatic functionality (compounds **154**, and **18**) activity compared to the *c*-Pent (compound **153**) could be associated with the structure in that the more 3-dimensional sp^3 hybridised compounds are less favoured perhaps due to the space present within the cleft. One point to note, however, is the comparable activity of Ph, methyl pyrazole, and Me within the LPC assay. As stated previously, this suggests compound **151** does not sit in the active site, and thus implies that the functionality on the nitrogen is less important. This hypothesis could be further validated with compound **122** which lacks substitution on the nitrogen, however, additional testing is required within the LPC assay to confirm the data.

Analysis of compounds **104**, **146**, **155-160**, **226**, and **227** (Table 21) which were the benzoic acid equivalents of the previous set of compounds, illustrated that there were similarities with these two data sets as to be expected.

For the benzoic acid compounds lacking substitution on the benzenoid ring (compounds **146**, **155-157**, and **226**, entry 1-5) no activity was observed within either assay, except for compound **157** which again displayed some activity within the LPC assay. This data correlated well with that obtained previously for the pyridyl compounds.

Moving to the 6-Cl substituted compounds **104**, **158-160**, and **227** (entry 6-10) it was again found that substitution on the indole nitrogen was important as **227** exhibited no activity. In terms of the functionality that was tolerated it was found that again Ph, methyl pyrazole, and Me were tolerated more than the *c*-Pent group. Again, this correlated with the data from the pyridyl series and as such it can be hypothesised that these two series are binding in a similar mode.

Table 21: Section D - Indole nitrogen substitution on benzoic acid system biological data.

Entry	Cpd. No. ^a	R	R'	Bis- <i>p</i> NPP Ki (μM) ⁹⁰	LPC IC ₅₀ (μM) ¹⁰³
1	157	H	Ph	20	1-10
2	146	H	1-methyl-1 <i>H</i> -pyrazole	>30	>30
3	155	H	Me	>30	>30
4	156	H	<i>c</i> -Pent	>30	>30
5	226	H	H	>30	>30
6	160	Cl	Ph	347 nM	<1
7	104	Cl	1-methyl-1 <i>H</i> -pyrazole	8.5	p
8	158	Cl	Me	133 nM	<1
9	159	Cl	<i>c</i> -Pent	>30	20-30
10	227	Cl	H	>30	>30

^aCompound number, p - data pending further analysis.

Looking at both the pyridyl acid and the benzoic acid series it became apparent that these displayed similar trends in that substitution on the indole nitrogen and the presence of the 6-Cl moiety on the benzenoid ring illustrated increased activity. In addition to this, it was found that in general the pyridyl compounds displayed comparable activity which was to be expected due to the similarity associated with these structures.

4.3.5 Assay Kinetics

One point to note, which became apparent after testing the compound library within the bis-*p*NPP assay, was the presence of abnormalities within the data generated. This became evident when the compound set was analysed in a single shot format at 30 μM, in order to prioritise the compounds for full curve analysis. As such, a cut off at 40% hydrolysis (60% inhibition) was implemented; anything above this would be deemed inactive, and anything below this would be deemed active enough to

require further biological analysis. From the original single shot data, it became apparent that in a number of cases the percentage hydrolysis seemed to stop at 40% as indicated in Figure 47 below. To further validate the data obtained a selection of compounds, which resided close to the 40% hydrolysis mark, were tested using an eight point dose response curve in order to prove the data generated using the single shot analysis.

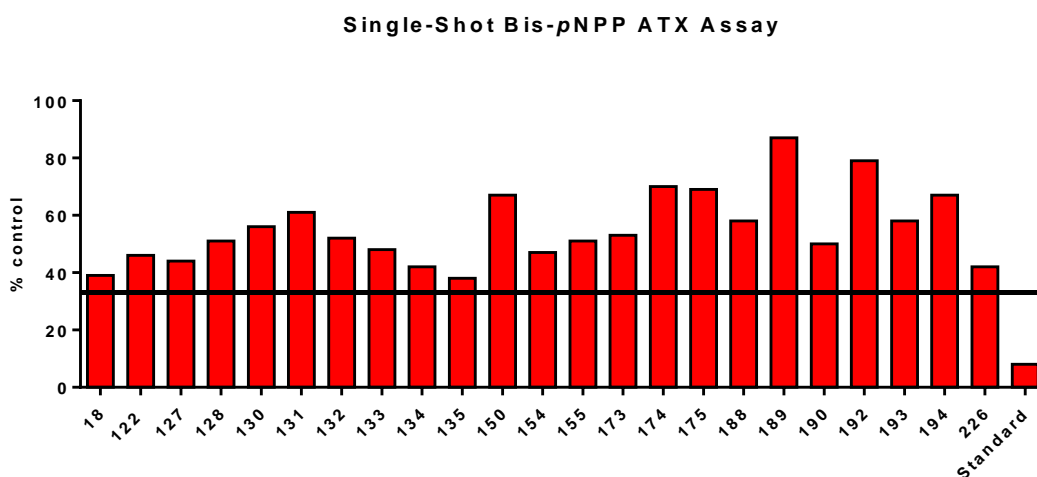


Figure 47: Single shot data at 30 μ M for a selection of the compounds tested.

From the full curve analysis it became evident that in the vast majority of cases the curve data also tailed off at 40% hydrolysis (Figure 48). This perhaps suggests that the compounds could be acting as non-competitive inhibitors (*i.e.* binding in a position other than the active site, thus altering the 3-D structure of the enzyme allowing it to still bind LPC but to a lesser extent). A similar situation has been recently described in the literature by Stein *et al.*⁴¹ who conducted an in-depth analysis of three main assays (bis-pNPP, pNP-TMP, and LPC) using similar chemotypes to those developed within this study. From the data analysis it became evident that there are stark differences between these assays in that the unnatural substrate assays (bis-pNPP, and pNP-TMP) contain this tailing off of the K_i curves, which is not observed when using the native LPC assay.

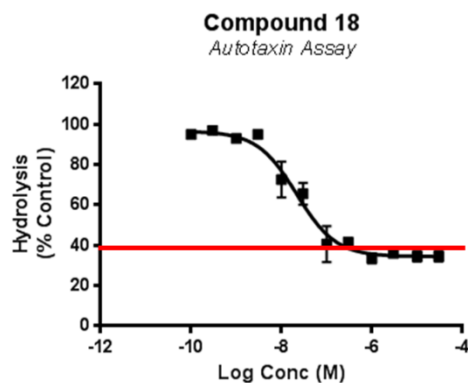


Figure 48: K_i curve data illustrating a tailing off at 40% hydrolysis indicated by the red line.

In addition to this, it was found that there were differences in activity when using the two different assays. This indicated that the compounds developed may in fact display more than one binding mode: those that bind within the active site, *i.e.*, exhibiting inhibition when using the bis-*p*NPP assay; and those that bind remote from the active site, *i.e.*, exhibit inhibition in only the LPC assay. Recent studies by Stein *et al.*,⁴¹ who have developed crystallographic data regarding this chemotype, have indicated that this type of structure can exhibit multiple binding modes depending on the functionality present within the compound. Of the four key structures outlined none contained the same binding mode, two exemplars are illustrated in Figure 49. The latter of these compounds **20** exhibits the most similar structure to the compounds developed within this study and as such it could be hypothesised that some of the compounds may be in fact reside within this binding mode. Looking at the binding interactions in more detail (Figure 50) it can be shown that this chemotype resides within the hydrophobic channel and is completely remote from LPA (pink).

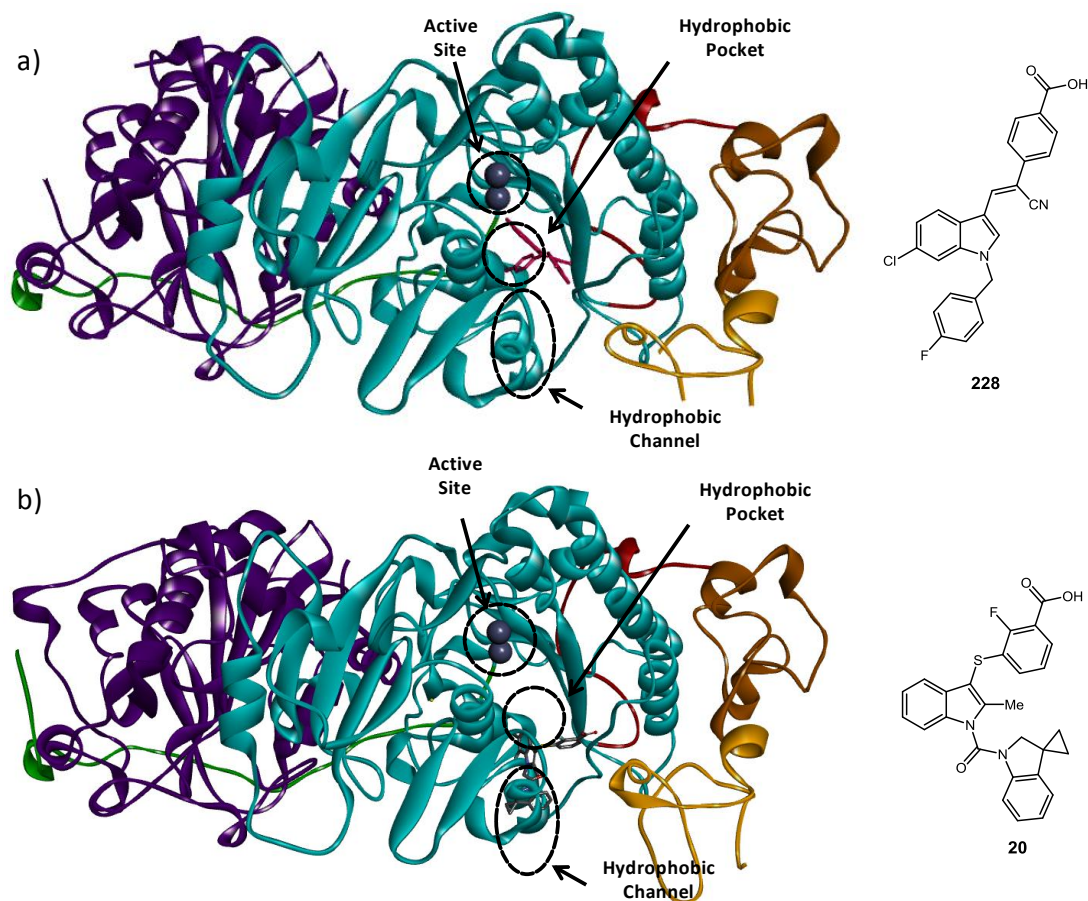


Figure 49: Ribbon representation of ATX coloured as follows: SMB1 domain in orange, SMB2 domain in brown, catalytic domain in cyan, nuclease-like domain in purple, L1 in red, L2 in green, and Zn²⁺ in grey. a) Structure of **228** complexed within ATX (PDB 4ZG7). b) Structure of **20** complexed within ATX (PDB 4ZG7).

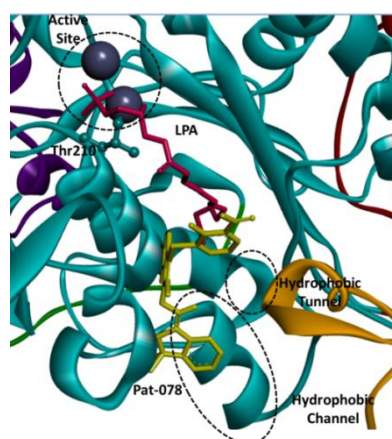


Figure 50: Structure of **20** in yellow and LPA 14:0 (**4**) in pink complexed within ATX, illustrating the remote binding of **20** from the active site.

4.4 Conclusions

Compound **18**, a known ATX inhibitor produced by Amira Pharmaceuticals, was used as the starting point for an extensive SAR study in order to determine what functionality was important for biological activity for this unique chemotype. To do this, a range of analogues were synthesised which focused on altering four main sections of the molecule. These were: Section A – substitution on the benzenoid ring; Section B – core changes; Section C – derivatisation of the acid warhead; and, Section D – indole nitrogen substitution, as illustrated in Figure 51.

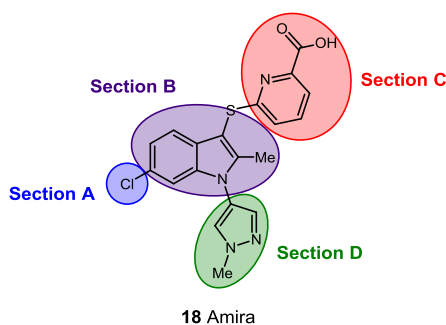


Figure 51: Four main sections probed in the SAR study.

The compound library produced was then screened using a dual assay procedure in order to gain as much information as possible regarding both the activity and potential binding mode of the synthesised compounds. From the biological data generated it became apparent that there was dissimilarity between the two assays. This was believed to be due to a possible different binding mode, remote from the active site, which has been illustrated previously in the literature.⁴¹

From the biological data generated it was found that there were in fact differences in activity between the two assays, thus indicating that the hypothesised binding mode developed from the docking studies was perhaps more complex than was first envisioned. Analysis of the data set as a whole led to the postulation that this chemotype may have multiple binding modes. A similar conclusion was drawn from the crystallographic data developed by Stein *et al*⁴¹ where a set of compounds, containing a similar structure to those discussed herein contained vastly different binding modes within the active site. The previously reported data, and that developed within this study, illustrated the complexity associated with this chemotype in terms of rationalisation of activity from specific binding interactions.

Conclusions

From the biological data generated several general trends were found (Figure 52), which were:

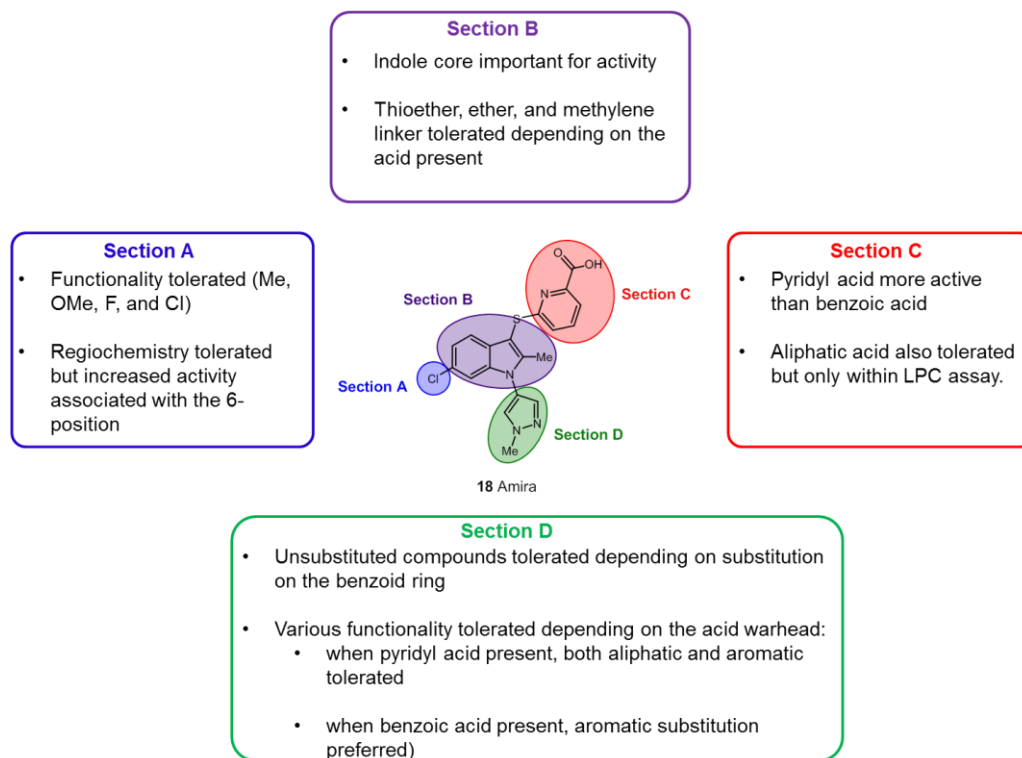


Figure 52: Summary of the associated SAR developed from the bis-pNNP data for the developed compound library.

Section A

The chlorine functionality was important; however, other functionalities such as Me, OMe, and F were also tolerated. In terms of the regiochemistry it was found that increased activity was associated with the 6-position, but, substitution in the 4-position was tolerated but led to a slight drop in activity (from $<1 \mu\text{M}$ to $1\text{-}10 \mu\text{M}$). In the vast majority of cases activity was illustrated with the presence of the methyl pyrazole on the nitrogen of the indole when functionality was present on the benzenoid ring.

Section B

The methylene, ether, and thioether linked compounds were all generally tolerated as long as the 6-Cl was present.

Section C

The presence of either aryl acids or aliphatic acids were tolerated. However, these are believed to adopt different binding modes.

Section D

Substitution on the indole nitrogen generally favoured the aromatic substituents. However, activity was also found with the aliphatic groups depending on the acid warhead present. Interestingly, however, a reversal in activity was associated with the introduction of the Ph group on the nitrogen of the indole where it as found that the 6-Cl (normally required for activity) led to inactivity compared to the unsubstituted equivalent (normally inactive).

4.5 Future Work

Further work on this compound library can be split into two main sections: additional biological evaluation and understanding, and supplementary SAR to probe the hypotheses described previously in Section 11.8.

4.5.1 Biological Evaluation

To validate the data obtained from the LPC assay further testing is required to confirm the results as those presented herein are preliminary $n=1$ results. In addition to this, due to the presence of H_2O_2 in this assay it is unknown whether this is having any effect on the compounds themselves, as there are a number of oxidisable groups present (sp^2 nitrogen and the thioether linker). This could be analysed by conducting high resolution mass spectrometry (HRMS) analysis of the assay solution prior and post assay, and compare the data to determine if any changes in mass have occurred.

Following on from this, an in-depth kinetic study of the three main assays used to test for ATX inhibition (bis-*p*NPP, *p*NP-TMP, and LPC) should be conducted, using the compound library developed, in an attempt to rationalise and understand the differences associated with these assays, especially the observed tailing off at 40% hydrolysis.

4.5.2 Supplementary SAR

In addition to the extra biological evaluation further analysis on the SAR of the original chemotype could be conducted taking into consideration the points established in Section 11.8. Firstly, due to the indication that the position of the chlorine is not as important as previously hypothesised an additional set of compounds could be synthesised which would keep the core chemotype intact, but with different functionality (e.g. Me, OMe, and F as in Section 11.8.1) at the 5-position of the indole ring, Figure 53. In doing this not only may it be possible to obtain comparable data to the original compound **18**, but it would also remove the issue of generating regioisomers (when using 3-substituted hydrazines) and hence higher yields, in theory, could be obtained.

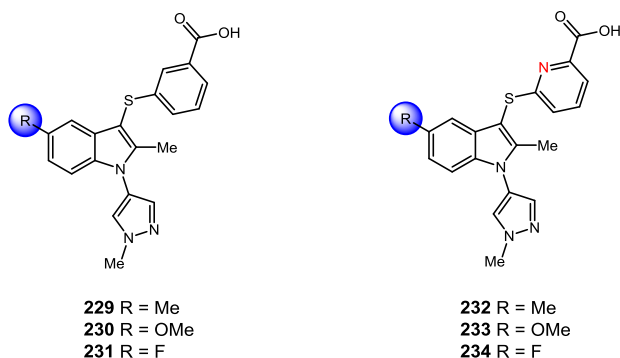


Figure 53: Proposed addition SAR surrounding the functionality of the indole ring.

A wider range of substituents could be introduced at each position of the benzenoid ring in order to further probe the space available in the cleft where the chlorine is believed to reside. Possible groups which could be introduced include bulky aromatic groups such as phenyl. This may not be the best compound in terms of medicinal chemistry properties (as it contains four aromatic rings), however, would allow for additional information regarding the binding mode. Alternative groups such as *c*-Pro (a common phenyl isostere), and *i*-Pr (to probe lipophilic tolerance) could also be introduced, Figure 54.

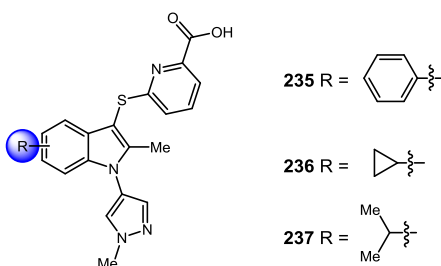


Figure 54: Alternative functionality on the benzenoid ring.

In addition to alterations on the benzenoid ring, and the nitrogen of the indole, another section which requires increased analysis is the acid warhead functionality. Although it has been hypothesised that the acid functionality is required to interact with one of the Zn^{2+} ions in the active site, this has not been proven experimentally within this study. Therefore, to confirm this, a range of compounds could be synthesised where the acid functionality is either masked (for example by an ester group) or completely removed leaving the pyridyl or benzyl ring. Following on from this, the introduction of a range of common carboxylic acid isosteres (for example,

phenol, tetrazole and sulphonic acid), could also probe the tolerance of alternative functionality at this position, Figure 55.

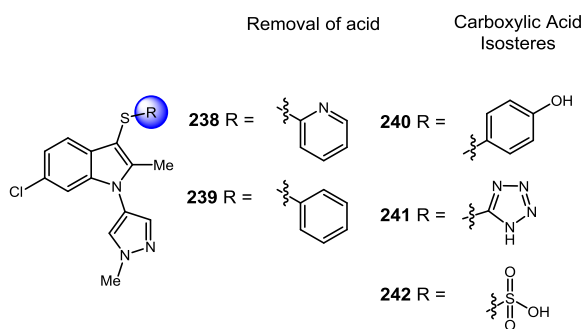


Figure 55: Additional SAR proposed for the acid region.

4.6 Experimental

4.6.1 General

All reagents and solvents were obtained from commercial suppliers and were used without further purification unless otherwise stated. Purification was carried out according to standard laboratory methods.⁹³

4.6.1.1 Purification of Solvents and Reagents

All solvents for dry reactions (DMF and pyridine) were distilled according to standard laboratory practice.⁹³ These solvents were transferred to a septum-sealed oven-dried flask over previously activated 4 Å molecular sieves and purged with and stored under nitrogen.

4.6.1.2 Experimental Details

Air-sensitive reactions were carried out using microwave vials. The vials were oven-dried and purged with N₂ before use. Purging refers to a vacuum/nitrogen-refilling procedure. Reactions were carried out at 0 °C using ice/water baths. Room temperature was generally ca. 18 °C. Reactions were carried out at elevated temperatures using a temperature-regulated hotplate/stirrer.

4.6.1.3 Purification of Products

Thin layer chromatography was carried out using Merck silica plates coated with fluorescent indicator UV254. These were analysed under 254 nm UV light or developed using potassium permanganate solution. Normal phase flash chromatography was carried out using ZEOprep 60 HYD 40-63 µm silica gel or IST Isolute Flash silica cartridges. Reverse-phase HPLC purification was carried out using a Gilson 151 preparative HPLC using an Agilent Zorbax SB-C18 column at room temperature. Purification was performed using a gradient method, eluting with 5-80% MeCN/water over 15 minutes at a flow rate of 10 mL/min. Fractions were collected automatically using a GX-271 liquid handler. Mass-directed automatic purification (MDAP) was carried out using a ZQ MS using alternate-scan positive and negative electrospray and a summed UV wavelength of 210 – 350 nm and an Xbridge C18 column (100 mm x 19 mm, 5 µm packing diameter, 20 mL/min flow rate) or Xbridge C18 column (150 mm x 30 mm, 5 µm packing diameter, 40 mL/min

flow rate). Purification was performed using a gradient method at room temperature with the mobile phases as (A) 10 mM aqueous $(\text{NH}_4)\text{HCO}_3$ solution, adjusted to pH 10 with 0.88 M aqueous NH_3 and (B) MeCN.

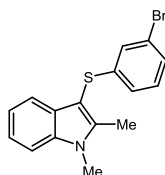
4.6.1.4 Analysis of Products

Fourier Transformed Infra-Red (FTIR) spectra were obtained on a Shimadzu IRAffinity-1 machine. ^1H and ^{13}C NMR spectra were obtained on a Bruker DPX 400 spectrometer at 400 and 101 MHz, respectively. Chemical shifts are reported in ppm and coupling constants are reported in Hz with CDCl_3 referenced at 7.26 (^1H) and 77.16 ppm (^{13}C), $(\text{CD}_3)_2\text{CO}$ at 2.50 (^1H) and 29.8 ppm (^{13}C), MeOD at 3.31 (^1H) and 49.0 ppm (^{13}C), and DMSO-d_6 at 2.50 (^1H) and 39.5 ppm (^{13}C), respectively. High-resolution mass spectra were obtained through analysis at the EPSRC National Mass Spectrometry Facility at Swansea University.

4.6.2 General Experimental Procedures

4.6.2.1 General Procedure A: Fischer Indole

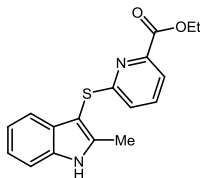
For example, for the preparation of 3-((3-bromophenyl)thio)-2-methyl-1*H*-indole, **208**



Phenylhydrazine hydrochloride (592.0 mg, 4.08 mmol, 1 equiv.) was added to a stirred solution of 1-((3-bromophenyl)thio)propan-2-one **205** (1.0 g, 4.08 mmol, 1 equiv.) in EtOH (20 mL, 0.2 M). The reaction mixture was then heated to reflux for 1 h. The reaction mixture was then allowed to cool to room temperature and concentrated under reduced pressure to a residue which was purified by silica chromatography (eluting with 0-10% EtOAc/petroleum ether) to afford the desired product as a brown oil (1.2 g, 91%).

4.6.2.2 General Procedure B: Alternative Fischer Indole

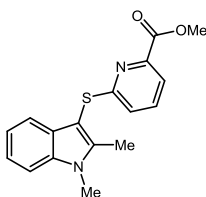
For example, for the preparation of ethyl 6-((2-methyl-1*H*-indol-3-yl)thio)picolinate, **187**



To a round bottomed flask ethyl 6-((2-oxopropyl)thio)picolinate **164** (1.02g, 4.24 mmol, 1 equiv.), and phenylhydrazine hydrochloride (0.61 g, 4.25 mmol, 1 equiv.) were dissolved in ^tBuOH (50 mL) and stirred at 80 °C overnight. Following this, HCl in ether (0.64 mL, 12.74 mmol, 3 equiv.) was added to the reaction mixture and stirred for a further 2 h before adding acetic acid (2 mL) and stirred for a further 1 h. The reaction mixture was cooled and then concentrated under vacuum. The resulting crude material was then purified by column chromatography (eluent 10-80% EtOAc in petroleum ether) to afford the desired compound as a brown solid (1.20 g, 92%).

4.6.2.3 General Procedure C: Indole N-Alkylation

For example, for the preparation of methyl 6-((1,2-dimethyl-1*H*-indol-3-yl)thio)picolinate, **152**

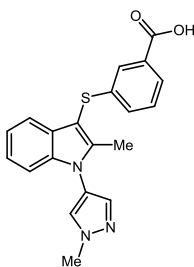


A solution of methyl ethyl 6-((6-chloro-2-methyl-1*H*-indol-3-yl)thio)picolinate **182** (138.5 mg, 0.4 mmol, 1 equiv.), NaH 60% w/w (63.5 mg, 1.6 mmol, 3 equiv.) in DMF (2 mL, 0.2 M) was heated to 60 °C for 1 h before adding MeI (0.07 mL, 1.2 mmol, 3 equiv.). The reaction mixture was heated to 60 °C for 16 h then allowed to cool to room temperature and concentrated under vacuum. The crude residue was purified

by silica chromatography (eluting with 10% EtOAc/petroleum ether) to afford the desired product as a pale yellow amorphous solid (27.7 mg, 21%).

4.6.2.4 General Procedure D: Ullman Cross-Coupling

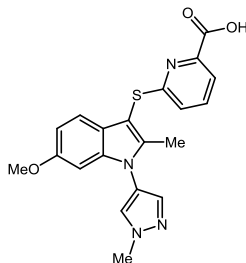
For example, for the preparation of 3-((2-methyl-1-(1-methyl-1*H*-pyrazol-4-yl)-1*H*-indol-3-yl)thio)benzoic acid, **104**



To a 5 mL microwave vial was added methyl 3-((2-methyl-1*H*-indol-3-yl)thio)benzoate **210** (202 mg, 0.67 mmol, 1 equiv.), 4-bromo-1-methyl-1*H*-pyrazole (0.21 mL, 2.02 mmol, 3 equiv.), K_2CO_3 (121 mg, 0.87 mmol, 1.3 equiv.), and CuO (107 mg, 1.35 mmol, 2 equiv.). The vial was then capped and purged with N_2 before the addition of pyridine (2 mL, 0.3 M) was added. The reaction mixture was then heated to 170 °C under pressure for 16 h. The reaction mixture was then allowed to cool to room temperature and, diluted with EtOAc (5 mL) and washed with H_2O (3 x 10 mL). The organic layers were combined, dried (hydrophobic frit), and concentrated under vacuum to residue that was purified by preparative HPLC to afford the desired product as a brown amorphous solid (22 mg, 9%).

4.6.2.5 General Procedure E: Alternative Ullman Cross-Coupling

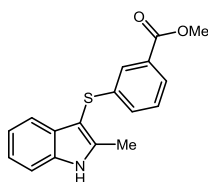
For example, for the preparation of 6-((6-methoxy-2-methyl-1-(1-methyl-1*H*-pyrazol-4-yl)-1*H*-indol-3-yl)thio)picolinic acid, **134**



To a microwave vial was added 1,10-phenanthroline (56 mg, 0.31 mmol, 1 equiv.), CuI (30 mg, 0.16 mmol, 0.5 equiv.), Cs₂CO₃ (204 mg, 0.63 mmol, 2 equiv.), 4-iodo-1-methyl-1*H*-pyrazole (130 mg, 0.63 mmol, 2 equiv.), and ethyl 6-((6-methoxy-2-methyl-1*H*-indol-3-yl)thio)picolinate **185** (107 mg, 0.31 mmol, 1 equiv.). The vial was then capped and purged with N₂ before addition of DMF (1.1 mL, 0.6 M). The reaction was then heated to 110 °C for 48 h. The reaction mixture was then allowed to cool to room temperature before the addition of NaOH (1 mL 2 M aq.) and stirred for 1 h at room temperature. The reaction mixture was then acidified using HCl (2 M) and extracted with EtOAc (3 x 10 mL). The combined organics were dried (hydrophobic frit), and concentrated under vacuum to a residue that was purified using MDAP to afford the desired product as a pink amorphous solid (32 mg, 26%).

4.6.2.6 General Procedure F: Carbonylation

For example, for the preparation of methyl 3-((2-methyl-1*H*-indol-3-yl)thio)benzoate, **210**



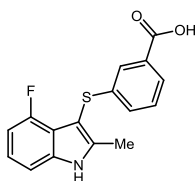
Trans-bis(acetato)bis[*o*-(*di*-*o*-tolylphosphino)benzyl]dipalladium(II) (183 mg, 0.2 mmol, 5 mol%) was added to a solution of 3-((3-bromophenyl)thio)-2-methyl-1*H*-indole **208** (1.16 g, 3.9 mmol, 1 equiv.), Mo(CO)₆ (1.03 g, 3.9 mmol, 1 equiv.), [tBu₃PH]BF₄ (226 mg, 0.78 mmol, 0.2 equiv.) and DBU (875 μL, 5.86 mmol, 1.5

Experimental

equiv.) in MeCN (4 mL, 1 M) and MeOH (16 mL, 0.2 M). The reaction mixture was heated to 70 °C for 16 h then allowed to cool to room temperature and concentrated under vacuum to a residue that was purified by silica chromatography (eluting with 20% EtOAc/petroleum ether) to afford the desired product as a brown solid (1 g, 89%).

4.6.2.7 General Procedure G: Hydrolysis

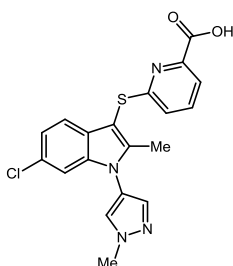
For example, for the preparation of 6-((4-fluoro-2-methyl-1*H*-indol-3-yl)thio)picolinic acid, **193**



2 M aq. NaOH (0.5 mL) was added to a solution of ethyl 6-((4-fluoro-2-methyl-1*H*-indol-3-yl)thio)picolinate **186** (51 mg, 0.15 mmol) in 0.5 mL THF (0.3 M) and stirred at room temperature for 16 h. The reaction mixture was acidified using aq. HCl (1 M) then extracted using EtOAc (2 x 10 mL). The combined organic layers were dried (hydrophobic frit) and concentrated under vacuum to afford the desired compound as a yellow amorphous solid (56 mg, 99%).

4.6.3 Compound Characterisation Data

Compound 18: 6-((6-chloro-2-methyl-1-(1-methyl-1*H*-pyrazol-4-yl)-1*H*-indol-3-yl)thio)picolinic acid



6-((6-chloro-2-methyl-1-(1-methyl-1*H*-pyrazol-4-yl)-1*H*-indol-3-yl)thio)picolinic acid
Chemical Formula: C₁₉H₁₅ClN₄O₂S
Molecular Weight: 398.87

Prepared according to General Procedure E using 1,10-phenanthroline (56 mg, 0.31 mmol, 1 equiv.), CuI (29 mg, 0.15 mmol, 0.5 equiv.), Cs₂CO₃ (200 mg, 0.62 mmol, 2 equiv.), 4-iodo-1-methyl-1*H*-pyrazole (130 g, 0.62 mmol, 2 equiv.), and ethyl 6-((6-chloro-2-methyl-1*H*-indol-3-yl)thio)picolinate **171** (110 mg, 0.31 mmol, 1 equiv.) in

Experimental

DMF (1.07 mL, 0.1 M) to afford the desired product as a pale yellow solid (10 mg, 8 %).

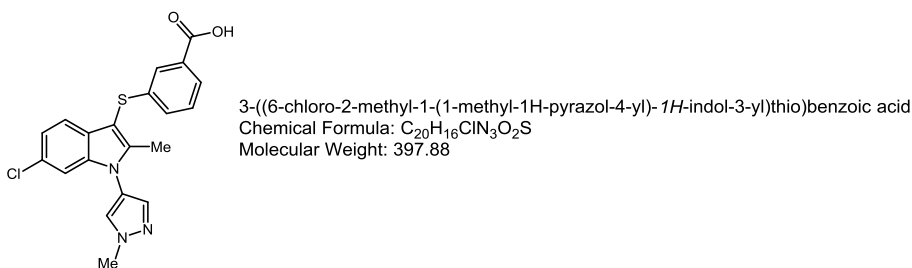
ν_{\max} (neat): 2947, 2924, 1712, 1577, 1465, 1438 cm^{-1} .

^1H NMR (400 MHz, MeOD): δ 8.04 (s, 1H), 7.68 - 7.81 (m, 2H), 7.58 (t, J = 7.70 Hz, 1H), 7.42 (d, J = 8.31 Hz, 1H), 7.20 (d, J = 1.71 Hz, 1H), 7.12 (dd, J = 8.31, 1.71 Hz, 1H), 6.80 (d, J = 8.07 Hz, 1H), 4.05 (s, 3H), 2.40 (s, 3H). CO_2H proton not observed.

^{13}C NMR (126 MHz, CDCl_3): δ 163.7, 161.5, 145.9, 144.9, 139.1, 138.6, 129.0, 128.2, 127.9, 127.6, 127.5, 126.8, 124.0, 122.3, 119.4, 110.7, 97.8, 39.9, 11.6.

HRMS: exact mass calculated for $[\text{M}+\text{H}^+]$ ($\text{C}_{19}\text{H}_{16}\text{ClN}_4\text{O}_2\text{S}$) requires m/z 399.0677, found m/z 399.0678.

Compound 104: 3-((6-Chloro-2-methyl-1-(1-methyl-1H-pyrazol-4-yl)-1H-indol-3-yl)thio)benzoic acid



Prepared according to General Procedure D using methyl 3-((2-methyl-1H-indol-3-yl)thio)benzoate **210** (188 mg, 0.57 mmol, 1 equiv.), CuO (90 mg, 1.13 mmol, 2 equiv.), K_2CO_3 (102 mg, 0.74 mmol, 1.3 equiv.) and 1-methyl-4-bromopyrazole (0.18 mL, 1.70 mmol, 3 equiv.) in pyridine (2 mL, 0.3 M) to afford the desired product as a white amorphous solid (24 mg, 11%).

ν_{\max} (neat): 2920, 2852, 1701, 1573, 1458, 1429 cm^{-1} .

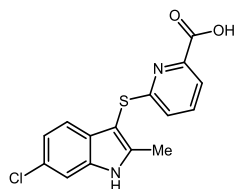
^1H NMR (400 MHz, MeOD): δ 8.04 (s, 1H), 7.78 - 7.72 (m, 3H), 7.35 - 7.30 (m, 1H), 7.30 - 7.25 (m, 1H), 7.18 - 7.14 (m, 1H), 7.13 (d, J = 2.2 Hz, 1H), 7.11 (s, 1H), 4.07 (s, 3H), 2.45 (s, 3H). CO_2H proton not observed.

^{13}C NMR (151 MHz, Acetone): δ 166.3, 146.7, 141.7, 140.3, 136.4, 131.2, 129.6, 128.9, 128.4, 126.3, 125.9, 125.3, 125.1, 122.8, 122.4, 118.6, 109.7, 38.9, 10.8. One carbon not observed/coincident.

Experimental

HRMS: exact mass calculated for $[M-H^+]$ ($C_{20}H_{15}ClN_3O_2S$) requires m/z 396.0579, found m/z 396.0572.

Compound 122: 6-((6-Chloro-2-methyl-1*H*-indol-3-yl)thio)picolinic acid



6-((6-chloro-2-methyl-1*H*-indol-3-yl)thio)picolinic acid
Chemical Formula: $C_{15}H_{11}ClN_2O_2S$
Molecular Weight: 318.78

Prepared according to General Procedure G using ethyl 6-((6-chloro-2-methyl-1*H*-indol-3-yl)thio)picolinate **171** (100 mg, 0.29 mmol, 1 equiv.) and 2 M aq. NaOH (1 mL) in THF (1 mL, 0.3 M) to afford the desired product as a yellow amorphous solid (79 mg, 86%).

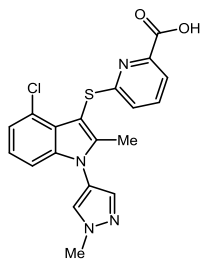
ν_{\max} (neat): 3302, 1734, 1685 cm^{-1}

1H NMR (400 MHz, MeOD): δ 7.77 (dd, $J = 7.6, 0.9$ Hz, 1H), 7.62 – 7.56 (m, 1H), 7.42 – 7.38 (m, 1H), 7.34 (d, $J = 8.5$ Hz, 1H), 7.04 (dd, $J = 8.4, 1.8$ Hz, 1H), 6.74 (dd, $J = 8.2, 0.9$ Hz, 1H), 2.49 (s, 3H).

^{13}C NMR (101 MHz, MeOD): δ 165.9, 163.6, 147.5, 143.3, 137.8, 136.7, 128.3, 127.4, 122.4, 120.5, 120.2, 118.5, 110.8, 95.9, 10.4.

HRMS: exact mass calculated for $[M+H^+]$ ($C_{15}H_{12}ClN_2O_2S$) requires m/z 319.0303, found m/z 319.0307.

Compound 127: 6-((4-Chloro-2-methyl-1-(1-methyl-1*H*-pyrazol-4-yl)-1*H*-indol-3-yl)thio)picolinic acid



6-((4-chloro-2-methyl-1-(1-methyl-1*H*-pyrazol-4-yl)-1*H*-indol-3-yl)thio)picolinic acid
 Chemical Formula: C₁₉H₁₅ClN₄O₂S
 Molecular Weight: 398.87

Prepared according to General Procedure E using 1,10-phenanthroline (54 mg, 0.30 mmol, 1 equiv.), CuI (30 mg, 0.15 mmol, 0.5 equiv.), Cs₂CO₃ (200 mg, 0.60 mmol, 2 equiv.), 4-iodo-1-methyl-1*H*-pyrazole (130 mg, 0.60 mmol, 2 equiv.), and ethyl 6-((7-chloro-2-methyl-1*H*-indol-3-yl)thio)picolinate **169** (100 mg, 0.30 mmol, 1 equiv.) in DMF (1.8 mL, 0.3 M) to afford the desired product as an off white solid (32 mg, 16%).

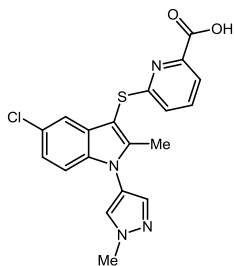
ν_{\max} (neat): 1735, 1500, 1510, 1402 cm⁻¹.

¹H NMR (600 MHz, CDCl₃): δ 7.84 (d, *J* = 7.5 Hz, 1H), 7.63 (m, 3H), 7.19 – 7.03 (m, 4H), 4.04 (s, 3H), 2.37 (s, 3H). CO₂H proton not observed.

¹³C NMR (151 MHz, MeOD): δ 160.1, 159.2, 142.0, 141.8, 136.3, 134.4, 133.2, 123.8, 121.7, 121.2, 120.6, 119.1, 119.0, 115.3, 115.0, 105.5, 93.2, 35.9, 7.7.

HRMS: exact mass calculated for [M+H⁺] (C₁₉H₁₆ClN₄O₂S) requires *m/z* 399.0677, found *m/z* 399.0680.

Compound 128: 6-((5-Chloro-2-methyl-1-(1-methyl-1*H*-pyrazol-4-yl)-1*H*-indol-3-yl)thio)picolinic acid



6-((5-chloro-2-methyl-1-(1-methyl-1*H*-pyrazol-4-yl)-1*H*-indol-3-yl)thio)picolinic acid
 Chemical Formula: C₁₉H₁₅ClN₄O₂S
 Molecular Weight: 398.8650

Prepared according to General Procedure E using 1,10-phenanthroline (58 mg, 0.32 mmol, 1 equiv.), CuI (31 mg, 0.16 mmol, 0.5 equiv.), Cs₂CO₃ (210 mg, 0.65 mmol, 2 equiv.), 4-iodo-1-methyl-1*H*-pyrazole (130 mg, 0.65 mmol, 2 equiv.) and ethyl 6-((5-chloro-2-methyl-1*H*-indol-3-yl)thio)picolinate **170** (110 mg, 0.32 mmol, 1 equiv.) in DMF (1.8 mL, 0.3 M) to afford the desired product as a white amorphous solid (28 mg, 22%).

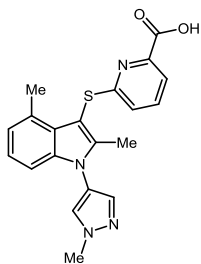
ν_{\max} (neat): 1730, 1577, 1558, 1531 cm⁻¹.

¹H NMR (400 MHz, CDCl₃): δ 7.88 (d, *J* = 7.5 Hz, 1H), 7.64 (m, 3H), 7.50 (d, *J* = 1.7 Hz, 1H), 7.19 – 7.05 (m, 3H), 4.05 (s, 3H), 2.38 (s, 3H). CO₂H proton not observed.

¹³C NMR (101 MHz, CDCl₃): δ 163.6, 161.3, 145.9, 145.6, 138.7, 137.1, 137.0, 130.2, 127.7, 127.5, 124.0, 123.2, 119.4, 119.1, 118.0, 111.7, 97.2, 39.9, 11.7.

HRMS: exact mass calculated for [M+H⁺] (C₁₉H₁₆ClN₃O₂S) requires *m/z* 399.0677, found *m/z* 399.0680.

Compound 130: 6-((2,4-Dimethyl-1-(1-methyl-1*H*-pyrazol-4-yl)-1*H*-indol-3-yl)thio)picolinic acid



6-((2,4-dimethyl-1-(1-methyl-1*H*-pyrazol-4-yl)-1*H*-indol-3-yl)thio)picolinic acid
 Chemical Formula: C₂₀H₁₈N₄O₂S
 Molecular Weight: 378.45

Prepared according to General Procedure E using 1,10-phenanthroline (49 mg, 0.27 mmol, 1 equiv.), CuI (26 mg, 0.14 mmol, 0.5 equiv.), Cs₂CO₃ (176 mg, 0.54 mmol, 2 equiv.), 4-iodo-1-methyl-1*H*-pyrazole (112 mg, 0.54 mmol, 2 equiv.), and ethyl 6-((2,4-dimethyl-1*H*-indol-3-yl)thio)picolinate **181** (88 mg, 0.27 mmol, 1 equiv.) in DMF (0.94 mL, 0.3 M) to afford the desired product as a white solid (24 mg, 24%).

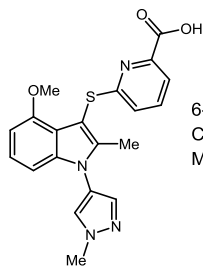
ν_{\max} (neat): 1720, 1619, 1581, 1574 cm⁻¹.

¹H NMR (600 MHz, DMSO): δ 7.16 (s, 1H), 6.94 (d, *J* = 7.5 Hz, 1H), 6.88 (s, 1H), 6.80 (t, *J* = 7.8 Hz, 1H), 6.30 – 6.18 (m, 2H), 6.13 – 5.98 (m, 2H), 4.01 (s, 3H), 1.78 (s, 3H), 1.56 (s, 3H). CO₂H proton not observed.

¹³C NMR (151 MHz, DMSO): δ 166.8, 163.9, 148.9, 143.5, 138.3, 137.0, 135.8, 129.2, 127.9, 125.7, 122.1, 121.3, 121.0, 119.0, 118.6, 107.3, 96.8, 37.5, 16.8, 9.2.

HRMS: exact mass calculated for [M+H⁺] (C₂₀H₁₉N₄O₂S) requires *m/z* 379.1223, found *m/z* 379.1220.

Compound 131: 6-((4-Methoxy-2-methyl-1-(1-methyl-1*H*-pyrazol-4-yl)-1*H*-indol-3-yl)thio)picolinic acid



6-((4-methoxy-2-methyl-1-(1-methyl-1*H*-pyrazol-4-yl)-1*H*-indol-3-yl)thio)picolinic acid
 Chemical Formula: C₂₀H₁₈N₄O₃S
 Molecular Weight: 394.4469

Prepared according to General Procedure E using 1,10-phenanthroline (53 mg, 0.3 mmol, 1 equiv.), CuI (28 mg, 0.15 mmol, 0.5 equiv.), Cs₂CO₃ (190 mg, 0.59 mmol, 2 equiv.), 4-iodo-1-methyl-1*H*-pyrazole (120 mg, 0.59 mmol, 2 equiv.) and ethyl 6-((4-methoxy-2-methyl-1*H*-indol-3-yl)thio)picolinate **182** (100 mg, 0.3 mmol, 1 equiv.) in DMF (2 mL, 0.2 M) to afford the desired product as an off-white amorphous solid (21 mg, 18%).

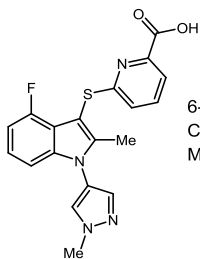
ν_{\max} (neat): 1602, 1556, 1494 cm⁻¹.

¹H NMR (600 MHz, MeOD): δ 7.96 (s, 1H), 7.68 (s, 1H), 7.60 (d, *J* = 7.3 Hz, 1H), 7.47 (t, *J* = 7.8 Hz, 1H), 7.07 (t, *J* = 8.1 Hz, 1H), 6.79 (d, *J* = 8.2 Hz, 1H), 6.75 (d, *J* = 7.8 Hz, 1H), 6.59 (d, *J* = 7.8 Hz, 1H), 4.02 (s, 3H), 3.64 (s, 3H), 2.35 (s, 3H). CO₂H proton not observed.

¹³C NMR (151 MHz, MeOD): δ 163.9, 153.8, 142.3, 140.4, 136.6, 136.6, 128.7, 123.0, 120.5, 119.6, 118.6, 118.2, 110.0, 103.3, 102.0, 97.5, 54.5, 4.25, 9.9. One carbon not observed/coincident.

HRMS: exact mass calculated for [M+H⁺] (C₂₀H₁₉N₄O₃S) requires *m/z* 395.1172, found *m/z* 395.1174.

Compound 132: 6-((4-Fluoro-2-methyl-1-(1-methyl-1*H*-pyrazol-3-yl)-1*H*-indol-3-yl)thio)picolinic acid



6-((4-fluoro-2-methyl-1-(1-methyl-1*H*-pyrazol-3-yl)-1*H*-indol-3-yl)thio)picolinic acid

Chemical Formula: C₁₉H₁₅FN₄O₂S

Molecular Weight: 382.4114

Prepared according to General Procedure E using 1,10-phenanthroline (80 mg, 0.44 mmol, 1 equiv.), CuI (42 mg, 0.22 mmol, 0.5 equiv.), Cs₂CO₃ (288 mg, 0.88 mmol, 2 equiv.), 4-iodo-1-methyl-1*H*-pyrazole (184 mg, 0.88 mmol, 2 equiv.), and ethyl 6-((7-chloro-2-methyl-1*H*-indol-3-yl)thio)picolinate **184** (146 mg, 0.44 mmol, 1 equiv.) in DMF (1.5 mL, 0.3 M) to afford the desired product as a red amorphous solid (6 mg, 3%).

ν_{\max} (neat): 1735, 1577, 1558, 1438 cm⁻¹.

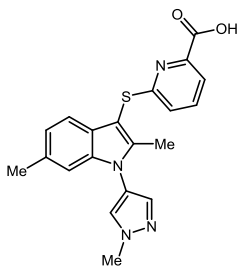
¹H NMR (600 MHz, CDCl₃): δ 7.87 (d, *J* = 7.3 Hz, 1H), 7.67 (d, *J* = 7.4 Hz, 1H), 7.63 (s, 1H), 7.61 (s, 1H), 7.22 (s, 1H), 7.11 (dd, *J* = 12.8, 8.0 Hz, 1H), 7.00 (d, *J* = 8.2 Hz, 1H), 6.88 – 6.75 (m, 1H), 4.05 (s, 3H), 2.37 (s, 3H). CO₂H proton not observed.

¹³C NMR (151 MHz, CDCl₃): δ = 162.1, 155.9 (d, ¹*J*_{C-F} = 249.1 Hz), 144.5, 142.2, 141.3 (d, ³*J*_{C-F} = 9.4 Hz), 138.5, 137.1, 127.6, 124.2, 123.1 (d, ³*J*_{C-F} = 7.5 Hz), 119.2, 117.5 (d, ²*J*_{C-F} = 17.9 Hz), 107.3 (d, ²*J*_{C-F} = 18.8 Hz), 106.8 (d, ⁴*J*_{C-F} = 3.3 Hz), 95.1, 39.9, 11.5. Two carbons not observed/coincident.

¹⁹F NMR (376 MHz, CDCl₃): δ -126.82.

HRMS: exact mass calculated for [M+H⁺] (C₁₉H₁₆FN₄O₂S) requires *m/z* 383.0973, found *m/z* 383.0975.

Compound 133: 6-((2,6-Dimethyl-1-(1-methyl-1*H*-pyrazol-4-yl)-1*H*-indol-3-yl)thio)picolinic acid



6-((2,6-dimethyl-1-(1-methyl-1*H*-pyrazol-4-yl)-1*H*-indol-3-yl)thio)picolinic acid
 Chemical Formula: C₂₀H₁₈N₄O₂S
 Molecular Weight: 378.45

Prepared according to General Procedure E using 1,10-phenanthroline (49 mg, 0.27 mmol, 1 equiv.), CuI (26 mg, 0.14 mmol, 0.5 equiv.), Cs₂CO₃ (176 mg, 0.54 mmol, 2 equiv.), 4-iodo-1-methyl-1*H*-pyrazole (112 mg, 0.54 mmol, 2 equiv.) and ethyl 6-((2,6-dimethyl-1*H*-indol-3-yl)thio)picolinate **184** (88 mg, 0.27 mmol, 1 equiv.) in DMF (0.94 mL, 0.3 M) to afford the desired product as a yellow amorphous solid (28mg, 28%).

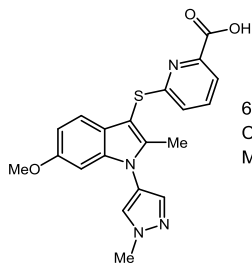
ν_{\max} (neat): 1680, 1615, 1558, 1573 cm⁻¹.

¹H NMR (400 MHz, MeOD): δ 7.99 (s, 1H), 7.72 (d, *J* = 0.6 Hz, 1H), 7.68 (d, *J* = 7.4 Hz, 1H), 7.51 (t, *J* = 7.8 Hz, 1H), 7.33 (d, *J* = 8.0 Hz, 1H), 7.01 (s, 1H), 6.97 (d, *J* = 8.0 Hz, 1H), 6.72 (d, *J* = 8.0 Hz, 1H), 4.03 (s, 3H), 2.40 (s, 3H), 2.38 (s, 3H). CO₂H proton not observed.

¹³C NMR (125 MHz, DMSO): δ = 166.0, 159.1, 153.9, 147.9, 146.5, 138.6, 134.2, 133.3, 132.4, 130.2, 124.9, 124.6, 123.8, 123.4, 120.7, 120.7, 102.5, 39.8, 21.2, 13.4.

HRMS: exact mass calculated for [M+H⁺] (C₂₀H₁₉N₄O₂S) requires *m/z* 379.1223, found *m/z* 379.1220.

Compound 134: 6-((6-Methoxy-2-methyl-1-(1-methyl-1*H*-pyrazol-4-yl)-1*H*-indol-3-yl)thio)picolinic acid



6-((6-methoxy-2-methyl-1-(1-methyl-1*H*-pyrazol-4-yl)-1*H*-indol-3-yl)thio)picolinic acid
 Chemical Formula: C₂₀H₁₈N₄O₃S
 Molecular Weight: 394.45

Prepared according to General Procedure E using 1,10-phenanthroline (56 mg, 0.31 mmol, 1 equiv.), CuI (30 mg, 0.16 mmol, 0.5 equiv.), Cs₂CO₃ (200 mg, 0.63 mmol, 2 equiv.), 4-iodo-1-methyl-1*H*-pyrazole (130 g, 0.63 mmol, 2 equiv.), and ethyl 6-((6-methoxy-2-methyl-1*H*-indol-3-yl)thio)picolinate **185** (110 g, 0.31 mmol, 1 equiv.) in DMF (1.09 mL, 0.3 M) to afford the desired product as a pink amorphous solid (32 mg, 26%).

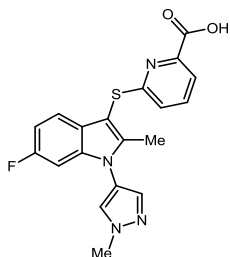
ν_{\max} (neat): 1755, 1616, 1583, 1556, 1438 cm⁻¹.

¹H NMR (600 MHz, CDCl₃): δ 7.85 (d, *J* = 7.4 Hz, 1H), 7.65 (s, 1H), 7.63 – 7.58 (m, 2H), 7.38 (d, *J* = 8.6 Hz, 1H), 7.09 (d, *J* = 8.1 Hz, 1H), 6.83 (dd, *J* = 8.6, 2.1 Hz, 1H), 6.70 (d, *J* = 2.2 Hz, 1H), 4.05 (s, 3H), 3.79 (s, 3H), 2.35 (s, 3H). CO₂H proton not observed.

¹³C NMR (151 MHz, CDCl₃): δ 163.8, 162.1, 157.3, 145.8, 142.8, 139.5, 138.5, 137.1, 127.6, 124.0, 122.9, 119.5, 119.2, 119.1, 111.1, 97.2, 94.6, 55.8, 39.9, 11.6.

HRMS: exact mass calculated for [M+H⁺] (C₂₀H₁₉N₄O₂S) requires *m/z* 395.1172, found *m/z* 395.1173.

Compound 135: 6-((6-Fluoro-2-methyl-1-(1-methyl-1*H*-pyrazol-3-yl)-1*H*-indol-3-yl)thio) picolinic acid



6-((6-fluoro-2-methyl-1-(1-methyl-1*H*-pyrazol-4-yl)-1*H*-indol-3-yl)thio)picolinic acid
 Chemical Formula: C₁₉H₁₅FN₄O₂S
 Molecular Weight: 382.41

Prepared according to General Procedure E using 1,10-phenanthroline (55 mg, 0.30 mmol, 1 equiv.), CuI (29 mg, 0.15 mmol, 0.5 equiv.), Cs₂CO₃ (197 mg, 0.61 mmol, 2 equiv.), 4-iodo-1-methyl-1*H*-pyrazole (126 mg, 0.61 mmol, 2 equiv.), and ethyl 6-((6-fluoro-2-methyl-1*H*-indol-3-yl)thio)picolinate **186** (135 mg, 0.30 mmol, 1 equiv.) in DMF (1.05 mL, 0.1 M) to afford the desired product as a yellow amorphous solid (25 mg, 22%).

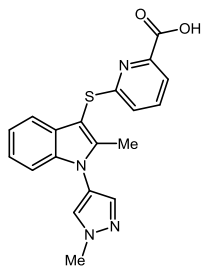
ν_{\max} (neat): 1700, 1618, 1575, 1558 cm⁻¹.

¹H NMR (600 MHz, MeOD) δ 8.01 (s, 1H), 7.73 (s, 1H), 7.71 (d, *J* = 7.6 Hz, 1H), 7.56 (t, *J* = 7.8 Hz, 1H), 7.42 (dd, *J* = 8.1, 5.2 Hz, 1H), 6.92 (d, *J* = 9.4 Hz, 2H), 6.77 (d, *J* = 8.1 Hz, 1H), 4.03 (s, 3H), 2.38 (s, 3H). CO₂H proton not observed.

¹³C NMR (126 MHz, Acetone): δ 162.0, 160.3 (d, ¹*J* = 237.2 Hz), 145.4, 138.9 (d, ³*J* = 12.5 Hz), 138.5, 136.2, 128.1, 125.5, 122.9, 119.9, 119.1 (d, ³*J* = 10.1 Hz), 118.6, 109.4 (d, ²*J* = 24.6 Hz), 97.4, 97.2 (d, ²*J* = 27.2 Hz), 39.0, 10.9. Two carbons not observed/coincident.

HRMS: exact mass calculated for [M+H⁺] (C₁₉H₁₆FN₄O₂S) requires *m/z* 383.0973, found *m/z* 383.0979.

Compound 136: 6-((2-Methyl-1-(1-methyl-1*H*-pyrazol-4-yl)-1*H*-indol-3-yl)thio)picolinic acid



6-((2-methyl-1-(1-methyl-1*H*-pyrazol-4-yl)-1*H*-indol-3-yl)thio)picolinic acid
 Chemical Formula: C₁₉H₁₆N₄O₂S
 Molecular Weight: 364.42

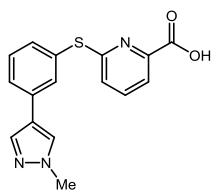
Prepared according to General Procedure D using methyl 3-((2-methyl-1*H*-indol-3-yl)thio)benzoate **187** (198 mg, 0.64 mmol, 1 equiv.), 4-bromo-1-methyl-1*H*-pyrazole (0.2 mL, 1.92 mmol, 3 equiv.), K₂CO₃ (115 mg, 0.83 mmol, 1.3 equiv.) and CuO (105 mg, 1.28 mmol, 2 equiv.) in pyridine (2 mL, 0.3 M) to afford the desired product as a yellow amorphous solid (15 mg, 6%).

ν_{\max} (neat): 1708, 1573, 1440 cm⁻¹.

¹H NMR (400 MHz, CDCl₃): δ 7.87 (d, *J* = 8.1 Hz, 1H), 7.67 (s, 1H), 7.63 (t, *J* = 7.8 Hz, 2H), 7.53 (dd, *J* = 7.0, 1.5 Hz, 1H), 7.25 – 7.18 (m, 3H), 7.10 (dd, *J* = 8.1, 0.6 Hz, 1H), 4.06 (s, 3H), 2.40 (s, 3H). CO₂H not observed.

¹³C NMR (101 MHz, CDCl₃): δ 191.1, 143.5, 141.3, 138.1, 136.5, 128.5, 127.2, 123.6, 122.5, 121.3, 118.7, 118.0, 110.1, 108.8, 100.6, 97.0, 94.1, 39.3, 11.1.

HRMS: exact mass calculated for [M+H⁺] (C₁₉H₁₇N₄O₂S) requires *m/z* 365.1067, found *m/z* 365.1070.

Compound 137: 6-((3-(1-Methyl-1H-pyrazol-4-yl)phenyl)thio)picolinic acid

6-((3-(1-methyl-1H-pyrazol-4-yl)phenyl)thio)picolinic acid
Chemical Formula: C₁₆H₁₃N₃O₂S
Molecular Weight: 311.36

To a round-bottomed flask was added Pd(OAc)₂ (2 mg, 0.01 mmol, 10 mol%) methyl 6-((3-bromophenyl)thio)picolinate **196** (280 mg, 0.86 mmol, 1 equiv.), 1-methylpyrazole-4-boronic acid pinacol ester (269 mg, 1.3 mmol, 1.5 equiv.), and S-Phos (707 mg, 1.72 mmol, 2 equiv.). The vessel was sealed and purged with N₂ before addition of THF (0.7 mL, 1.2 M) and H₂O (0.1 mL). The reaction was then heated to 50 °C for 16 h. The reaction was allowed to cool to room temperature before addition of 2 M aq. NaOH (0.3 mL). The reaction was stirred at room temperature and monitored until completion by TLC. The reaction mixture was then quenched with sat. aq. NH₄Cl (2 mL), acidified using aqueous HCl (1 M) solution and extracted with EtOAc. (2 x 10 mL) The combined organics were dried (hydrophobic frit), and concentrated under vacuum before purification by preparative HPLC to afford the desired product (37 mg, 9% over two steps).

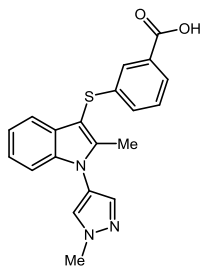
ν_{max} (neat): 3140, 1680, 1537, 1403 cm⁻¹.

¹H NMR (400 MHz, CDCl₃): δ 7.90 (d, *J* = 7.3 Hz, 1H), 7.77 (s, 1H), 7.75 – 7.67 (m, 2H), 7.64 (s, 1H), 7.62 – 7.55 (m, 1H), 7.51 – 7.42 (m, 2H), 7.24 (s, 1H), 3.95 (s, 3H). CO₂H not observed.

¹³C NMR (101 MHz, CDCl₃): δ 138.6, 138.2, 136.3, 134.3, 132.7, 131.7, 130.6, 129.9, 128.9, 126.7, 126.5, 121.6, 93.7, 42.4, 38.7. One carbon not observed/coincident.

HRMS: exact mass calculated for [M+H⁺] (C₁₆H₁₄N₃O₂S) requires *m/z* 312.0801, found *m/z* 312.0801.

Compound 146: 3-((2-Methyl-1-(1-methyl-1*H*-pyrazol-4-yl)-1*H*-indol-3-yl)thio)benzoic acid



3-((2-methyl-1-(1-methyl-1*H*-pyrazol-4-yl)-1*H*-indol-3-yl)thio)benzoic acid
 Chemical Formula: C₂₀H₁₇N₃O₂S
 Molecular Weight: 363.43

Prepared according to General Procedure D using methyl 3-((2-methyl-1*H*-indol-3-yl)thio)benzoate **206** (202 mg, 0.67 mmol, 1 equiv.), 4-bromo-1-methyl-1*H*-pyrazole (0.21 mL, 2.02 mmol, 3 equiv.), CuO (107 mg, 1.35 mmol, 2 equiv.), and K₂CO₃ (121 mg, 0.87 mmol, 1.3 equiv.) in pyridine (2 mL, 0.3 M), to afford the desired product as a dark red amorphous solid (22 mg, 9%).

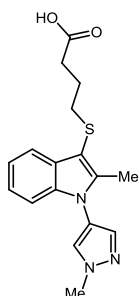
ν_{\max} (neat): 3327, 1710 cm⁻¹.

¹H NMR (400 MHz, CDCl₃): δ 8.33 (s, 1H), 7.81 (t, *J* = 1.7 Hz, 1H), 7.71 (dt, *J* = 7.5, 1.5 Hz, 1H), 7.52 (d, *J* = 7.8 Hz, 1H), 7.33 (dd, *J* = 4.8, 3.9 Hz, 1H), 7.19 (t, *J* = 7.5 Hz, 2H), 7.16 – 7.12 (m, 2H), 7.11 (d, *J* = 1.0 Hz, 1H), 3.86 (s, 3H), 2.51 (s, 3H). CO₂H proton not observed.

¹³C NMR (126 MHz, CDCl₃): δ 166.9, 141.3, 140.3, 135.5, 130.6, 130.1, 129.9, 128.7, 126.6, 125.8, 122.3, 120.8, 118.8, 110.8, 98.7, 52.2, 12.1. Three carbons not observed/coincident.

HRMS: exact mass calculated for [M-H⁺] (C₂₀H₁₆N₃O₂S) requires *m/z* 362.0969, found *m/z* 362.0967.

Compound 147: 4-(2-Methyl-1-(1-methyl-1*H*-pyrazol-4-yl)-1*H*-indol-3-yl)butanoic acid



4-((2-methyl-1-(1-methyl-1*H*-pyrazol-4-yl)-1*H*-indol-3-yl)thio)butanoic acid
 Chemical Formula: C₁₇H₁₉N₃O₂S
 Molecular Weight: 329.4167

Prepared according to General Procedure D using 4-(2-methyl-1*H*-indol-3-yl)butanoic acid **218** (200 mg, 0.80 mmol, 1 equiv.), CuO (128 mg, 1.60 mmol, 2 equiv.), K₂CO₃ (144 mg, 1.04 mmol, 1.3 equiv.) and 1-methyl-4-bromopyrazole (0.25 mL, 2.40 mmol, 3 equiv.) in pyridine (2 mL, 0.4 M) to afford the desired product as a brown oil (4 mg, 2%).

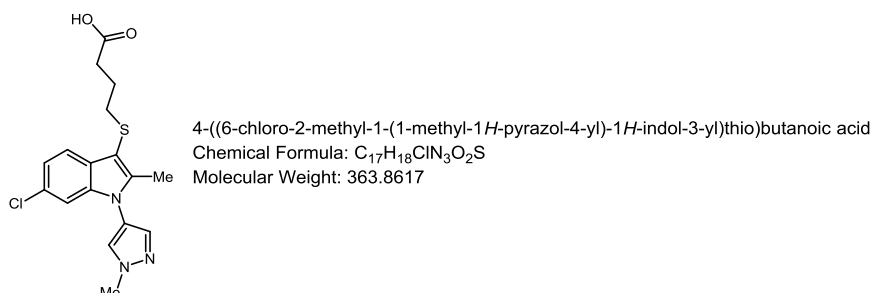
ν_{max} (neat): 1718, 1580, 1500, 1456 cm⁻¹.

¹H NMR (400 MHz, CDCl₃): δ 7.71 (dd, *J* = 6.5, 1.4 Hz, 1H), 7.60 (s, 1H), 7.54 (s, 1H), 7.22 – 7.13 (m, 3H), 4.03 (s, 3H), 2.73 (t, *J* = 7.1 Hz, 2H), 2.52 (m, 2H), 2.40 (s, 3H), 1.84 (quin., *J* = 7.2 Hz, 2H). CO₂H proton not observed.

¹³C NMR (126 MHz, CDCl₃) δ 178.7, 140.0, 135.3, 130.5, 121.9, 120.3, 118.6, 110.6, 101.8, 35.1, 32.5, 24.7, 12.2.

HRMS: exact mass calculated for [M+H⁺] (C₁₇H₂₀N₃O₂) requires *m/z* 330.1271, found *m/z* 333.1267.

Compound 148: 4-((6-chloro-2-methyl-1-(1-methyl-1*H*-pyrazol-4-yl)-1*H*-indol-3-yl)thio)butanoic acid



Prepared according to General Procedure D using 4-(2-methyl-1*H*-indol-3-yl)butanoic acid **219** (400 mg, 1.41 mmol, 1 equiv.), CuO (224 mg, 2.81 mmol, 2 equiv.), K₂CO₃ (254 mg, 1.83 mmol, 1.3 equiv.), and 1-methyl-4-bromopyrazole (0.44 mL, 4.23 mmol, 3 equiv.) in pyridine (4 mL, 0.4 M) to give the desired product as a brown oil (7 mg, 1%).

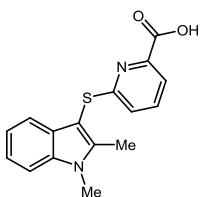
ν_{\max} (neat): 3409, 1681, 1437, 1407 cm⁻¹.

¹H NMR (400 MHz, CDCl₃): δ 7.59 (d, *J* = 8.4 Hz, 2H), 7.55 (s, 1H), 7.14 (dd, *J* = 8.3, 1.8 Hz, 1H), 7.11 (d, *J* = 1.6 Hz, 1H), 4.03 (s, 3H), 2.71 (t, *J* = 7.1 Hz, 2H), 2.51 (t, *J* = 7.4 Hz, 2H), 2.38 (s, 3H), 1.83 (quin, *J* = 7.2 Hz, 2H). CO₂H proton not observed.

¹³C NMR (101 MHz, CDCl₃): δ 176.6, 142.8, 138.2, 136.6, 136.6, 128.0, 127.7, 120.9, 119.0, 110.0, 109.7, 102.5, 39.3, 34.8, 31.7, 24.3, 11.1.

HRMS: exact mass calculated for [M+H⁺] (C₁₇H₁₉ClN₃O₂) requires *m/z* 364.0881, found *m/z* 364.0878.

Compound 149: 6-((1,2-Dimethyl-1*H*-indol-3-yl)thio)picolinic acid



6-((1,2-dimethyl-1*H*-indol-3-yl)thio)picolinic acid
Chemical Formula: C₁₆H₁₄N₂O₂S
Molecular Weight: 298.36

Prepared according to General Procedure G using ethyl 6-((1,2-dimethyl-1*H*-indol-3-yl)thio)picolinate **187** (49.5 mg, 0.16 mmol, 1 equiv.) and 2 M aq. NaOH (0.25 mL) in THF (0.25 mL, 0.6 M) to afford the desired product as a dark red amorphous solid (34.7 mg, 74%).

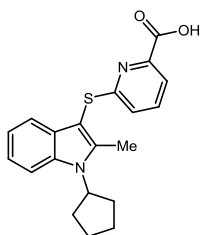
ν_{\max} (neat): 2992, 1693, 1571, 1440, 1408 cm⁻¹.

¹H NMR (500 MHz, CDCl₃): δ 7.83 (d, J = 7.5 Hz, 1H), 7.57 (dd, J = 9.7, 5.9 Hz, 1H), 7.52 (d, J = 7.8 Hz, 1H), 7.39 (d, J = 8.1 Hz, 1H), 7.29 (d, J = 7.3 Hz, 1H), 7.17 (t, J = 7.4 Hz, 1H), 6.98 (d, J = 8.1 Hz, 1H), 3.81 (s, 3H), 2.53 (s, 3H). CO₂H proton not observed.

¹³C NMR (101 MHz, CDCl₃): δ 145.2, 137.9, 137.9, 123.5, 123.4, 122.2, 121.8, 120.7, 120.5, 118.6, 118.5, 118.0, 110.5, 108.9, 29.2, 10.4.

HRMS: exact mass calculated for [M+H⁺] (C₁₆H₁₅N₂O₂S) requires m/z 299.0854, found m/z 299.0853.

Compound 150: 6-((1-Cyclopentyl-2-methyl-1*H*-indol-3-yl)thio)picolinic acid



6-((1-cyclopentyl-2-methyl-1*H*-indol-3-yl)thio)picolinic acid
 Chemical Formula: C₂₀H₂₀N₂O₂S
 Molecular Weight: 352.45

Prepared according to General Procedure G using ethyl 6-((2-methyl-1*H*-indol-3-yl)thio)picolinate **182** (300 mg, 0.96 mmol, 1 equiv.), distilled bromocyclopentane (0.31 mL, 2.89 mmol, 3 equiv.), NaH 60% w/w (68.7 mg, 2.86 mmol, 3 equiv.), and DMF (3 mL, 0.3 M) to afford the desired product as a yellow amorphous solid (36 mg, 11%).

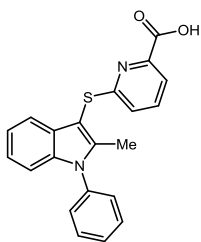
ν_{\max} (neat): 3275, 2918, 1714, 1570, 1429, 1404 cm⁻¹.

¹H NMR (400 MHz, CDCl₃): δ 9.10 (s, 1H), 7.70 (d, *J* = 7.6 Hz, 1H), 7.49 (d, *J* = 7.8 Hz, 1H), 7.39 (t, *J* = 7.8 Hz, 2H), 7.24 – 7.19 (m, 1H), 7.16 – 7.11 (m, 1H), 6.79 (d, *J* = 8.7 Hz, 1H), 5.46 (m, 1H), 2.53 (s, 3H), 2.07 – 1.96 (m, 2H), 1.93 – 1.75 (m, 4H), 1.65 (m, 2H).

¹³C NMR (101 MHz, CDCl₃): δ 164.3, 163.7, 147.7, 141.4, 136.7, 135.3, 129.3, 121.9, 121.8, 120.3, 119.9, 118.1, 110.6, 96.9, 78.3, 32.2, 23.3, 11.7.

HRMS: exact mass calculated for [M-H⁺] (C₂₀H₁₉N₂O₂S) requires *m/z* 351.1173, found *m/z* 351.1170.

Compound 151: 6-((2-Methyl-1-phenyl-1*H*-indol-3-yl)thio)picolinic acid



6-((2-methyl-1-phenyl-1*H*-indol-3-yl)thio)picolinic acid
 Chemical Formula: C₂₁H₁₆N₂O₂S
 Molecular Weight: 360.43

Prepared according to General Procedure D using ethyl 6-((2-methyl-1*H*-indol-3-yl)thio)picolinate **187** (200 mg, 0.64 mmol, 1 equiv.), bromobenzene (0.20 mL, 1.92 mmol, 3 equiv.), CuO (110 mg, 1.28 mmol, 2 equiv.) and K₂CO₃ (115 mg, 0.83 mmol, 1.3 equiv.) in pyridine (2 mL, 0.3 M) to afford the desired product as a brown amorphous solid (12 mg, 5%).

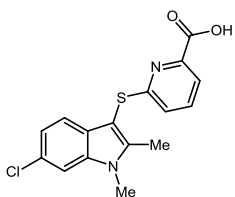
ν_{\max} (neat): 2920, 1693, 1573, 1409 cm⁻¹.

¹H NMR (400 MHz, CDCl₃): δ 7.87 (d, *J* = 7.4 Hz, 1H), 7.67 – 7.49 (m, 5H), 7.40 (m, 2H), 7.23 – 7.14 (m, 3H), 7.12 (d, *J* = 8.0 Hz, 1H), 2.39 (s, 3H). CO₂H proton not observed.

¹³C NMR (101 MHz, CDCl₃): δ 163.2, 161.6, 145.3, 142.9, 138.0, 137.7, 136.7, 129.3, 128.2, 127.4, 123.6, 122.3, 121.1, 118.7, 118, 110.3, 96.9, 11.2, 0.51.

HRMS: exact mass calculated for [M+H⁺] (C₂₁H₁₇N₂O₂S) requires *m/z* 361.1010, found *m/z* 361.1010.

Compound 152: 6-((6-Chloro-1,2-dimethyl-1*H*-indol-3-yl)thio)picolinic acid



6-((6-chloro-1,2-dimethyl-1*H*-indol-3-yl)thio)picolinic acid
Chemical Formula: C₁₆H₁₃ClN₂O₂S
Molecular Weight: 332.80

Prepared according to General Procedure C using ethyl 6-((6-chloro-2-methyl-1*H*-indol-3-yl)thio)picolinate **171** (138.5 mg, 0.4 mmol, 1 equiv.), NaH 60% w/w (63.5 mg, 1.6 mmol, 3 equiv.) and MeI (0.07 mL, 1.19 mmol, 3 equiv.) in DMF (2 mL, 0.2 M) to afford the desired product as a yellow amorphous solid (27.7 mg, 21%).

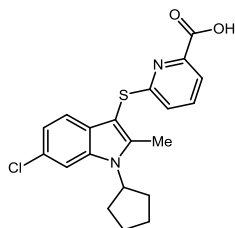
ν_{\max} (neat): 2916, 2848, 1703, 1573, 1556, 1440 cm⁻¹.

¹H NMR (400 MHz, CDCl₃): δ 7.84 (d, J = 7.3 Hz, 1H), 7.58 (t, J = 7.8 Hz, 1H), 7.43 – 7.36 (m, 2H), 7.12 (d, J = 8.3 Hz, 1H), 6.94 (d, J = 7.9 Hz, 1H), 3.76 (s, 3H), 2.51 (s, 3H). CO₂H proton not observed.

¹³C NMR (101 MHz, CDCl₃): δ 161.7, 143.5, 138.0, 137.2, 127.8, 127.7, 127.1, 123.3, 121.1, 118.9, 118.8, 109.2, 95.4, 30.2, 29.2, 10.6.

HRMS: exact mass calculated for [M+H⁺] (C₁₆H₁₄ClN₂O₂S) requires m/z 333.0462, found m/z 333.0463.

Compound 153: 6-((6-Chloro-1-cyclopentyl-2-methyl-1*H*-indol-3-yl)thio)picolinic acid



6-((6-chloro-1-cyclopentyl-2-methyl-1*H*-indol-3-yl)thio)picolinic acid
 Chemical Formula: C₂₀H₁₉ClN₂O₂S
 Molecular Weight: 386.90

Prepared according to General Procedure C using ethyl 6-((6-chloro-2-methyl-1*H*-indol-3-yl)thio)picolinate **171** (192.6 mg, 0.58 mmol, 1 equiv.), NaH 60% w/w (184.5 mg 4.61 mmol, 3 equiv.) and distilled bromocyclopentane (0.4 mL, 3.46 mmol, 6 equiv.) in DMF (3 mL, 0.2 M) to afford the desired product as an off white solid (19.2 mg, 9%).

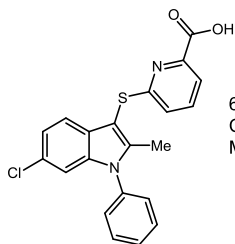
ν_{max} (neat): 2958, 2872, 1699, 1570, 1440 cm⁻¹.

¹H NMR (400 MHz, CDCl₃): δ 7.85 (dd, *J* = 7.5, 0.8 Hz, 1H), 7.65 – 7.57 (m, 1H), 7.48 – 7.43 (m, 2H), 7.42 (s, 1H), 7.11 (dd, *J* = 8.4, 1.7 Hz, 1H), 6.96 (dd, *J* = 8.1, 0.8 Hz, 1H), 4.85 (quin, *J* = 9.0 Hz, 1H), 2.54 (s, 3H), 2.33 – 2.20 (m, 2H), 2.20 – 2.04 (m, 4H), 1.90 – 1.77 (m, 2H).

¹³C NMR (126 MHz, CDCl₃): δ 163.6, 162.1, 145.7, 144.1, 138.5, 135.2, 128.6, 127.7, 123.9, 121.3, 119.7, 119.2, 111.6, 96.1, 57.5, 30.2, 25.3, 11.9.

HRMS: exact mass calculated for [M-H⁺] (C₂₀H₁₈ClN₂O₂S) requires *m/z* 385.0783, found *m/z* 385.0778.

Compound 154: 6-((6-Chloro-2-methyl-1-phenyl-1*H*-indol-3-yl)thio)picolinic acid



6-((6-chloro-2-methyl-1-phenyl-1*H*-indol-3-yl)thio)picolinic acid
 Chemical Formula: $C_{21}H_{15}ClN_2O_2S$
 Molecular Weight: 394.87

Prepared according to General Procedure E using 1,10-phenanthroline (104 mg, 0.58 mmol, 1 equiv.), CuI (55 mg, 0.29 mmol, 0.5 equiv.), Cs_2CO_3 (376 mg, 1.15 mmol, 2 equiv.), iodobenzene (0.13 mL, 1.15 mmol, 2 equiv.), and ethyl 6-((6-chloro-2-methyl-1*H*-indol-3-yl)thio)picolinate **171** (200 mg, 0.58 mmol, 1 equiv.) in 2 mL DMF (0.1 M) to afford the desired product as a white amorphous solid (9 mg, 4%).

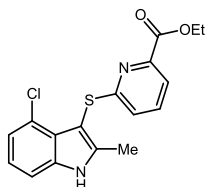
ν_{max} (neat): 3081, 1770, 1597, 1558, 1500 cm^{-1} .

1H NMR (500 MHz, $CDCl_3$) δ 7.88 (d, $J = 7.3$ Hz, 1H), 7.66 (t, $J = 7.8$ Hz, 1H), 7.61 (t, $J = 7.4$ Hz, 2H), 7.55 (t, $J = 7.4$ Hz, 1H), 7.47 (d, $J = 8.4$ Hz, 1H), 7.40 – 7.36 (m, 2H), 7.19 – 7.13 (m, 2H), 7.11 (d, $J = 8.1$ Hz, 1H), 2.37 (s, 3H).

^{13}C NMR (151 MHz, MeOD): δ 162.6, 144.6, 138.6, 137.8, 136.8, 129.8, 128.8, 128.3, 127.8, 127.7, 122.1, 121.5, 120.2, 119.1, 110.1, 110.0, 98.3, 10.3. One carbon not observed/coincident.

HRMS: exact mass calculated for $[M+H^+]$ ($C_{21}H_{16}ClN_2O_2S$) requires m/z 395.0616, found m/z 395.0617.

Compound 169: Ethyl 6-((7-chloro-2-methyl-1*H*-indol-3-yl)thio)picolinate



ethyl 6-((7-chloro-2-methyl-1*H*-indol-3-yl)thio)picolinate
 Chemical Formula: $C_{17}H_{15}ClN_2O_2S$
 Molecular Weight: 346.83

Prepared according to general procedure G ethyl 6-((2-oxopropyl)thio)picolinate (0.5 g, 2.09 mmol) and (3-chlorophenyl)hydrazine hydrochloride (0.4 g, 2.09 mmol) in 12

Experimental

mL EtOH (0.2 M) to afford the desired product as a white amorphous solid (125 mg, 17%).

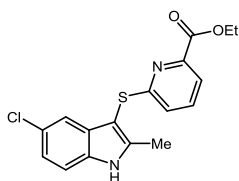
ν_{max} (neat): 1720, 1571, 1537, 1433 cm^{-1} .

^1H NMR (600 MHz, MeOD): δ 7.75 – 7.71 (m, 1H), 7.58 (t, J = 7.9 Hz, 1H), 7.33 (dd, J = 8.0, 0.5 Hz, 1H), 7.07 (t, J = 7.9 Hz, 1H), 7.00 (dd, J = 7.6, 0.5 Hz, 1H), 6.82 (dd, J = 8.2, 0.6 Hz, 1H), 4.42 (q, J = 7.1 Hz, 2H), 2.49 (s, 3H), 1.41 (t, J = 7.1 Hz, 3H). NH not observed.

^{13}C NMR (151 MHz, MeOD): δ 165.8, 164.8, 147.2, 144.1, 137.7, 137.5, 125.4, 124.8, 122.7, 122.0, 121.2, 120.0, 109.9, 95.2, 61.6, 13.1, 10.4.

HRMS: exact mass calculated for $[\text{M}+\text{H}^+]$ ($\text{C}_{17}\text{H}_{16}\text{ClN}_2\text{O}_2\text{S}$) m/z requires 347.0616, m/z found 347.0617.

Compound 170: Ethyl 6-((5-chloro-2-methyl-1H-indol-3-yl)thio)picolinate



ethyl 6-((5-chloro-2-methyl-1H-indol-3-yl)thio)picolinate
Chemical Formula: $\text{C}_{17}\text{H}_{15}\text{ClN}_2\text{O}_2\text{S}$
Molecular Weight: 346.83

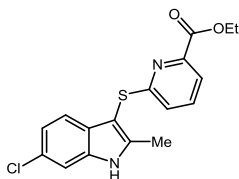
Prepared according to General Procedure A using ethyl 6-((2-oxopropyl)thio)picolinate **164** (1 g, 4.18 mmol, 1 equiv.) and (4-chlorophenyl)hydrazine hydrochloride (0.75 g, 4.18 mmol, 1 equiv.) in EtOH (25 mL, 0.2 M) to afford the desired product as a brown amorphous solid (460 mg, 32%).

ν_{max} (neat): 3263, 1720, 1570, 1500, 1463 cm^{-1} .

^1H NMR (400 MHz, MeOD): δ 7.75 (dd, J = 7.6, 0.8 Hz, 1H), 7.59 (t, J = 7.9 Hz, 1H), 7.41 (d, J = 1.8 Hz, 1H), 7.11 (dd, J = 8.6, 2.0 Hz, 1H), 6.75 (dd, J = 8.1, 0.8 Hz, 1H), 4.43 (q, J = 7.1 Hz, 2H), 2.49 (s, 3H), 1.42 (t, J = 7.1 Hz, 3H). CO_2H protons not observed.

^{13}C NMR (101 MHz, MeOD): δ 164.7, 163.8, 147.5, 144.1, 137.7, 134.6, 130.9, 126.0, 122.3, 121.7, 120.4, 116.8, 112.1, 95.4, 61.6, 13.1, 10.4.

HRMS: exact mass calculated for $[\text{M}+\text{H}^+]$ ($\text{C}_{17}\text{H}_{16}\text{ClNO}_2\text{S}$) requires m/z 347.0616, found m/z 347.0626.

Compound 171: Ethyl 6-((6-chloro-2-methyl-1H-indol-3-yl)thio)picolinate⁶⁹

ethyl 6-((6-chloro-2-methyl-1H-indol-3-yl)thio)picolinate
Chemical Formula: C₁₇H₁₅ClN₂O₂S
Molecular Weight: 346.83

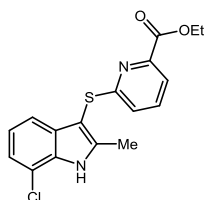
Prepared according to General Procedure B using ethyl 6-((2-oxopropyl)thio)picolinate **164** (512 mg, 2.09 mmol, 1 equiv.) and (3-chlorophenyl)hydrazine hydrochloride (374 mg, 2.09 mmol, 1 equiv.) in ^tBuOH (25 mL, 0.1 M) with additional 1 M HCl in Et₂O (0.31 mL) and AcOH (0.3 mL) to afford the desired product as a brown amorphous solid (517 mg, 71%).

ν_{\max} (neat): 1720, 1573, 1435, 1398 cm⁻¹.

¹H NMR (600 MHz, MeOD): δ 7.73 (dd, $J = 7.6, 0.8$ Hz, 1H), 7.59 – 7.54 (m, 1H), 7.39 (d, $J = 1.8$ Hz, 1H), 7.31 (d, $J = 8.4$ Hz, 1H), 7.02 (dd, $J = 8.4, 1.8$ Hz, 1H), 6.74 (dd, $J = 8.2, 0.8$ Hz, 1H), 4.42 (q, $J = 7.1$ Hz, 2H), 2.48 (s, 3H), 1.41 (t, $J = 7.1$ Hz, 3H). NH proton not observed.

¹³C NMR (151 MHz, MeOD): δ 164.7, 163.9, 147.5, 143.3, 137.7, 136.6, 128.3, 127.4, 122.4, 120.5, 120.3, 118.5, 110.8, 95.9, 61.6, 13.1, 10.4.

HRMS: exact mass calculated for [M+H⁺] (C₁₇H₁₆ClN₂O₂S) requires m/z 347.0916, found m/z 347.0916.

Compound 172: Ethyl 6-((7-chloro-2-methyl-1H-indol-3-yl)thio)picolinate

ethyl 6-((7-chloro-2-methyl-1H-indol-3-yl)thio)picolinate
Chemical Formula: C₁₇H₁₅ClN₂O₂S
Molecular Weight: 346.83

Prepared according to General Procedure A using ethyl 6-((2-oxopropyl)thio)picolinate **164** (0.55 g, 2.3 mmol, 1 equiv.) and (2-chlorophenyl)hydrazine hydrochloride (0.41 g, 2.3 mmol, 1 equiv.) in EtOH (12 mL, 0.2 M) to afford the desired product as a yellow amorphous solid (386 mg, 45%).

Experimental

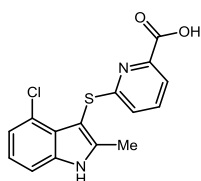
ν_{\max} (neat): 1722, 1571, 1431 cm^{-1} .

^1H NMR (400 MHz, MeOD): δ 7.74 (d, $J = 7.2$ Hz, 1H), 7.57 (t, $J = 7.9$ Hz, 1H), 7.32 (d, $J = 7.9$ Hz, 1H), 7.15 (d, $J = 7.6$ Hz, 1H), 7.02 (t, $J = 7.8$ Hz, 1H), 6.74 (d, $J = 8.1$ Hz, 1H), 4.43 (q, $J = 7.1$ Hz, 2H), 2.52 (s, 3H), 1.42 (t, $J = 7.1$ Hz, 3H). CO_2H proton not observed.

^{13}C NMR (101 MHz, MeOD): δ 164.6, 163.8, 147.5, 143.7, 137.7, 133.2, 131.4, 122.4, 121.1, 120.9, 120.3, 116.3, 116.3, 96.9, 61.6, 13.1, 10.3.

HRMS: exact mass calculated for $[\text{M}+\text{H}^+]$ ($\text{C}_{17}\text{H}_{16}\text{ClN}_2\text{O}_2\text{S}$) requires m/z 347.0616, found m/z 347.0616.

Compound 173: 6-((4-Chloro-2-methyl-1H-indol-3-yl)thio)picolinic acid



6-((4-chloro-2-methyl-1H-indol-3-yl)thio)picolinic acid
Chemical Formula: $\text{C}_{15}\text{H}_{11}\text{ClN}_2\text{O}_2\text{S}$
Molecular Weight: 318.7750

Prepared according to general procedure G using ethyl 6-((4-chloro-2-methyl-1H-indol-3-yl)thio)picolinate **164** (50 mg, 0.14 mmol) and 2 M aq. NaOH (1 mL) in 1 mL THF (0.1 M) to afford the desired product as a brown amorphous solid (40 mg, 87%).

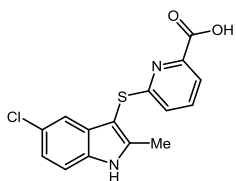
ν_{\max} (neat): 3138, 1745, 1573, 1558, 1535 cm^{-1} .

^1H NMR (400 MHz, MeOD): δ 7.76 (dd, $J = 7.6, 0.9$ Hz, 1H), 7.64 – 7.58 (m, 1H), 7.33 (dd, $J = 8.0, 1.0$ Hz, 1H), 7.07 (t, $J = 7.8$ Hz, 1H), 7.00 (dd, $J = 7.7, 1.0$ Hz, 1H), 6.84 (dd, $J = 8.2, 0.9$ Hz, 1H), 2.49 (s, 3H). NH and CO_2H protons not observed.

^{13}C NMR (101 MHz, MeOD): δ 166.0, 165.5, 147.1, 144.1, 137.7, 125.4, 124.8, 122.8, 122.0, 121.2, 119.9, 109.9, 95.1, 10.4. One carbon not observed/coincident.

HRMS: exact mass calculated for $[\text{M}+\text{H}^+]$ ($\text{C}_{15}\text{H}_{12}\text{ClN}_2\text{O}_2\text{S}$) m/z requires 319.0303, m/z found 319.0303.

Compound 174: 6-((5-Chloro-2-methyl-1*H*-indol-3-yl)thio)picolinic acid



6-((5-chloro-2-methyl-1*H*-indol-3-yl)thio)picolinic acid
 Chemical Formula: C₁₅H₁₁ClN₂O₂S
 Molecular Weight: 318.7750

Prepared according to General Procedure G using ethyl 6-((5-chloro-2-methyl-1*H*-indol-3-yl)thio)picolinate **170** (46 mg, 0.13 mmol, 1 equiv.) and 2 M aq. NaOH (0.5 mL) in THF (0.5 mL, 0.3 M) to afford the desired product as a pale brown amorphous solid (37 mg, 88%).

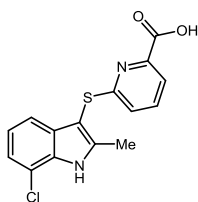
ν_{\max} (neat): 3304, 1751, 1656, 1577, 1440 cm⁻¹.

¹H NMR (600 MHz, MeOD) δ 7.79 (dd, *J* = 7.6, 0.8 Hz, 1H), 7.63 – 7.58 (m, 1H), 7.37 (d, *J* = 8.6 Hz, 1H), 7.35 (d, *J* = 1.9 Hz, 1H), 7.13 (dd, *J* = 8.6, 2.0 Hz, 1H), 6.77 (dd, *J* = 8.2, 0.8 Hz, 1H), 2.51 (s, 3H).

¹³C NMR (151 MHz, MeOD): δ 166.0, 163.6, 147.7, 144.1, 137.8, 134.6, 130.9, 126.0, 122.3, 121.8, 120.2, 116.8, 112.2, 95.4, 10.4.

HRMS: exact mass calculated for [M+H⁺] (C₁₅H₁₂ClNO₂S) requires *m/z* 319.0303, found *m/z* 319.0307.

Compound 175: 6-((7-Chloro-2-methyl-1*H*-indol-3-yl)thio)picolinic acid



6-((7-chloro-2-methyl-1*H*-indol-3-yl)thio)picolinic acid
 Chemical Formula: C₁₅H₁₁ClN₂O₂S
 Molecular Weight: 318.78

Prepared according to General Procedure A using ethyl 6-((2-oxopropyl)thio)picolinate **172** (1 g, 4.18 mmol, 1 equiv.) and (2-chlorophenyl)hydrazine hydrochloride (0.75 g, 4.18 mmol, 1 equiv.) in EtOH (25 mL, 0.2 M), followed by General Procedure x using 2 M aq. NaOH (6 mL) in THF (6 mL, 0.7 M) to afford the desired product as a pale yellow amorphous solid (289 mg, 22% over 2 steps).

ν_{\max} (neat): 3130, 1591, 1429, 1396, 1367 cm⁻¹.

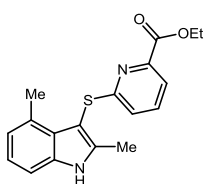
Experimental

^1H NMR (400 MHz, MeOD): δ 7.59 (dd, $J = 7.6, 0.9$ Hz, 1H), 7.47 – 7.39 (m, 1H), 7.37 – 7.31 (m, 1H), 7.17 – 7.11 (m, 1H), 7.05 – 6.97 (m, 1H), 6.56 – 6.48 (m, 1H), 2.52 (s, 3H). NH and CO_2H protons not observed.

^{13}C NMR (151 MHz, MeOD): δ 171.4, 162.1, 154.9, 143.4, 137.0, 133.1, 131.6, 121.0, 120.7, 119.6, 118.9, 116.5, 116.2, 97.8, 10.3.

HRMS: exact mass calculated for $[\text{M}+\text{H}^+]$ ($\text{C}_{15}\text{H}_{12}\text{ClN}_2\text{O}_2\text{S}$) requires m/z 319.0303, found m/z 319.0306.

Compound 181: Ethyl-6-((2,4-dimethyl-1H-indol-3-yl)thio)picolinate



ethyl 6-((2,4-dimethyl-1H-indol-3-yl)thio)picolinate
Chemical Formula: $\text{C}_{18}\text{H}_{18}\text{N}_2\text{O}_2\text{S}$
Molecular Weight: 326.41

Prepared according to General Procedure A using ethyl 6-((2-oxopropyl)thio)picolinate **164** (1 g, 4.43 mmol, 1 equiv.) and *m*-tolylhydrazine hydrochloride (0.67 mL, 4.43 mmol, 1 equiv.) in EtOH (25 mL, 0.2 M) to afford the desired product as a yellow amorphous solid (156 mg, 11%).

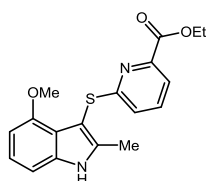
ν_{max} (neat): 3153, 1720, 1674, 1573, 1433 cm^{-1} .

^1H NMR (400 MHz, MeOD): δ 7.72 (dd, $J = 7.6, 0.9$ Hz, 1H), 7.60 – 7.54 (m, 1H), 7.21 (d, $J = 8.1$ Hz, 1H), 7.02 – 6.96 (m, 1H), 6.82 – 6.73 (m, 2H), 4.42 (q, $J = 7.1$ Hz, 2H), 2.54 (s, 3H), 2.45 (s, 3H), 1.41 (t, $J = 7.1$ Hz, 3H). NH not observed.

^{13}C NMR (101 MHz, MeOD): δ 166.2, 164.7, 147.3, 142.3, 137.7, 136.4, 129.5, 127.1, 122.5, 121.8, 121.4, 120.0, 108.9, 95.1, 61.6, 17.5, 13.1, 10.3.

HRMS: exact mass calculated for $[\text{M}+\text{H}^+]$ ($\text{C}_{18}\text{H}_{19}\text{N}_2\text{O}_2\text{S}$) requires m/z 327.1162, found m/z 327.1161.

Compound 182: Ethyl 6-((4-methoxy-2-methyl-1*H*-indol-3-yl)thio)picolinate



ethyl 6-((4-methoxy-2-methyl-1*H*-indol-3-yl)thio)picolinate
 Chemical Formula: C₁₈H₁₈N₂O₃S
 Molecular Weight: 342.4121

Prepared according to General Procedure A using ethyl 6-((2-oxopropyl)thio)picolinate **164** (1 g, 4.2 mmol, 1 equiv.) and (3-methoxyphenyl)hydrazine hydrochloride (0.7 g, 4.18 mmol, 1 equiv.) in 25 mL EtOH (0.2 M) to afford the desired product as a yellow amorphous solid (282 mg, 20%).

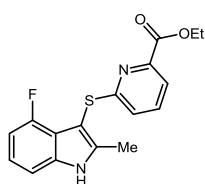
ν_{\max} (neat): 3288, 1714, 1575, 1543, 1506 cm⁻¹.

¹H NMR (600 MHz, MeOD): δ 7.72 (dd, $J = 7.5, 0.8$ Hz, 1H), 7.57 (t, $J = 7.9$ Hz, 1H), 7.04 (t, $J = 7.9$ Hz, 1H), 6.99 (dd, $J = 8.1, 0.6$ Hz, 1H), 6.88 (dd, $J = 8.2, 0.8$ Hz, 1H), 6.51 (d, $J = 7.7$ Hz, 1H), 4.43 (q, $J = 7.1$ Hz, 2H), 3.62 (s, 3H), 2.44 (s, 3H), 1.42 (t, $J = 7.1$ Hz, 3H). NH proton not observed.

¹³C NMR (151 MHz, MeOD): δ 166.4, 164.7, 153.5, 146.7, 140.6, 137.9, 137.3, 123.1, 122.4, 119.8, 118.6, 104.4, 101.0, 94.3, 61.6, 54.4, 13.1, 10.2.

HRMS: exact mass calculated for [M+H⁺] (C₁₈H₁₉N₂O₃S) requires m/z 343.1111, found m/z 343.1112.

Compound 183: Ethyl 6-((4-fluoro-2-methyl-1*H*-indol-3-yl)thio)picolinate



ethyl 6-((4-fluoro-2-methyl-1*H*-indol-3-yl)thio)picolinate
 Chemical Formula: C₁₇H₁₅FN₂O₂S
 Molecular Weight: 330.3766

Prepared according to General Procedure A using ethyl 6-((2-oxopropyl)thio)picolinate **164** (1 g, 4.18 mmol, 1 equiv.) and (3-fluorophenyl)hydrazine hydrochloride (0.7 mg, 4.18 mmol, 1 equiv.) in EtOH (25 mL, 0.2 M) to afford the desired product as a yellow amorphous solid (332 mg, 24%).

ν_{\max} (neat): 1718, 1573, 1435 cm⁻¹.

Experimental

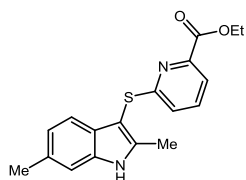
^1H NMR (400 MHz, MeOD): δ 7.74 (dd, $J = 7.6, 0.9$ Hz, 1H), 7.62 – 7.57 (m, 1H), 7.19 (d, $J = 8.0$ Hz, 1H), 7.06 (m, 1H), 6.86 (dd, $J = 8.1, 0.7$ Hz, 1H), 6.69 (m, 1H), 4.42 (q, $J = 7.1$ Hz, 2H), 2.47 (s, 3H), 1.41 (t, $J = 7.1$ Hz, 3H). NH proton not observed.

^{13}C NMR (101 MHz, MeOD): δ 165.1, 164.7, 155.9 (d, $^1J_{\text{C-F}} = 246.5$ Hz), 147.2, 142.8, 139.0 (d, $^3J_{\text{C-F}} = 10.3$ Hz), 137.6, 122.5, 122.0 (d, $^3J_{\text{C-F}} = 7.6$ Hz), 120.1, 117.7 (d, $^2J_{\text{C-F}} = 17.2$ Hz), 107.2 (d, $^4J_{\text{C-F}} = 3.7$ Hz), 105.2 (d, $^2J_{\text{C-F}} = 19.2$ Hz), 93.2, 61.6, 13.1, 10.1.

^{19}F NMR (376 MHz, DMSO): δ -130.41.

HRMS: exact mass calculated for $[\text{M}+\text{H}^+]$ ($\text{C}_{17}\text{H}_{16}\text{FN}_2\text{O}_2\text{S}$) requires m/z 331.0911, found m/z 331.0917.

Compound 184: Ethyl 6-((2,6-dimethyl-1H-indol-3-yl)thio)picolinate



ethyl 6-((2,6-dimethyl-1H-indol-3-yl)thio)picolinate
Chemical Formula: $\text{C}_{18}\text{H}_{18}\text{N}_2\text{O}_2\text{S}$
Molecular Weight: 326.41

Prepared according to General Procedure A using ethyl 6-((2-oxopropyl)thio)picolinate **164** (1 g, 4.43 mmol, 1 equiv.) and *m*-tolylhydrazine hydrochloride (0.7 mL, 4.43 mmol, 1 equiv.) in EtOH (25 mL, 0.2 M) to afford the desired product as a yellow amorphous solid (189 mg, 13%).

ν_{max} (neat): 3296, 1720, 1573, 1435, 1400 cm^{-1} .

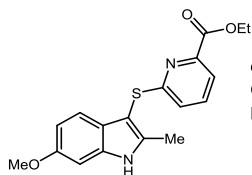
^1H NMR (400 MHz, MeOD): δ 7.70 (dd, $J = 7.6, 0.9$ Hz, 1H), 7.53 – 7.46 (m, 1H), 7.22 (d, $J = 8.1$ Hz, 1H), 7.19 – 7.16 (m, 1H), 6.86 (dd, $J = 8.0, 0.9$ Hz, 1H), 6.72 (dd, $J = 8.2, 0.9$ Hz, 1H), 4.41 (q, $J = 7.1$ Hz, 2H), 2.45 (s, 3H), 2.40 (s, 3H), 1.41 (t, $J = 7.1$ Hz, 3H). CO_2H proton not observed.

^{13}C NMR (101 MHz, MeOD): δ 164.7, 147.3, 141.4, 137.5, 136.6, 131.4, 127.3, 122.5, 121.6, 120.1, 117.1, 110.8, 95.0, 61.6, 20.3, 13.1, 10.3. One carbon not observed/coincident.

Experimental

HRMS: exact mass calculated for $[M+H]^+$ ($C_{18}H_{19}N_2O_2S$) requires m/z 327.1162, found m/z 327.1162.

Compound 185: Ethyl 6-((6-methoxy-2-methyl-1*H*-indol-3-yl)thio)picolinate



ethyl 6-((6-methoxy-2-methyl-1*H*-indol-3-yl)thio)picolinate
Chemical Formula: $C_{18}H_{19}N_2O_3S$
Molecular Weight: 342.41

Prepared according to General Procedure A using ethyl 6-((2-oxopropyl)thio)picolinate **164** (1 g, 4.18 mmol, 1 equiv.) and (3-methoxyphenyl)hydrazine hydrochloride (0.7 g, 4.18 mmol, 1 equiv.) in EtOH (25 mL, 0.2 M) to afford the desired product as a brown amorphous solid (521 mg, 36%).

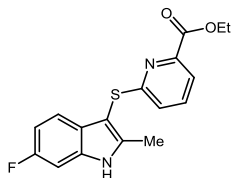
ν_{\max} (neat): 1726, 1627, 1452 cm^{-1} .

1H NMR (600 MHz, MeOD): δ 7.73 (dd, $J = 7.6, 0.8$ Hz, 1H), 7.61 – 7.51 (m, 1H), 7.22 (d, $J = 8.6$ Hz, 1H), 6.93 (d, $J = 2.2$ Hz, 1H), 6.77 (dd, $J = 8.2, 0.8$ Hz, 1H), 6.71 (dd, $J = 8.6, 2.2$ Hz, 1H), 4.43 (q, $J = 7.1$ Hz, 2H), 3.81 (s, 3H), 2.44 (s, 3H), 1.42 (t, $J = 7.1$ Hz, 3H). NH not observed.

^{13}C NMR (151 MHz, MeOD): δ 164.6, 164.5, 156.7, 147.1, 140.9, 137.7, 136.9, 123.6, 122.6, 120.2, 118.0, 109.7, 94.9, 94.7, 61.6, 54.7, 13.1, 10.3.

HRMS: exact mass calculated for $[M+H]^+$ ($C_{16}H_{19}N_2O_3S$) requires m/z 343.1111, found m/z 343.1113.

Compound 186: Ethyl 6-((6-fluoro-2-methyl-1*H*-indol-3-yl)thio)picolinate



ethyl 6-((6-fluoro-2-methyl-1*H*-indol-3-yl)thio)picolinate
Chemical Formula: $C_{17}H_{15}FN_2O_3S$
Molecular Weight: 330.38

Prepared according to General Procedure A using ethyl 6-((2-oxopropyl)thio)picolinate **164** (1 g, 4.18 mmol, 1 equiv.) and (3-

Experimental

fluorophenyl)hydrazine hydrochloride (0.68 g, 4.18 mmol, 1 equiv.) in EtOH (25 mL, 0.2 M) to afford the desired product as a yellow amorphous solid (563 mg, 48%).

ν_{\max} (neat): 3296, 1722, 1627, 1573, 1560 cm^{-1} .

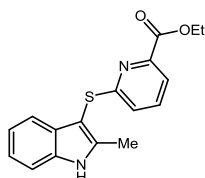
^1H NMR (400 MHz, MeOD): δ 7.72 (dd, $J = 7.6, 0.9$ Hz, 1H), 7.58 – 7.51 (m, 1H), 7.30 (dd, $J = 8.6, 5.2$ Hz, 1H), 7.09 (dd, $J = 9.6, 2.2$ Hz, 1H), 6.81 (ddd, $J = 9.8, 8.7, 2.3$ Hz, 1H), 6.74 (dd, $J = 8.2, 0.9$ Hz, 1H), 4.42 (q, $J = 7.1$ Hz, 2H), 2.46 (s, 3H), 1.41 (t, $J = 7.1$ Hz, 3H). NH not observed.

^{13}C NMR (101 MHz, MeOD): δ 164.6, 164.1, 159.9 (d, $^1J_{\text{C-F}} = 236.1$ Hz), 147.4, 142.8 (d, $^4J_{\text{C-F}} = 2.9$ Hz), 137.7, 136.1 ($^3J_{\text{C-F}} = 12.5$ Hz), 126.0, 122.4, 120.3, 118.3 (d, $^3J_{\text{C-F}} = 10.1$ Hz), 108.2 (d, $^2J_{\text{C-F}} = 24.7$ Hz), 97.2 (d, $^2J_{\text{C-F}} = 26.5$ Hz), 95.6, 61.6, 13.1, 10.4.

^{19}F NMR (376 MHz, MeOD): δ -123.5.

HRMS: exact mass calculated for $[\text{M}+\text{H}^+]$ ($\text{C}_{17}\text{H}_{16}\text{FN}_2\text{O}_2\text{S}$) requires m/z 331.0911, found m/z 331.0917.

Compound 187: Ethyl 6-((2-methyl-1*H*-indol-3-yl)thio)picolinate



ethyl 6-((2-methyl-1*H*-indol-3-yl)thio)picolinate
Chemical Formula: $\text{C}_{17}\text{H}_{16}\text{N}_2\text{O}_2\text{S}$
Molecular Weight: 312.39

Prepared according to General Procedure B using ethyl 6-((2-oxopropyl)thio)picolinate **164** (1.0 g, 4.24 mmol, 1 equiv.), phenyl hydrazine hydrochloride (0.6 g, 4.25 mmol, 1 equiv.) in $^t\text{BuOH}$ (50 mL, 0.1 M), with additional 1 M HCl in Et_2O (0.64 mL), to afford the desired product as a brown amorphous solid (1.2 g, 92%).

ν_{\max} (neat): 3280, 1733, 1573, 1406, 1290 cm^{-1} .

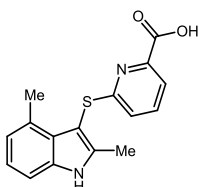
^1H NMR (400 MHz, CDCl_3) δ 8.59 (s, 1H), 7.74 (dd, $J = 7.6, 0.8$ Hz, 1H), 7.51 (d, $J = 7.9$ Hz, 1H), 7.41 (d, $J = 8.0$ Hz, 1H), 7.37 (d, $J = 8.7$ Hz, 1H), 7.24 – 7.19 (m, 1H), 7.13 (td, $J = 7.7, 1.0$ Hz, 1H), 6.76 (d, $J = 8.1$ Hz, 1H), 4.47 (q, $J = 7.1$ Hz, 2H), 2.53 (s, 3H), 1.43 (t, $J = 7.1$ Hz, 3H).

Experimental

^{13}C NMR (101 MHz, CDCl_3): δ 165.1, 164.1, 148.0, 141.6, 137.2, 135.7, 129.8, 122.5, 122.4, 120.9, 120.5, 118.8, 110.9, 97.8, 61.9, 14.3, 12.2.

HRMS: exact mass calculated for $[\text{M}+\text{H}^+]$ ($\text{C}_{17}\text{H}_{17}\text{N}_2\text{O}_2\text{S}$) requires m/z 313.1005, found m/z 313.1005.

Compound 188: 6-((2,4-Dimethyl-1*H*-indol-3-yl)thio)picolinic acid



6-((2,4-dimethyl-1*H*-indol-3-yl)thio)picolinic acid
Chemical Formula: $\text{C}_{16}\text{H}_{14}\text{N}_2\text{O}_2\text{S}$
Molecular Weight: 298.36

Prepared according to General Procedure E using 1,10-phenanthroline (49 mg, 0.27 mmol, 1 equiv.), CuI (26 mg, 0.14 mmol, 0.5 equiv.), Cs_2CO_3 (176 mg, 0.54 mmol, 2 equiv.), 4-iodo-1-methyl-1*H*-pyrazole (112 mg, 0.54 mmol, 2 equiv.), and ethyl 6-((2,4-dimethyl-1*H*-indol-3-yl)thio)picolinate **181** (88 mg, 0.27 mmol, 1 equiv.) in DMF (0.94 mL, 0.3 M) to afford the desired product as an off white amorphous solid (31 mg, 39%).

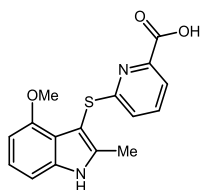
ν_{max} (neat): 3302, 1690, 1580, 1558, 1454 cm^{-1} .

^1H NMR (400 MHz, MeOD): δ 7.76 (dd, $J = 7.6, 0.9$ Hz, 1H), 7.63 – 7.55 (m, 1H), 7.23 (d, $J = 8.1$ Hz, 1H), 7.05 – 6.97 (m, 1H), 6.84 – 6.75 (m, 2H), 2.56 (s, 3H), 2.47 (s, 3H). NH and CO_2H protons not observed.

^{13}C NMR (101 MHz, MeOD): δ 166.1, 165.9, 147.4, 142.3, 137.8, 136.4, 129.5, 127.1, 122.5, 121.8, 121.4, 119.9, 108.9, 95.2, 17.5, 10.3.

HRMS: exact mass calculated for $[\text{M}+\text{H}^+]$ ($\text{C}_{16}\text{H}_{15}\text{N}_2\text{O}_2\text{S}$) requires m/z 299.0849, found m/z 299.0849.

Compound 189: 6-((4-Methoxy-2-methyl-1*H*-indol-3-yl)thio)picolinic acid



6-((4-methoxy-2-methyl-1*H*-indol-3-yl)thio)picolinic acid
 Chemical Formula: C₁₆H₁₄N₂O₃S
 Molecular Weight: 314.3590

Prepared according to General Procedure G using ethyl 6-((4-methoxy-2-methyl-1*H*-indol-3-yl)thio)picolinate **182** (47.2 mg 0.14 mmol, 1 equiv.) and 2 M aq. NaOH (0.5 mL) in THF (0.5 mL, 0.3 M), to afford the desired product as a yellow amorphous solid (41.7 mg, 96%).

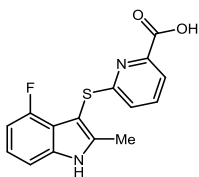
ν_{\max} (neat): 3273, 1716, 1583, 1539, 1483 cm⁻¹.

¹H NMR (400 MHz, MeOD): δ 7.72 (d, *J* = 7.5 Hz, 1H), 7.55 (t, *J* = 7.9 Hz, 1H), 7.06 – 6.93 (m, 2H), 6.89 (d, *J* = 8.2 Hz, 1H), 6.49 (d, *J* = 7.5 Hz, 1H), 3.59 (s, 3H), 2.43 (s, 3H). NH and CO₂H protons not observed.

¹³C NMR (101 MHz, MeOD): δ 165.9, 165.9, 153.5, 146.7, 140.7, 137.8, 137.5, 123.1, 122.4, 119.7, 118.6, 104.4, 101.0, 94.2, 54.4, 10.2.

HRMS: exact mass calculated for [M+H⁺] (C₁₆H₁₅N₂O₃S) requires *m/z* 315.0798, found *m/z* 315.0798.

Compound 190: 6-((4-Fluoro-2-methyl-1*H*-indol-3-yl)thio)picolinic acid



6-((4-fluoro-2-methyl-1*H*-indol-3-yl)thio)picolinic acid
 Chemical Formula: C₁₅H₁₁FN₂O₂S
 Molecular Weight: 302.3234

Prepared according to General Procedure G using ethyl 6-((4-fluoro-2-methyl-1*H*-indol-3-yl)thio)picolinate **183** (51 mg, 0.15 mmol, 1 equiv.) and 2 M aq. NaOH solution (0.5 mL) in THF (0.5 mL, 0.3 M) to afford the desired product as a yellow amorphous solid (56 mg, 99%).

ν_{\max} (neat): 1687, 1573, 1413 cm⁻¹.

Experimental

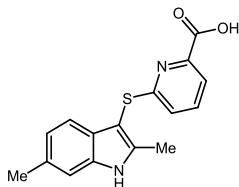
^1H NMR (600 MHz, MeOD): δ 7.75 (dd, $J = 7.5, 0.7$ Hz, 1H), 7.58 (t, $J = 7.9$ Hz, 1H), 7.18 (d, $J = 8.2$ Hz, 1H), 7.05 (td, $J = 8.0, 4.9$ Hz, 1H), 6.86 (d, $J = 8.2$ Hz, 1H), 6.68 (dd, $J = 11.1, 7.9$ Hz, 1H), 2.46 (s, 3H). NH and CO_2H protons not observed.

^{13}C NMR (151 MHz, MeOD): δ 166.1, 164.7, 155.9 (d, $^1J_{\text{C-F}} = 246.5$ Hz), 147.3, 142.8, 139.0 (d, $^3J_{\text{C-F}} = 10.3$ Hz), 137.7, 122.5, 121.9 (d, $^3J_{\text{C-F}} = 7.7$ Hz), 120.0, 117.7 (d, $^2J_{\text{C-F}} = 17.3$ Hz), 107.2 (d, $^4J_{\text{C-F}} = 3.8$ Hz), 105.3 (d, $^2J_{\text{C-F}} = 19.2$ Hz), 93.2 (d, $^4J_{\text{C-F}} = 1.6$ Hz), 10.1.

^{19}F NMR (376 MHz, MeOD): δ -129.6.

HRMS: exact mass calculated for $[\text{M}+\text{H}^+]$ ($\text{C}_{15}\text{H}_{12}\text{FN}_2\text{O}_2\text{S}$) requires m/z 303.0598, found m/z 303.0568.

Compound 191: 6-((2,6-Dimethyl-1H-indol-3-yl)thio)picolinic acid



6-((2,6-dimethyl-1H-indol-3-yl)thio)picolinic acid
Chemical Formula: $\text{C}_{16}\text{H}_{14}\text{N}_2\text{O}_2\text{S}$
Molecular Weight: 298.36

Prepared according to General Procedure E using 1,10-phenanthroline (49 mg, 0.27 mmol, 1 equiv.), CuI (26 mg, 0.14 mmol, 0.5 equiv.), Cs_2CO_3 (176 mg, 0.54 mmol, 2 equiv.), 4-iodo-1-methyl-1H-pyrazole (112 mg, 0.54 mmol, 2 equiv.), and ethyl 6-((2,6-dimethyl-1H-indol-3-yl)thio)picolinate (88 mg, 0.27 mmol, 1 equiv.) in DMF (0.94 mL, 0.3 M) to afford the desired product as a yellow amorphous solid (8 mg, 10%).

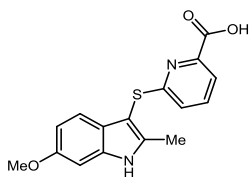
ν_{max} (neat): 3279, 1720, 1580, 1578, 1441 cm^{-1} .

^1H NMR (400 MHz, MeOD): δ 7.64 (d, $J = 7.5$ Hz, 1H), 7.46 (t, $J = 7.8$ Hz, 1H), 7.24 (d, $J = 8.0$ Hz, 1H), 7.18 (d, $J = 0.5$ Hz, 1H), 6.88 (dd, $J = 8.0, 0.9$ Hz, 1H), 6.63 (d, $J = 8.0$ Hz, 1H), 2.45 (s, 3H), 2.42 (s, 3H). NH and CO_2H not observed.

^{13}C NMR (101 MHz, MeOD): δ 169.2, 163.5, 151.7, 141.2, 137.1, 136.6, 131.4, 127.5, 121.5, 120.9, 119.2, 117.6, 110.75, 95.7, 20.3, 10.3.

HRMS: exact mass calculated for $[\text{M}+\text{H}^+]$ ($\text{C}_{16}\text{H}_{15}\text{N}_2\text{O}_2\text{S}$) requires m/z 299.0849, found m/z 299.0849.

Compound 192: 6-((6-Methoxy-2-methyl-1*H*-indol-3-yl)thio)picolinic acid



6-((6-methoxy-2-methyl-1*H*-indol-3-yl)thio)picolinic acid
 Chemical Formula: C₁₆H₁₄N₂O₃S
 Molecular Weight: 314.36

Prepared according to General Procedure G using ethyl 6-((6-methoxy-2-methyl-1*H*-indol-3-yl)thio)picolinate **185** (46.4 mg, 0.14 mmol, 1 equiv.) and 2 M aq. NaOH (0.5 mL) in THF (0.5 mL, 0.3 M) to afford the desired product as a brown amorphous solid (36.2 mg, 85%).

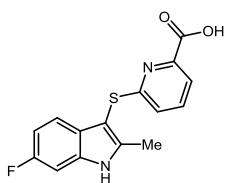
ν_{\max} (neat): 3286, 1724, 1627, 1581, 1500 cm⁻¹.

¹H NMR (400 MHz, MeOD): δ 7.75 (dd, *J* = 7.6, 0.9 Hz, 1H), 7.58 – 7.51 (m, 1H), 7.21 (d, *J* = 8.6 Hz, 1H), 6.93 (d, *J* = 2.1 Hz, 1H), 6.78 (dd, *J* = 8.1, 0.9 Hz, 1H), 6.70 (dd, *J* = 8.6, 2.2 Hz, 1H), 3.80 (s, 3H), 2.50 – 2.39 (m, 3H). NH and CO₂H protons not observed.

¹³C NMR (101 MHz, MeOD): δ 165.8, 164.3, 156.7, 147.1, 140.9, 137.9, 136.9, 123.5, 122.7, 120.1, 118.0, 109.7, 94.8, 94.7, 54.7, 10.4.

HRMS: exact mass calculated for [M-H⁺] (C₁₆H₁₃N₂O₂S) requires *m/z* 315.0798, found *m/z* 315.0798.

Compound 193: 6-((6-Fluoro-2-methyl-1*H*-indol-3-yl)thio)picolinic acid



6-((6-fluoro-2-methyl-1*H*-indol-3-yl)thio)picolinic acid
 Chemical Formula: C₁₅H₁₁FN₂O₂S
 Molecular Weight: 302.32

Prepared according to General Procedure G using ethyl 6-((6-fluoro-2-methyl-1*H*-indol-3-yl)thio)picolinate **185** (50 mg, 0.15 mmol, 1 equiv.) and 2 M aq. NaOH (0.5 mL) in THF (0.5 mL, 0.3 M) to afford the desired product as a brown amorphous solid (3 mg, 7%).

ν_{\max} (neat): 3338, 1732, 1608, 1583, 1556 cm⁻¹.

Experimental

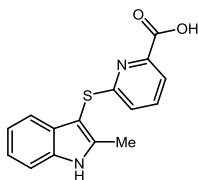
^1H NMR (400 MHz, MeOD): δ 7.62 (d, $J = 7.5$ Hz, 1H), 7.46 (t, $J = 7.8$ Hz, 1H), 7.33 (dd, $J = 8.6, 5.3$ Hz, 1H), 7.09 (dd, $J = 9.6, 2.2$ Hz, 1H), 6.82 (ddd, $J = 9.8, 8.7, 2.3$ Hz, 1H), 6.57 (d, $J = 8.0$ Hz, 1H), 2.46 (s, 3H). NH and CO_2H protons not observed.

^{13}C NMR (101 MHz, MeOD): δ 169.1, 163.0, 160.0 (d, $^1J_{\text{C-F}} = 235.9$ Hz), 151.6, 142.7 (d, $^2J_{\text{C-F}} = 26.4$ Hz), 137.3, 136.1 (d, $^3J_{\text{C-F}} = 12.6$ Hz), 126.1, 120.9, 119.5, 118.4 (d, $^3J_{\text{C-F}} = 10$ Hz), 108.1 (d, $^2J_{\text{C-F}} = 24.7$ Hz), 97.2 (d, $^2J_{\text{C-F}} = 26.4$ Hz), 96.1, 10.4.

^{19}F NMR (376 MHz, MeOD): δ -123.86.

HRMS: exact mass calculated for $[\text{M}+\text{H}^+]$ ($\text{C}_{15}\text{H}_{12}\text{FN}_2\text{O}_2\text{S}$) requires m/z 303.0598, found m/z 303.0596.

Compound 194: 6-((2-Methyl-1*H*-indol-3-yl)thio)picolinic acid



6-((2-methyl-1*H*-indol-3-yl)thio)picolinic acid
Chemical Formula: $\text{C}_{15}\text{H}_{12}\text{N}_2\text{O}_2\text{S}$
Molecular Weight: 284.3330

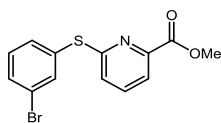
Prepared according to General Procedure G using ethyl 6-((2-methyl-1*H*-indol-3-yl)thio)picolinate **187** (56 mg, 0.18 mmol, 1 equiv.) and 2 M aq. NaOH (0.5 mL) in THF (0.5 mL, 0.4 M) to afford the desired product as a brown amorphous solid (27 mg, 53%).

ν_{max} (neat): 3280, 1749, 1575, 1558, 1438 cm^{-1} .

^1H NMR (400 MHz, MeOD): δ 7.75 (dd, $J = 7.6, 0.8$ Hz, 1H), 7.56 (t, $J = 7.9$ Hz, 1H), 7.42 – 7.34 (m, 2H), 7.18 – 7.10 (m, 1H), 7.10 – 7.01 (m, 1H), 6.75 (dd, $J = 8.1, 0.8$ Hz, 1H), 2.49 (s, 3H). NH and CO_2H protons not observed.

^{13}C NMR (101 MHz, MeOD): δ 166.2, 164.1, 163.2, 147.6, 142.1, 137.6, 136.2, 129.6, 122.4, 121.6, 120.0, 117.4, 110.9, 95.4, 10.4.

HRMS: exact mass calculated for $[\text{M}+\text{H}^+]$ ($\text{C}_{15}\text{H}_{13}\text{N}_2\text{O}_2\text{S}$) requires m/z 285.0692, found m/z 285.0692.

Compound 196: Methyl 6-((3-bromophenyl)thio)picolinate

methyl 6-((3-bromophenyl)thio)picolinate
Chemical Formula: C₁₃H₁₀BrNO₂S
Molecular Weight: 324.19

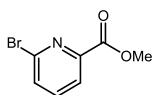
To a round-bottomed flask was added ethyl 6-bromopicolinate **197** (499.3 mg, 2.17 mmol, 1 equiv.), Cs₂CO₃ (1.42 g, 4.36 mmol, 2 equiv.), and 4-bromothiophenol (0.22 mL, 2.17 mmol, 1 equiv.). The reaction vessel was sealed and purged with N₂ before addition of DMF (10 mL, 0.2 M). The reaction mixture was then heated to 45 °C under for 16 h. The reaction mixture was allowed to cool to room temperature and diluted with H₂O (30 mL) and extracted using EtOAc (3 x 30 mL). The combined organics were dried (hydrophobic frit), and concentrated under vacuum to a residue that was purified using silica chromatography (10-40% EtOAc in petroleum ether) to afford the desired product as a white amorphous solid (0.26 g, 37%).

ν_{\max} (neat): 1724, 1560, 1440, 1390 cm⁻¹.

¹H NMR (400 MHz, CDCl₃) δ 7.86 (d, *J* = 7.6 Hz, 1H), 7.83 – 7.79 (m, *J* = 1.5 Hz, 1H), 7.63 (t, *J* = 7.9 Hz, 1H), 7.55 (t, *J* = 8.2 Hz, 2H), 7.32 (d, *J* = 7.9 Hz, 1H), 7.06 (d, *J* = 8.1 Hz, 1H), 3.98 (s, 3H).

¹³C NMR (101 MHz, CDCl₃) δ 165.0, 151.4, 143.9, 142.3, 140.7, 137.00 136.2, 135.1, 128.8, 127.9, 126.7, 125.5, 55.9.

HRMS: exact mass calculated for [M-H⁺] (C₁₃H₉⁷⁹BrNO₂S) requires *m/z* 323.9692, found 323.9692, (C₁₃H₉⁸¹BrNO₂S) requires *m/z* 325.9666, found *m/z* 325.9666.

Compound 197. Methyl 6-bromopicolinate

methyl 6-bromopicolinate
Chemical Formula: C₇H₆BrNO₂
Molecular Weight: 216.03

In a round bottomed flask 6-bromopicolic acid (1 g, 4.96 mmol, 1 equiv.) was dissolved in MeOH (30 mL, 0.2 M). To the reaction mixture conc. H₂SO₄ (0.35 mL) was added and the reaction mixture was heated to reflux under N₂ for 16 h. The reaction mixture was then cooled to 0 °C and 35% NH₄OH (1.6 mL) was added. The resulting solution was then reduced under vacuum, dissolved in CH₂Cl₂ (50 mL), and washed with brine (50 mL). The combined organics were dried (hydrophobic frit),

Experimental

and concentrated under vacuum to afford the desired product as a white amorphous solid (0.9 g, 85%).

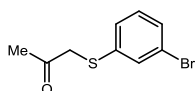
ν_{\max} (neat): 1718, 1687, 1562, 1446 cm^{-1} .

^1H NMR (500 MHz, CDCl_3): δ 8.09 (dd, $J = 7.0, 1.5$ Hz, 1H), 7.73 – 7.66 (m, 2H), 4.00 (s, 3H).

^{13}C NMR (101 MHz, CDCl_3): δ 164.4, 148.7, 142.1, 139.2, 131.8, 124.0, 53.1.

HRMS: exact mass calculated for $[\text{M}-\text{H}^+]$ ($\text{C}_7\text{H}_5^{79}\text{BrNO}_2$) requires m/z 215.9655, found m/z 215.9653, ($\text{C}_7\text{H}_5^{81}\text{BrNO}_2$) requires m/z 217.9634, found m/z 217.9632.

Compound 205: 1-((3-Bromophenyl)thio)propan-2-one



1-((3-bromophenyl)thio)propan-2-one
Chemical Formula: $\text{C}_9\text{H}_9\text{BrOS}$
Molecular Weight: 245.14

To a flask bromothiophenol (0.27 mL, 2.65 mmol, 1 equiv.) and THF (15 mL, 0.2 M) were added and cooled to 0 °C. DIPEA (2.3 mL, 13.22 mmol, 5 equiv.) was added portion wise and allowed to stir for 30 min before the addition of chloroacetone (2.3 mL, 5.65 mmol, 2.1 equiv.). The reaction mixture was then allowed to warm to room temperature and stirred for 16 h. The reaction mixture was concentrated under vacuum, diluted with EtOAc (30 mL) and washed with H_2O (30 mL). The combined organics were dried (hydrophobic frit) and concentrated under vacuum to a residue that was purified using silica chromatography (0-40% EtOAc in petroleum ether) to afford the desired product as a colourless oil (0.5 g, 84%).

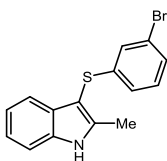
ν_{\max} (neat): 3050, 1571, 1559, 1454, 1392 cm^{-1} .

^1H NMR (400 MHz, CDCl_3): δ 7.45 (t, $J = 1.8$ Hz, 1H), 7.33 – 7.29 (m, 1H), 7.24 – 7.20 (m, 1H), 7.15 – 7.10 (m, 1H), 3.68 (s, 2H), 2.26 (s, 3H).

^{13}C NMR (101 MHz, CDCl_3): δ 202.8, 137.2, 131.7, 130.4, 129.8, 127.6, 122.9, 44.3, 28.1.

HRMS: exact mass calculated for $[\text{M}+\text{H}^+]$ ($\text{C}_9\text{H}_{10}^{79}\text{BrOS}$) requires m/z 246.9609, found m/z 246.9601, ($\text{C}_9\text{H}_{10}^{81}\text{BrOS}$) requires m/z 246.9609, found m/z 246.9601.

Compound 208: 3-((3-Bromophenyl)thio)-2-methyl-1H-indole



3-((3-bromophenyl)thio)-2-methyl-1H-indole
 Chemical Formula: C₁₅H₁₂BrNS
 Molecular Weight: 318.2320

Prepared according to General Procedure A using phenyl hydrazine hydrochloride (592.0 mg, 4.08 mmol, 1 equiv.) and 1-((3-bromophenyl)thio)propan-2-one **205** (1.0 g, 4.08 mmol, 1 equiv.) in EtOH (20 mL, 0.2 M) to afford the title compound as a brown oil (1.2 g, 91%).

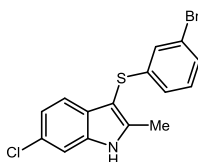
ν_{max} (neat): 3392, 3055, 2980, 1573, 1556 cm⁻¹.

¹H NMR (400 MHz, CDCl₃): δ : 8.30 (br s, 1H), 7.52 (d, J = 7.8 Hz, 1H), 7.36 (d, J = 8.0 Hz, 1H), 7.21 (td, J = 7.0, 1.3 Hz, 1H), 7.18-7.11 (m, 3H), 7.00 (t, J = 8.1 Hz, 1H), 6.93 (dt, J = 8.0, 1.4 Hz, 1H), 2.52 (s, 3H).

¹³C NMR (101 MHz, CDCl₃): δ : 142.1, 141.5, 135.6, 130.1, 127.9, 127.7, 124.1, 123.0, 122.5, 121.0, 118.9, 110.9, 98.5, 12.3. One carbon not observed/coincident.

HRMS: exact mass calculated for [M+H⁺] (C₁₅H₁₃⁷⁹BrNS) requires m/z 317.9947, found m/z 317.9951, (C₁₅H₁₃⁸¹BrNS) requires m/z 319.9925, found m/z 319.9931.

Compound 209: 3-((3-Bromophenyl)thio)-6-chloro-2-methyl-1H-indole⁶⁹



3-((3-bromophenyl)thio)-6-chloro-2-methyl-1H-indole
 Chemical Formula: C₁₅H₁₁BrClNS
 Molecular Weight: 352.6740

Prepared according to General Procedure A using (3-chlorophenyl)hydrazine (2.0 g, 8.18 mmol, 1 equiv.) and 1-((3-bromophenyl)thio)propan-2-one **205** (1.5 g, 8.18 mmol, 1 equiv.) in EtOH (40 mL, 0.2 M) to afford the desired compound as a cream amorphous solid (639.0 mg, 22%).

ν_{max} (neat): 3409, 1573, 1557, 1536 cm⁻¹.

¹H NMR (400 MHz, CO(CD₃)₂): δ 10.97 (br s, 1H), 7.48 (d, J = 1.9 Hz, 1H), 7.38 (d, J = 8.4 Hz, 1H), 7.24 (ddd, J = 7.9, 1.9, 1.0 Hz, 1H), 7.15 (t, J = 7.9 Hz, 1H), 7.11 (t,

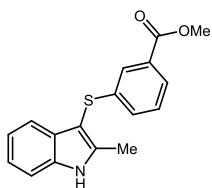
Experimental

$J = 1.8$ Hz, 1H), 7.08 (dd, $J = 8.4$ Hz, 1H), 7.02 (ddd, $J = 7.9, 1.8, 1.0$ Hz, 1H), 2.52 (s, 3H).

^{13}C NMR (101 MHz, CDCl_3): δ 143.0, 142.8, 136.3, 132.3, 129.5, 127.3, 127.0, 125.4, 123.5, 122.4, 122.2, 121.8, 109.1, 97.8, 11.7.

HRMS: exact mass calculated for $[\text{M}+\text{H}^+]$ ($\text{C}_{15}\text{H}_{12}^{79}\text{BrCINS}$) requires m/z 351.9557, found m/z 351.9555, ($\text{C}_{15}\text{H}_{12}^{81}\text{BrCINS}$) requires m/z 353.9534, found m/z 353.9529.

Compound 210: 3-((2-Methyl-1H-indol-3-yl)thio)benzoate



methyl 3-((2-methyl-1H-indol-3-yl)thio)benzoate
Chemical Formula: $\text{C}_{17}\text{H}_{15}\text{NO}_2\text{S}$
Molecular Weight: 297.3720

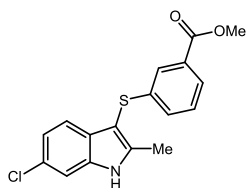
Prepared according to General Procedure F using *trans*-bis(acetato)bis[o-(di-*o*-tolylphosphino)benzyl]dipalladium(II) (183 mg, 0.195 mmol, 5 mol %), 3-((3-bromophenyl)thio)-2-methyl-1H-indole **208** (1.16 g, 3.91 mmol, 1 equiv.), $\text{Mo}(\text{CO})_6$ (1.03 g, 3.91 mmol, 1 equiv.), $[\text{tBu}_3\text{P}]\text{BF}_4$ (226 mg, 0.781 mmol, 20 mol %) and DBU (875 μL , 5.86 mmol, 1.5 equiv.) in MeCN (4 mL) and MeOH (16 mL, 0.2 M) to afford the desired compound as a brown amorphous solid (1.03 g, 89%).

ν_{max} (neat): 3327, 1500, 1710 cm^{-1} .

^1H NMR (500 MHz, CDCl_3): δ 8.49 (s, 1H), 7.81 (s, 1H), 7.70 (d, $J = 7.6$ Hz, 1H), 7.51 (d, $J = 7.8$ Hz, 1H), 7.34 (d, $J = 8.0$ Hz, 1H), 7.22 – 7.09 (m, 4H), 3.86 (s, 3H), 2.50 (s, 3H).

^{13}C NMR (126 MHz, CDCl_3): δ 166.9, 141.4, 140.4, 135.6, 130.6, 130.1, 129.8, 128.7, 126.6, 125.8, 122.3, 120.8, 118.8, 110.8, 52.1, 29.1, 12.1.

HRMS: exact mass calculated for $[\text{M}-\text{H}^+]$ ($\text{C}_{17}\text{H}_{14}\text{NO}_2\text{S}$) requires m/z 296.0751, found m/z 296.0753.

Compound 211: Methyl 3-((6-chloro-2-methyl-1H-indol-3-yl)thio)benzoate

methyl 3-((6-chloro-2-methyl-1H-indol-3-yl)thio)benzoate
 Chemical Formula: C₁₇H₁₄ClNO₂S
 Molecular Weight: 331.8140

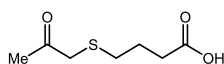
Prepared according to general procedure using *trans*-bis(acetato)bis[o-(di-*o*-tolylphosphino)benzyl]dipalladium(II) (90 mg, 0.096 mmol, 5 mol%), 3-((3-bromophenyl)thio)-6-chloro-2-methyl-1H-indole **209** (639 mg, 1.93 mmol, 1 equiv.), Mo(CO)₆ (510 mg, 1.93 mmol, 1 equiv.), [tBu₃PH]BF₄ (112 mg, 0.39 mmol, 20 mol %) and DBU (432 μL, 2.90 mmol, 1.5 equiv.) MeCN (4 mL) MeOH (16 mL, 0.3 M) to afford the desired compound as a cream amorphous solid (463 mg, 71%).

ν_{max} (neat): 3405, 3321, 2950, 1699, 1621, 1591, 1575, 1539 cm⁻¹.

¹H NMR (400 MHz, CO(CD₃)₂): δ 10.92 (br s, 1H), 7.73-7.66 (m, 2H), 7.47 (d, *J* = 1.8 Hz, 1H), 7.38 (d, *J* = 8.4 Hz, 1H), 7.32 (td, *J* = 7.7, 0.9 Hz, 1H), 7.25-7.18 (m, 1H), 7.07 (dd, *J* = 8.4, 1.9 Hz, 1H), 3.81 (s, 3H), 2.53 (s, 3H).

¹³C NMR (101 MHz, CO(CD₃)₂): δ 166.8, 144.4, 141.2, 137.4, 131.9, 130.6, 130.0, 129.7, 128.1, 126.9, 126.6, 121.6, 120.6, 112.1, 98.4, 52.4, 12.0.

HRMS: exact mass calculated for [M+H⁺] (C₁₇H₁₅ClNO₂S) requires *m/z* 332.0507, found *m/z* 332.0505,

Compound 215: 4-((2-Oxopropyl)thio)butanoic acid

4-((2-oxopropyl)thio)butanoic acid
 Chemical Formula: C₇H₁₂O₃S
 Molecular Weight: 176.2334

A solution of 4-mercaptobutanoic acid **216** (1.2 g, 10.02 mmol, 1 equiv.), DIPEA (4.4 mL, 25.06 mmol, 2.5 equiv.) in THF (30 mL, 0.3M) was cooled to 0 °C. To the cooled solution chloroacetone (0.98 mL, 10.52 mmol, 1 equiv.) was added portionwise. The reaction mixture was then allowed to warm to room temperature and stirred for 16 h. The reaction was then diluted with EtOAc (50 mL) and washed with water (3 x 30 mL) and brine (1 x 30 mL). The organic layer was then collected, dried (hydrophobic frit) and concentrated to a residue which was purified by silica

Experimental

chromatography (eluent DCM) to afford the desired compound as a clear oil (266.0 mg, 15%).

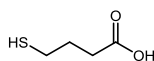
ν_{\max} (neat): 2924, 1701 cm^{-1} .

^1H NMR (400 MHz, CDCl_3): δ 3.20 (s, 2H), 2.48 (dt, $J = 33.2, 7.2$ Hz, 4H), 2.27 (s, 3H), 1.87 (p, $J = 7.3$ Hz, 2H). CO_2H proton not observed.

^{13}C NMR (101 MHz, CDCl_3): δ 203.7, 178.2, 41.1, 32.1, 30.6, 27.3, 23.2.

HRMS: exact mass calculated for $[\text{M}+\text{H}^+]$ ($\text{C}_7\text{H}_{13}\text{O}_3\text{S}$) requires m/z 177.0580, found m/z 177.0575.

Compound 216: 4-Mercaptobutanoic acid



4-mercaptobutanoic acid
Chemical Formula: $\text{C}_4\text{H}_8\text{O}_2\text{S}$
Molecular Weight: 120.1701

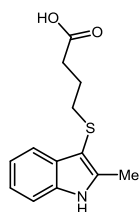
A solution of 4-bromobutyric acid (3.01 g, 18 mmol, 1 equiv.) and thiourea (2.05 g, 27 mmol, 1.5 equiv.) in EtOH (26 mL, 1 M) was heated at reflux for 3 h, then allowed to cool to room temperature and concentrated under vacuum. The residue was then dissolved in 7.5 M aq. NaOH (20 mL) and refluxed for 16 h. The reaction mixture was then cooled to 0 °C and acidified using 2 M aq. H_2SO_4 and extracted using CH_2Cl_2 (3 x 20 mL). The organics were combined, dried (hydrophobic frit) and concentrated under vacuum to afford the desired product as a colourless oil (1.73 g, 80%).

ν_{\max} (neat): 1703 cm^{-1} .

^1H NMR (400 MHz, CDCl_3) δ 10.07 (s, 1H), 2.62 – 2.53 (m, $J = 15.1, 7.1$ Hz, 2H), 2.49 (t, $J = 7.3$ Hz, 2H), 1.91 (quin., $J = 7.2$ Hz, 2H), 1.35 (t, $J = 8.1$ Hz, 1H).

^{13}C NMR (101 MHz, CDCl_3): δ 179.5, 32.4, 28.6, 23.9.

HRMS: exact mass calculated for $[\text{M}+\text{H}^+]$ ($\text{C}_4\text{H}_9\text{O}_2\text{S}$) requires m/z 121.0318, found m/z 121.0315.

Compound 218: 4-(2-Methyl-1H-indol-3-yl)butanoic acid

4-((2-methyl-1H-indol-3-yl)thio)butanoic acid
Chemical Formula: C₁₃H₁₅NO₂S
Molecular Weight: 249.3287

Prepared according to General Procedure B using 4-((2-oxopropyl)thio)butanoic acid **215** (340 mg, 2.27 mmol, 1 equiv.) and phenyl hydrazine hydrochloride (328 mg, 2.27 mmol, 1 equiv.) in ^tBuOH (15 mL, 0.15 M) with additional 1 M HCl in Et₂O (0.4 mL) and AcOH (1 mL) to afford the desired product as a yellow oil (308 mg, 66%).

ν_{\max} (neat): 3323, 2926, 1622, 1566, 1496, 1435 cm⁻¹.

¹H NMR (400 MHz, CDCl₃) δ 8.09 (s, 1H), 7.70 – 7.63 (m, 1H), 7.31 – 7.27 (m, 1H), 7.19 – 7.13 (m, 2H), 2.69 (t, J = 7.0 Hz, 2H), 2.53 (s, 3H), 2.50 (t, J = 7.4 Hz, 2H), 1.80 (quin., J = 7.2 Hz, 2H).

¹³C NMR (126 MHz, CDCl₃): δ 178.7, 140.0, 135.3, 130.5, 121.9, 120.3, 118.6, 110.6, 101.8, 35.1, 32.5, 24.7, 12.2.

HRMS: exact mass calculated for [M+H⁺] (C₁₃H₁₅NO₂) requires m/z 248.0751, found m/z 248.0752.

4.7 Biology

4.7.1 Autotaxin Inhibition Assay

Molecules were tested for their ability to inhibit autotaxin activity using the Autotaxin Inhibitor Screening Kit (Cayman Chemical) with modifications to the manufacturer's protocol. Briefly, In a 96 well plate 20 ng/mL autotaxin was incubated with 3 mM bis-pNPP at 30 °C for 30 min in 50 mM Tris-HCl buffer (pH8.5) containing 10 mM CaCl₂ and 0.02% triton X. Liberated bis-p-nitrophenol was measured using a Wallac Victor2 1420 multilabel counter (Perkin Elmer, Beaconsfield, UK) in absorbance mode at 405nm. The background was determined by incubating bis-pNPP in the absence of enzyme. Activity of the compounds was determined by subtracting the average background OD from all results and expressing the compound activity as a

percentage of the enzyme-substrate reaction in the absence of compound. PF-8380 in the concentration range of 0.1-300 nM in half log units was included as a standard compound in every assay plate. The potential inhibitors were initially tested against autotaxin at a concentration of 30 μ M (n=2); samples which showed inhibition of 60% or greater were considered to be active. Dose response curves, in the concentration range of 30 nM to 30 μ M in half log units, to calculate K_i values were performed on compounds reaching the designated activity threshold (n=3). Data was expressed as mean \pm SEM was plotted using Graph Pad Prism version 6.00 for Windows, GraphPad Software, La Jolla California USA, www.graphpad.com

4.7.2 Choline Release Assay

All biochemical studies were performed with hATX. ATX lysoPLD activity was measured by choline release from LPC. 20 nM ATX (prepared from HEK 293 Flp-In cells) was incubated with 150 μ M LPC(18:1) in a final volume of 100 μ l buffer containing 50 mM Tris pH 7.4, 0.01% Triton X-100, 50 mM CaCl_2 , 1 Unit ml^{-1} choline oxidase, 2 Unit ml^{-1} horseradish peroxidase, 2 mM homovanilic acid (HVA). The relative amount of released choline was measured by HVA fluorescence in a 96-well plate (Corning). Fluorescent intensity was determined at $\lambda_{\text{ex}}/\lambda_{\text{em}} = 320/450$ nm every 30 seconds for 90 minutes with a Fluorostar plate reader (BMG Labtech). Data analysis was performed using GraphPad Prism version 6.00 for Windows, GraphPad Software, La Jolla California USA, www.graphpad.com.

5 References

- (1) PHD; IHPHPS; RAMP. *Living Well for Longer: National Support for Local Action to Reduce Premature Avoidable Mortality*; 2014.
- (2) Version, E. Statistics Fact Sheet 8
<http://www.macmillan.org.uk/Documents/AboutUs/Research/Keystats/StatisticsFactsheet.pdf>.
- (3) <Http://www.iarc.fr/en/publications/books/wcr/wcr-order.php>. *World Cancer Report*; 2014.
- (4) NCRI. *The National Cancer Research Institution (NCRI) Cancer Research in the UK 2002-2011: An Overview of the Research Funded by NCRI Partners*; 2013.
- (5) Cooper, G. M. *The Cell: A Molecular Approach*, Second Edi.; Sinauer Associates: Sunderland (MA), 2000.
- (6) Sergew, A.; Brown, K. K. Idiopathic Pulmonary Fibrosis and Other Interstitial Lung Diseases. In *Clinical Respiratory Medicine*; Elsevier, 2012; pp 599–606.
- (7) *The Burden of Lung Disease: A Statistial Report from the Brithish Thoracic Society*, Second Edi.; London, 2006.
- (8) Gibson, K.; Kaminski, N. The Mechanisms of Idiopathic Pulmonary Fibrosis: Can We See the Elephant? *Drug Discov. Today Dis. Mech.* **2004**, 1 (1), 117–122.
- (9) King, T. E.; Pardo, A.; Selman, M. Idiopathic Pulmonary Fibrosis. *Lancet* **2011**, 378 (9807), 1949–1961.
- (10) Navaratnam, V.; Fleming, K. M.; West, J.; Smith, C. J. P.; Jenkins, R. G.; Fogarty, A.; Hubbard, R. B. The Rising Incidence of Idiopathic Pulmonary Fibrosis in the U.K. *Thorax* **2011**, 66 (6), 462–467.
- (11) Vancheri, C.; Failla, M.; Crimi, N.; Raghu, G. Idiopathic Pulmonary Fibrosis: A Disease with Similarities and Links to Cancer Biology. *Eur. Respir. J.* **2010**, 35 (3), 496–504.

-
- (12) Selman, M.; Pardo, A. Role of Epithelial Cells in Idiopathic Pulmonary Fibrosis: From Innocent Targets to Serial Killers. *Proc. Am. Thorac. Soc.* **2006**, *3* (4), 364–372.
- (13) Ren, Y.; Guo, L.; Tang, X.; Apparsundaram, S.; Kitson, C.; Deguzman, J.; Fuentes, M. E.; Coyle, L.; Majmudar, R.; Allard, J.; Truitt, T.; Hamid, R.; Chen, Y.; Qian, Y.; Budd, D. C. Comparing the Differential Effects of LPA on the Barrier Function of Human Pulmonary Endothelial Cells. *Microvasc. Res.* **2012**, *85*, 59–67.
- (14) du Bois, R. M. Strategies for Treating Idiopathic Pulmonary Fibrosis. *Nat. Rev. Drug Discov.* **2010**, *9* (2), 129–140.
- (15) Montesi, S. B.; Mathai, S. K.; Brenner, L. N.; Gorshkova, I. A.; Berdyshev, E. V.; Tager, A. M.; Shea, B. S. Docosatetraenoyl LPA Is Elevated in Exhaled Breath Condensate in Idiopathic Pulmonary Fibrosis. *BMC Pulm. Med.* **2014**, *14*, 5.
- (16) Yang, S. Y.; Lee, J.; Park, C. G.; Kim, S.; Hong, S.; Chung, H. C.; Min, S. K.; Han, J. W.; Lee, H. W.; Lee, H. Y. Expression of Autotaxin (NPP-2) Is Closely Linked to Invasiveness of Breast Cancer Cells. *Clin. Exp. Metastasis* **2002**, *19* (7), 603–608.
- (17) N. Panupinthu, H. Y. Lee, G. B. M.; Panupinthu, N.; Lee, H. Y.; Mills, G. B. Lysophosphatidic Acid Production and Action: Critical New Players in Breast Cancer Initiation and Progression. *Br. J. Cancer* **2010**, *102* (6), 941–946.
- (18) Stassar, M. J. J. G.; Devitt, G.; Brosius, M.; Rinnab, L.; Prang, J.; Schradin, T.; Simon, J.; Petersen, S.; Kopp-Schneider, A.; Zöller, M. Identification of Human Renal Cell Carcinoma Associated Genes by Suppression Subtractive Hybridization. *Br. J. Cancer* **2001**, *85* (9), 1372–1382.
- (19) Kehlen, A.; Englert, N.; Seifert, A.; Klonisch, T.; Dralle, H.; Langner, J.; Hoang-Vu, C. Expression, Regulation and Function of Autotaxin in Thyroid Carcinomas. *Int. J. Cancer* **2004**, *109* (6), 833–838.
- (20) Chun, J.; Lin, M.-E.; Mirendil, H. *Lysophospholipid Receptors: Signalling and Biochemistry*, Chun, J., Hla, T., Spiegel, S., Moolenaar, W., Eds.; John Wiley

& Sons, Inc.: Hoboken, NJ, USA, 2013.

- (21) Oikonomou, N.; Mouratis, M. A.; Tzouveleki, A.; Kaffe, E.; Valavanis, C.; Vilaras, G.; Karameris, A.; Prestwich, G. D.; Bouros, D.; Aidinis, V. Pulmonary Autotaxin Expression Contributes to the Pathogenesis of Pulmonary Fibrosis. *Am. J. Respir. Cell Mol. Biol.* **2012**, *47* (5), 566–574.
- (22) Tager, A. M.; LaCamera, P.; Shea, B. S.; Campanella, G. S.; Selman, M.; Zhao, Z.; Polosukhin, V.; Wain, J.; Karimi-Shah, B. a; Kim, N. D.; Hart, W. K.; Pardo, A.; Blackwell, T. S.; Xu, Y.; Chun, J.; Luster, A. D. The Lysophosphatidic Acid Receptor LPA1 Links Pulmonary Fibrosis to Lung Injury by Mediating Fibroblast Recruitment and Vascular Leak. *Nat. Med.* **2008**, *14* (1), 45–54.
- (23) Huang, L. S.; Fu, P.; Patel, P.; Harijith, A.; Sun, T.; Zhao, Y.; Garcia, J. G. N.; Chun, J.; Natarajan, V. Lysophosphatidic Acid receptor–2 Deficiency Confers Protection against Bleomycin-Induced Lung Injury and Fibrosis in Mice. *Am. J. Respir. Cell Mol. Biol.* **2013**, *49* (6), 912–922.
- (24) Ohashi, T.; Yamamoto, T. Antifibrotic Effect of Lysophosphatidic Acid Receptors LPA 1 and LPA 3 Antagonist on Experimental Murine Scleroderma Induced by Bleomycin. *Exp. Dermatol.* **2015**, *24* (9), 698–702.
- (25) Albers, H. M. H. G.; Ovaa, H. Chemical Evolution of Autotaxin Inhibitors. *Chem. Rev.* **2012**, *112* (5), 2593–2603.
- (26) Stefan, C.; Jansen, S.; Bollen, M. Modulation of Purinergic Signaling by NPP-Type Ectophosphodiesterases. *Purinergic Signal.* **2006**, *2* (2), 361–370.
- (27) Stracke, M. L.; Krutzsch, H. C.; Unsworth, E. J.; Arestad, A.; Cioce, V.; Schiffmann, E.; Liotta, L. A. Identification, Purification, and Partial Sequence Analysis of Autotaxin, a Novel Motility-Stimulating Protein. *J. Biol. Chem.* **1992**, *267* (4), 2524–2529.
- (28) Tokumura, A.; Majima, E.; Kariya, Y.; Tominaga, K.; Kogure, K.; Yasuda, K.; Fukuzawa, K. Identification of Human Plasma Lysophospholipase D, a Lysophosphatidic Acid-Producing Enzyme, as Autotaxin, a Multifunctional Phosphodiesterase. *J. Biol. Chem.* **2002**, *277* (42), 39436–39442.

-
- (29) Umezu-Goto, M.; Kishi, Y.; Taira, A.; Hama, K.; Dohmae, N.; Takio, K.; Yamori, T.; Mills, G. B.; Inoue, K.; Aoki, J.; Arai, H. Autotaxin Has Lysophospholipase D Activity Leading to Tumor Cell Growth and Motility by Lysophosphatidic Acid Production. *J. Cell Biol.* **2002**, *158* (2), 227–233.
- (30) T. Akira, H. Kengo, F. Kenji, T. H. No Title. *BBA-Lipid Lipid Met.* **1986**, *875*, 31–38.
- (31) Perrakis, A.; Moolenaar, W. H. Autotaxin: Structure-Function and Signaling. *J. Lipid Res.* **2014**, *55* (6), 1010–1018.
- (32) Lin, M. E.; Herr, D. R.; Chun, J. Lysophosphatidic Acid (LPA) Receptors: Signaling Properties and Disease Relevance. *Prostaglandins Other Lipid Mediat.* **2010**, *91* (3-4), 130–138.
- (33) Qian, Y.; Hamilton, M.; Sidduri, A.; Gabriel, S.; Ren, Y.; Peng, R.; Kondru, R.; Narayanan, A.; Truitt, T.; Hamid, R.; Chen, Y.; Zhang, L.; Fretland, A. J.; Sanchez, R. A.; Chang, K. C.; Lucas, M.; Schoenfeld, R. C.; Laine, D.; Fuentes, M. E.; Stevenson, C. S.; Budd, D. C. Discovery of Highly Selective and Orally Active Lysophosphatidic Acid Receptor-1 Antagonists with Potent Activity on Human Lung Fibroblasts. *J. Med. Chem.* **2012**, *55* (17), 7920–7939.
- (34) Di, L.; Kerns, E. H. Profiling Drug-like Properties in Discovery Research. *Curr. Opin. Chem. Biol.* **2003**, *7* (3), 402–408.
- (35) Zhao, Y.; Natarajan, V. Lysophosphatidic Acid Signaling in Airway Epithelium: Role in Airway Inflammation and Remodeling. *Cell. Signal.* **2009**, *21* (3), 367–377.
- (36) Mills, G. B.; Moolenaar, W. H. The Emerging Role of Lysophosphatidic Acid in Cancer. *Nat. Rev. Cancer* **2003**, *3* (8), 582–591.
- (37) Benesch, M. G. K.; Ko, Y. M.; McMullen, T. P. W.; Brindley, D. N. Autotaxin in the Crosshairs: Taking Aim at Cancer and Other Inflammatory Conditions. *FEBS Lett.* **2014**, *588* (16), 2712–2727.
- (38) Giganti, A.; Rodriguez, M.; Fould, B.; Moulharat, N.; Coge, F.; Chomarar, P.; Galizzi, J.-P.; Valet, P.; Saulnier-Blache, J.-S.; Boutin, J. A.; Ferry, G. Murine

- and Human Autotaxin A, B, and Y Isoforms: Gene Organisation, Tissue Distribution, and Biochemical Characterization. *J. Biol. Chem.* **2008**, *283* (12), 7776–7789.
- (39) Hausmann, J.; Kamtekar, S.; Christodoulou, E.; Day, J. E.; Wu, T.; Fulkerson, Z.; Albers, H. M. H. G.; Meeteren, L. A. Van; Zeijl, L. Van; Jansen, S.; Andries, M.; Hall, T.; Pegg, L. E.; Benson, T. E.; Kasiem, M.; Harlos, K.; Kooi, C. Vander; Susan, S.; Ovaa, H.; Bollen, M.; Morris, A. J.; Moolenaar, W. H.; Perrakis, A. Structural Basis of Substrate Discrimination and Integrin Binding by Autotaxin. *Nat. Struct. Mol. Biol.* **2011**, *18* (2), 198–204.
- (40) Nishimasu, H.; Okudaira, S.; Hama, K.; Mihara, E.; Dohmae, N.; Inoue, A.; Ishitani, R.; Takagi, J.; Aoki, J.; Nureki, O. Crystal Structure of Autotaxin and Insight into GPCR Activation by Lipid Mediators. *Nat. Struct. Mol. Biol.* **2011**, *18* (2), 205–212.
- (41) Stein, A. J.; Bain, G.; Prodanovich, P.; Santini, A. M.; Darlington, J.; Stelzer, N. M. P.; Sidhu, R. S.; Schaub, J.; Goulet, L.; Lonergan, D.; Calderon, I.; Evans, J. F.; Hutchinson, J. H. Structural Basis for Inhibition of Human Autotaxin by Four Potent Compounds with Distinct Modes of Binding. *Mol. Pharmacol.* **2015**, *88* (6), 982–992.
- (42) Barbayianni, E.; Magrioti, V.; Moutevelis-Minakakis, P.; Kokotos, G. Autotaxin Inhibitors: A Patent Review. *Expert Opin. Ther. Pat.* **2013**, *23* (9), 1123–1132.
- (43) Gijssbers, R.; Aoki, J.; Arai, H.; Bollen, M. The Hydrolysis of Lysophospholipids and Nucleotides by Autotaxin (NPP2) Involves a Single Catalytic Site. *FEBS Lett.* **2003**, *538* (1-3), 60–64.
- (44) Moolenaar, W. H.; Perrakis, A. Insights into Autotaxin: How to Produce and Present a Lipid Mediator. *Nat. Rev. Mol. Cell Biol.* **2011**, *12* (10), 674–679.
- (45) Nishimasu, H.; Ishitani, R.; Aoki, J.; Nureki, O. A 3D View of Autotaxin. *Trends Pharmacol. Sci.* **2012**, *33* (3), 138–145.
- (46) Albers, H. M. H. G.; Hendrickx, L. J. D.; Van Tol, R. J. P.; Hausmann, J.; Perrakis, A.; Ovaa, H. Structure-Based Design of Novel Boronic Acid-Based Inhibitors of Autotaxin. *J. Med. Chem.* **2011**, *54* (13), 4619–4626.

-
- (47) Clair, T.; Aoki, J.; Koh, E.; Bandle, R. W.; Nam, S. W.; Ptaszynska, M. M.; Mills, G. B.; Schiffmann, E.; Liotta, L. a.; Stracke, M. L. Autotaxin Hydrolyzes Sphingosylphosphorylcholine to Produce the Regulator of Migration, Sphingosine-1-Phosphate. *Cancer Res.* **2003**, *63* (17), 5446–5453.
- (48) Van Meeteren, L. A.; Ruurs, P.; Christodoulou, E.; Goding, J. W.; Takakusa, H.; Kikuchi, K.; Perrakis, A.; Nagano, T.; Moolenaar, W. H. Inhibition of Autotaxin by Lysophosphatidic Acid and Sphingosine 1-Phosphate. *J. Biol. Chem.* **2005**, *280* (22), 21155–21161.
- (49) Postma, F. R.; Jalink, K.; Hengeveld, T.; Moolenaar, W. H. Sphingosine-1-Phosphate Rapidly Induces Rho-Dependent Neurite Retraction: Action through a Specific Cell Surface Receptor. *The EMBOJournal* **1996**, *15*, 2388–2392.
- (50) Hait, N. C.; Oskeritzian, C. A.; Paugh, S. W.; Milstien, S.; Spiegel, S. Sphingosine Kinases, Sphingosine 1-Phosphate, Apoptosis and Diseases. *Biochim. Biophys. Acta - Biomembr.* **2006**, *1758* (2006), 2016–2026.
- (51) Gududuru, V.; Zeng, K.; Tsukahara, R.; Makarov, N.; Fujiwara, Y.; Pigg, K. R.; Baker, D. L.; Tigyi, G.; Miller, D. D. Identification of Darmstoff Analogs as Selective Agonists and Antagonists of Lysophosphatidic Acid Receptors. *Bioorg. Med. Chem. Lett* **2006**, *16*, 451–456.
- (52) Fells, J. I.; Lee, S. C.; Fujiwara, Y.; Norman, D. D.; Lim, K. G.; Tsukahara, R.; Liu, J.; Patil, R.; Miller, D. D.; Kirby, R. J.; Nelson, S.; Seibel, W.; Papoian, R.; Parrill, A. L.; Baker, D. L.; Bittman, R.; Tigyi, G. Hits of a High-Throughput Screen Identify the Hydrophobic Pocket of Autotaxin/lysophospholipase D as an Inhibitory Surface. *Mol. Pharmacol.* **2013**, *84* (3), 415–424.
- (53) Albers, H. M. H. G.; van Meeteren, L. A.; Egan, D. A.; van Tilburg, E. W.; Moolenaar, W. H.; Ovaa, H. Discovery and Optimization of Boronic Acid Based Inhibitors of Autotaxin. *J. Med. Chem.* **2010**, *53* (13), 4958–4967.
- (54) Takakusa, H.; Kikuchi, K.; Urano, Y.; Sakamoto, S.; Yamaguchi, K.; Nagano, T. Design and Synthesis of an Enzyme-Cleavable Sensor Molecule for Phosphodiesterase Activity Based on Fluorescence Resonance Energy Transfer. *J. Am. Chem. Soc.* **2002**, *124* (8), 1653–1657.

-
- (55) Ferguson, C. G.; Bigman, C. S.; Richardson, R. D.; van Meeteren, L. A.; Moolenaar, W. H.; Prestwich, G. D. Fluorogenic Phospholipid Substrate to Detect Lysophospholipase D/Autotaxin Activity. *Org. Lett.* **2006**, *8* (10), 2023–2026.
- (56) Morris, A. J.; Smyth, S. S. Measurement of Autotaxin/Lysophospholipase D Activity. *Methods Enzymol.* **2007**, *434*, 89–104.
- (57) North, E. J.; Howard, A. L.; Wanjala, I. W.; Pham, T. C. T.; Baker, D. L.; Parrill, A. L. Pharmacophore Development and Application Toward the Identification of Novel, Small-Molecule Autotaxin Inhibitors. *J. Med. Chem.* **2010**, *53* (8), 3095–3105.
- (58) Fells, J. I.; Lee, S. C.; Norman, D. D.; Tsukahara, R.; Kirby, J. R.; Nelson, S.; Seibel, W.; Papoian, R.; Patil, R.; Miller, D. D.; Parrill, A. L.; Pham, T. C.; Baker, D. L.; Bittman, R.; Tigyi, G. Targeting the Hydrophobic Pocket of Autotaxin with Virtual Screening of Inhibitors Identifies a Common Aromatic Sulfonamide Structural Motif. *FEBS J.* **2014**, *281* (4), 1017–1028.
- (59) Hoeglund, A. B.; Howard, A. L.; Wanjala, I. W.; Pham, T. C. T.; Parrill, A. L.; Baker, D. L. Characterization of Non-Lipid Autotaxin Inhibitors. *Bioorganic Med. Chem.* **2010**, *18* (2), 769–776.
- (60) Kihara, Y.; Mizuno, H.; Chun, J. Lysophospholipid Receptors in Drug Discovery. *Exp. Cell Res.* **2015**, *333* (2), 171–177.
- (61) Ohta, H.; Sato, K.; Murata, N.; Damirin, A.; Malchinkhuu, E.; Kon, J.; Kimura, T.; Tobo, M.; Yamazaki, Y.; Watanabe, T.; Yagi, M.; Sato, M.; Suzuki, R.; Murooka, H.; Sakai, T.; Nishitoba, T.; Im, D.-S.; Nochi, H.; Tamoto, K.; Tomura, H.; Okajima, F. Ki16425, a Subtype-Selective Antagonist for EDG-Family Lysophosphatidic Acid Receptors. *Mol. Pharmacol.* **2003**, *64* (4), 994–1005.
- (62) Swaney, J. S.; Chapman, C.; Correa, L. D.; Stebbins, K. J.; Broadhead, a R.; Bain, G.; Santini, a M.; Darlington, J.; King, C. D.; Baccei, C. S.; Lee, C.; Parr, T. a; Roppe, J. R.; Seiders, T. J.; Ziff, J.; Prasit, P.; Hutchinson, J. H.; Evans, J. F.; Lorrain, D. S. Pharmacokinetic and Pharmacodynamic Characterization of an Oral Lysophosphatidic Acid Type 1 Receptor-Selective

- Antagonist. *J. Pharmacol. Exp. Ther.* **2011**, 336 (3), 693–700.
- (63) Swaney, J. S.; Chapman, C.; Correa, L. D.; Stebbins, K. J.; Bunday, R. a; Prodanovich, P. C.; Fagan, P.; Baccei, C. S.; Santini, a M.; Hutchinson, J. H.; Seiders, T. J.; Parr, T. a; Prasit, P.; Evans, J. F.; Lorrain, D. S. A Novel, Orally Active LPA(1) Receptor Antagonist Inhibits Lung Fibrosis in the Mouse Bleomycin Model. *Br. J. Pharmacol.* **2010**, 160 (7), 1699–1713.
- (64) Gierse, J.; Thorarensen, A.; Beltey, K.; Bradshaw-Pierce, E.; Cortes-Burgos, L.; Hall, T.; Johnston, A.; Murphy, M.; Nemirovskiy, O.; Ogawa, S.; Pegg, L.; Pelc, M.; Prinsen, M.; Schnute, M.; Wendling, J.; Wene, S.; Weinberg, R.; Wittwer, A.; Zweifel, B.; Masferrer, J. A Novel Autotaxin Inhibitor Reduces Lysophosphatidic Acid Levels in Plasma and the Site of Inflammation. *J. Pharmacol. Exp. Ther.* **2010**, 334 (1), 310–317.
- (65) Schiemann, K.; Schultz, M.; Staehle, W. Piperidine and Piperazine Derivatives as Autotaxin Inhibitors. PCT Int. Appl. WO2010/115491 A2, 2014.
- (66) St-Cœur, P.-D.; Ferguson, D.; Morin, P. J.; Touaibia, M. PF-8380 and Closely Related Analogs: Synthesis and Structure-Activity Relationship towards Autotaxin Inhibition and Glioma Cell Viability. *Arch. Pharm. (Weinheim)*. **2013**, 346 (2), 91–97.
- (67) Data Generated Using SciFinder and Espacenet and Searching for Papers with the Term ATX.
- (68) Roppe, J. R.; Parr, T. A.; Hutchinson, J. H. Heterocyclic Autotaxin Inhibitors and Uses Therof. U.S. Pat. Appl. 20130029948 A1, 2013.
- (69) Roppe, J. R.; Parr, T. A.; Stock, N. S.; Volkotos, D.; Hutchinson, J. H. Autotaxin Inhibitors and Uses Therof. PCT Int. Appl. WO2012024620A2, 2012.
- (70) Hutchinson, J. H.; Lonergan, D.; Huang, F.; Rowbottom, M.; Calderon, I. Autotaxin Inhibitor Compounds. PCT Int. Appl. WO2015/048301 A1, 2015.
- (71) Hutchinson, J. H.; Lonergan, D.; Rowbottom, M.; Lai, A. G. Tetracyclic Autotaxin Inhibitors. PCT Int. Appl. WO2015/077502 A1, 2015.

-
- (72) Hutchinson, J. H.; Parr, T. A.; Bunker, K. D.; Lonergan, D. Vinyl Autotaxin Inhibitor Compounds. PCT Int. Appl. WO2015/042053 A1, 2015.
- (73) Autotaxin Inhibitors. U. S. Pat. Appl. 2014/0171403 A1, 2014.
- (74) Autotaxin Inhibitors. PCT Int. Appl. WO2015/008229 A1, 2015.
- (75) Sun, H.; Tawa, G.; Wallqvist, A. Classification of Scaffold-Hopping Approaches. *Drug Discov. Today* **2012**, *17* (7-8), 310–324.
- (76) Duffy, E. L. Lead Identification of Receptor and Enzyme Targets for the Treatment of IPF, University of Strathclyde, 2015.
- (77) ChemAxon. JChem for Excel (Version 16.1.1800). 2010.
- (78) Walters, W. P.; Murcko, A.; Murcko, M. a. Recognizing Molecules with Drug-like Properties. *Curr. Opin. Chem. Biol.* **1999**, *3* (4), 384–387.
- (79) Veber, D. F.; Johnson, S. R.; Cheng, H.-Y.; Smith, B. R.; Ward, K. W.; Kopple, K. D. Molecular Properties That Influence the Oral Bioavailability of Drug Candidates. *J. Med. Chem.* **2002**, *45* (12), 2615–2623.
- (80) Yang, Y., Coward, J. K. Synthesis of P-Aminophenyl Aryl H-Phosphinic Acids and Esters via Cross-Coupling Reactions: Elaboration to Phosphinic Acid Pseudopeptide Analogues of Pteroyl Glutamic Acid and Related Antifolates. *J. Org. Chem* **2007**, *72* (15), 5748–5758.
- (81) Prat, D.; Hayler, J.; Wells, A. A Survey of Solvent Selection Guides. *Green Chem.* **2014**, *16* (10), 4546–4551.
- (82) McGonagle, F. I.; MacMillan, D. S.; Murray, J.; Sneddon, H. F.; Jamieson, C.; Watson, A. J. B. Development of a Solvent Selection Guide for Aldehyde-Based Direct Reductive Amination Processes. *Green Chem.* **2013**, *15*, 1159–1165.
- (83) MacMillan, D. S.; Murray, J.; Sneddon, H. F.; Jamieson, C.; Watson, A., J. B. Evaluation of Alternative Solvents in Common Amide Coupling Reactions: Replacement of Dichloromethane and N,N-Dimethylformamide. *Green Chem.* **2012**, No. 15, 596–200.

-
- (84) MacMillan, D. S.; Murray, J.; Sneddon, H. F.; Jamieson, C.; Watson, A. J. B. Replacement of Dichloromethane Within Chromatographic Purification: A Guide to Alternative Solvents. *Green Chem.* **2012**, No. 14, 3016–3019.
- (85) Malacria, M., Maestri, G. Palladium/Norbornene Catalytic System: Chelation as a Tool To Control Regioselectivity of Pd(IV) Reductive Elimination. *J. Org. Chem* **2013**, *78* (4), 1323–1328.
- (86) DiscoverX. PathHunter b-arrestin GPCR assay platform <https://www.discoverx.com/arrestin>.
- (87) See SI for Full Details.
- (88) Zhang, H.; Xu, X.; Gajweiak, J.; Tsukahara, R.; Fujiwara, Y.; Liu, J.; Fells, J. I.; Perygin, D.; Parrill, A. L.; Tigyi, G.; Prestwich, G. D. Dual Activity Lysophosphatidic Acid Receptor Pan-Antagonist/autotaxin Inhibitor Reduces Breast Cancer Cell Migration in Vitro and Causes Tumor Regression in Vivo. *Cancer Res.* **2009**, *69*, 5411–5449.
- (89) Castagna, D.; Duffy, E. L.; Semaan, D.; Young, L. C.; Pritchard, J. M.; Macdonald, S. J. F.; Budd, D. C.; Jamieson, C.; Watson, A. J. B. Identification of a Novel Class of Autotaxin Inhibitors through Cross-Screening. *Med. Chem. Commun.* **2015**, *6* (6), 1149–1155.
- (90) Biological Data Generated by Collaborators at Strathclyde Institute of Pharmacology & Biomedical Sciences (SIPBS).
- (91) Gleeson, P. M. Generation of a Set of Simple, Interpretable ADMET Rules of Thumb. *J. Med. Chem* **2008**, *51*, 817–834.
- (92) Fra, L.; Millán, A.; Souto, J. A.; Muñiz, K. Indole Synthesis Based On A Modified Koser Reagent. *Angew. Chemie Int. Ed.* **2014**, *53* (28), 7349–7353.
- (93) Armarego, W. L. F.; Perrin, D. D. *Purification of Laboratory Chemicals*, Sixth Edit.; Elsevier Inc., 2009.
- (94) Gragg, B. R.; Layton, W. J.; Niedenzu, K. A ¹³C NMR Study on Some Phenylborane Derivatives. *J. Organomet. Chem.* **1977**, *132* (1), 29–36.
- (95) Xie, P.; Xie, Y.; Qian, B.; Zhou, H.; Xia, C.; Huang, H. Palladium-Catalyzed

Oxidative Carbonylation of Benzylic C–H Bonds via Nondirected C(sp³)–H Activation. *J. Am. Chem. Soc.* **2012**, *134* (24), 9902–9905.

- (96) Chouhan, G.; Alper, H. Synthesis of Ring-Fused Oxazolo- and Pyrazoloisoquinolinones by a One-Pot Pd-Catalyzed Carboxamidation and Aldol-Type Condensation Cascade Process. *J. Org. Chem.* **2009**, *74* (16), 6181–6189.
- (97) Data Generated by Collaborators at GSK.
- (98) Hert, J.; Hunziker, D.; Mattei, P.; Mauser, H.; Tang, G.; Wang, L. New Bicyclic Derivatives. WO 2014/048865 A1, 2014.
- (99) Molecular Operating Environment (MOE), 2013.08. Chemical Computing Group Inc.: Sherbooke St. West 2016.
- (100) *Molecular Modelling Conducted by Collaborators at GSK Using MOE.*
- (101) Castagna, D.; Miller, L. M.; Duffy, E. L.; Potjewyd, F. M.; Young, L. C.; Macdonald, S. J. F.; Jamieson, C.; Watson, A. J. B. Structure-Activity Relationship of Autotaxin Inhibitors. *Manuscr. Prep.*
- (102) Ketone Supplied Outsourced by Our Collaborators at GSK.
- (103) Data Generated by Collaborators at NKI in the Netherlands.